

198 pages

12824

NASA Contractor Report 174919

e/s W 0802171

# Analysis and Tests for Design of an Electro-Impulse De-Icing System

(NASA-CR-174919) ANALYSES AND TESTS FOR  
DESIGN OF AN ELECTRO-IMPULSE DE-ICING SYSTEM  
Interim Report (Wichita State Univ.) 198 p  
HC A09/MF A01 CSCL 01C

N86-27268

Unclas

G3/03

43300

G.W. Zumwalt, R.L Schrag, W.D. Bernhart,  
and R.A. Friedberg  
*Wichita State University*  
*Wichita, Kansas*

May 1985

Prepared for  
Lewis Research Center  
Under Grant NAG 3-284

Date for general release June 1986



## TABLE OF CONTENTS

	PAGE
<b>CHAPTER 1</b>	
<b>THE EIDI DEVELOPMENT PROJECT</b>	
I. Introduction . . . . .	1
II. The Basic Principles . . . . .	1
III. Prior History . . . . .	6
IV. Current NASA/WSU/Industry Project . . . . .	7
V. References . . . . .	9
 <b>CHAPTER 2</b>	
<b>ELECTRODYNAMIC STUDIES AND TESTS</b>	
I. Electro-Impulse Circuit Characteristics and Design Aspects . . . . .	11
II. Ballistics Pendulum Studies . . . . .	23
III. Magnetic Field Diagnostics Experiment . . . . .	39
IV. Electrodynamics Modeling . . . . .	60
V. References . . . . .	75
 <b>CHAPTER 3</b>	
<b>STRUCTURAL DYNAMIC TESTS AND STUDIES</b>	
I. Introduction . . . . .	77
II. Strain Measurements Near EIDI Coils . . . . .	81
III. Boeing (BCAC) 767 Leading Edge Slat Strain . . . . .	84
IV. 2.5 Inch Radius Semi-Cylinder Studies . . . . .	87
V. Recent Developments Related to EIDI Force Measurements . . . . .	94
VI. References . . . . .	96
VII. Figures 3-1 to 3-32 . . . . .	97
 <b>CHAPTER 4</b>	
<b>FABRICATION TECHNIQUES</b>	
I. Coil Wire Rolling . . . . .	129
II. Coil Making . . . . .	129
III. Coil Mounts . . . . .	136
IV. Electrical Leads . . . . .	140
V. Weight Estimates . . . . .	140
VI. Coil Attachment . . . . .	141
VII. Icing Tunnel Models . . . . .	141
VIII. Test Model Instrumentation . . . . .	143
 <b>CHAPTER 5</b>	
<b>ICING TUNNEL TESTS</b>	
I. Oct. 25 - Nov. 5, 1982 Tests . . . . .	147
II. April 18-22, 1983 Tests . . . . .	149
III. August 15-18, 1983 Tests . . . . .	153
IV. November 7-9, 1983 Tests . . . . .	157
V. May 14-23, 1984 Tests . . . . .	161
VI. August 13-17, 1984 Tests . . . . .	164
VII. Sept. 17-21, 1984 Tests . . . . .	166
VIII. Nov. 26 - Dec. 4, 1984 Tests . . . . .	172
IX. References . . . . .	175

TABLE OF CONTENTS  
(Continued)

CHAPTER 6

FLIGHT TESTS

I. NASA Icing Research Aircraft . . . . .	177
II. Cessna TV 206 Flights (1984) . . . . .	180
III. References . . . . .	187

CHAPTER 7

PLANS AND PROSPECTS . . . . .	189
-------------------------------	-----

CHAPTER 8

APPENDICES

WSU Participants on EIDI Project . . . . .	191
Industrial Participants . . . . .	192
Prospects and Problems for Applying EIDI to Helicopter Blades . . . . .	193

## CHAPTER 1. THE EIDI DEVELOPMENT PROJECT

### I. Introduction

Ice accumulation on aircraft wings in flight has been a danger since the earliest days of flight. The total accumulation needs not be large to be fatal. Although ice normally is accrued on frontward facing surfaces only, giving a few centimeters thickness on the front 2 percent of the wing chord, this is enough to cause flow separation and destroy lift, particularly if the aircraft slows or maneuvers. Also, drag may increase enough to exhaust fuel reserves or destabilize the flight. Helicopter rotors are even more vulnerable to the detrimental effects of ice, and engine inlet diffusers require icing protection to a greater degree than lifting surfaces. This need brought the NASA Lewis Research Center into aircraft icing research almost from its start.

Although several methods of de-icing or anti-icing are available, all have some undesirable aspects in regard to energy requirements. A method suggested (Ref. 1-1) as early as 1937 offers an alternative which has not been adequately developed. The electro-magnetic impulse phenomenon has been used for metals forming, and holds the promise of ice removing with very low energy, minimal maintenance (no moving parts), great reliability, and weight and cost competitive with existing methods.

This report summarizes work done under a NASA-Lewis grant to develop the Electro-Impulse De-Icing (EIDI) system. Wichita State University has been the grant recipient, charged with researching the phenomena to provide the underlying technology, and also with coordinating the efforts of a team of participating industries. The program has consisted of basic analyses, laboratory tests, icing tunnel tests and flight tests. At the two-and-a-half year point, the EIDI system has been tested and refined and shown to be a low-energy, highly reliable de-icing method. This report is a status report and an outline of design methods developed to this date.

### II. The Basic Principles

The physical form of the Electro-Impulse De-Icing (EIDI) method is shown in Figure 1-1. Flat-wound coils made of copper ribbon wire are placed just inside the leading edge of a wing's skin with a small gap separating skin and coil. Either one or two coils are placed at a given spanwise station, depending on the size of the leading edge. Two methods of supporting coils are shown; support by the front spar or from a beam attached to ribs is generally used, but mounting to the skin itself is sometimes used.

The coils are connected by low resistance, low inductance cables to a high voltage capacitor bank, and energy is discharged through the coil by a

remote signal to a silicon-controlled-rectifier ("thyristor"). Discharge of the capacitor through the coils creates a rapidly forming and collapsing electro-magnetic field which induces eddy currents in the metal skin. The fields resulting from current flow in the coil and skin create a repulsive force of several hundred pounds magnitude, but a duration only a fraction of a millisecond. A small amplitude, high acceleration movement of the skin acts to shatter, debond and expel the ice. Two or three such "hits" are performed sequentially, separated by the time required to recharge the capacitors, then ice is permitted to accumulate until it again approaches an undesirable thickness.

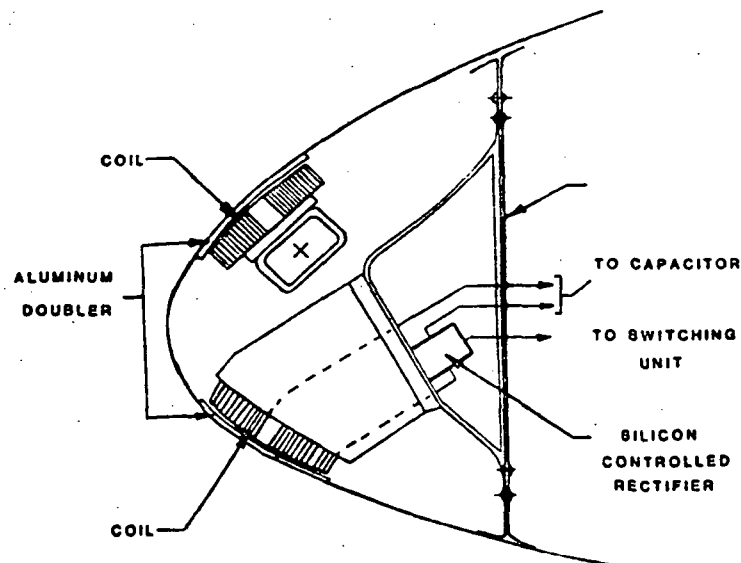


Fig. 1-1 Impulse Coils in a Leading Edge

Figure 1-1 also shows "doublers," unalloyed aluminum discs, slightly larger than the coils, bonded to the skin opposite the coil. These are used when the skin thickness is less than the minimum required to provide adequate conductance for the eddy currents. Composite, non-metallic, leading edges require a similar special treatment. A fundamental study of the phenomena and parameters for electro-impulse was undertaken to provide a basis for such geometric and electrical design choices. Prof. R. L. Schrag of Wichita State University has led this study which is presented in Chapter 2. Ref. 1-2 reported initial results of this work.

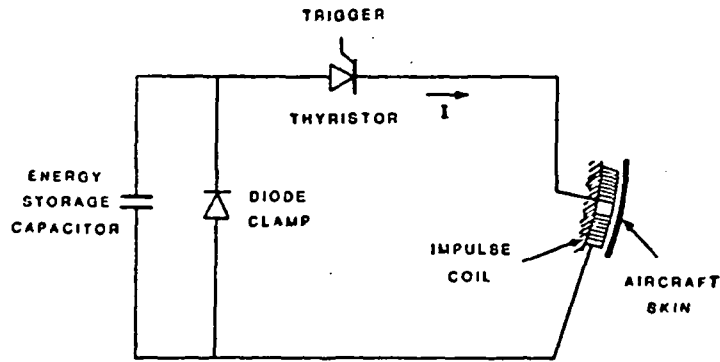


Fig. 1-2 Basic Circuit

In Figure 1-2, the basic circuit is illustrated. An electro-impulse is initiated by supplying a trigger pulse to the thyristor, allowing the capacitor to discharge through the coil. A typical current waveform is shown in Figure 1-3. Since a thyristor has diode properties, the current follows the first positive loop of the RLC response, after which the thyristor re-opens the circuit. This leaves the capacitor reverse-charged. Such reverse charging reduces capacitor life substantially. For that reason a clamping diode is placed across the capacitor. A typical current and resulting skin displacement are shown in Figure 1-3.

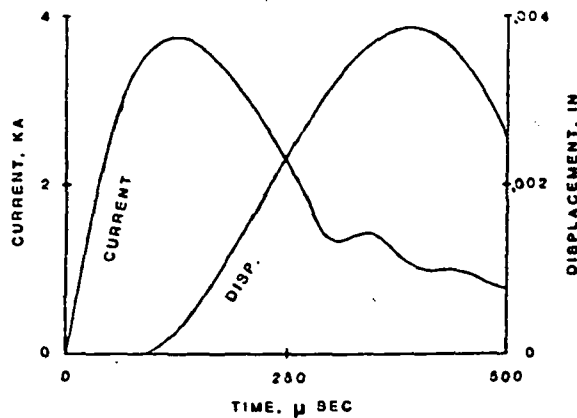


Fig. 1-3 Typical Coil Current and Skin Displacement

Figure 1-4 is a flat geometry illustration of the coil's magnetic field and induced eddy currents in the electrically conducting skin. The magnetic field due to the eddy currents is not shown, but it has a significant influence (by self induction) on the magnitude, time history, and radial distribution of the eddy currents. In addition, the electromagnetic "skin effect" phenomenon affects the eddy current distribution across the aluminum skin thickness. Current densities are greatest on the coil side. A reverse coupling effect is also present. Time-changing eddy currents induce a voltage in the impulse coil, modifying its current. From a circuit aspect, the consequence is a modification of the effective inductance and resistance of the coil. The effective inductance decreases, and the effective resistance increases, due to the proximity of the metal sheet.

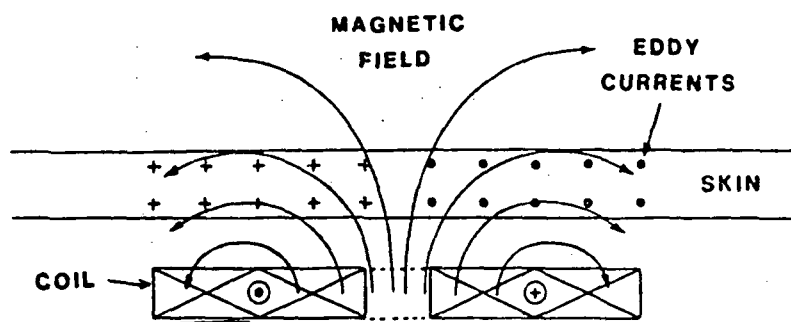


Fig. 1-4 Coil Magnetic Field Pattern and Resulting Eddy Currents

When the aircraft skin moves in response to the electro-impulse force the coil-to-skin gap changes and that modifies the magnitude of the proximity influence. In addition, the skin's movement relative to the coil's magnetic field further modifies (by motional induction) the electromotive forces that drive the eddy currents. These influences due to skin motion are, however relatively small because of the time delay involved in the motion, and appear to be negligible when the skin is ice loaded. The assertion is, in effect, that the coil current and the strength of the force impulse may be calculated without the need to also analyze the complex structural response. This is discussed in detail in Chapter 2.

Figure 1-5 shows a wing with coils placed spanwise, separated by about 0.4 meters. These are all supplied by a single power unit. A more effective modified version is shown in Fig. 1-6. Energy requirements are small, being comparable to those typical of landing lights for the same size aircraft. De-icing has been accomplished in the icing wind tunnel and in flight for typical general aviation wings under a wide range of velocities, angles of attack, icing rates and temperatures.

Just as effective de-icing by electro-impulse requires a matching of electric circuit dynamics and skin electrical properties, so also does it

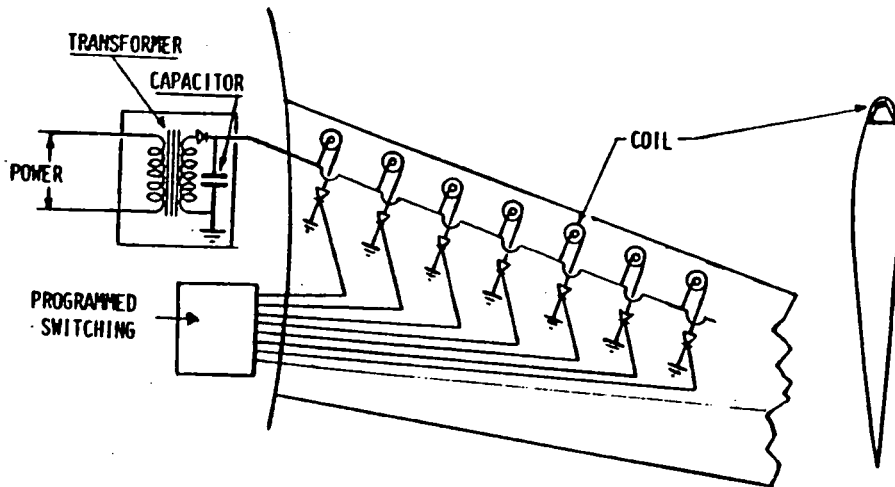


Fig. 1-5 Electro-Impulse Coils  
Installed in a Wing

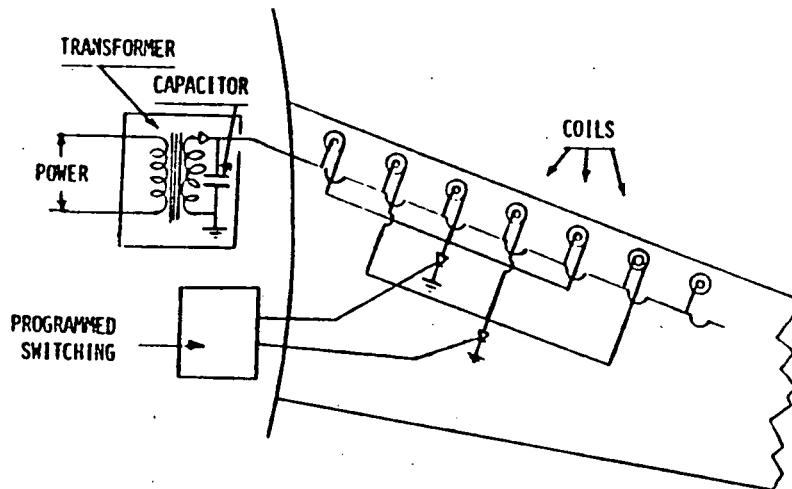


Fig. 1-6 E.I.D.I. with Series-Connected Coils  
("Odds and Evens")

demand properly related structural dynamic matching. The propagation of skin movement in chordwise and spanwise directions from the EIDI coil is necessary. It is also a complex, three-dimensional, transient structural dynamic analysis problem; Ref. 1-3. Coil location and pulse duration must have the proper relations to the structural vibrational mode to be excited. Failure to do so severely impairs the effectiveness of de-icing.

The imposed force cannot be modeled as a simple impulse, since its duration is comparable to the period of the first vibrational mode. Similarly, the force cannot be treated as a concentrated "point" load, since the width of the coil is of the same order as the wave lengths of low-order vibrational modes. Thus, structure-dynamic analysis must include the details of the spacial and temporal results of the electro-dynamic analysis.

Under the leadership of Professor Walter D. Bernhart, analytical and experimental studies have been carried out on the structural dynamics of leading edge structures under EIDI-type impulsive loading. These are reported in Chapter 3.

The participation of industry in the project provided constant reminder of the practical aspects of safety, weight, cost and manufacturability. While research and testing were carried on, parallel efforts were made to develop fabricating and design method for the hardware. In particular, coil making and mounting were developed under the leadership of Robert Friedberg. The current state of materials and processes for these, together with testing methods, are given in Chapter 4.

Icing tunnel tests (eight sets at the time of this report writing) have been essential to the system development. The unique capabilities of the NASA-Lewis Icing Research Tunnel (IRT) provide testing conditions for confident evaluation of the system in flight. Chapter 5 summarizes the IRT tests and results. Reference 1-4 reports in more detail the engine nacelle and large wing testing.

Chapter 6 gives a brief account of the two flight test programs completed to date. These were earlier reported in References 1-5 and 1-6. A third is in progress at the time of writing this interim report. Finally, plans and prospects for the project are delineated in Chapter 7.

### III. Prior History

The use of electro-magnetic impulse force to remove ice was first suggested by Rudolf Goldschmidt, a German national residing in London before World War II. He was granted a patent (Ref. 1-1) and a series of patent extensions in 1937 through 1939. His patents, now expired, anticipated most of the applications now being used or considered. However, there is no evidence that Goldschmidt ever attempted to build the devices he imagined.

During the 1950's and 1960's, electro-impulse methods were used for metals forming in various industrial processes, but no record can be found of the use for de-icing until researchers in the USSR either discovered Goldschmidt's patents or rediscovered this application independently. In 1965, I.A. Levin in the Soviet Ministry of Power and Electrification, seeking methods for cleaning frozen and sticky materials from surfaces (coal bunkers, transformer boxes, towers, etc.) published work on electro-impulse possibilities. He immediately received inquiries from other ministries (aviation, fisheries, dairy, housing) regarding de-icing of vehicles, buildings, ships, and for cleaning of dry milk from hoppers (Ref. 1-7 and 1-8). Responding to their requests involved him in bureaucratic territorial struggles and he was fired. Eventually, however, he was set up in his own

laboratory under the State Committee for Meteorology and Environmental Monitoring, and apparently made some installations in aircraft; the Il-18 has been cited as having been the first, but confirmation by Western observers is difficult to obtain.

In any case, in the early 1970's, Russian representatives were granted EIDI patents in several Western nations, including the USA, and USSR salesmen began calling on American and European aircraft companies offering to sell their design and construction services for an EIDI system. Their lack of candor discouraged most customers, but interest was stirred and during the 1970's, work was done on this method in France (Air-Equipment division of DBA), Great Britain (Lucas Aerospace and B.A.C.), and the United States (Lockheed and McDonnell-Douglas). For various reasons, the development stopped short of full implementation. The system still lacked a well developed underlying technology and known design parameters.

#### IV. Current NASA/WSU/Industry Project

##### A. Initial Feasibility Demonstration

In mid-1982, NASA Lewis Research Center funded a six-month grant to Wichita State University to work with two small plane makers, Beech and Cessna, and an aircraft electrical system manufacturer, the Engine Systems Division of Simmonds-Precision, to do a feasibility study resulting in an icing tunnel demonstration in Oct.-Nov. 1982. Two wing sections were tested, mid-wing portions from a Beech Bonanza and a Cessna 206. These were similar in size and flight speeds, but had very different leading edge structures, one very stiff and small, the other flexible and large in extension from the front spar. Good cleaning was accomplished with fairly low energy expenditure for air speeds from 96 to 230 knots, air temperatures from 29° to -15°F (-2° to -26°C), angles of attack from 2 to 8 degrees and liquid moisture contents from 0.6 to 2.4 g/m<sup>3</sup>.

##### B. The Industry Consortium

The results were encouraging enough to lead NASA to expand the aim to full development of the method for the whole range of civil aircraft. A consortium of participating industries was formed for this purpose. Each company agreed to contribute some services or equipment to the project, and in return became eligible to submit its own products for de-icing design and tests by the EIDI method. WSU was charged with doing the needed research into the electrodynamic and structural dynamic phenomena involved, and developing manufacturing methods for coils and their mountings. In addition, WSU coordinated the effort and conducted further tests in the

NASA/Lewis Icing Research Tunnel (IRT). The industries represented a wide scope of aircraft sizes, air speeds, skin thicknesses and of attitudes regarding the introduction of a new device.

Realizing the ultimate requirement for certification, FAA personnel were invited into the group meeting so that their concerns could be considered as early as possible.

Consortium members for the 1982-83 period were:

Small Aircraft: Beech Aircraft Co., Wichita, KS  
Cessna-Pawnee Div., Wichita, KS  
Business Jet Aircraft: Gates Learjet Corporation,  
Wichita, KS  
Cessna-Wallace Div., Wichita, KS  
Composite, High Performance: LearFan Ltd., Reno, NV  
Transport Aircraft: Boeing Commercial, Seattle, WA  
McDonnell-Douglas, Co., Long Beach, CA  
Electrical Equipment: Simmonds-Precision, Norwich, NY

In late 1983, Rohr Industries of Chula Vista, CA, joined the group with an interest in de-icing engine inlets. In 1984, a second aircraft electrical equipment developer was added, Electro-Delta of White Oak, Texas, and the first helicopter maker, Sikorsky Aircraft Co., Stratford, CT. also joined. At the time of preparation of this report, Bell Helicopter of Ft. Worth, TX, and the Boeing/Vertol Co. of Philadelphia, PA, have requested membership.

### C. Objectives

The program objectives were, from the start, quite comprehensive:

1. Develop computer models for the structural dynamics of leading edge portions of wings and engine inlets to provide design guidance for coil location, coil size, impulse intervals and coil spanwise spacing. An alternative approach was also desired, namely the development of a standard measurement method for existing structures to extract the structural dynamics characteristics needed for the design.
2. Develop a computer model for the electro-dynamics and provide detailed design data for the electro-impulse equipment, including coil design, power, voltage, insulation, pulse duration, and switching equipment.

3. Test wing sections and engine inlets in the IRT to guide and prove EIDI designs.
4. Consider practical aspects of retro-fitting the EIDI system to existing aircraft.
5. Devise methods for optimal design of a wing structure for using the system.
6. Estimate and attempt to minimize the cost of the EIDI system in terms of weight, maintenance and capital outlay.
7. Details to be considered are:
  - (a) Limits of application (size, stiffness, etc.)
  - (b) Standardization of components
  - (c) Fatigue of skin, mountings, switching gear, bondings
  - (d) Electro-magnetic interference problems and solutions
  - (e) Use with composite materials
  - (f) Integration with present avionics and electrical systems
8. Conduct flight demonstrations using aircraft from NASA and participating industries.
9. Carry out at least the first stages of FAA certification.

#### V. References

- 1-1. British Patent Specification No. 505,433 issued to Rudolf Goldschmidt; May 5, 1939.
- 1-2. R.L. Schrag and G.W. Zumwalt, "Electro-Impulse De-icing: Concept and Electrodynamic Studies," AIAA 22nd Aerospace Sciences Meeting, Reno, NV, Jan. 9-12, 1984, Paper No. 84-0021.
- 1-3. W.D. Bernhart and G.W. Zumwalt, "Electro-Impulse De-icing: Structural Dynamic Studies, Icing Tunnel Tests and Applications," AIAA 22nd Aerospace Sciences Meeting, Reno, NV, Jan. 9-12, 1984, AIAA Paper No. 84-0022.
- 1-4. G.W. Zumwalt, "Icing Tunnel Tests of Electro-Impulse De-Icing of an Engine Inlet and High-Speed Wings," AIAA 23rd Aerospace Sciences Meeting, Reno, Nevada, January 14-17, 1985. AIAA Paper No. 85-0466.

V. References  
(continued)

- 1-5. G.W. Zumwalt and A.A. Mueller, "Flights and Wind Tunnel Tests of an Electro-Impulse De-Icing System", AIAA/NASA General Aviation Technology Conference, Hampton, VA, July 10-12, 1984. AIAA Paper No. 84-2234.
- 1-6. Mueller, A.A., D.R. Ellis and D.C. Bassett, "Flight Evaluation of an Electro-Impulse De-icing System on a Light General Aviation Airplane." AIAA/AHS Aircraft Designs, Systems and Operations Meeting, San Diego, CA., October 1984. AIAA Paper No. 84-2495.
- 1-7. "From the Sky to the Earth," Pravda, (unsigned), Dec. 10, 1978.
- 1-8. "Development of De-icing System," Pravada, (unsigned), Feb. 11, 1980.

## CHAPTER 2

### ELECTRODYNAMIC STUDIES AND TESTS

#### I. Electro-Impulse Circuit Characteristics and Design Aspects

##### A. Theoretical Low Frequency Inductance and Resistance for Isolated Pancake Shaped Coils

Procedures can be found in the literature for calculating the inductance of flat pancake shaped coils wound spirally with rectangular wire. The procedure given in Reference 2-1 was used to calculate a table of values (Table 2-1) for coils having a fixed thickness of .188 inch and a fixed inner diameter of 0.25 inch. Insulation thickness of .003 was assumed. The table also lists theoretical d.c. coil resistance, assuming annealed copper, and the ribbon wire thickness. It is particularly useful for design purposes, once the outer diameter and inductance are selected.

One comparison was made between calculated inductance and a bridge measurement. The coil had 30 turns and a 2 inch diameter. The bridge measured 19.8  $\mu\text{H}$ , compared with a calculated 18.9  $\mu\text{H}$ . The difference may have been due to about 18 inches of connecting leads.

TABLE 2-1  
COIL DIAMETER, INCHES

TURNS	1.5			2.0			2.5			3.0		
	L	R	b	L	R	b	L	R	b	L	R	b
20	6.5	7.0	28.4									
25	11.3	11.2	22.1	12.6	9.9	32.1						
30	18.8	16.6	17.9	18.9	14.6	26.3	21.9	13.5	34.6			
35	30.6	23.2	14.9	27.3	20.2	22.1	30.4	18.7	29.2	35.0	17.7	36.4
40				38.5	26.9	19.0	40.9	24.8	25.2	46.3	23.4	31.4
45							53.7	31.8	22.1	59.7	30.0	27.6
50							69.5	39.9	19.6	75.1	37.5	24.6
55										93.4	46.0	22.0

L = Inductance in  $\mu\text{H}$

R = D.C. resistance in  $\text{m}\Omega$   
(Assumes annealed copper)

b = Ribbon wire thickness in Mils

Fixed Dimensions:

Ribbon width 0.188 inch

Insulation thickness 0.003 inch

Inner coil diameter 0.25 inch

B. Influence of Frequency on L and R

ORIGINAL PAGE IS  
OF POOR QUALITY

Bridge measurements were made at various frequencies on the 30-turn, 2 inch diameter coil. The inductance was found to be practically independent of frequency, decreasing only 5 percent as the frequency was scanned from 500 Hz to 20 kHz.

The resistance exhibited a much greater frequency effect. Figure 2-1 shows a plot of the ratio of a.c. resistance to d.c. resistance vs. frequency. The d.c. resistance value was measured by the ammeter-voltmeter method, and exceeded the value given in Table 2-1 by 40 percent. This is probably due to the fact that the wire was not annealed subsequent to a rolling operation. The increase in R with frequency suggests the presence of skin effect.

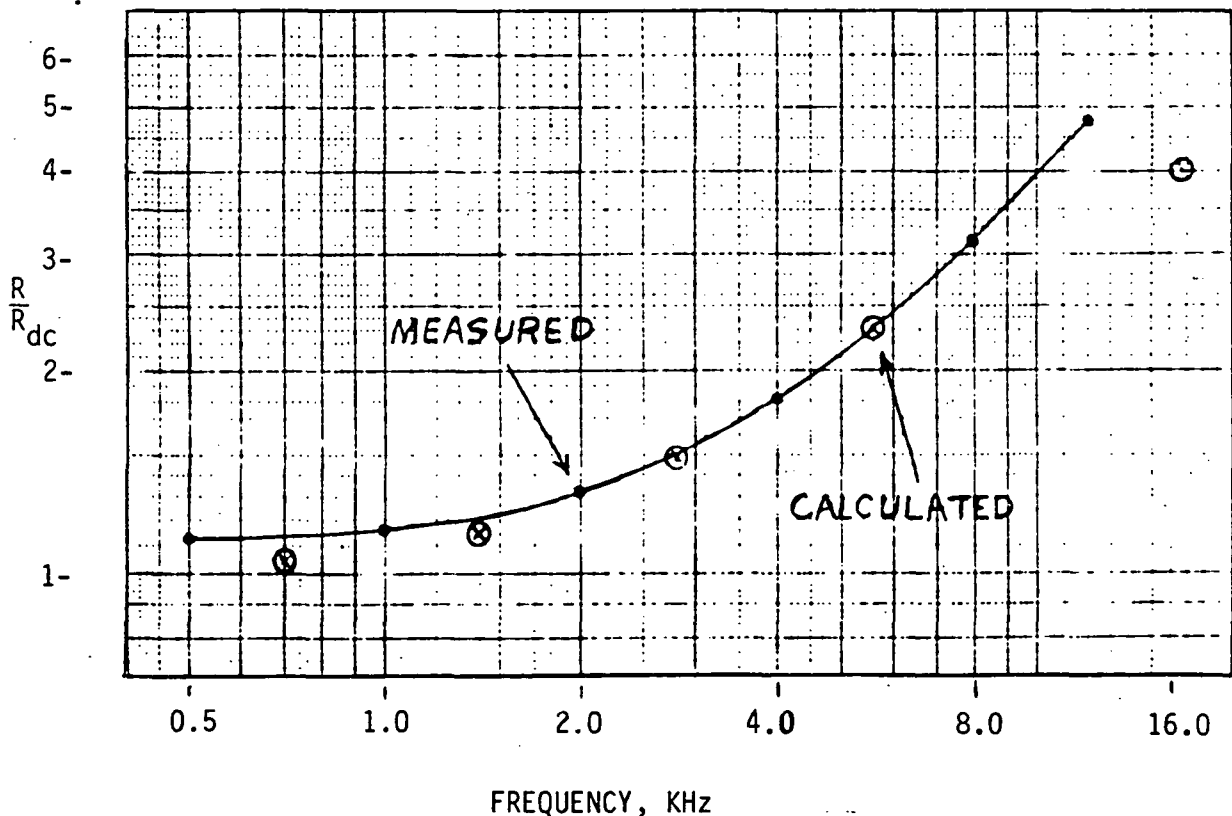


Fig. 2-1 Coil Resistance vs. Frequency

Assuming a metal plate of thickness "b" with symmetrical excitation on both surfaces, one can derive the following formula for the resistance ratio:

$$\frac{R_{a.c.}}{R_{d.c.}} = \operatorname{Re} \left[ \frac{\frac{\tau b}{2}}{\tanh\left(\frac{\tau b}{2}\right)} \right]$$

where

$$\tau = (1 + j)/\delta$$

and  $\delta$  is the skin depth given by

$$\delta = \sqrt{2/\omega\mu\sigma}$$

In order to explain the experimental data, the "b" dimension had to be taken as the width (not thickness) of the ribbon wire. With that assumption, the calculated results agree well with the measurements (see Figure 2-1) up to about 6 kHz. Beyond that frequency there appears to be some added complication to the theoretical model.

It is concluded that the primary frequency affect on resistance in the audio frequency range is due to energy diffusion into the ribbon wire via the coil surfaces. Diffusion into the ribbon via its narrow dimension should occur at a much higher frequency and may, in part, be involved in the added complication referred to above.

### C. Proximity Effects of Metal Plates

In designing a coil for electro-impulse de-icing, one should recognize the fact that the apparent inductance and resistance of the coil will be modified by the close proximity of the aluminum skin. A suitable theoretical model would, presumably, account for this modification.

Limited bridge measurements were made in order to get a feel for the magnitudes of the proximity effects. The coil used in the tests was the 30-turn, 2 inch diameter coil. Two "target" configurations were tried.

The first was a .032 inch 2024-T3 aluminum plate with a .05 inch gap (approximately .078 inch between the plate and the copper surface of the coil). For the second test a .021 inch copper "doubler" was added onto the coil side of the .032 inch aluminum plate, still maintaining a .050 inch gap from coil-to-doubler. The experimental results are given in Tables 2-2 and 2-3.

TABLE 2-2

INFLUENCE OF .032" Al PLATE  
WITH .05" GAP

Frequency	Inductance Factor	Resistance Factor
1 kHz	.85	1.8
2 kHz	.75	2.6
4 kHz	.65	2.9

These are ratios of values with the plate present to values without the plate (at the same frequency).

TABLE 2-3

INFLUENCE OF .032" Al PLATE +  
.021" Cu DOUBLER WITH .05" GAP

Frequency	Inductance Factor	Resistance Factor
1 kHz	.68	1.8
2 kHz	.61	1.9
4 kHz	.58	1.8

Note that the addition of the doubler causes a greater inductance reduction, but less resistance increase at the higher frequencies.

D. Theoretical Waveforms for Current and Capacitor Voltage Assuming an Ideal R-L-C Circuit

In spite of the fact that the coil parameters (especially resistance) are functions of frequency, the experimental waveforms for current and capacitor voltage resemble those for an ideal under-damped R-L-C circuit. It would be useful to summarize the properties of the ideal waveforms, sketched in Figure 2-2. These waveforms assume no clamping diode across the capacitor.

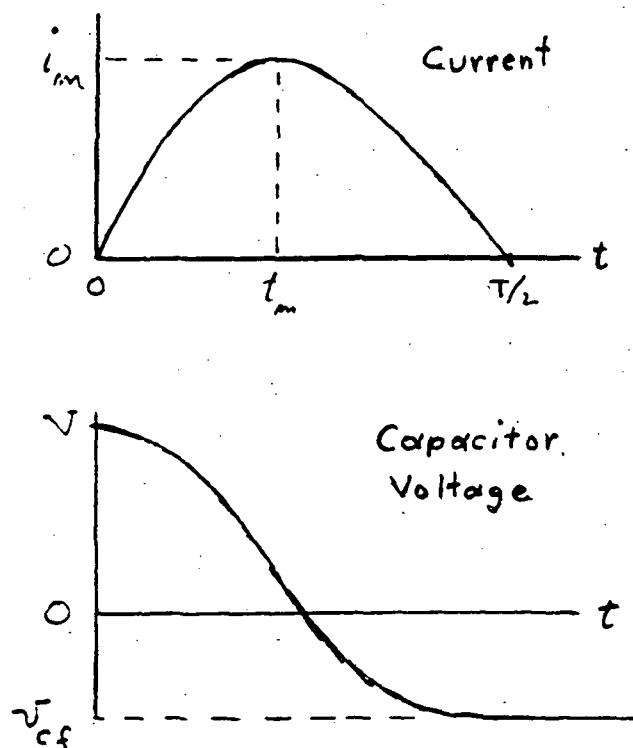


Fig. 2-2 Approximate Waveforms for Coil Current and Capacitor Voltage without a Diode Clamp

If we define a damping parameter by

$$m = \frac{1}{\sqrt{\frac{4L}{R^2C} - 1}} \quad (2-1)$$

then the period of damped oscillation is

$$T = 2\pi\sqrt{LC} \sqrt{m^2 + 1} \quad (2-2)$$

The time for the maximum current can be expressed in alternate forms

$$\begin{aligned} t_m &= \sqrt{LC} \sqrt{m^2 + 1} \tan^{-1}\left(\frac{1}{m}\right) \\ &= \frac{T}{2\pi} \tan^{-1}\left(\frac{1}{m}\right) \\ &= \frac{1}{2} RC \frac{m^2 + 1}{m} \tan^{-1}\left(\frac{1}{m}\right) \end{aligned} \quad (2-3)$$

If the initial stored energy is  $W$ , then the maximum current is

$$i_m = \sqrt{\frac{2W}{L}} e^{-m \tan^{-1}\left(\frac{1}{m}\right)} \quad (2-4)$$

Without the clamping diode, the capacitor will become reverse-charged with the final voltage

$$v_{cf} = -V e^{-\pi m} \quad (2-5)$$

where  $V$  is the initial capacitor voltage. Finally, the maximum stored inductor energy and the final re-stored capacitor energy are, respectively,

$$\frac{1}{2} L i_m^2 = W e^{-2m \tan^{-1}\left(\frac{1}{m}\right)} \quad (2-6)$$

and

$$\frac{1}{2} C v_{cf}^2 = W e^{-2\pi m} \quad (2-7)$$

A reliable technique for determining the effective circuit resistance and inductance from the current and voltage waveforms is the measure  $T/2$ ,  $i_m$ , and  $v_{cf}$  ( $C$  and  $V$  are assumed to be known). Then the following sequence of calculations can be made:

$$m = \frac{1}{\pi} \ln \left( -\frac{V}{v_{cf}} \right) \quad (2-8)$$

$$L_{\text{eff}} = \left( \frac{V}{i_m} \right)^2 C e^{-2m \tan^{-1} \left( \frac{1}{m} \right)} \quad (2-9)$$

$$R_{\text{eff}} = \frac{2\pi Lm}{T}$$

#### E. Circuit Parameters of the Energy System

Additional bridge measurements were made to determine the circuit parameters contributed by the Simmonds Energy system. The following Table lists the breakdown of parameter distributions for the discharge circuit assuming the 30-turn, 2 inch diameter impulse coil (without a target).

	Capacitance ( $\mu\text{F}$ )	Inductance ( $\mu\text{H}$ )	Resistance ( $\Omega$ )
30-Turn 2 Inch Dia. Coil		19.8	.0273 (at 1 kHz)
600 $\mu\text{F}$ Capacitor	600.0		.003 (at 1 kHz)
22 ft Cable		1.7	.043
Totals	600.0	21.5	.0733

Discharge waveform data for this same circuit were determined to be:

$$\begin{aligned}V &= 500 \text{ volts} \\V_{cf} &= -260 \text{ volts} \\i_m &= 2025 \text{ amps} \\T/2 &= 368 \mu\text{sec}\end{aligned}$$

Then, following the calculations outlined in Sec. D, one obtains,

$$\begin{aligned}m &= 0.2083 \\L_{\text{eff}} &= 20.7 \mu\text{h} \\R_{\text{eff}} &= 0.0736 \Omega\end{aligned}$$

These inductance and resistance values are in substantial agreement with the total values deduced from bridge measurements.

#### F. Example of Coil Design

An elementary coil design procedure will be described assuming prior determination (or estimation) of the following:

	<u>Sample Design Value</u>
(1) Initial capacitor energy required (estimate from de-icing test experience)	W = 250 Joules
(2) Natural period of the surface mode to be excited	1.2 msec
(3) Initial capacitor voltage	V = 1000 volts
(4) Cable resistance	.03 $\Omega$
(5) Cable inductance	negligible
(6) Capacitance, $C = \frac{2W}{V^2}$	500 $\mu\text{F}$
(7) Coil Thickness	0.188 Inch
(8) Coil inner diameter	0.25 Inch
(9) Coil outer diameter	2.5 Inches

Items (7) through (9) look like they ought to belong to the coil "design" activity. We do not, to date, have a sufficiently extensive design procedure to yield optimum dimensions.\* The coil thickness and inner diameter values for the sample design are those that were assumed for the calculation of Table 2-1. They also are the thickness and inner diameter values for nearly all the coils that were used in the de-icing tests. The selection of 2.5 inches for the outer coil diameter is somewhat arbitrary. Ballistic pendulum tests have indicated that larger diameter coils (other parameters remaining the same) result in increased delivered force impulse. Diameter optimization most probably will be based on weight-performance tradeoffs.

The remaining coil design steps, illustrated with the sample values, proceed as follows:

(a) Electric Circuit Period

In order to minimize peak skin stresses, the force impulse should be made as "soft" as possible, consistent with its ability to excite mechanical motion. The rule of thumb for yielding the desired pulse duration will be to make the (undamped) electrical period equal to half the natural period of the surface mode to be excited. See sample design:

$$T = \frac{1}{2} (1.2 \text{ ms}) = 0.6 \text{ ms}$$

(b) Coil Inductance

The required values of coil inductance is fixed by T and C, according to

$$\text{Sample Design: } L_{\text{eff}} = \frac{1}{500 \times 10^{-6}} \left[ \frac{1}{C} \left( \frac{T}{2\pi} \right)^2 \right]^2 = 18 \mu\text{H}$$

This is the effective inductance for the mounted coil. When unmounted, the inductance will be greater (see Tables 2-2 and 2-3). Taking the skin "proximity factor" to be 0.6, then the required coil inductance for the sample design is

$$L = \frac{18 \mu\text{H}}{0.6} = 30 \mu\text{H}$$

---

\*The computer modeling activities should yield more definite bases for selecting optimum dimensions.

(c) Number of Turns and Wire Thickness

These design values are read from Table 2-1. To achieve 30  $\mu\text{H}$  with a 2.5 inch diameter coil, then

$$N = 35 \text{ Turns}$$

$$b = .029 \text{ Inch (Ribbon Wire Thickness)}$$

(d) Effective Coil Resistance

The d.c. coil resistance for the sample design is also indicated in Table 2-1 as

$$R_{\text{d.c.}} = .0187 \ \Omega$$

The effective a.c. resistance is higher. Since the electrical frequency is

$$f = \frac{1}{T} = 1.67 \text{ kHz}$$

Figure 2-1 indicates an increase factor of about 1.25. Thus

$$R_{\text{a.c.}} = 1.25(.0187) = .023 \ \Omega$$

Finally, applying a correction factor to account for skin proximity (Tables 2-2 and 2-3)

$$R_{\text{a.c.}} \Big|_{\text{eff}} = 1.8(.023) = .0414 \ \Omega$$

(e) Doubler Design

A conservative criterion for the doubler design is to pick a doubler thickness that equals one-half the electrical skin depth at the circuit frequency. If this answer is comparable to the aluminum skin thickness, then a somewhat thinner doubler might be used.

Sample design: Suppose 1145 Al is used as doubler material. It has about 62 percent conductivity so the recommended thickness is

$$\begin{aligned} \Delta_{\text{Doub}} &= \frac{1}{2} \sqrt{\frac{2}{\omega \mu \sigma}} = \frac{1}{2} \sqrt{\frac{2}{2\pi(1667)(4\pi \times 10^{-7})(.62 \times 5.8 \times 10^7)}} \\ &= 1.028 \times 10^{-3} \text{ m} = .040 \text{ Inch} \end{aligned}$$

(f) Estimate of Peak Current

The peak current can be calculated from Eq. (2-4)

$$i_m = \sqrt{\frac{2W}{L}} e^{-m \tan^{-1}\left(\frac{1}{m}\right)}$$

where

$$m = \frac{1}{\sqrt{\frac{4L}{R^2C} - 1}}$$

For the sample design,

$$R_{\text{ckt}} = R_{\text{coil}} + R_{\text{cable}} = .0414 + .03 = .0714$$

$$L = 18 \mu\text{H}, \quad C = 500 \mu\text{F}$$

$$W = 250 \text{ J}$$

Thus

$$\frac{4L}{R^2C} = \frac{4(18)}{(.0714)^2(500)} = 28.25$$

So

$$m = \frac{1}{\sqrt{27.25}} = .1916$$

and the current modification due to losses is

$$e^{-m \tan^{-1}\left(\frac{1}{m}\right)} = .767$$

Finally

$$i_m = \sqrt{\frac{2(250)}{18 \times 10^{-6}}} (.767) = 4.04 \text{ KA}$$

(g) Design Iteration

Results from previous steps need to be inspected to see if they present any particular system design problems, and adjustments made accordingly. For example, one may be committed to use a thyristor for which 4.04 KA peak current is dangerously high. An increased inductance is then called for. If that results in too long a pulse, then C can be reduced and the operating voltage increased.

## II. Ballistic Pendulum Studies

A ballistic pendulum was constructed and utilized to study the effects of parameter variations on impulse production. A schematic drawing of the apparatus is shown in Fig. 2-3. The maximum pendulum swing ( $\theta_{\max}$ ) was measured by an electrical output from the precision potentiometer, and the delivered impulse was determined from the formula:

$$\text{Impulse} = \frac{4\pi J}{1T} \sin \frac{\theta_{\max}}{2} \text{ lb-sec} \quad (2-10)$$

where

J = Moment of inertia of the  
pendulum = .387 lb-ft-sec<sup>2</sup> (calculated)  
l = Pendulum length, pivot to target  
center = 3.727 ft.  
T = Free oscillation period = 2.09 sec  
(measured)

Numerically,

$$4\pi J/(1T) = 0.624 \text{ lb-sec.}$$

This section describes the various test conditions and the test results. In most cases a "dummy coil" was included in series with the "active coil" to simulate double coil operation. When dummy coils were used, they were always identical to the active coils and were fitted with identical targets (except where noted otherwise).

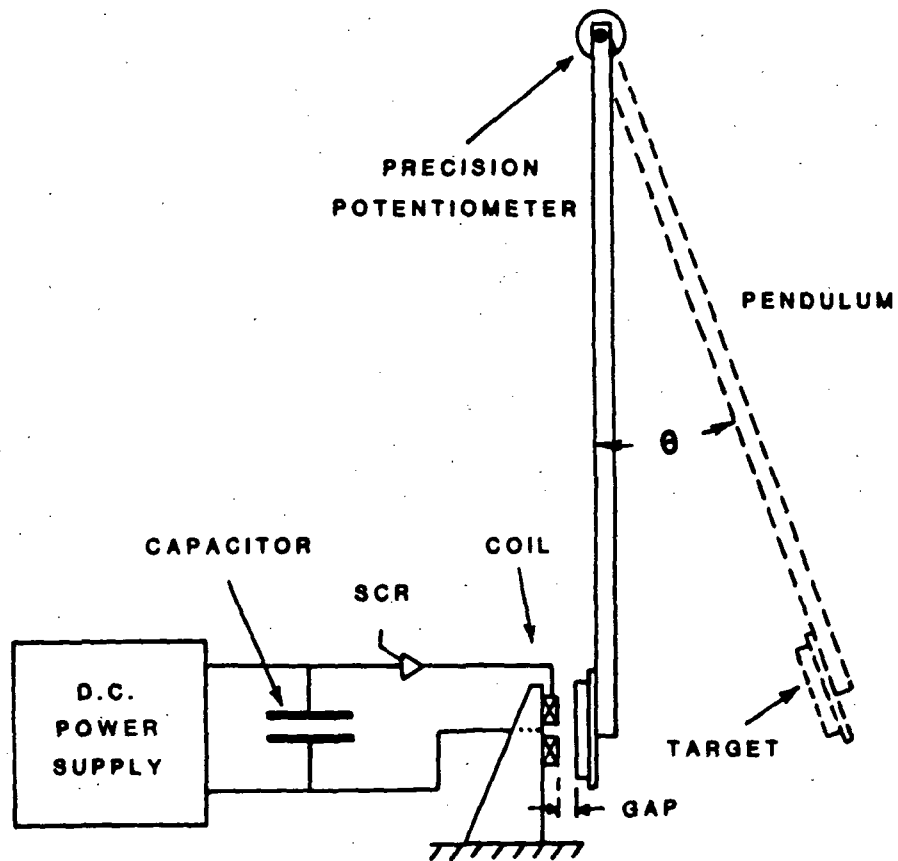


Fig. 2-3 Ballistic Pendulum Apparatus

A. Varying Voltage

TEST 1

ELECTRICAL	ACTIVE COIL	DUMMY COIL	TARGET
Volts <u>Var.</u>	Turns <u>30</u>	Used <u>yes</u>	Mat. <u>Al 2024-T3</u>
$\mu$ F <u>600</u>	Dia. <u>2.0"</u>	With Target	Thickness <u>.032"</u>
Joules <u>Var.</u>	Thickness <u>.188"</u>	<u>no</u>	Gap <u>.050"</u>

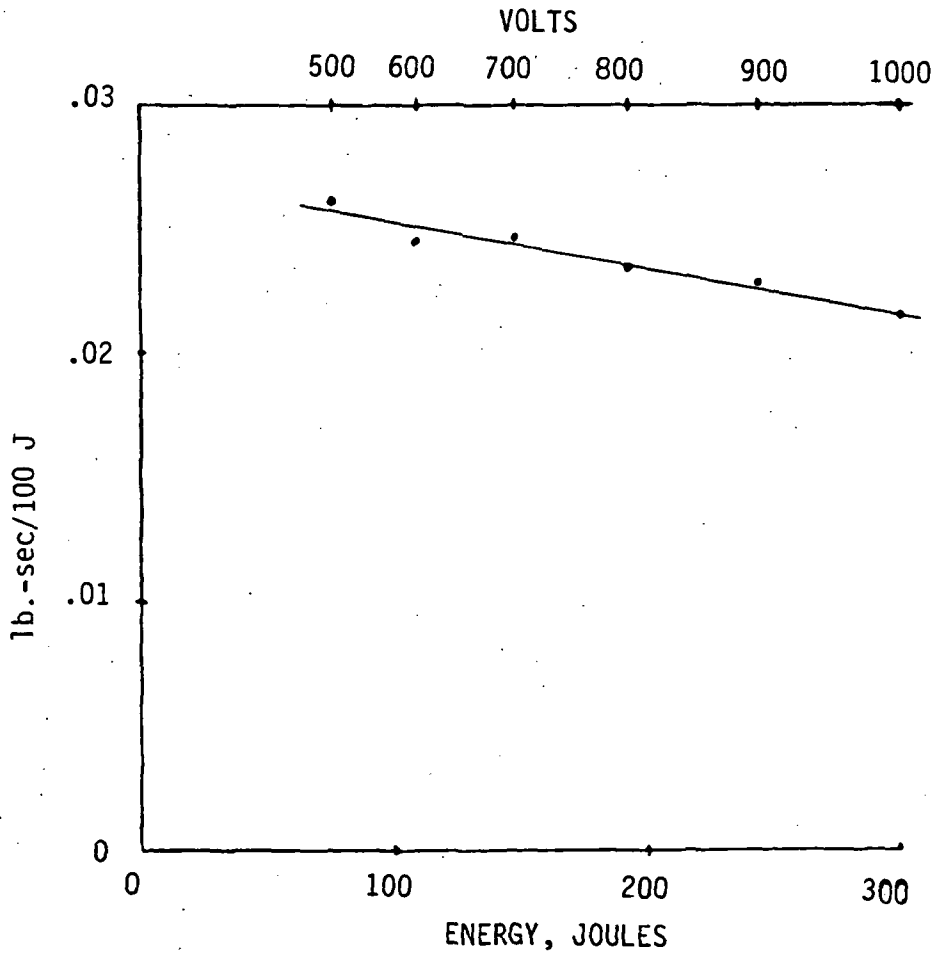


Fig. 2-4 Impulse Per Unit Energy  
with Voltage Varied

TEST 2

ELECTRICAL	ACTIVE COIL	DUMMY COIL	TARGET
Volts <u>Var.</u>	Turns <u>30</u>	Used <u>yes</u>	Mat. <u>Al 1100</u>
$\mu$ F <u>400</u>	Dia. <u>2.0"</u>	With Target	Thickness <u>.050"</u>
Joules <u>Var.</u>	Thickness <u>.195</u>	<u>yes</u>	Gap <u>.050"</u>

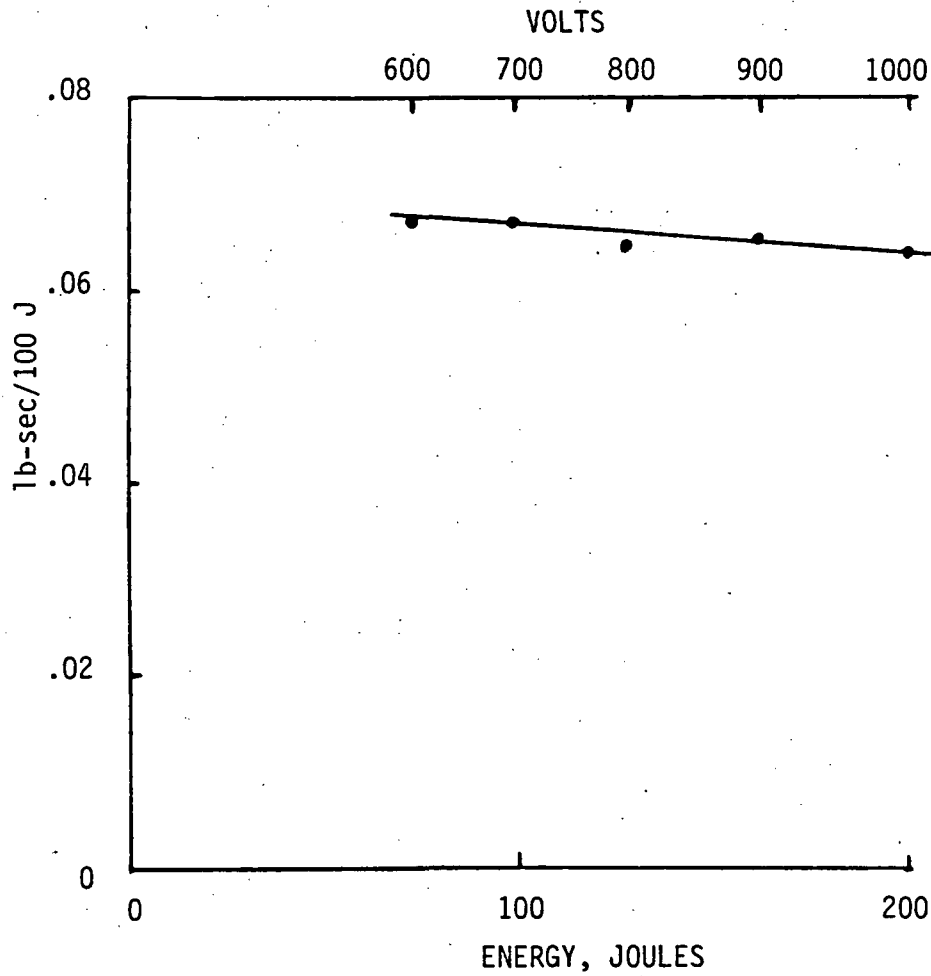


Fig. 2-5 Impulse Per Unit Energy  
with Voltage Varied

### Coil Current Data For Test 2

Volts	$i_m$ (KA)	KA/KV	$t_m$ ( $\mu$ s)
600	1.40	2.33	163
800	1.85	2.31	163
1000	2.31	2.31	163

Comments: This test was intended to verify that the impulse is proportional to the square of the capacitor voltage. The experimental data show some small deviation from a proportionality, both for a thin poor-conductivity target and a thicker good-conductivity target. This deviation is relatively inconsequential. Impulse values can still be extrapolated with fair accuracy from one voltage to another by assuming proportionality to  $V^2$ .

#### B. Varying Capacitance, Fixed Energy

##### TEST 3

ELECTRICAL	ACTIVE COIL	DUMMY COIL	TARGET
Volts <u>Var.</u>	Turns <u>30</u>	Used <u>yes</u>	Mat. <u>A1 2024-T3</u>
$\mu$ F <u>Var.</u>	Dia. <u>2.0"</u>	With Target	Thickness <u>.032"</u>
Joules <u>150</u>	Thickness <u>.188"</u>	<u>no</u>	Gap <u>.050"</u>

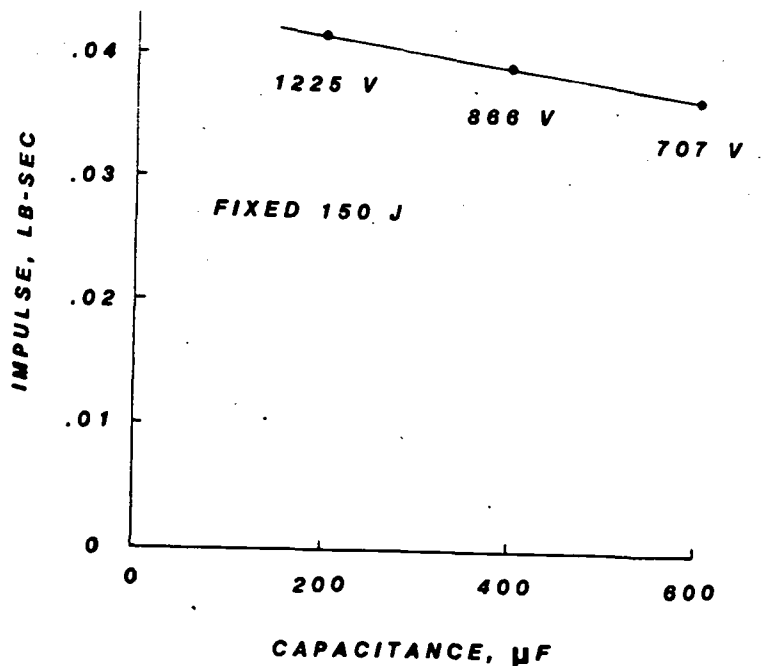


Fig. 2-6 Impulse vs Capacitance with Fixed Energy

TEST 4

ELECTRICAL	ACTIVE COIL	DUMMY COIL	TARGET
Volts <u>Var.</u>	Turns <u>40</u>	Used <u>yes</u>	Mat. <u>Al 1100</u>
$\mu$ F <u>Var.</u>	Dia. <u>2.28"</u>	With Target	Thickness <u>.050"</u>
Joules <u>120</u>	Thickness <u>.195"</u>	<u>yes</u>	Gap <u>.050"</u>

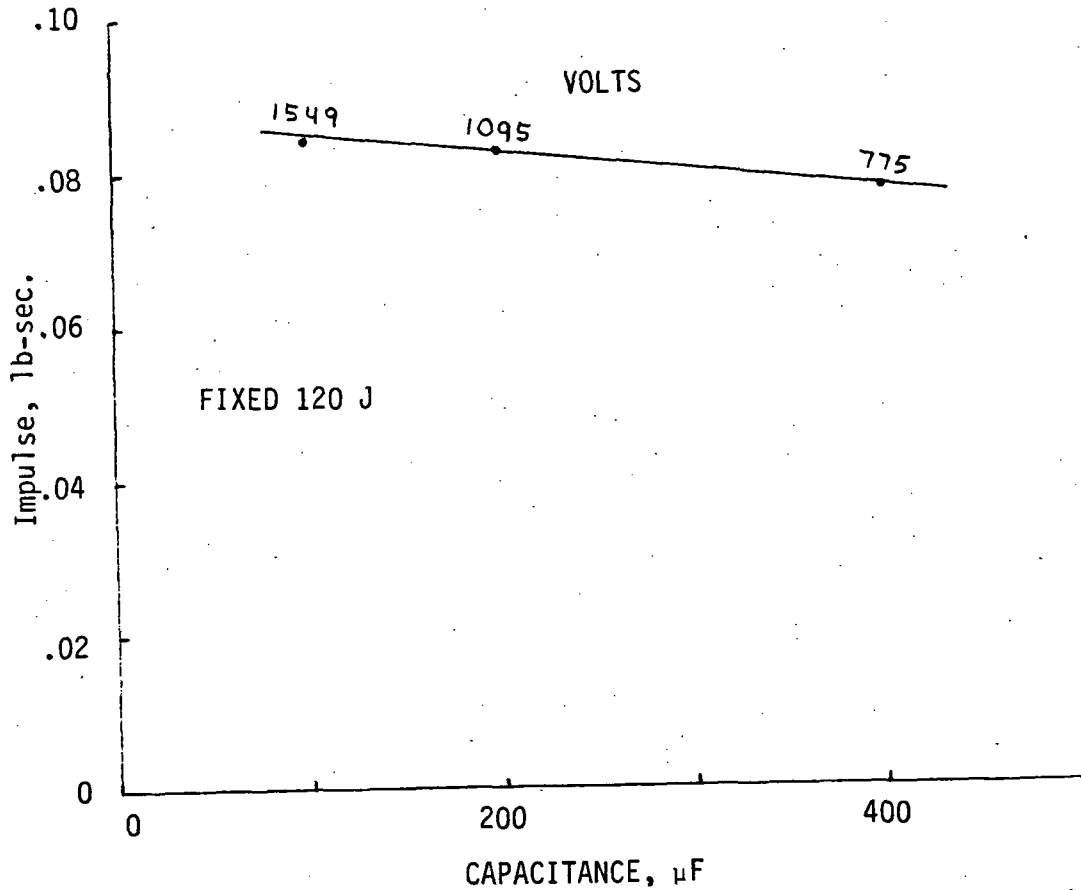


Fig. 2-7 Impulse vs Capacitance with Fixed Energy

Coil Current Data For Test 4

$\mu\text{F}$	Volts	$i_m$ (KA)	$t_m$ ( $\mu\text{s}$ )
100	1549	2.18	80
200	1095	2.00	115
400	775	1.79	163

Comments: This test explored the relative effectiveness of different capacitance - voltage combinations with fixed energy. Both tests (3 and 4) showed small advantages of high voltage - low capacitance combinations.

C. Varying Coil-to-Target Gap

TEST 5

ELECTRICAL	ACTIVE COIL	DUMMY COIL	TARGET
Volts <u>800</u>	Turns <u>30</u>	Used <u>yes</u>	Mat. <u>Al 2024-T3</u>
$\mu\text{F}$ <u>600</u>	Dia. <u>2.0"</u>	With Target	Thickness <u>.032"</u>
Joules <u>192</u>	Thickness <u>.188"</u>	<u>no</u>	Gap <u>Var.</u>

See Figure 2-8 on following page.

TEST 5

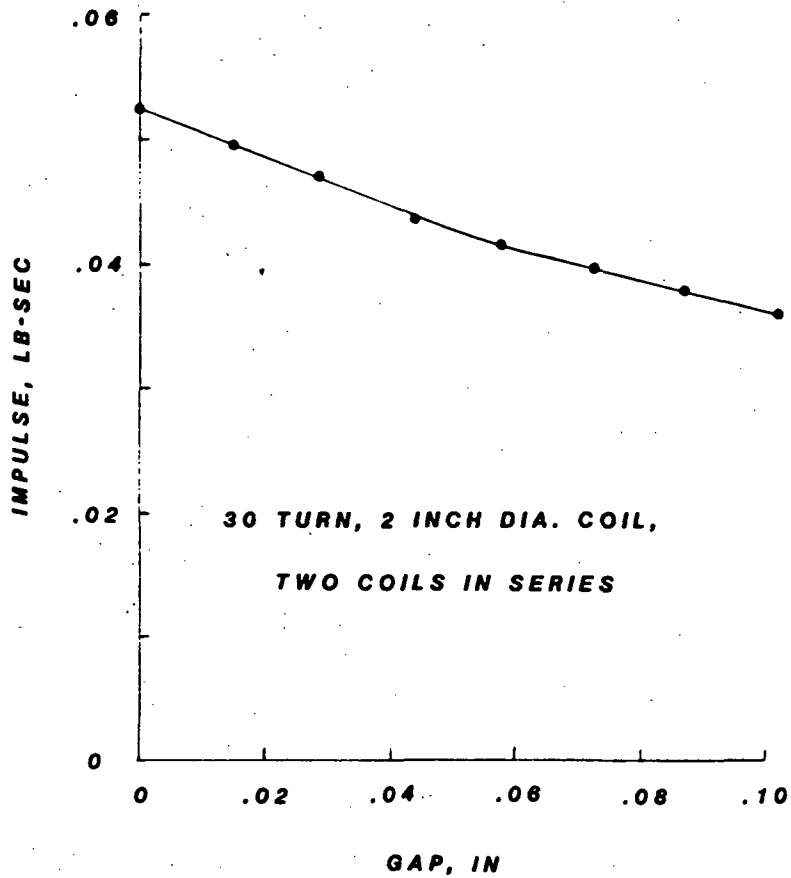


Fig. 2-8 Impulse vs Coil-to Target Gap

Comments: As expected, the delivered impulse decreased with increased coil-to-target gap. This reduction was about 20 percent for the gap increase from zero to 0.05 inch.

D. Varying Target Material and Thickness

TEST 6

ELECTRICAL	ACTIVE COIL	DUMMY COIL	TARGET
Volts <u>800</u>	Turns <u>30</u>	Used <u>yes</u>	Mat. <u>Var.</u>
$\mu$ F <u>600</u>	Dia. <u>2.0"</u>	With Target	Thickness <u>Var.</u>
Joules <u>192</u>	Thickness <u>.188"</u>	<u>no</u>	Gap <u>.050"</u>

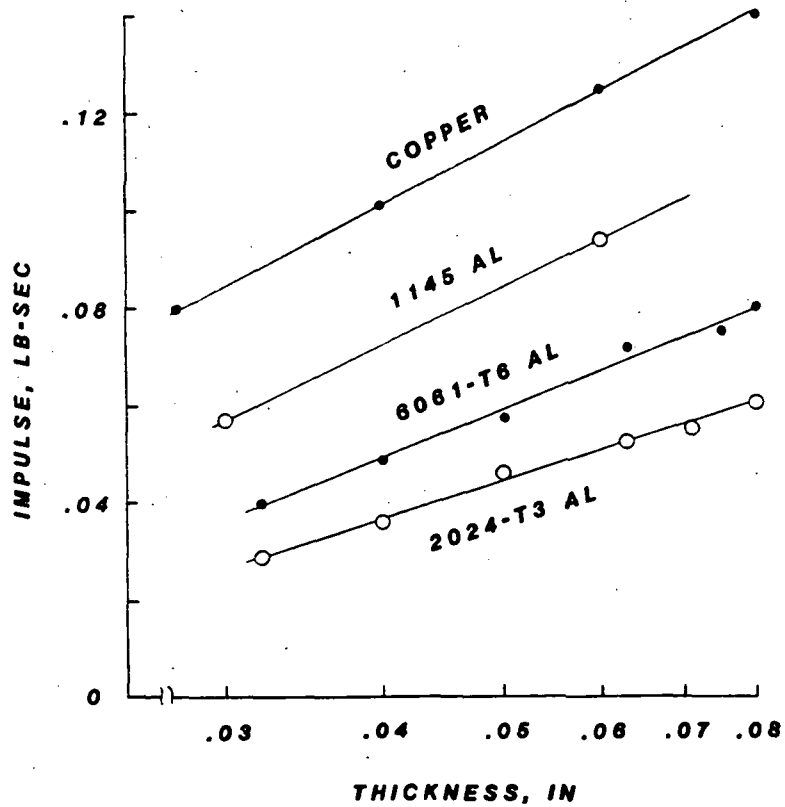


Fig. 2-9. Impulse vs Target Material and Thickness

Comments: These data show large gains in impulse performance when high electrical conductivity targets are used. The published conductivities in percent of annealed copper for the three aluminum types are:

1145 - 62%  
 6061-T6 - 43%  
 2024-T3 - 30%

Increasing the target thickness also increases the impulse, but with diminishing returns. A rule of thumb criterion is that the desired thickness from the standpoint of impulse production is about one electrical skin depth calculated from the formula

$$\delta = \frac{1}{\sqrt{\pi f \mu_0 \sigma}}$$

where  $\sigma$  is the electrical conductivity of the target in mhos per meter,  $\mu_0 = 4\pi \times 10^{-7}$ , and  $f$  is the resonant frequency ( $\text{sec}^{-1}$ ) of the electrical circuit.

E. Varying Coil Diameter and Turns

TEST 7

ELECTRICAL	ACTIVE COIL	DUMMY COIL	TARGET
Volts <u>600</u>	Turns <u>Var.</u>	Used <u>no</u>	Mat. <u>Cu</u>
$\mu$ F <u>600</u>	Dia. <u>Var.</u>	With Target	Thickness <u>.021"</u>
Joules <u>108</u>	Thickness <u>.188"</u>	<u>n/a</u>	Gap <u>.050"</u>

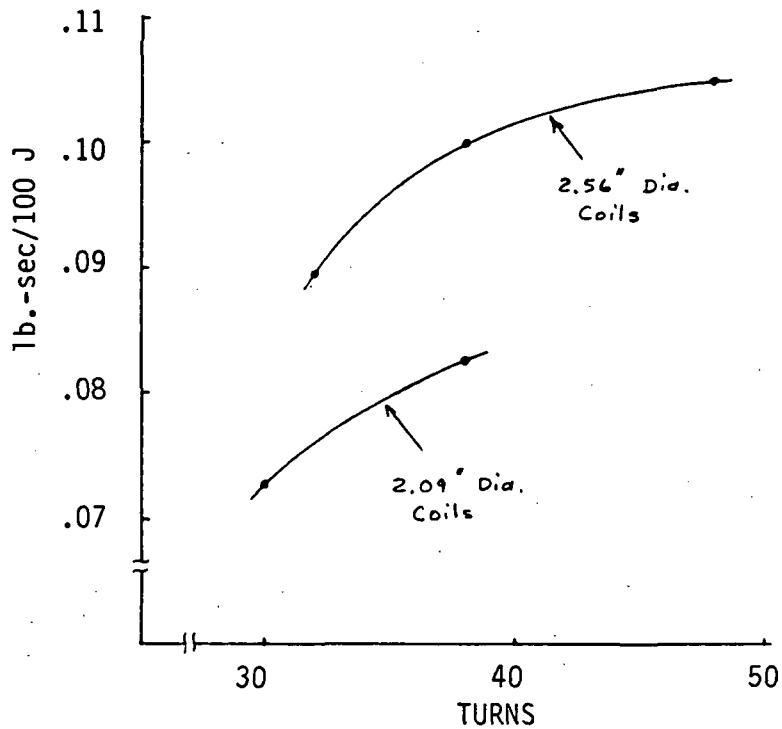


Fig. 2-10 Impulse Per Unit Energy with Two Coil Diameters and Variable Turns

Coil Current Data  
For Test 7

Coil Dia. (In)	Turns	$i_m$ (KA)	$t_m$ ( $\mu$ s)
2.09	30	3.58	117
2.09	38	2.83	137
2.56	32	3.18	137
2.56	38	2.78	146
2.56	48	2.14	174

Comments: This test measured the relative effectiveness of five coil designs for which the number of turns and the outer diameters were varied. A greater number of turns for a given coil diameter was achieved by rolling the ribbon wire thinner.

No dummy coils were used in the impulse tests. Voltage and capacitance were held fixed, so the energy was also fixed. In general, the data showed that given diameter coils produced more impulse as turns were increased, and that coils with a given number of turns produced more impulse as the diameter was increased.

#### TEST 8

ELECTRICAL	ACTIVE COIL	DUMMY COIL	TARGET
Volts <u>Var.</u>	Turns <u>40</u>	Used <u>yes</u>	Mat. <u>Al 1100</u>
$\mu$ F <u>400</u>	Dia. <u>2.28"</u>	With Target	Thickness <u>.050"</u>
Joules <u>Var.</u>	Thickness <u>Var.</u>	<u>yes</u>	Gap <u>.050"</u>

#### Current Data at V = 800 Volts

Coil Thickness (In)	$i_m$ (KA)	$t_m$ ( $\mu$ s)
.195	1.85	163
.150	1.79	158
.100	1.66	146

Comments: For this test, six identical 40-turn coils were constructed. Each had a thickness of 0.195" (the ribbon wire width after the rolling operation). Then one pair was milled to a reduced thickness of 0.150", and another pair to 0.100". Finally, the various pairs (one active, the other dummy) were installed into the ballistic pendulum apparatus for tests.

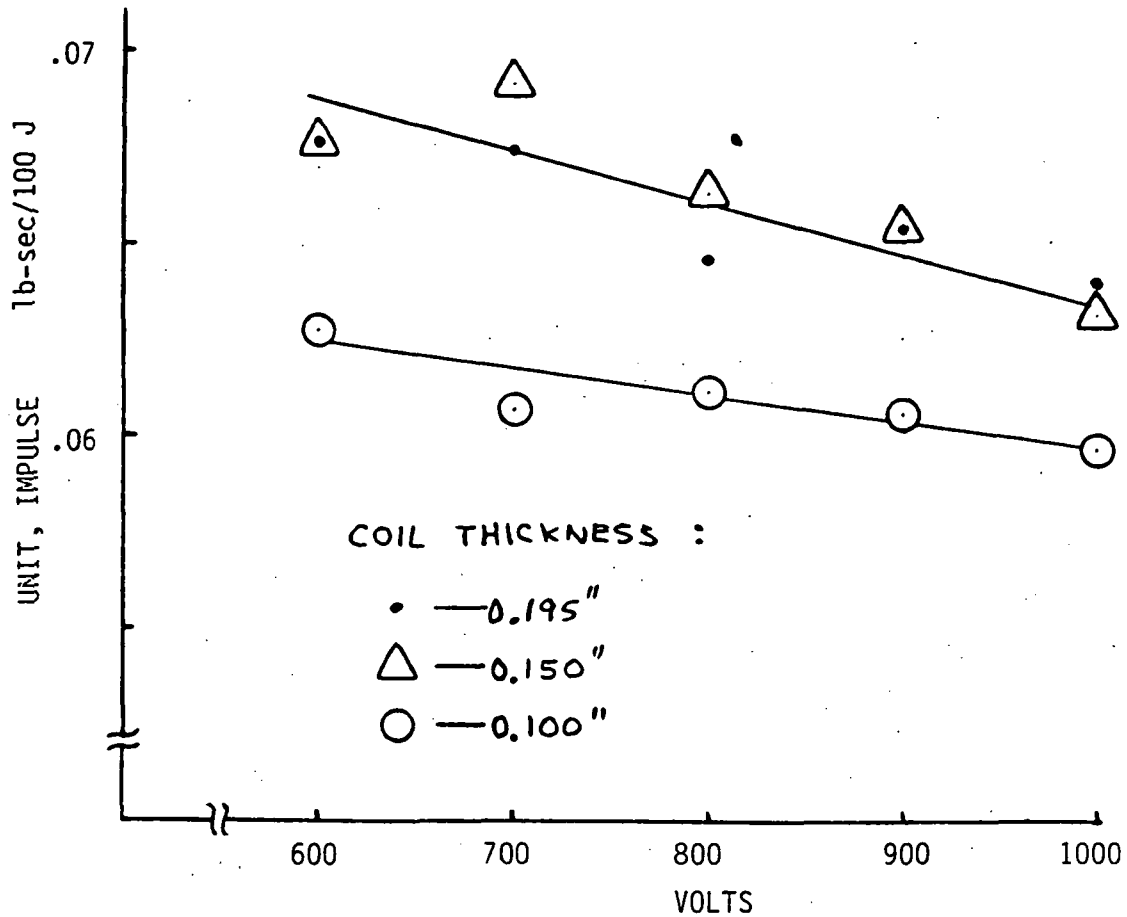


Fig. 2-11 Impulse Per Unit Energy with Three Coil Thicknesses

The results show no detectable degradation in performance for the 0.150" thick coil, but an approximately 7 percent impulse reduction for the 0.100" thick coil (relative to the 0.195" thick coil). The performance loss for the thinnest coil was, presumably, due to its excessive resistance. Data on resistance values were as follows:

	d.c. ohms
0.195" thick coils	.035 each
0.150" thick coils	.045 each
0.100" thick coils	.068 each
Supply cable	.043

G. Series vs Parallel Coils

TEST 9

ELECTRICAL	ACTIVE COIL	DUMMY COIL	TARGET
Volts <u>Var.</u>	Turns <u>40</u>	Used <u>yes</u>	Mat. <u>Al 1100</u>
$\mu$ F <u>Var.</u>	Dia. <u>2.28"</u>	With Target	Thickness <u>.050"</u>
Joules <u>60/Coil</u>	Thickness <u>.195"</u>	<u>yes</u>	Gap <u>.050"</u>

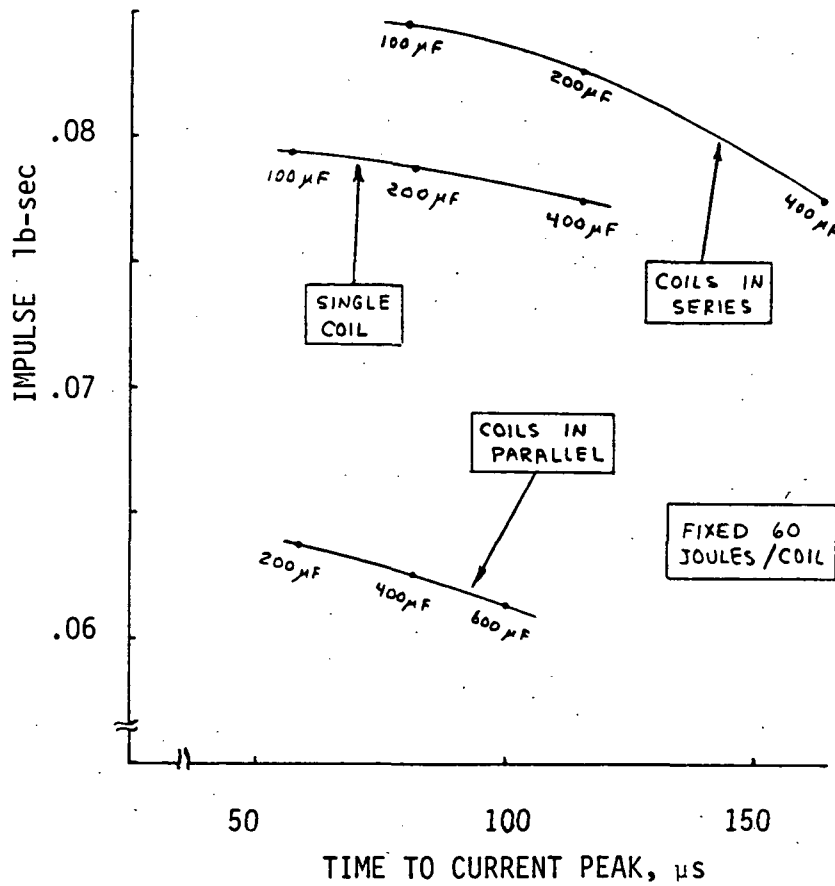


Fig. 2-12 Impulse vs Time to Current Peak, with Series and Parallel Coil Operation Compared

(TEST 9 - continued)

Peak Currents For  $t_m = 80\mu s$

	KA
Series Coils (C = 100 $\mu F$ )	1.55
Single Coil (C = 200 $\mu F$ )	1.49
Parallel Coils (C = 400 $\mu F$ )	1.34/coil

Comments: This test utilized the two 0.195" thick coils from Test 8. The object of the experiment was to compare impulse production with coils (active and dummy) placed in series, to that with the coils in parallel, to that for single operation. Various capacitance values were used, with voltage adjusted for fixed 60 Joules/coil.

Relative to single coil operation, the series combination showed improved performance while the parallel combination showed substantially worse performance. If the coil currents were identical (same peak values and same time to peak) then the impulse values should be the same. The Table above, which lists peak currents with fixed risetimes, shows the greatest current for coils in series and least current for coils in parallel. Furthermore the impulse ratios agree approximately with the ratios of the peak currents squared.

It appears that the explanation for the relative impulse performance lies in the varying degrees of circuit damping. Without resistance in the supply cable, then the damping factors should be the same in all cases. However the (constant) supply cable resistance causes the damping to be greatest with parallel coil operation.

H. Effect of the Diode Clamp

Some impulse measurements were made with and without the (reverse-charge prevention) diode in place. The conditions and results were as follows:

TEST 10

ELECTRICAL	ACTIVE COIL	DUMMY	TARGET
Volts <u>Var.</u>	Turns <u>30</u>	Used <u>no</u>	Mat. <u>Cu</u>
$\mu F$ <u>Var.</u>	Dia. <u>2.0"</u>	With Target	Thickness <u>.021"</u>
Joules <u>Var.</u>	Thickness <u>.188"</u>	_____	Gap <u>.050"</u>

RESULTS

(TEST 10 - continued)

C( $\mu$ F)	V (Volts)	<u>Impulse with Diode</u> <u>Impulse w/o Diode</u>
600	500	.92
400	600	.92
200	800	1.00

Comment: The diode introduces a slight performance degradation, but it is a small penalty to pay for increased capacitor life.

### III. Magnetic Field Diagnostics

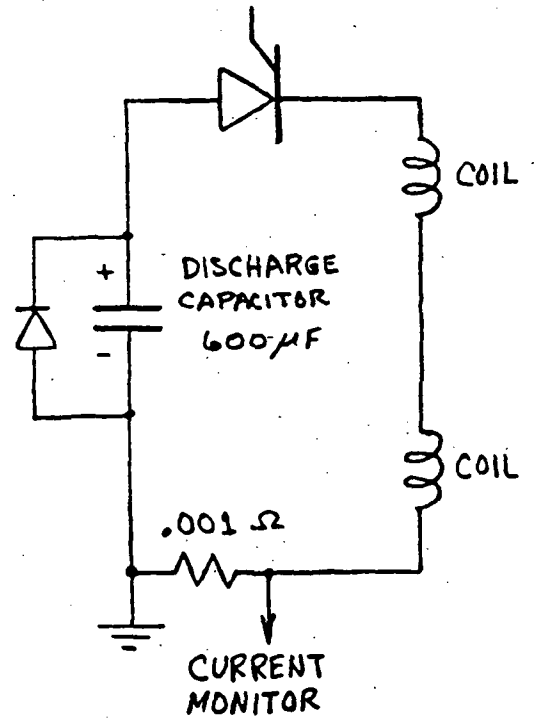
#### Experiment

This section describes a magnetic field measurement method for studying the distribution of eddy currents within, and pressure distribution on, a flat metallic plate subjected to an axially symmetric transient magnetic field produced by an pulsed circular coil. The pulsing system, coil and target ( including coil-to-target gap) closely simulated conditions that existed during electro-impulse-de-icing tests conducted by Wichita State University. For this experiment, the target was rigidly supported, and reduced voltage was used (energy about 15% of that required for de-icing).

#### A. Experimental Apparatus

Figure 2-13 shows the energy discharge system, omitting the capacitor charging circuit and the thyristor firing circuit. Two identical pulsing coils were operated in series, because that was the arrangement used in most of the de-icing tests. However, only one of the two coils were located in the coil-target assembly which is detailed in Fig. 2-14. The effective gap between the coil (copper) surface and the near surface of the target was .078 inch.

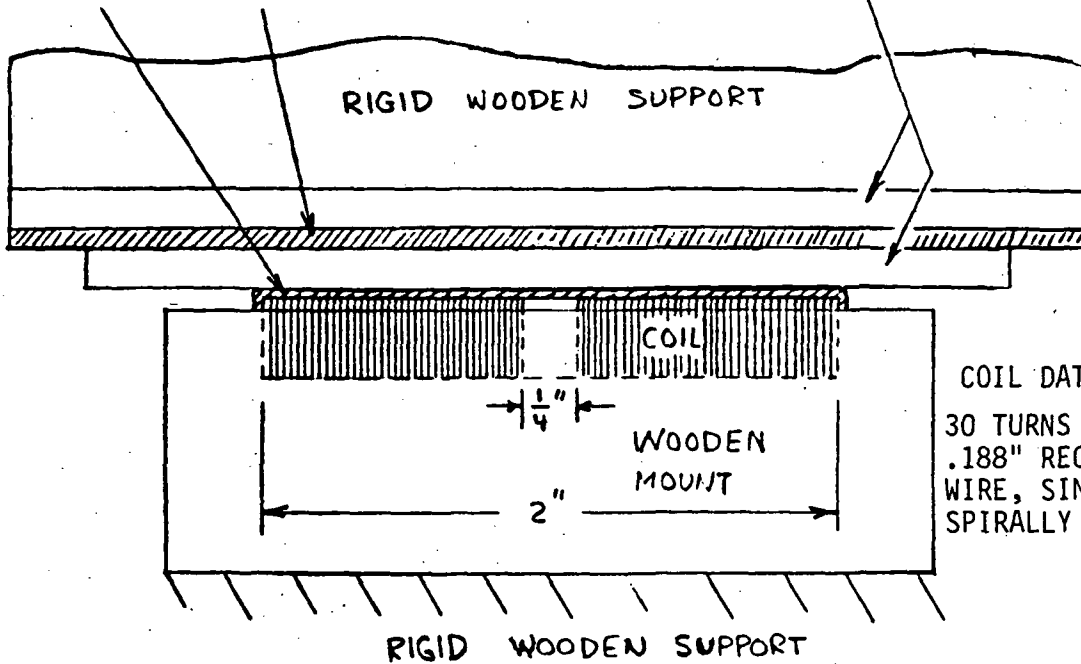
Fig. 2-13 Energy Discharge Circuit



.028" THICK  
POTTING  
LAYER,  
POLYESTER  
RESIN

.032" Al TARGET  
5" DIA. DISC  
2024 T3

.050" PHENOLIC  
SPACER  
PLATES



COIL DATA:  
30 TURNS OF .024" x  
.188" RECTANGULAR COPPER  
WIRE, SINGLE LAYER  
SPIRALLY WOUND

2-14 Details of the Coil-Target Assembly

Each coil consisted of 30 turns of .024" x .188" rectangular copper wire spirally wound in a single layer from an inner radius of .125" to an outer radius of 1.00".

The initial capacitor voltage utilized for this experimental study was 400 volts, and the resulting discharge current waveforms are shown in Fig. 2-15. One trace is with the aluminum target removed, the other is with the target in place.

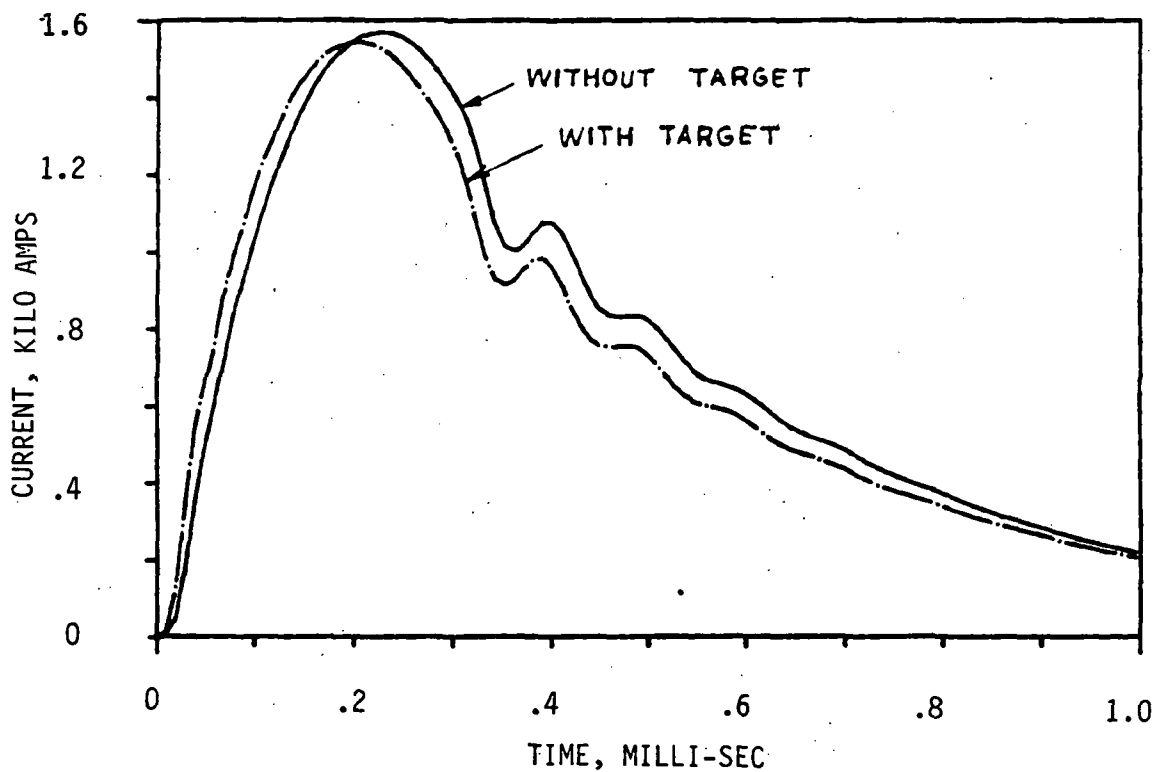


Fig. 2-15 Discharge Current With and Without the Aluminum Target Present

## B. Magnetic Field Measurements

A field measuring plate was constructed in a manner illustrated in Fig. 2-16. Shallow concentric grooves were cut into both sides of a .050" thick phenolic disc with radius increments of 0.2", starting at  $r = 0.2$ " and ending at  $r = 2.0$ ". Single-turn loops of .006" diameter wire were then cemented into these grooves, and their twisted leads brought out to solder tabs through radial channels. Figure 2-17 is a photograph of the finished plate.

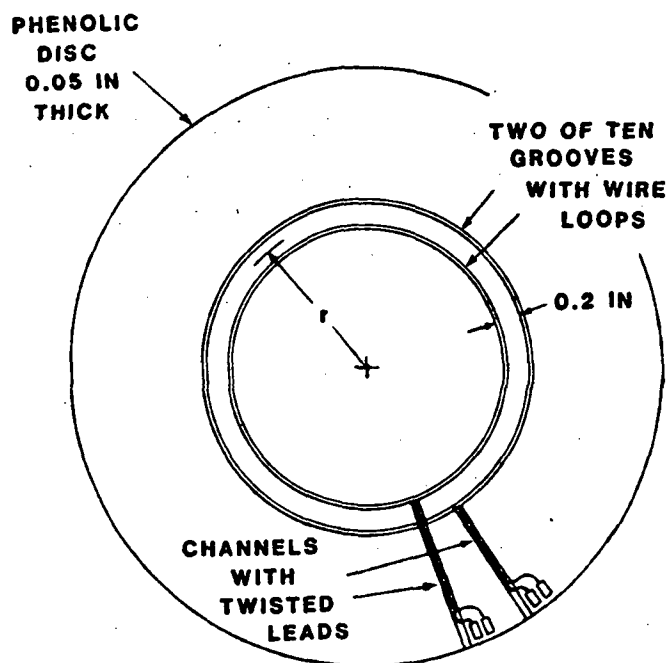


Fig. 2-16 Partial Illustration of the Field Measuring Plate

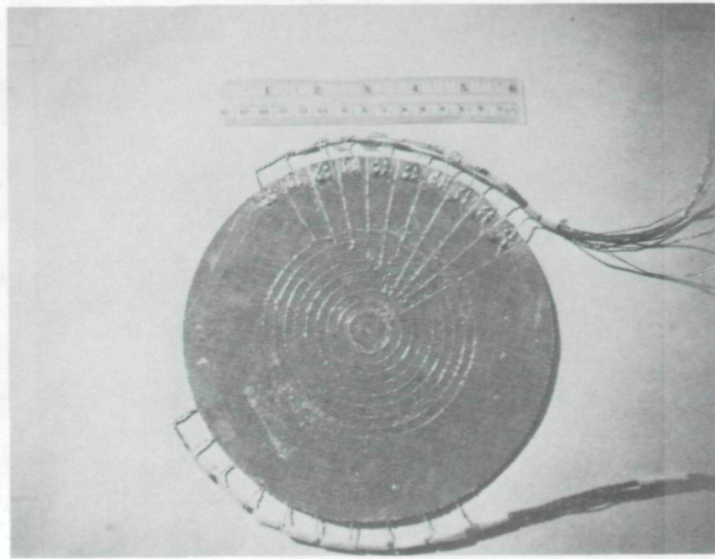


Fig. 2-17 Photograph of the Field  
Measuring Plate

For measuring the fields on either side of the target, the measuring plate simply substituted for the corresponding spacer plate in Fig. 2-14. A measurement of the flux density component perpendicular to the plate was derived from the induced voltage in any two neighboring loops connected in series opposition. For the two loops illustrated in Fig. 2-16, for example,

$$B_{\perp}(t) = 1550 \frac{\int_0^t v \, dt}{\pi(r_2^2 - r_1^2)} \text{ Teslas} \quad (2-11)$$

where  $r$  is in inches and  $v$  in volts. This value is the average perpendicular flux density over the area between the two induction loops. In deriving further results, we will assume the answer to apply at a radius midway between the two loops.

To measure the tangential (radial) component of flux density at any radius, the front and back loops at that radius are connected in series opposition, and calculations are made from

$$B_r(t) = 1550 \frac{\int_0^t v dt}{2\pi rh} \text{Teslas}$$

where r is the radius of the two induction loops and h is their separation, both in inches.

The specific tests are identified in the following Test Table, and the data appear on Figs. 2-18 through 2-24.

TEST TABLE

Test	Configuration	Measurements Made	Data
1	Target removed, Field Measurement Plate against coil surface	$B_{\perp}$ on both sides of Meas. Plate	Peak $B_{\perp}$ vs r (2-18) plotted in Fig.
		$B_r$	Peak $B_r$ vs r (2-19) plotted in Fig.
2	Target removed, .041" spacer between coil and Meas. Plate	$B_r$	$B_r$ vs time in Fig. (2-20)
3	Target in place, Meas. Plate between coil and target	$B_{\perp}$ adjacent to target	$B_{\perp}$ vs time in Fig. (2-21)
		$B_r$	$B_r$ vs time in Fig. (2-22)
4	Target in place, Meas. Plate beyond target	$B_{\perp}$ adjacent to target	$B_{\perp}$ vs time in Fig. (2-23)
		$B_r$	$B_r$ vs time in Fig. (2-24)

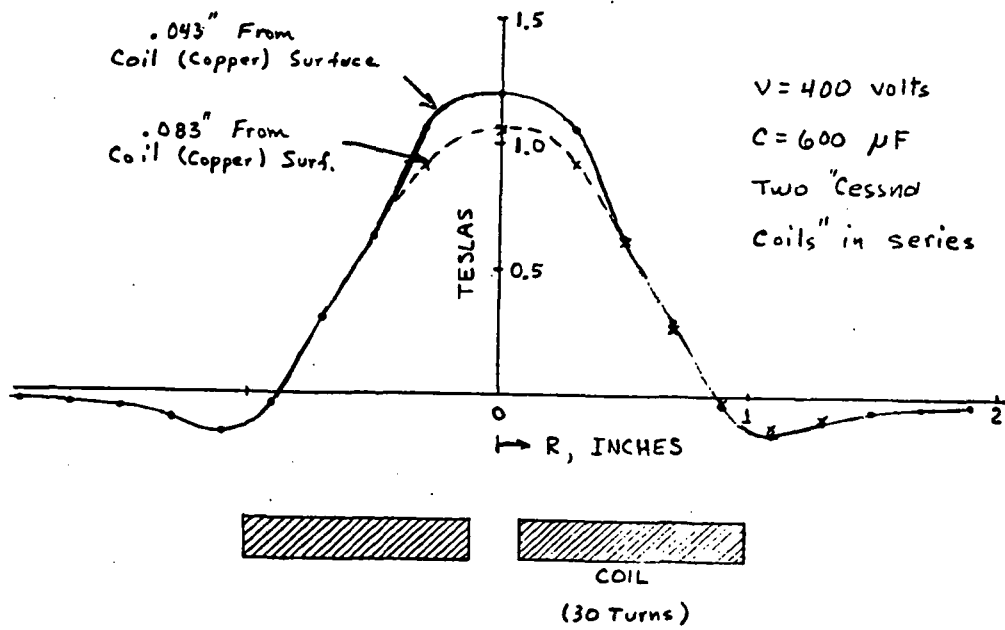


Fig. 2-18 Maximum  $B_{\perp}$  vs Radius, no Target Present

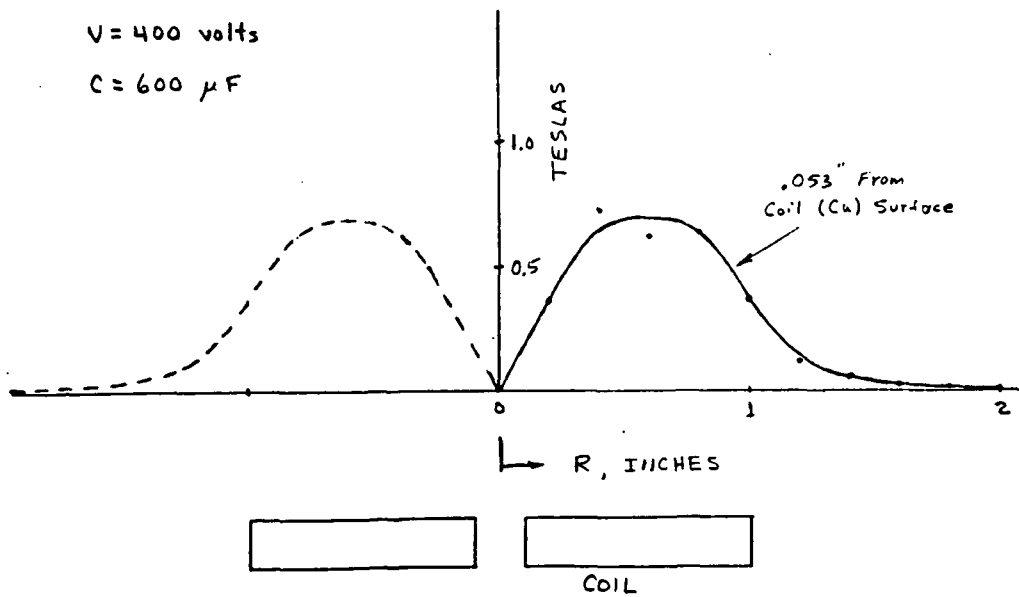


Fig. 2-19 Maximum  $B_{\parallel}$  vs Radius, no Target Present

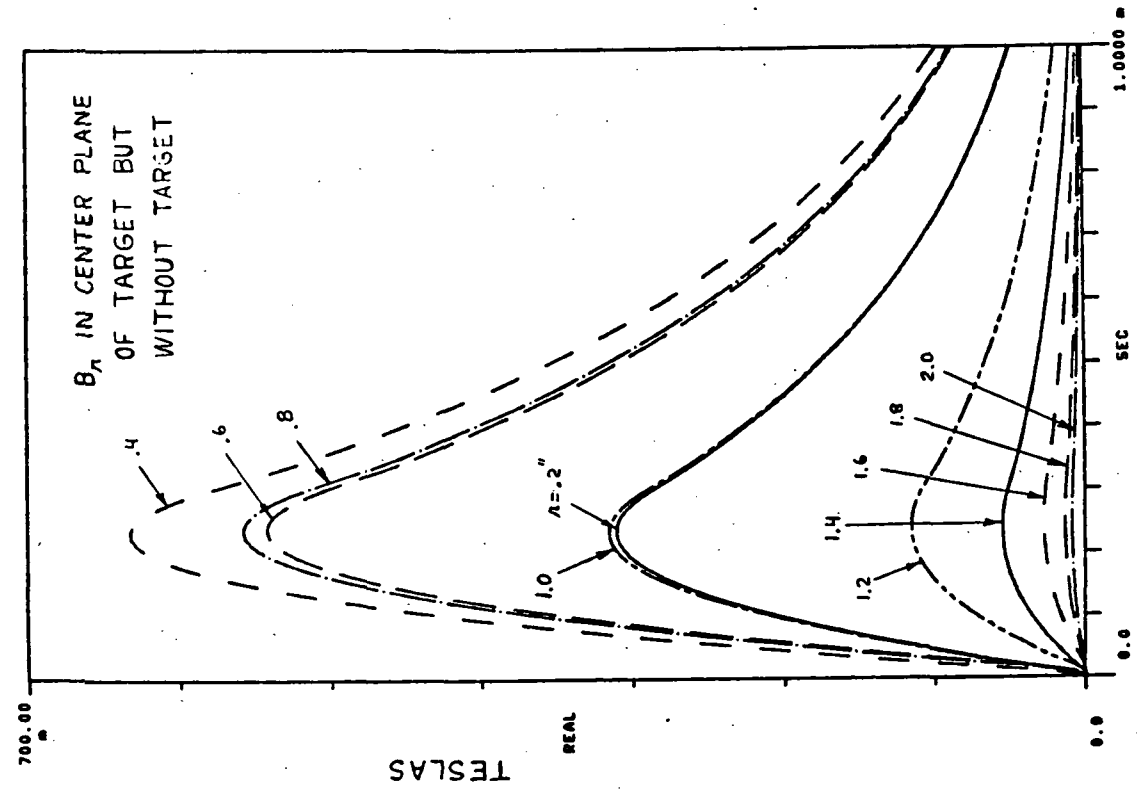


Fig. 2-20  $B_r$  in the Center Plane of the Target but with the Target Removed

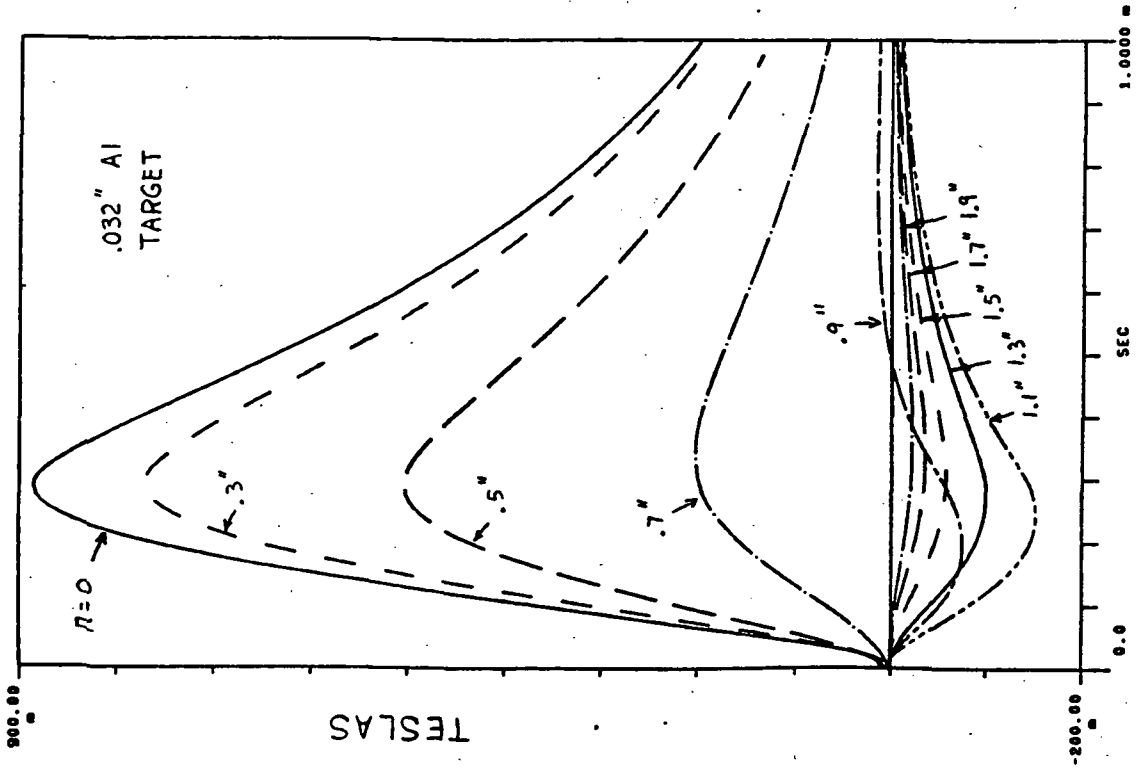


Fig. 2-21  $B_l$  on the Near Side

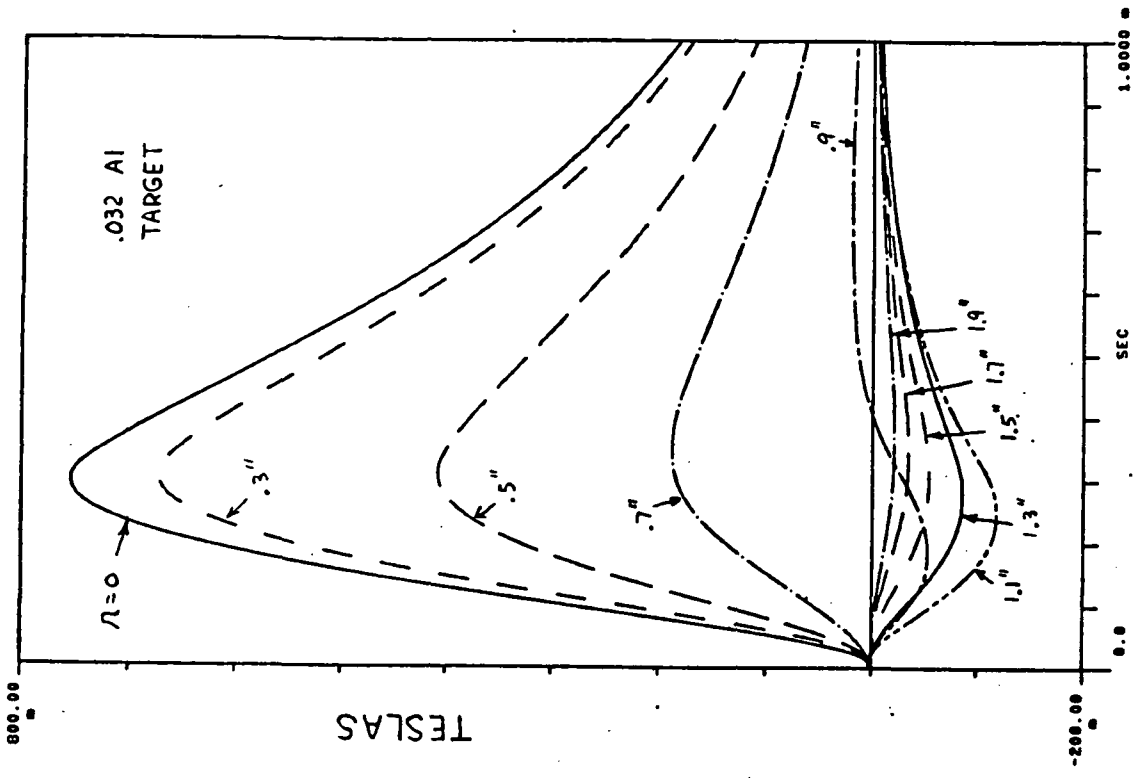


Fig. 2-23  $B_I$  on the Far Side

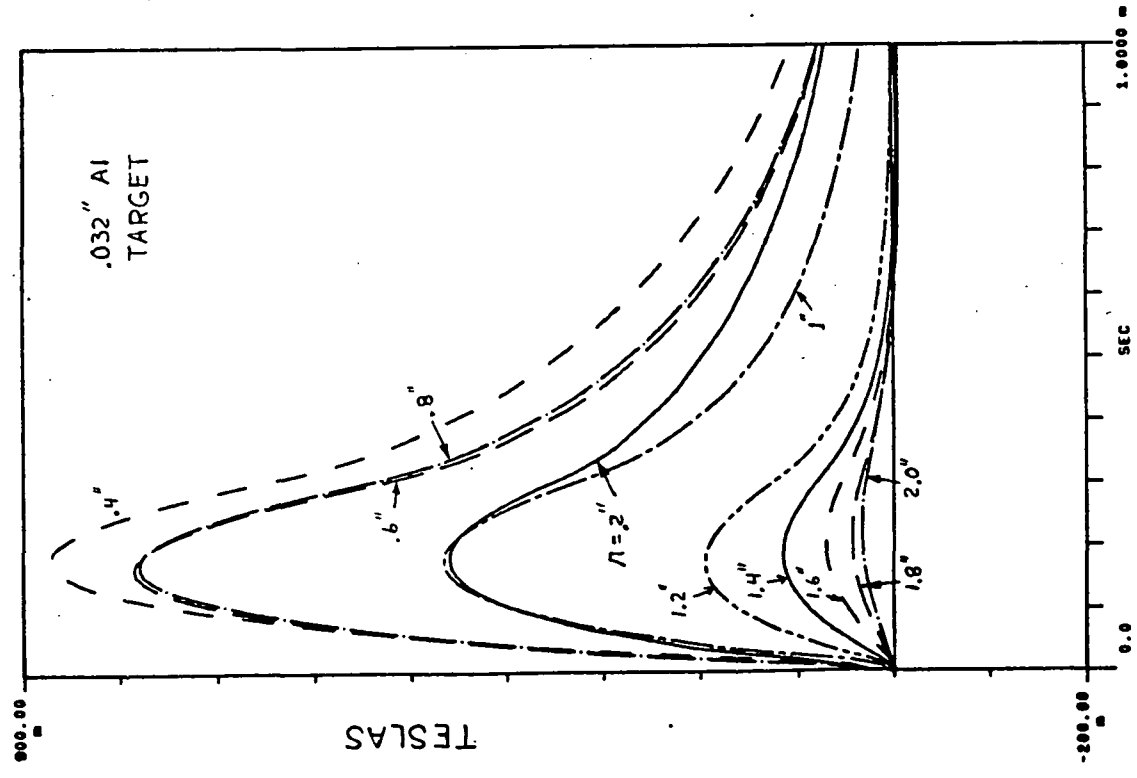


Fig. 2-22  $B_r$  on the Near Side

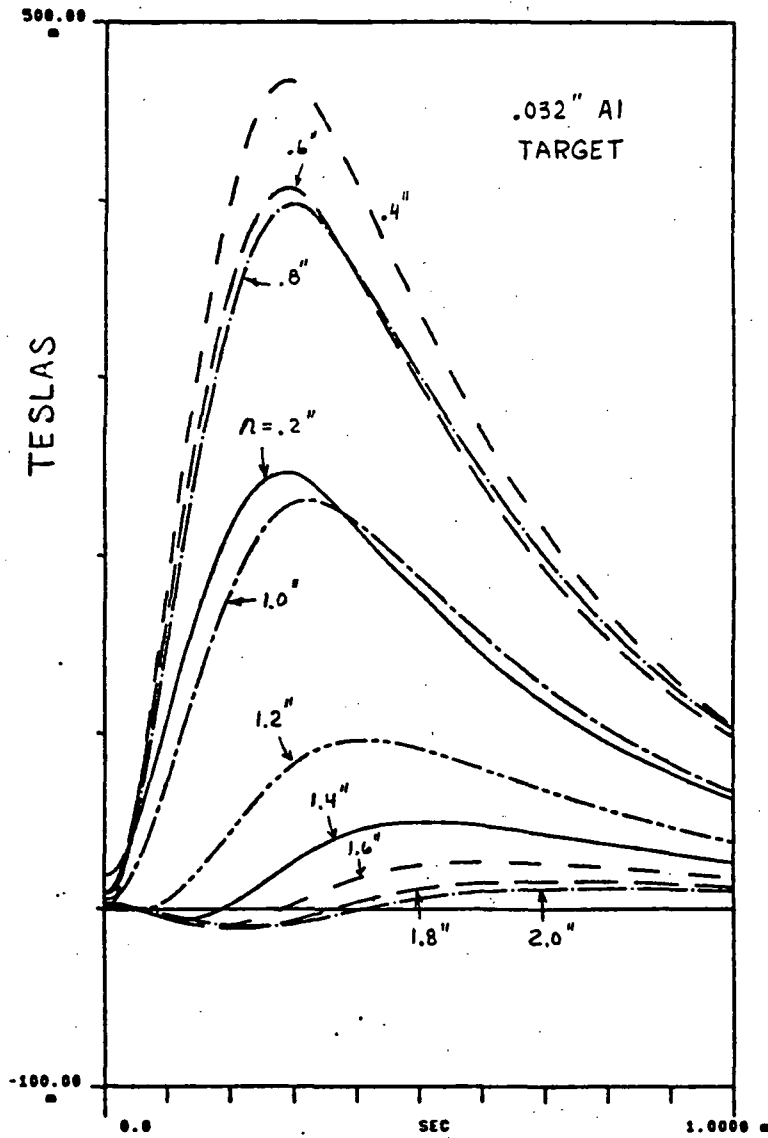


Fig. 2-24  $B_{\perp}$  on the Far Side

The purpose of Test 2 was to obtain  $B_r$  data, due to the coil alone, at the mid-plane position of the target to be added for Tests 3 and 4. These data will be used in the pressure calculation.

All  $B_r$  data showed an anomolous behavior (irregularities) at  $r = .4$  relative to  $r = .6$ . A separate check was made, in which the plate was reversed (interchanging the two sides). This produced a reversal of the irregularities, so the effect was probably due to an inaccuracy in the construction of the plate.

### C. Eddy Currents

Information on the magnitude and distribution of eddy currents in the target was obtained from a finite increment version of Ampere's Law,

$$\Delta I_{\text{eddy}} = \frac{1}{\mu_0} \oint \bar{B} \cdot d\bar{L} \quad (2-13)$$

One of the circulation paths is illustrated by the dotted rectangle in Fig. 2-25.

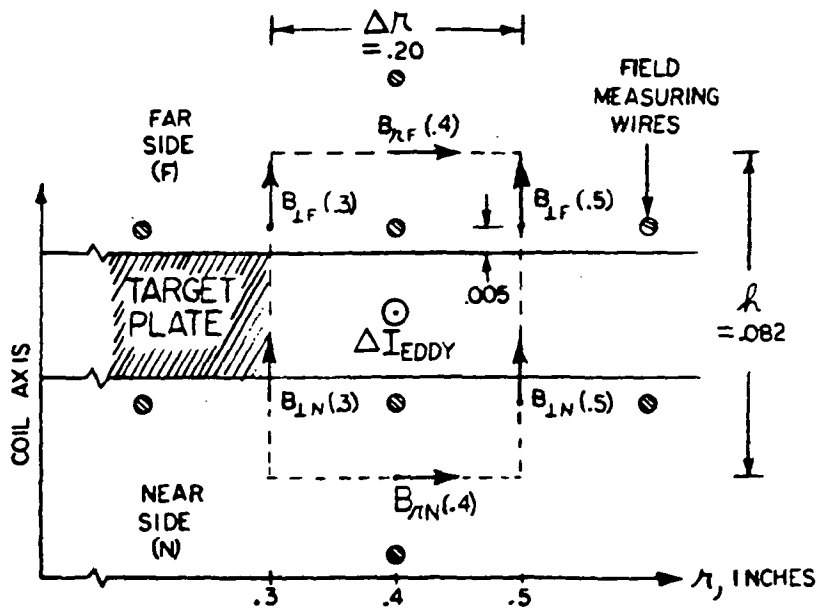


Fig. 2-25 Illustration of a Circulation Path For Evaluating Eddy Currents

It is imagined that the current in the drive coil (below the target) is referenced into the view, and the eddy currents are referenced out of the view. Thus, a counterclockwise circulation is taken, and the result is divided by  $\mu_0 \Delta r$  to obtain the current per inch of radius, assumed to apply at  $r = .4$ ". For the path illustrated in Fig. 2-25,

$$\Delta I_{\text{eddy}} = \frac{1}{\mu_0} \left( \frac{B_{\perp N}(.5) + B_{\perp F}(.5)}{2} h - \frac{B_{\perp F}(.3) + B_{\perp N}(.3)}{2} h + [B_{rN}(.4) - B_{rF}(.4)] \Delta r \right) \quad (2-14)$$

Numerically,

$$K_{\text{eddy}} = \frac{\Delta I_{\text{eddy}}}{\Delta r} = 4.14 [B_{\perp N}(.5) + B_{\perp F}(.5) - B_{\perp F}(.3) - B_{\perp N}(.3)] + 20.2 [B_{rN}(.4) - B_{rF}(.4)] \text{ KA/In} \quad (2-15)$$

where all B components are in Teslas.

Calculated results for  $K_{\text{eddy}}$  vs time at various radii are graphed in Fig. 2-26, and plots of  $K_{\text{eddy}}$  vs radius are shown in Fig. 2-27. The latter figure includes the drive coil current density for comparison. It is observed that a reasonable (about 50%) current transfer efficiency occurs very early in the process, whereas the eddy currents are only about 10% of the drive current at the time of 250  $\mu\text{s}$ . Eventually, the eddy currents reverse, due to the reversed EMF from the collapsing magnetic field.

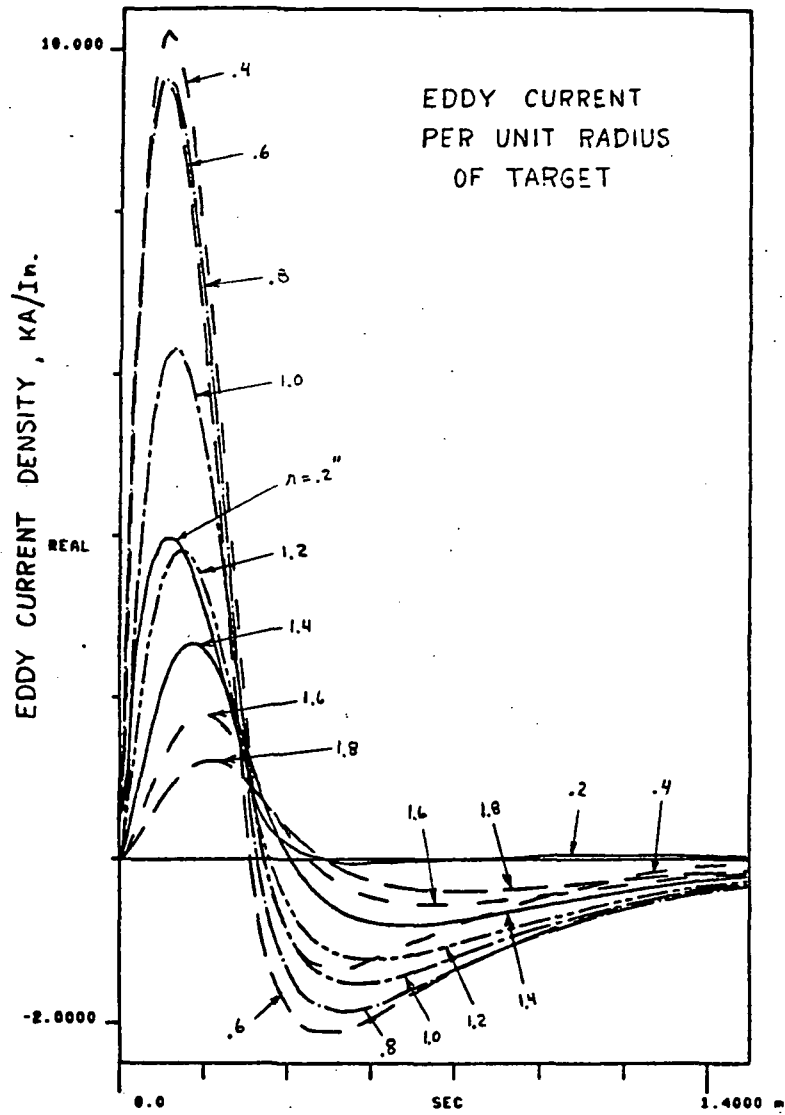


Fig. 2-26 Calculated Eddy Current Densities vs Time, at Various Radii

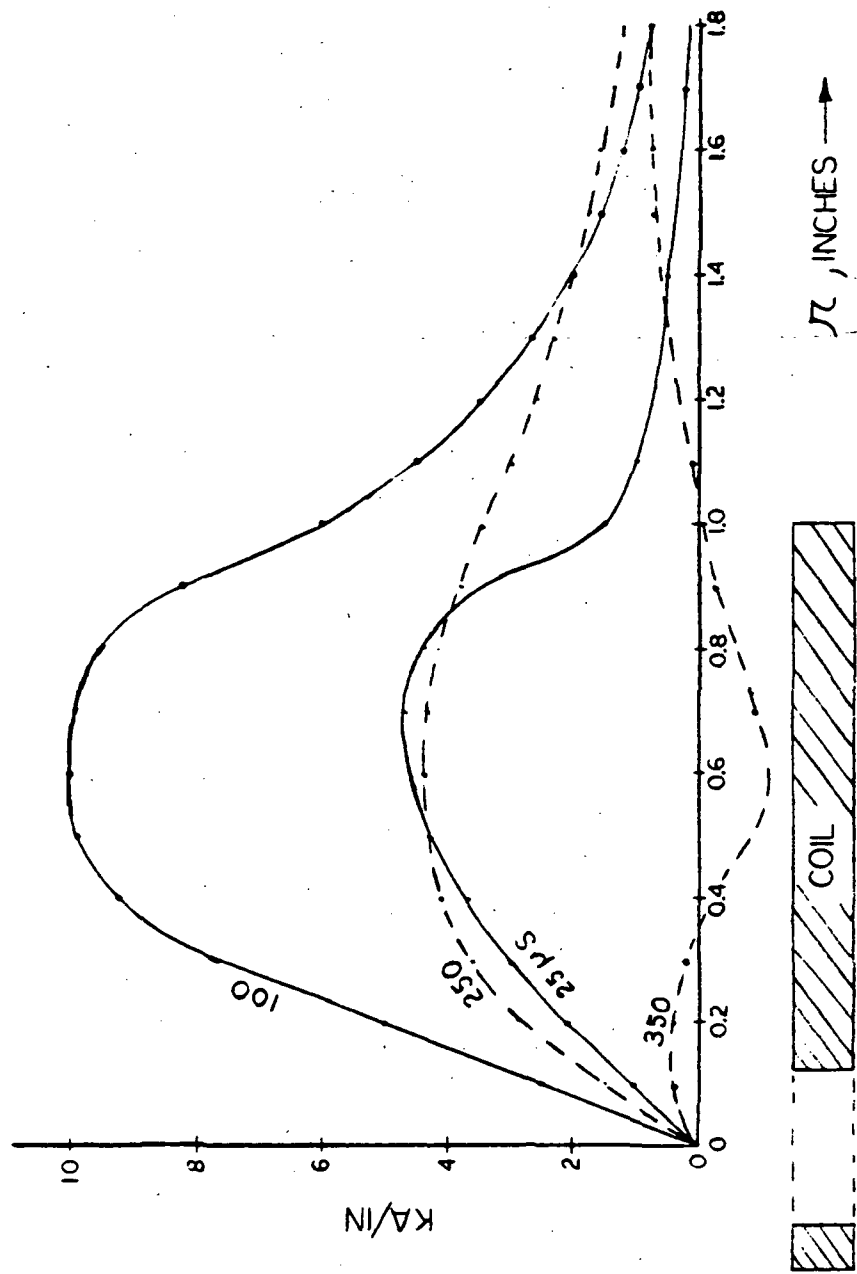


Fig. 2-27 Eddy Current Profiles

#### D. Pressure on the Target

Having evaluated the eddy currents, the pressure on the target can be found by the "conductor force equation," utilizing data for  $B_r$  along the center plane of the target. The  $B_r$  data used was that from Test 2, corrected for change in coil current due to the presence of the target. Thus the  $B_r$  data from Test 2 were multiplied by the factor

$$\frac{I_{\text{coil}}(t) \text{ in Test 3}}{I_{\text{coil}}(t) \text{ in Test 2}}$$

The difference in the two currents is small, as seen from Fig. 2-15.

Figure 2-27 illustrates the factors involved in the pressure calculation. The normal force exerted on a typical ring from  $r$  to  $r+\Delta r$  is

$$\Delta F_L = B_r \Delta I_{\text{eddy}} 2\pi r ,$$

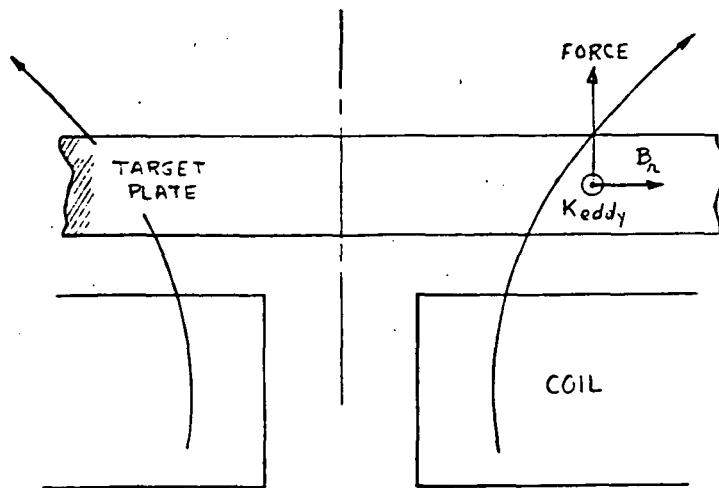


Fig. 2-28 Illustration For Pressure Calculations

yielding the following pressure formula:

$$p = 5.71 B_r K_{\text{eddy}} \text{ PSI} \quad (2-16)$$

where  $K_{\text{eddy}}$  is in KA/In, and  $B_r$  in Teslas.

Calculated results for  $p$  vs  $t$  at various radii are graphed in Fig. 2-29, and pressure "footprints" for several values of time are shown in Fig. 2-30.

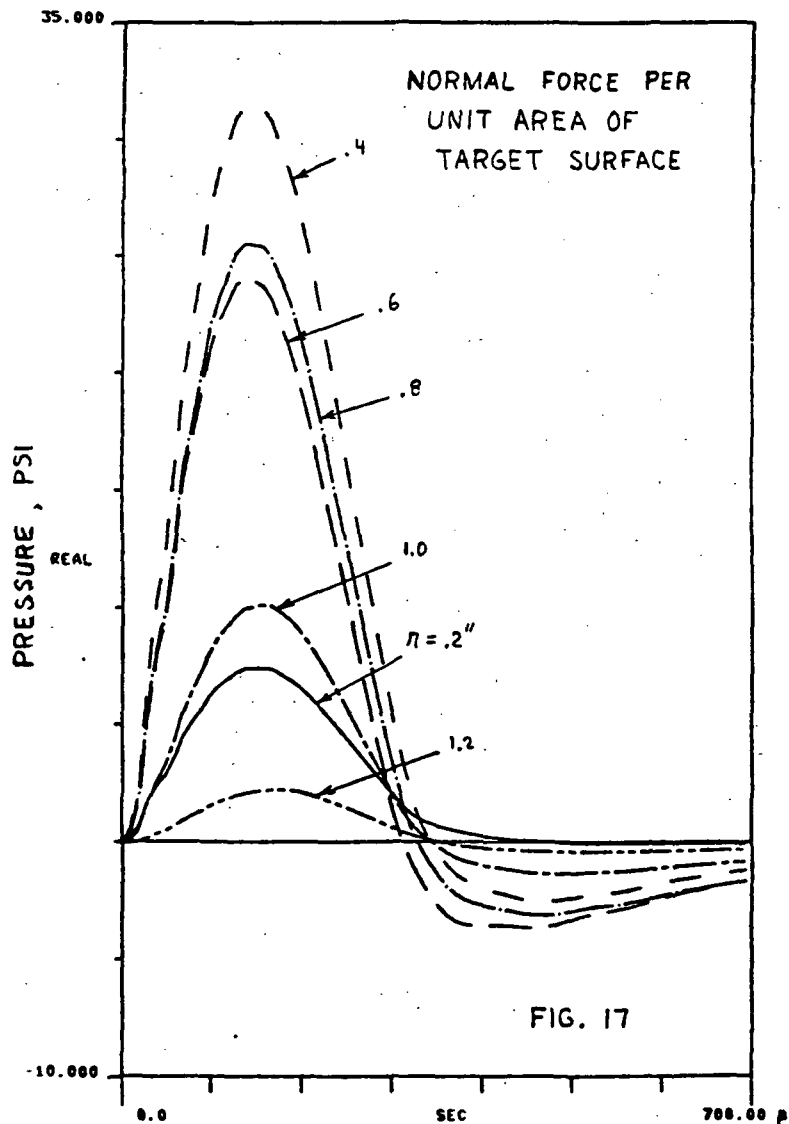


Fig. 2-29 Pressure vs Time at Various Radii

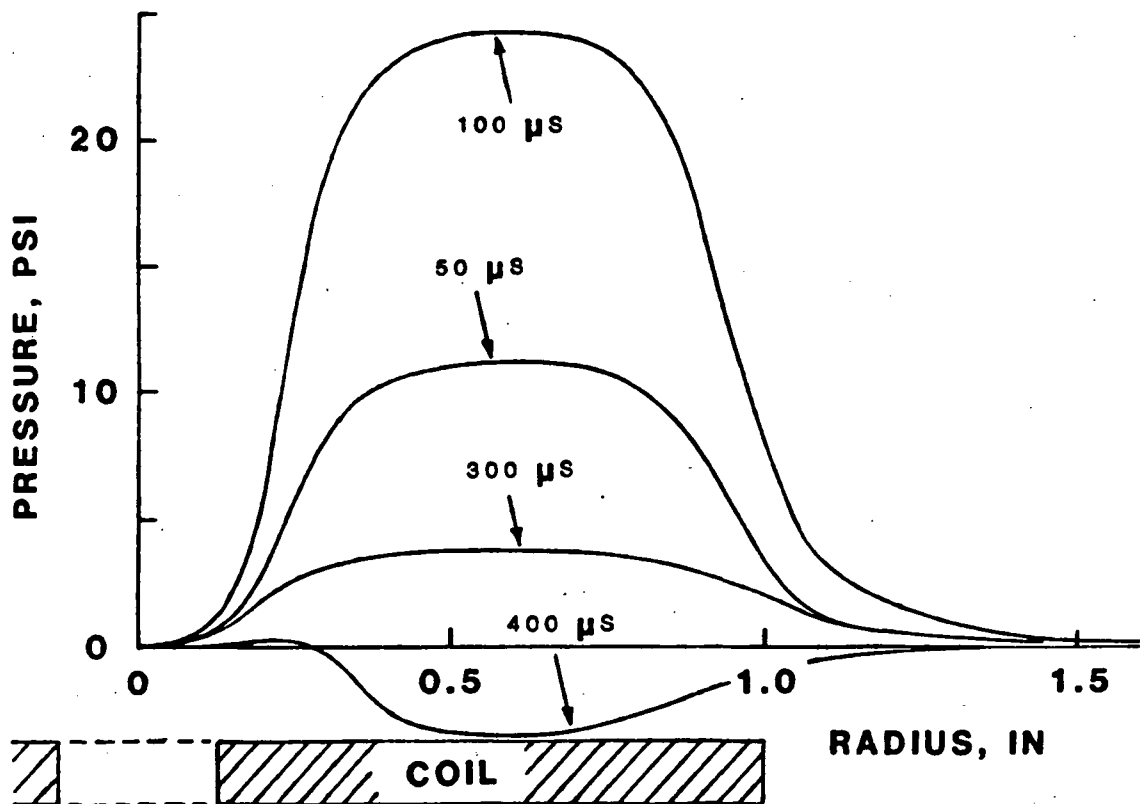


Fig. 2-30 Pressure Distribution with Radius

E. Total Normal Force and Impulse

The total normal force on the target was evaluated by the finite interval version of

$$\text{Force} = \int_{r=0}^{\infty} p \cdot 2\pi r dr \quad (2-17)$$

and is graphed in Fig. 2-31, and its time integral in Fig. 2-32. The latter figure shows an impulse degradation of about 25%, due to the collapsing magnetic field.

An independent measurement of the impulse was made with a ballistic pendulum, and the pendulum value exceeded the .0112 lb-sec value on Fig. 2-32 by about 10%.

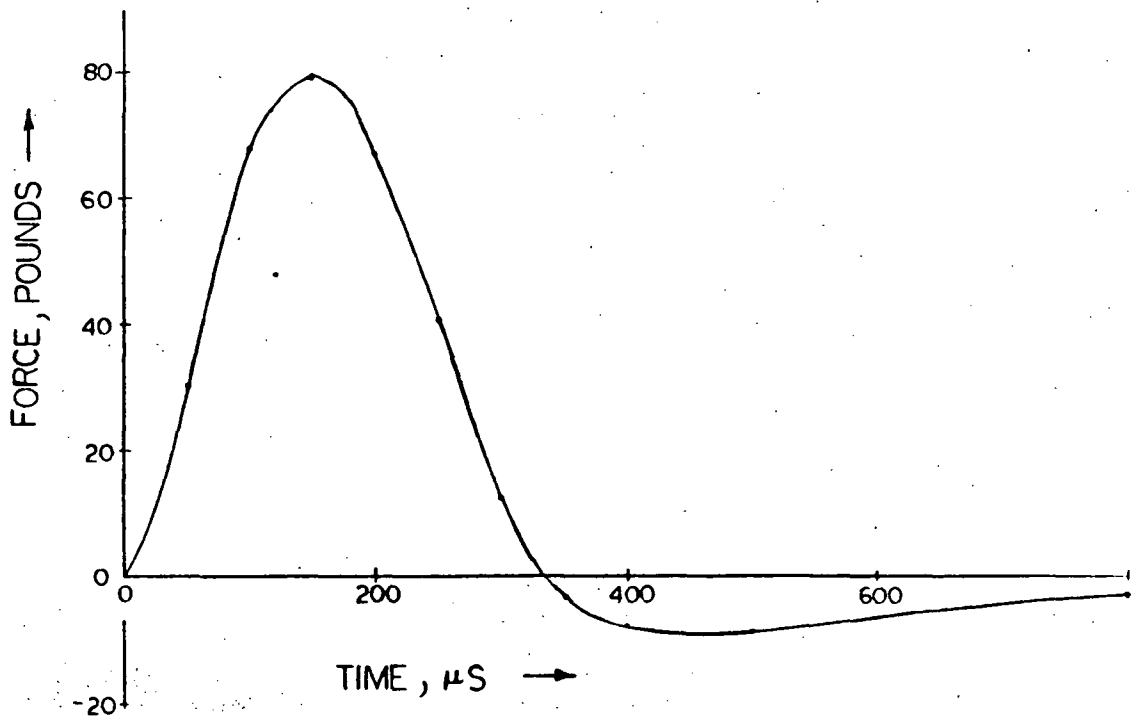


Fig. 2-31 Total Normal Force vs Time

#### F. Radial Forces in the Target

If  $B_{\perp}$  were used in the force calculation (Fig. 2-28), the result would be the radially acting force tending to compress the target. This force would turn to an expansive force when either  $B_{\perp}$  or  $K_{\text{eddy}}$  become opposite to the reference directions.

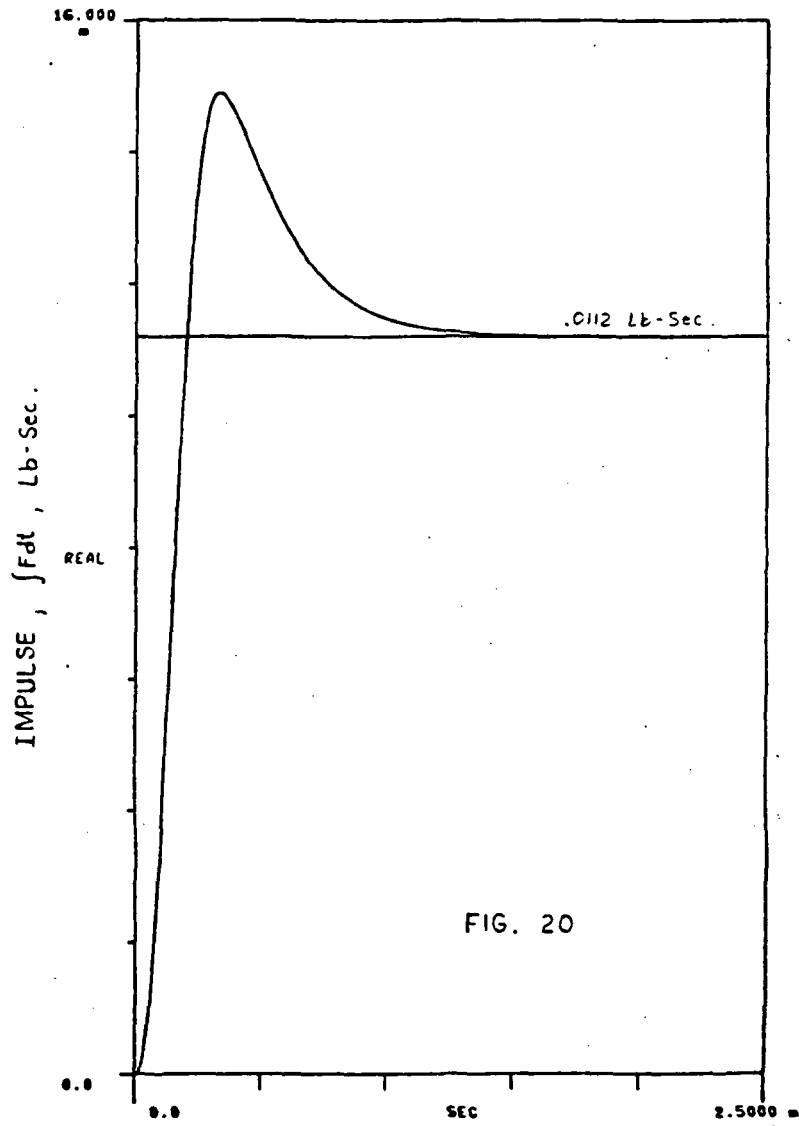


FIG. 20

Fig. 2-32 Time Integral of the  
Total Normal Force

The radial force acting on the incremental target area  $r \Delta\phi \Delta r$  is

$$\Delta F_r = -(K_{\text{eddy}} \Delta r) r \Delta\phi B_{\perp}, \quad (2-18)$$

and the force per unit of target (surface) area is

$$p_r = -B_{\perp} K_{\text{eddy}} \quad (2-19)$$

The specific formula, for example, to evaluate  $p_r$  at  $r = .6$ " is

$$p_r(.6) = -1.43 \left[ B_{\perp F}(.5) + B_{\perp N}(.5) + B_{\perp F}(.7) + B_{\perp N}(.7) \right] K_{\text{eddy}}(.6) \text{ PSI} \quad (2-20)$$

where the B components are in Teslas, and  $K_{\text{eddy}}$  in KA/In.  $B_{\perp F}$  data are from Test 4 and  $B_{\perp N}$  data from Test 3.

Figure 2-33 shows graphs of  $p_r$  vs time, at various  $r$  locations, and Fig. 2-34 shows  $p_r$  vs  $r$  at various times. At early stages, the radial forces are compressive at small radii, and expansive at large radii. This action is reversed in later stages.

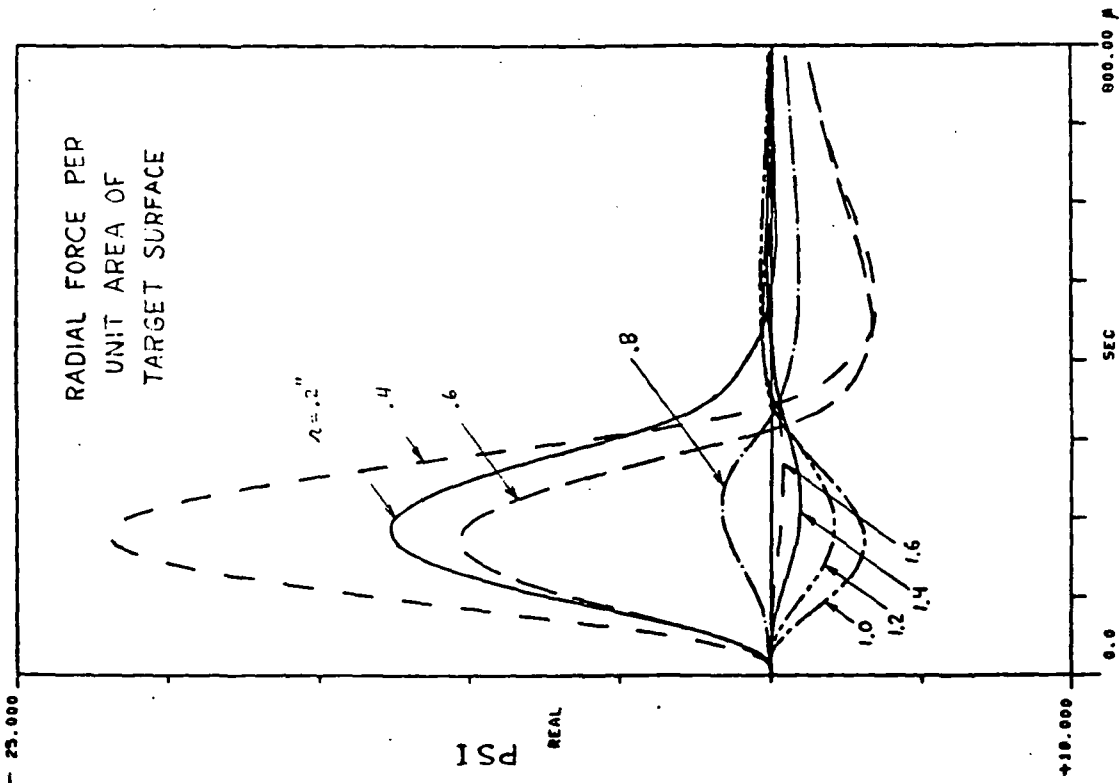


Fig. 2-33 In-Plane Force Per Unit Target Area

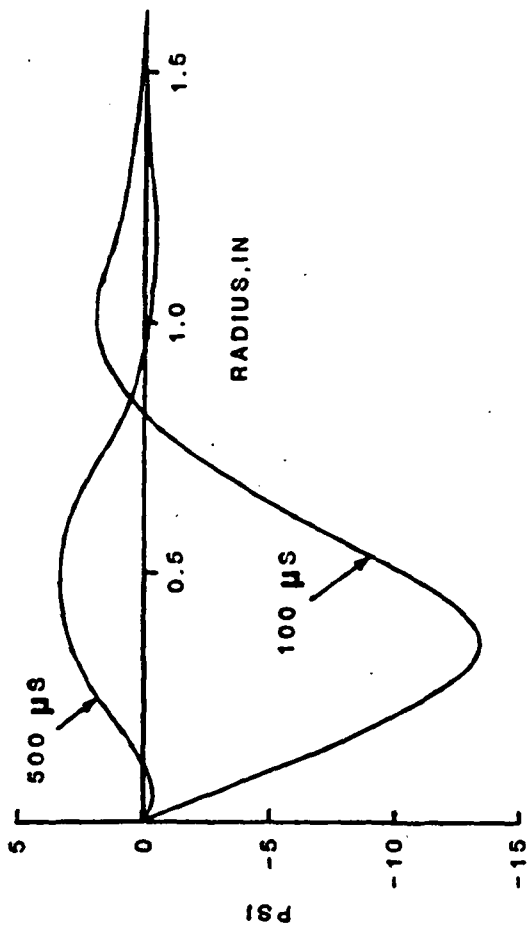


Fig. 2-34 Radial Distribution of In-Plane Force Per Unit Target Area



$$\begin{Bmatrix} E_{\phi}(\lambda, z) \\ H_r(\lambda, z) \end{Bmatrix} = \int_{r=0}^{\infty} \begin{Bmatrix} E_{\phi}(r, z) \\ H_r(r, z) \end{Bmatrix} J_1(\lambda, r) r dr \quad (2-21)$$

These are said to be the fields in "Hankel Space". El-Markabi shows that when Maxwell's Equations for axially symmetrical fields are transformed into Hankel Space, and displacement current ignored, then the resulting equations are analogous to those characterizing one-dimensional transmission lines. Thus, the field problem can be modeled by an equivalent transmission circuit in Hankel Space. El-Markabi's solution assumes the coil current to be sinusoidal, and the fields are then phasors. He also approximates the volume-distributed coil current by several current sheets. A three-sheet approximation is pictured in Fig. 2-35, and is assumed for the equivalent transmission line model pictured in Fig. 2-36, on the following page.

In the T-line model,  $E_{\phi}(\lambda, \omega)$  is analogous to voltage and  $H_r(\lambda, \omega)$  is analogous to current. The model consists of six line sections. The extreme left section ( $z < z_0$ ) extends to  $z = -\infty$ , so there is no reflected wave on it. This section may then be replaced by its characteristic impedance  $Z_a$ . The same reasoning applies to the section ( $z > z_4$ ). All other sections have been represented in Fig. 2-36 by their 4-terminal network parameters (A,B,C,D). The three sheet current sources are assumed to be the same. This assumption may be removed in some future work, to account for skin effect. Then the middle source would have a phase delay and reduced amplitude.

Formulas for the characteristic impedances,  $Z$ , and for the propagation constants,  $\gamma$ , are:

#### Air Sections

$$Z_a = j\omega\mu_0/\lambda$$

$$\gamma_a = \lambda$$

#### Metal Plate

$$Z_p = Z_a \left( 1 + \frac{j\omega\mu_0\sigma}{\lambda^2} \right)^{-1/2}$$

$$\gamma_p = \frac{\lambda Z_a}{Z_p}$$

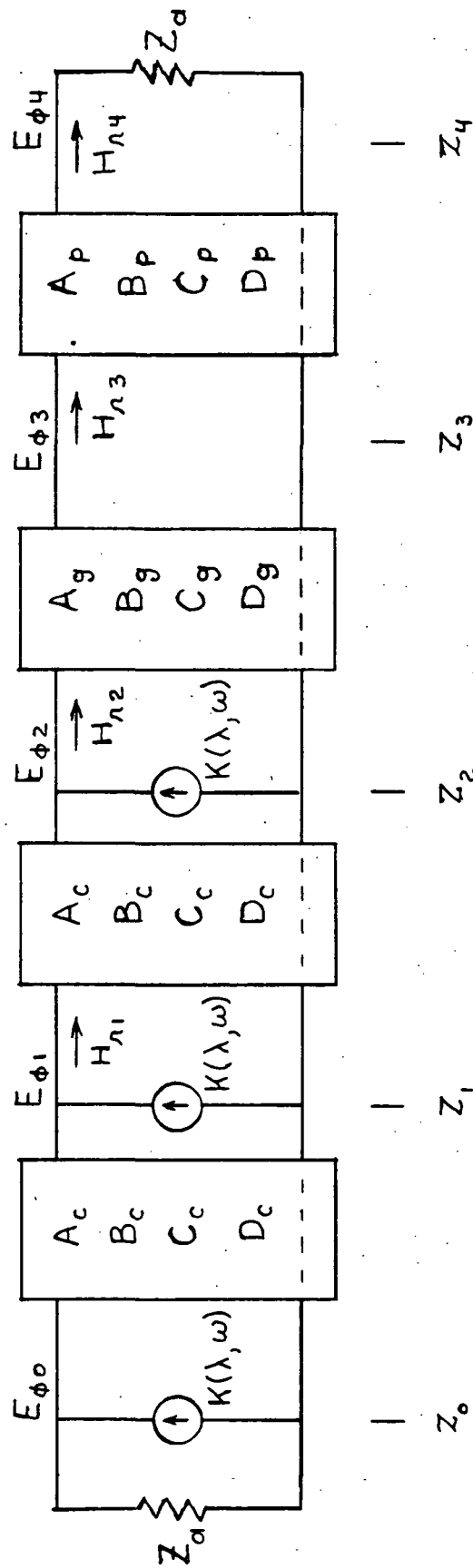


Fig. 2-36 Hankel Space Transmission Model  
of the Field Problem

Formulas for the 4-terminal network parameters are:

$$A_c = D_c = \text{COSH} (\lambda h/3)$$

$$B_c = Z_a \text{ SINH} (\lambda h/3)$$

$$C_c = B_c Z_a^{-2}$$

$$A_g = D_g = \text{COSH} (\lambda g)$$

$$B_g = Z_a \text{ SINH} (\lambda g)$$

$$C_g = B_g Z_a^{-2}$$

$$A_p = D_p = \text{COSH} (\gamma_p d)$$

$$B_p = Z_p \text{ SINH} (\gamma_p d)$$

$$C_p = B_p Z_p^{-2}$$

The Hankel Space current sources are calculated from

$$K(\lambda, \omega) = \frac{N I(\omega)}{3(R_2 - R_1)} \int_{R_1}^{R_2} J_1(\lambda r) r dr \quad (2-22)$$

where N is the number of coil turns, and I(ω) is the Fourier transform of the coil current.

Analysis of the network (Fig. 2-36) is done by a computer. If fields are desired in real space, then the inverse Hankel transformation must be calculated:

$$\begin{Bmatrix} E_\phi(r, z) \\ H_r(r, z) \end{Bmatrix} = \int_{\lambda=0}^{\infty} \begin{Bmatrix} E_\phi(\lambda, z) \\ H_r(\lambda, z) \end{Bmatrix} J_1(\lambda r) \lambda d\lambda, \quad (2-23)$$

and if they are desired as time functions, then an additional calculation must be performed for the inverse Fourier transform.

## B. The Circuit Problem

The electrical circuit can be represented as shown in Figs. 2-37 (a) and (b). Both circuits have

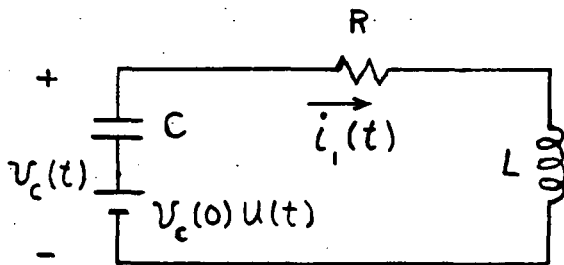


Fig. 2-37 (a)

Applies up to time  $t_x$ ,  
when the diode clamp  
begins to conduct.

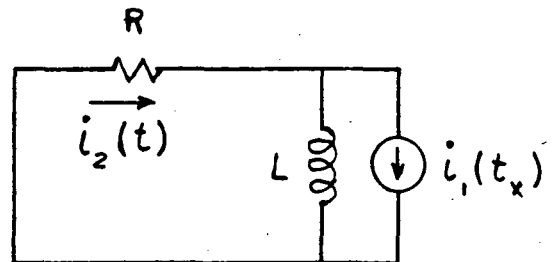


Fig. 2-37 (b)

Applies for  $t > t_x$

initial conditions represented as external sources. Direct time-domain solutions for these circuits cannot be written because  $R$  and  $L$  are functions of frequency.

Figures 2-38 (a) and (b) are the frequency domain circuits. They show a breakdown of elements of the physical circuit. It is assumed that this circuit contains a series-connected dummy coil in free space (no target).

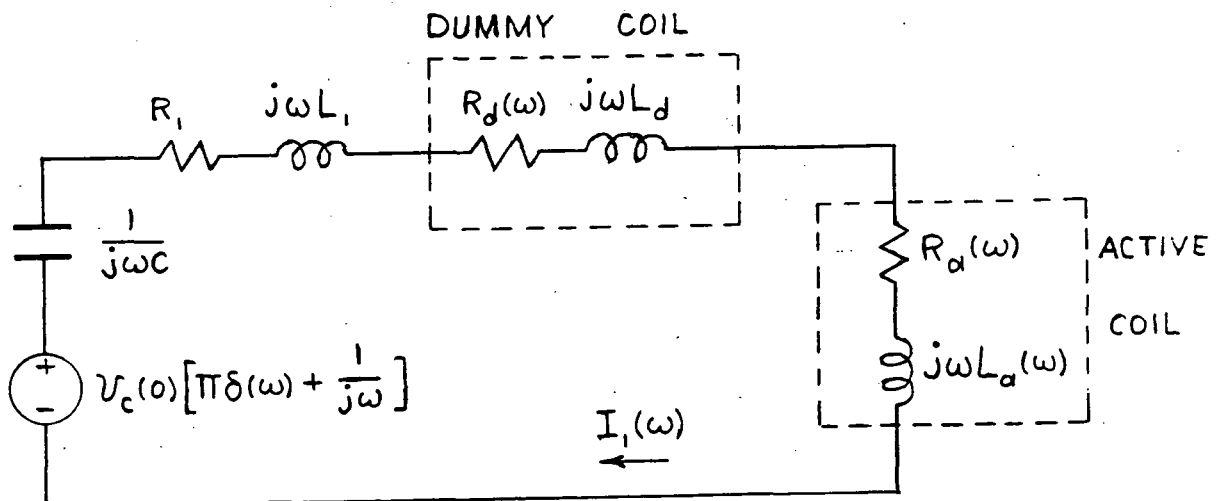


Fig. 2-38 (a) Frequency Domain  
Circuit ( $t < t_x$ )

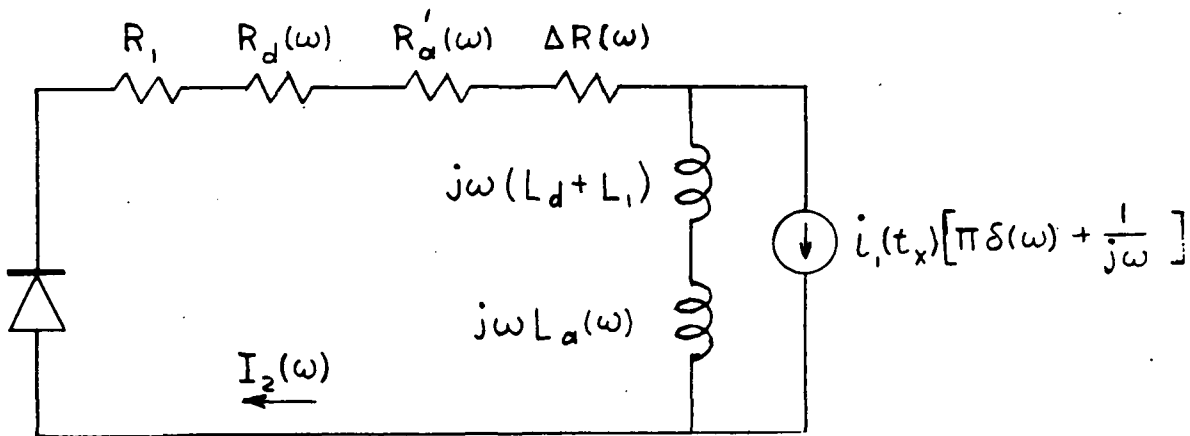


Fig. 2-38 (b) Frequency Domain  
Circuit ( $t > t_x$ )

The symbols in Fig. 2-38 represent:

$R_1$  = Equivalent resistance of the capacitor and the cable.

$L_1$  = Equivalent inductance of the capacitor and the cable.

$R_d(\omega)$  = A.C. resistance of the dummy coil.

$L_d$  = Inductance of the dummy coil.

$R'_d(\omega)$  = Effective resistance of the active coil.

$R'_a(\omega)$  = Portion of  $R_a(\omega)$  that is the free-space A.C. resistance.

$\Delta R(\omega)$  = Portion of  $R_a(\omega)$  that is field-induced. It is due to the presence of the metal plate.

$L_a(\omega)$  = Inductance of the active coil in the presence of the metal plate.

Data on  $R_d(\omega)$  and  $R'_a(\omega)$  can be estimated by procedures given in Section I.

The field-induced impedance of the active coil

$$Z(\omega) = \Delta R(\omega) + j\omega L_a(\omega)$$

must also be found before the circuit problem can be solved. This impedance is defined as the phasor voltage across the coil terminals, resulting from  $E_\phi$  in Fig. 2-35, per ampere of coil current. Thus, a preliminary solution to the field problem must be carried out. The simplest procedure is to set  $I(\omega)$  in Eq. 2-22 equal to unity, and then solve the transmission network for  $E_{\phi_0}$ ,  $E_{\phi_1}$ , and  $E_{\phi_2}$ .

Basing the calculation on the average of these three fields, and following El-Markabi's reasoning, the formula for calculating  $Z(\omega)$  becomes

$$Z(\omega) = \frac{2}{3} \frac{\pi N}{R_2 - R_1} \int_0^{\infty} \left\{ \lambda \left[ E_{\phi_0}(\lambda) + E_{\phi_1}(\lambda) + E_{\phi_2}(\lambda) \right] \int_{R_1}^{R_2} J_1(\lambda r) r dr \right\} d\lambda. \quad (2-24)$$

Now the circuit problem can be solved.

$I_1(\omega)$  is first found from the circuit of Fig. 2-38 (a), and its inverse transform,  $i_1(t)$ , calculated, along with the corresponding  $v_{C_1}(t)$ . The value of  $t$  (called  $t_x$  in Figs. 2-37 (a) and (b)) for the first zero crossing of  $v_{C_1}(t)$  is noted. The circuit in Fig. 2-38 (b) is then solved for  $i_2(t)$ , using  $i_1(t_x)$  as the initial condition. The circuit current is finally constructed from the two solution parts by

$$i(t) = i_1(t) [1 - u(t - t_x)] + i_2(t - t_x), \quad (2-25)$$

and its Fourier transform  $I(\omega)$  found. This is the current spectral information which enters into the Hankel Space current sources (Eq. 2-22).

### C. Pressure and Force on the Target

Starting with the equation for the force per unit volume within the target

$$\frac{\bar{F}}{\text{vol}} = \bar{J} \times \bar{B} \quad (2-26)$$

where  $\bar{J}$  is the local current density, and neglecting displacement current, then the pressure becomes

$$\begin{aligned} P(r) &= \int_{z_3}^{z_4} \left( \frac{F_z}{\text{vol}} \right) dz = -\frac{1}{\mu_0} \int_{z_3}^{z_4} B_r \left( \frac{\partial B_r}{\partial z} - \frac{\partial B_z}{\partial r} \right) dz \\ &= \frac{1}{\mu_0} \left[ \frac{B_r^2(z_3)}{2} - \frac{B_r^2(z_4)}{2} + \int_{z_3}^{z_4} B_r \frac{\partial B_z}{\partial r} dz \right]. \end{aligned} \quad (2-27)$$

Also utilizing  $\nabla \cdot \bar{B} = 0$ , Eq. 2-27 can be further modified into

$$P(r) = \frac{1}{\mu_0} \left[ \frac{B_r^2(z_3) - B_z^2(z_3)}{2} - \frac{B_r^2(z_4) - B_z^2(z_4)}{2} + \int_{z_3}^{z_4} \frac{1}{r} \frac{\partial}{\partial r} (rB_r B_z) dz \right]. \quad (2-28)$$

The force contributed by the integral term in Eq. 2-28 is

$$\begin{aligned} \int_{r=0}^{\infty} 2\pi r \left[ \int_{z_3}^{z_4} \frac{1}{r} \frac{\partial}{\partial r} (rB_r B_z) dz \right] dr \\ = 2\pi \int_{z_3}^{z_4} \int_{r=0}^{\infty} \frac{\partial}{\partial r} (rB_r B_z) dr dz. \end{aligned}$$

However,

$$\int_{r=0}^{\infty} \frac{\partial}{\partial r} (rB_r B_z) dr = (rB_r B_z) \Big|_{\text{at } r=\infty} - (rB_r B_z) \Big|_{\text{at } r=0} = 0$$

Thus, while the integral term in Eq. 2-28 may influence the distribution of pressure, it does not contribute to the total force. This total force should then be given by

$$F(t) = \int_{r=0}^{\infty} \frac{2\pi r}{2\mu_0} \left[ B_r^2(z_3) - B_z^2(z_3) - B_r^2(z_4) + B_z^2(z_4) \right] dr. \quad (2-29)$$

The calculation for pressure distribution appears to be difficult (no formula has yet been discovered that utilizes only field information at the two surfaces of the target). On the other hand, the force seems to be more readily calculable.

#### D. Preliminary Results

All of the computational work to date has been for the problem conditions that existed in the Magnet Field Diagnostics experiment, so that calculated results might be compared with experimental results. A tabulation of the conditions are:

##### Coils

(Active and Dummy Alike)

$$\begin{aligned} N &= 30 \text{ turns, } R_1 = .125 \text{ inch,} \\ R_2 &= 1.00 \text{ inch, } h = .188 \text{ inch,} \\ R_{dc} &= .0235 \Omega, L_d = 22\mu\text{H.} \end{aligned}$$

##### Target

$$\begin{aligned} &2024-T3 \text{ Aluminum } (\sigma = 3.48 \times 10^7 \text{ } \psi/\text{m}), \\ &d = .032 \text{ inch.} \end{aligned}$$

##### Gap

$$g = .1095 \text{ inch}$$

##### Circuit

$$\begin{aligned} C &= 600\mu\text{F, } R_1 = .054 \Omega, \\ L_1 &= 1 \mu\text{H, } v_c(o) = 400 \text{ volts} \end{aligned}$$

Calculations have been completed for the coil impedance  $Z(\omega)$ , the circuit current  $i(t)$  and its spectrum  $I(\omega)$ , and the Hankel-space fields  $B_{r_3}(\lambda, \omega)$  and  $B_{r_4}(\lambda, \omega)$ . Time-domain fields on the target surfaces have not yet been calculated, nor has the target force.

Figures 2-39 through 2-43 show results pertaining to coil impedance. Fig. 2-39 is a plot of the inductance of the active coil at three frequencies, as calculated from Eq. 2-24, as the upper limit on  $\lambda$  is varied. This plot gives an indication of what  $\lambda$  range provides the largest contribution. Figure 2-40 is a similar plot for the real part of  $Z(\omega)$ , which is the field-induced resistance.

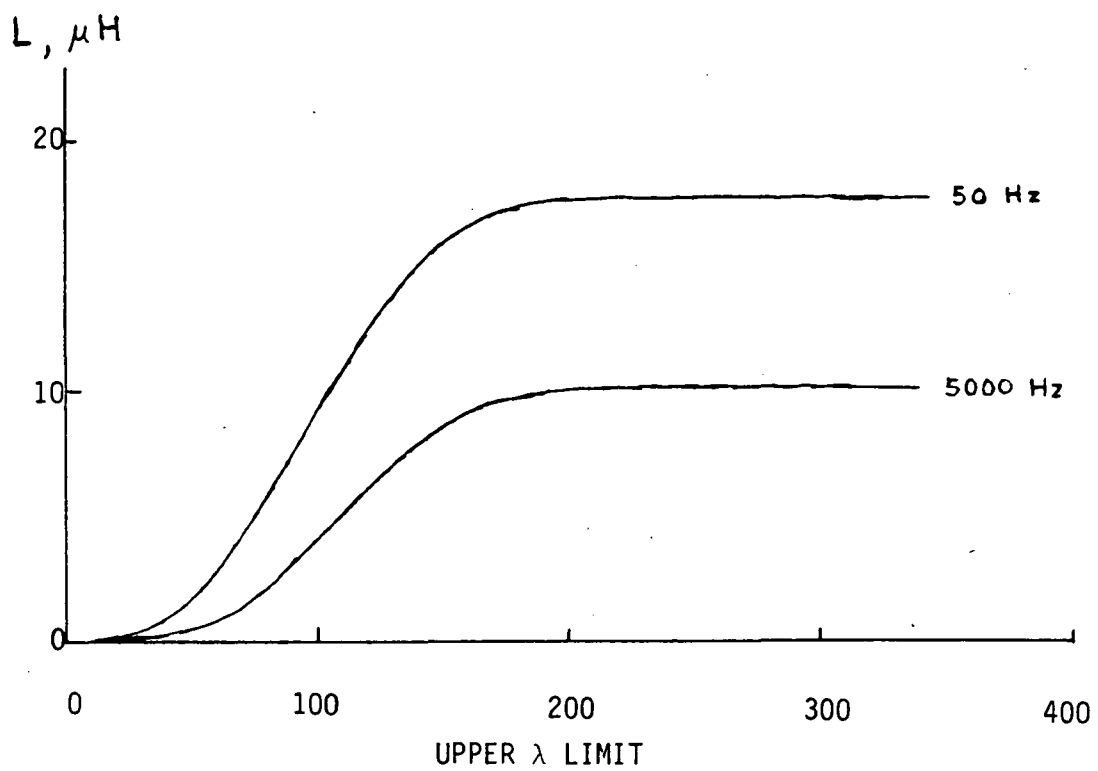


Fig. 2-39 Calculated Coil Inductance,  
vs. Upper  $\lambda$  Limit

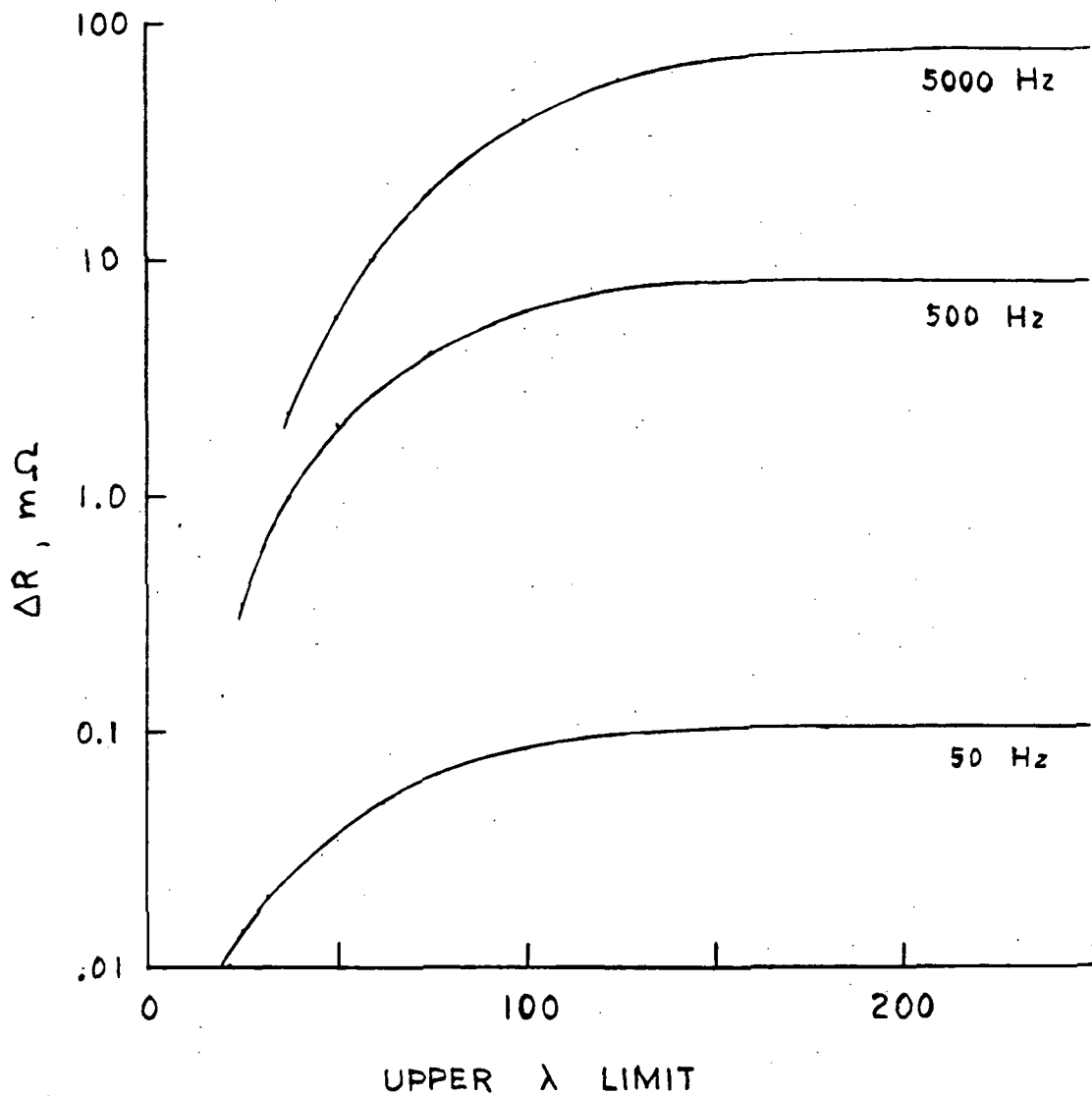


Fig. 2-40 Calculated Coil Resistance  
Contributed by the Metal  
Plate vs Upper  $\lambda$  Limit

Figure 2-41 is a graph of coil inductance vs frequency, with math model calculations, formula calculations, and experimental measurements compared. These comparisons are fair, but could be better.

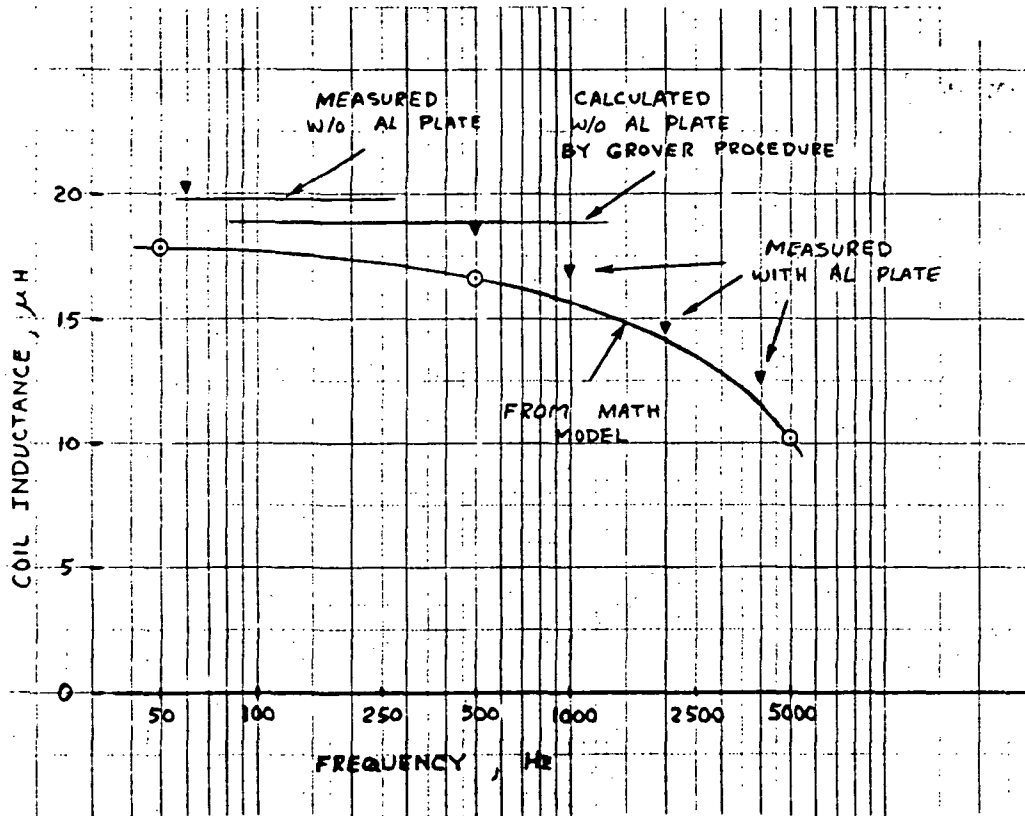


Fig. 2-41 Coil Inductance, Comparative Results

ORIGINAL PAGE IS  
OF POOR QUALITY

Figure 2-42 shows the calculated field-induced resistance as a function of frequency, along with bridge measured data. The measured values are the difference between the measurement without the target plate and a re-measurement with the target brought into position.

ORIGINAL PAGE IS  
OF POOR QUALITY

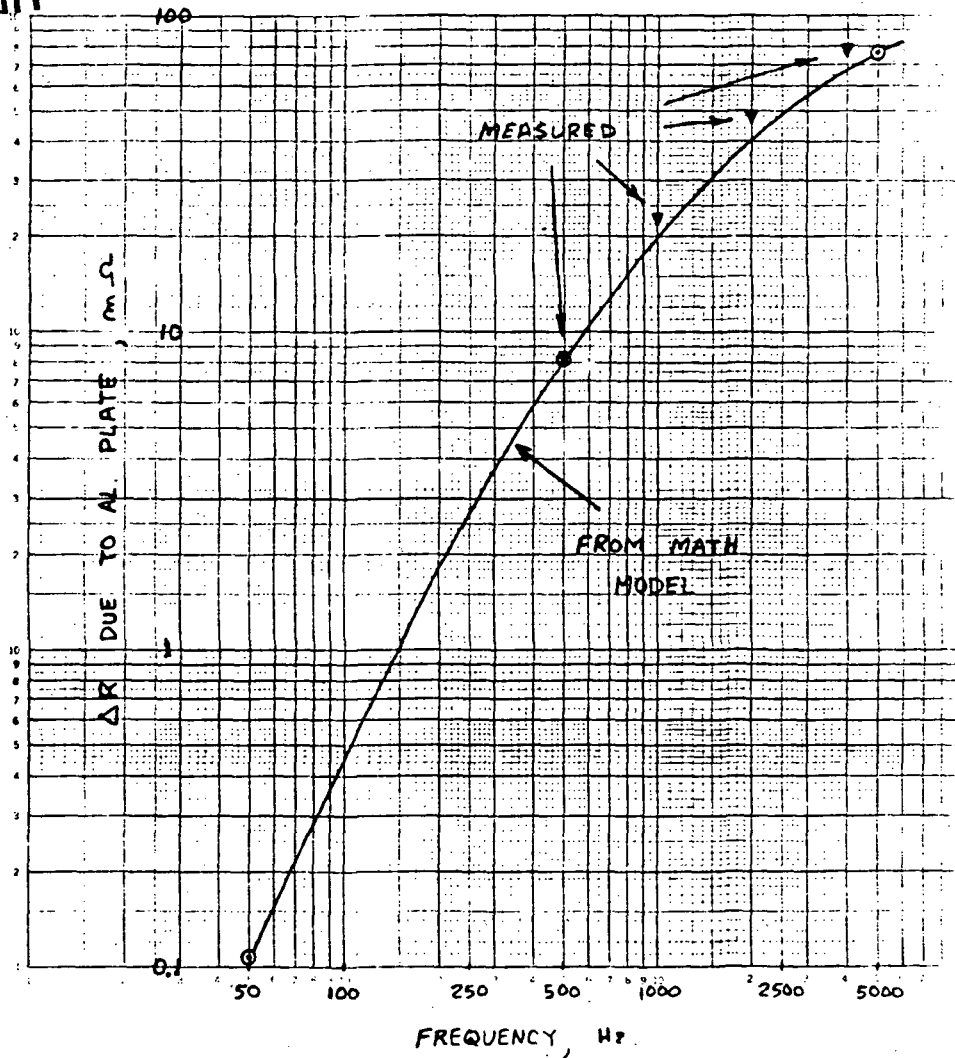


Fig. 2-42 Coil Resistance Due to the Metal Plate vs Frequency

Figure 2-43 shows no additional results from the math model. Rather, it puts the field-induced coil resistance in perspective, relative to the D.C. and A.C. resistance values for the series combination of the active and dummy coils. At 4000 Hz, for example, the resistance almost doubles as a result of  $\Delta R$ .

ORIGINAL PAGE IS  
OF POOR QUALITY

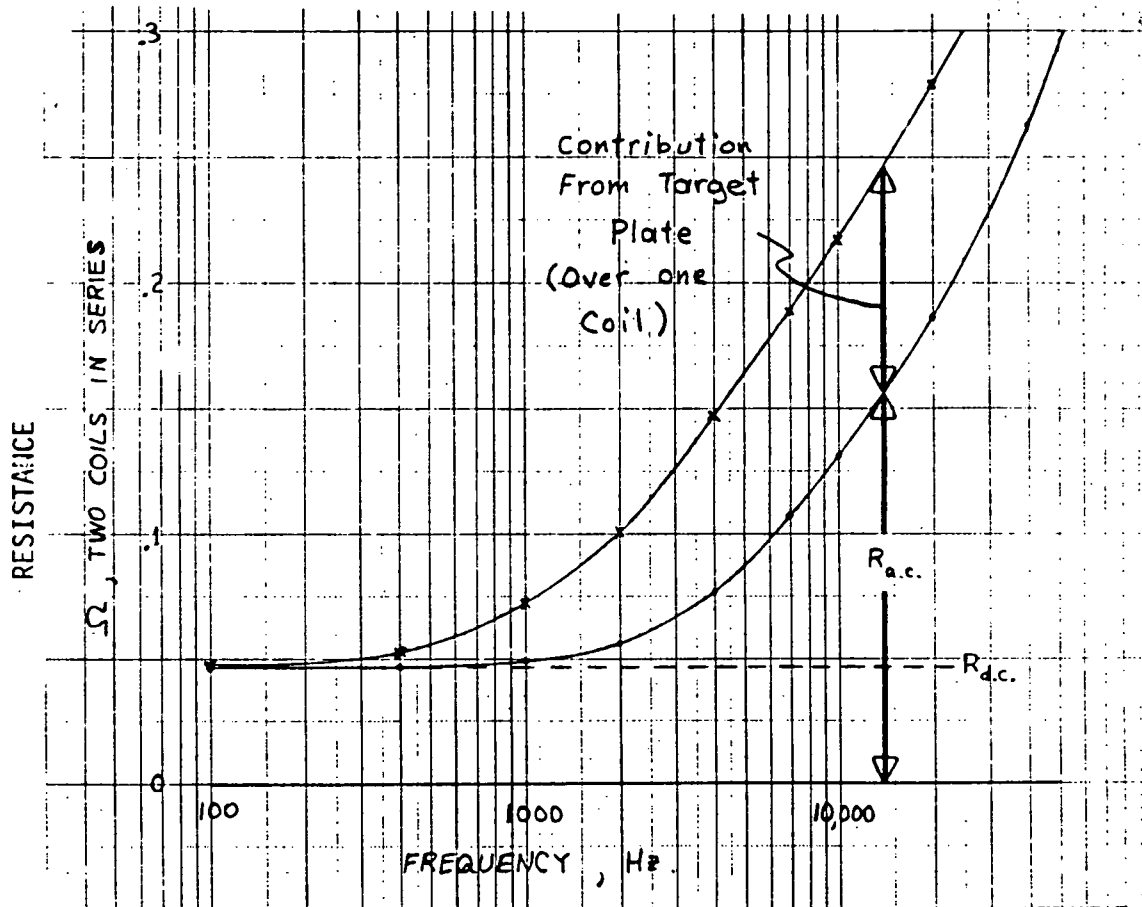


Fig. 2-43 Comparison of Various Contributions to Coil Resistance

Figure 2-44 shows a comparison of the coil current calculated from the math model Eq. 2-25 and the measured current.

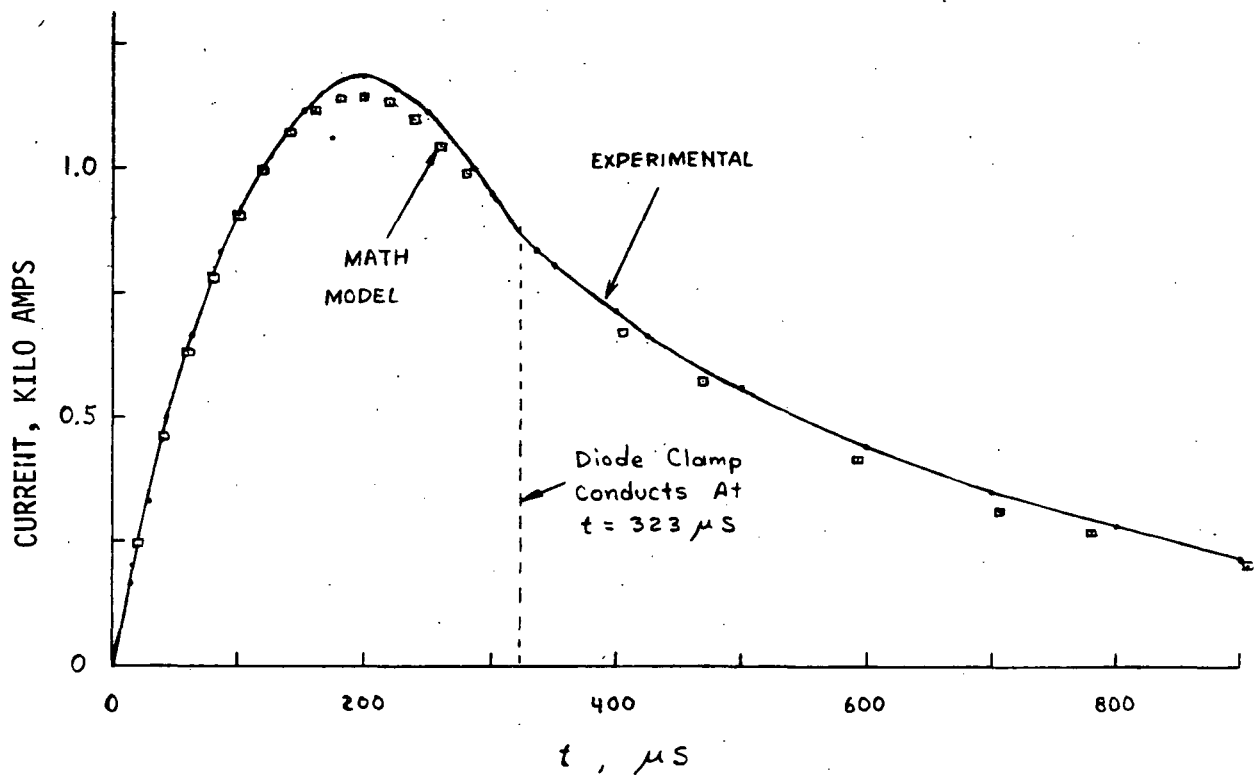


Fig. 2-44 Comparison of Coil Current Calculated from the Math Model with that Measured

## V. References

- 2-1 Frederick W. Grover, "Inductance Calculations, Working Formulas and Tables," Dover Publications, Inc., 1962
- 2-2 El-Markabi, M.H.S., et al, "Electromagnetic Properties of a Circular Cylindrical Coil in a Set of Planar Ferromagnetic Regions", IEE Proceedings (London), Vol. 129, Part A, No. 8, pp 582-589, Nov. 1982.

## CHAPTER 3. STRUCTURAL DYNAMIC TESTS AND STUDIES.

### I. Introduction

The structural dynamics associated with electro impulse de-icing has proved to be a difficult and challenging problem. The EIDI project was begun in May 1982 and the structural dynamic investigations conducted to date have raised as many new questions as have been answered. The project has been a modest activity from the standpoint of structures personnel and suitable instrumentation. The majority of the resources have been utilized in the proof of concept through subjective optimization of the numerous IRT test demonstrations for the participants in the industrial consortium. Eight IRT tests and two flight test demonstrations are summarized in Chapters 5 and 6. This Chapter is divided into the following sections:

- II. Transient Strain Measurements near EIDI Coils.
- III. Boeing (BCAC) 767 Leading Edge Slat Strain Survey.
- IV. Semi-Cylinder Leading Edge Investigations:
  - A. Experimental Results.
  - B. Analytical Studies and Models.
- V. Recent Developments Related to EIDI Force Measurements.

In Section II, the problem of strain measurement in both mild shock environments and strong magnetic fields is discussed and the project solutions to these problems are presented in Section III. The semi-cylindrical leading edge structure was developed by Wichita State University personnel and represents a portion of the graduate dissertation of Mr. Robert Friedberg. The goal of this study is to gain some fundamental correlation between experimental and analytical models for the simple geometry afforded by a semi-cylindrical shell. For the past two years, Mr. Friedberg has served as the principal designer for such items as coil winding and fabrication, coil mounts and the structural integrity of the coil supporting structures, and he is largely responsible for the concept of skin-mounted coils. In addition, he has also served as the University observer on the two flight tests conducted to date. These demands have left little time for any serious analytical investigations of the structural dynamics of the EIDI process. Thus, during the first two years of the project, the emphasis was on preparing the coils and their mountings and preparation of the test article for the associated IRT test. During this same period the project did manage to assemble certain resources that would serve to permit some fundamental investigations of the structural dynamics associated with EIDI.

The project began its activities with a single suitable accelerometer and charge amplifier, and a HP-5423A Structural Dynamics Analyzer. This two channel instrument has a 25 kilohertz bandwidth and a sample time of approximately 10 microseconds, which proved to be adequate for acceleration measurements but inadequate for the proper resolution of strain measurements in magnetic fields. This problem is discussed and demonstrated in Section II. The project did acquire several transducers, amplifiers, and other miscellaneous instrumentation; and in May 1984, a Nicolet 3091 Digital Oscilloscope was purchased. This two channel instrument has a digital sample time of 1 microsecond and channel subtraction capability and was ideally suited for the proper resolution of the strain measurement problem. Thus, during late 1984, the first reliable strain measurements were available to the project and some of these results are reported in Section IV. A. Unfortunately, the only output was an analog xy-recorder, hence the signals had to be captured, processed, and displayed immediately. During November 1984, the project acquired a Zenith Z-150 micro-computer that was interfaced with the Nicolet oscilloscope and the floppy disk units have provided a means of permanently storing the various signals. A HP-7245B Digital Plotter is now interfaced with the micro-computer and this plot capability is displayed in Section III. The most recent improvement is an interface between the micro-computer and the University main frame IBM-3081 computer, permitting the transfer of signals to the 3081 for subsequent processing and display.

The second major resource was the installation of the MSC/NASTRAN code on the IBM-3081, in October 1984. This finite element code has provided the capability of performing structural dynamic investigations for various EIDI applications. In September 1984, three graduate students majoring in structural dynamics began to develop analytical models for the transient response of pulsed leading edge structures. The majority of these studies have been confined to the semi-cylinder and are reported in Section IV. B.

The simple concept of a semi-cylindrical leading edge simulation has also attracted the attention of the McDonnell Douglas participants in the EIDI program; Mr. David Blyther, Dr. Don Kerans, and Mr. Lou Barretto. The EIDI project group has designed and fabricated a duplicate of the semi-cylinder described in Section IV for McDonnell Douglas and they plan to fully instrument the shell and conduct an IRT test in June or August, 1985. The principal goal of this study is a time correlation of acceleration, strains, and high speed photography in a serious attempt to answer the question of the basic ice shedding mechanism in the EIDI pulse.

While all of these elements and resources are encouraging and appear to be converging on a true analytical and experimental correlation of the EIDI problem, there remains one major unsolved area, namely, an adequate

representation of the spatial and temporal behavior of the coil pulse. This behavior was first shown by Schrag, Ref. 3-1, for a single case of coil size, gap, target material, and electrical parameters. The experimental result was conducted with a special magnetic field measuring plate fabricated by WSU personnel, described in Section 2. B of this report. This experimental result was generalized into a separated solution of spatial and temporal behavior by Bernhart, Ref. 3-2, and used successfully in a transient response study of a flat plate subject to a EIDI pulse. While this limited study did show favorable agreement with experimental results, it also clearly identified the response sensitivity to both rise time and pulse duration. Mr. John Walsh, who is a graduate student in Aeronautical Engineering, will be repeating the experiment using the magnetic field measuring plate for a wider range of parameters during the summer of 1985. These results will be compared to ballistic pendulum results presented by Schrag, Ref. 3-1, and several British authors, Ref. 3-3. A very recent parallel experimental development designed to measure the temporal behavior of the EIDI pulse is reported in Section V. This experiment employs fundamental one dimensional wave mechanics in a 48 inch long polycarbonate circular rod with a propagation time of approximately 850 microseconds. This time delay is adequate to measure the plane wave behavior of the force pulse. Preliminary results appear to be very encouraging, however a proper model for the dispersion mechanism in the rod is currently under study.

The question of fatigue has been raised on several occasions by various observers. It is important to recognize that a prolonged fatigue test of a representative leading edge structure at this point in the EIDI program, would essentially be a longevity test of the electrical components in the EIDI pulsing system. The question does need to be addressed, but only after certain question related to the potential usage of the system are answered; e.g., number of hours of operation per year, and a suitable pulsing system becomes available to the project. The EIDI project has developed several coil attachment concepts that serve to reduce peak stress levels but raise other questions related to bonding fatigue subject to shock environments. This potential reduction is shown for the Boeing 767 slat in Section III.

The basic goal of these structural dynamics studies and tests is the development of an analytic design procedure for the EIDI program. The studies conducted to date are briefly summarized as follows:

A finite element model study of a semi-cylindrical leading edge has been completed. The study has demonstrated that a proper finite element model is adequate to duplicate, and hence predict, the peak accelerations and strains that have been observed in various airfoil tests. The development of a finite element model for a airfoil leading edge with more complex geometry and boundary conditions is in progress. The EIDI project personnel are currently

conducting parallel studies to develop an analytical model for the EIDI pressure pulse with appropriate experimental verification. This model will become an integral part of the aforementioned structural dynamics computational code. The pressure pulse format will include both the spatial and temporal behavior of the impulse for a variety of electrical parameters such as voltage level, storage capacitance, and coil inductance; as well as the target material thickness and conductivity, and air gap.

When these basic elements are joined and supported by experimental verification; meaningful parametric studies may be conducted that will yield the dynamic response of a proposed airfoil leading edge structure and coil configuration. The computational code will have the flexibility of examining the effects of one or more coils that can be positioned at arbitrary location in the leading edge cavity. This capability can then be easily extended to simulate magnetic doublers, skin mounted coils, coil mountings, internal ribs, and various boundary conditions.

Dr. Don Kearns, McDonnell-Douglas Corp., is currently adding simulated ice accretions to his structural dynamic model of a semi-cylinder. The McDonnell-Douglas tests, scheduled for the summer of 1985, will hopefully serve to partially answer the question of the fundamental ice shedding mechanism in the EIDI process. If this test is successful, it will lead to optimization studies to maximize a specific performance criteria, e.g., acceleration, strain, strain rate, etc., that is associated with optimum ice shedding.

## II. Strain Measurements Near EIDI Coils.

Strain measurements in the magnetic field produced by a EIDI coil has proved to be a difficult problem and the following demonstration problems are intended to portray some of the difficulties. The EIDI coil can generate magnetic flux densities in excess of 10,000 gauss, and the field strength is developed in 100 to 300 microseconds. Any strain gage in the proximity of the coil is subject to transverse magnetic flux which results in induced voltage in the gage. If the resulting induced voltage is not cancelled, eliminated or minimized, it obscures the strain signal developed in the gage. Thus, the problem is likened to a signal plus noise phenomena. The typical strain signal is be on the order of 1 to 10 millivolts, whereas the induced or noise voltage may be of the same order and in some cases greater than the strain signal.

Contacts with strain gage manufacturers revealed that the Measurement Group, Inc., (Ref. 3-1) had solved a similar problem for the Princeton University Plasma Physics Laboratory in connection with the Tokamak Fusion Test Reactor. The application involved magnetic flux densities as high as 50,000 gauss and a time duration of approximately one second. A special gage was employed, identified as a "dual element gage", which consists of two identical overlaid grids, laminated in precise alignment with one another, and connected in series such that the current passes through them in opposite directions. The gage is shown in conceptual form in Fig. 3-1. Since the grids are very close together with respect to the field gradients, induced voltage in the grids tend to be equal and of opposite sign, rendering the gages largely immune to magnetic effects. The Measurements Group also recommends a woven cable product commercially known as Inter-8 Weave to minimize the magnetic noise in the cabling. Several of the "dual element gages" (WK-13-125-WS-700) were obtained and installed on a representative leading edge structure. The lead attachments to the "dual element gages" posed very special soldering problems and several gages were lost during installation. The recommended cabling also proved to be excessive in weight for the relatively light weight structures common to aircraft leading edges.

The first time the "dual element gages" were tested on a EIDI pulsed airfoil, the gages sheared along the bonding plane between the grids and the resulting misalignment rendered them useless to the project. Thus, the EIDI strain gage environment is not only harsh due to the magnetic flux, it is also subject to very high acceleration levels which can reach peak values of 10,000 to 20,000 g's in 100 microseconds or less. This failure prompted

Dr. R. L. Schrag to propose a modification to a standard strain gage which is herein identified as a "compensated gage", and is also shown in Fig. 3-1. This modification incorporates the installation of a single loop of 32 gauge enameled wire which serves to partially compensate or minimize the induced magnetic effect. The compensation loop is also bonded to the gage where appropriate. Standard Wheatstone bridges are used in the EIDI project with a complete avoidance of any wire wound potentiometers or other electrical components. Gage leads consist of twisted pairs of 28 or 32 gauge insulated wire twisted with a drill motor. The leads are both inexpensive and light weight.

Strain measurement must be completed in two steps. After performing a resistance balance of the bridge, the first step is to remove the bridge excitation DC voltage source and pulse the EIDI coil to establish the induced magnetic effect in the gage. In the second step, the bridge excitation is restored and the EIDI coil is pulsed a second time to establish the induced magnetic effect plus the mechanical strain. Subtracting the two signals yields the desired mechanical strain. This two step operation is of course difficult to achieve in the IRT tests. Some data have been obtained by using a pre-recorded magnetic effect pulse and subtracting it from the pulse data obtained under icing conditions.

The two step process is identified as a DC-bridge measurement by project personnel and has been used with varying levels of success. Figs. 3-2 and 3-3 depict some additional problems for the DC-bridge related to the digital sample time of the transient capture instrumentation. The data contained in the two figures represent strain measurements for a 2.5 inch radius semi-cylinder, 66 inches in length described in Section IV. This simulated leading edge structure contains a single coil located at the mid-length and compensated strain gages placed on the outer and inner surfaces of the 0.040 inch thick skin. The data in Fig. 3-2 represents the two signals for each location and the resulting subtraction when using a HP-5423A Signal Analyzer, whose sample time is approximately 10 microseconds. The desired strain signal is literally obscured during the first 150 microseconds and the establishment of a peak strain is difficult. Fig. 3-3 represents the same data acquired with a two channel Nicolet 3091 Digital Oscilloscope using a 1 microsecond sample time. The figure clearly indicates the desired levels of the two strain signals for a well compensated gage. The resulting data can be reported with confidence as has been done in Section IV. of this Chapter.

A recent improvement in strain measurements has also been developed by Dr. R. L. Schrag. The development is an AC-bridge, wherein the carrier frequency is 100 kilohertz, which is considerably higher than any known strain gage instrumentation. The principal advantage of the instrument is the

single step measurement process. The AC-bridge does require both resistance as well as capacitance balancing and is exceedingly sensitive to lead wire movements during the balancing and pulsing operations. In spite of some of these difficulties, the instrument exhibits great promise and hopefully funds can be obtained for future improvements and the fabrication of multiple channels. A schematic diagram of the AC-bridge is shown in Fig. 3-4.

Figs. 3-5 through 3-7 are strain measurements for a single gage on the Boeing 767 leading edge slat; details related to the gage location and the slat structure may be found in Section III. Fig. 3-5 is the data for an noncompensated gage and standard strain gage leads using the DC-bridge process; while Fig. 3-6 is the same data with a compensating loop added to the gage with twisted leads. The improvement resulting from the compensating loop is obvious. Fig. 3-7 represents AC-bridge measurements for both the noncompensated and compensated gage. The compensating loop neither adds or detracts from the performance. A brief summary of the peak strain level developed by the four measurements is summarized below. The peak circumferential (chordwise) strain taken as the average of the four measurements is 2070 micro-strain.

Figure 3-5. 1940 micro-strain

Figure 3-6. 1850 micro-strain

Figure 3-7. 2220 micro-strain

Figure 3-7. 2270 micro-strain

### III. Boeing (BCAC) 767 Leading Edge Slat Strain Survey.

A 76 inch long section of the BCAC 767 leading edge slat was fitted with EIDI coils and tested in the NASA Lewis IRT on August 13, 14; 1984. A sketch of the leading edge cavity is shown in Fig. 3-8. Prior to the test, this geometric definition was used in a simple two dimensional computer code to approximate the fundamental mode shapes of the leading edge section. The mode shape plots are displayed in Fig. 3-9 and are used in the preliminary design of coil placement in both the upper and lower surfaces. A short 4 inch long section of the leading edge cavity was also dynamically tested to verify the analytically predicted frequencies. The first two frequencies compared favorably with the computer code.

The 76 inch long section is divided into two equal length bays of 38 inches each with ribs on each end and at the center of the span. The selected EIDI coil types and positions used in the IRT test are summarized below.

Coil No.	--Description--	Spanwise Position	Chordwise Position (measured from nose)	
1	2 side coils-nose attached	6.3" from lower rib	Lower Sfc 1.6"	Upper Sfc 2.5"
2	2 side coils-spar mounted	20.0" from lower rib	3.1"	2.5"
3	2 side coils-spar mounted	32.7" from lower rib	3.1"	2.6"
4	2 side coils-spar mounted	32.7" from upper rib	2.5"	2.5"
5	2 side coils-spar mounted	20.0" from upper rib	2.7"	2.4"
6	2 side coils-skin mounted	6.3" from upper rib	1.4"	1.4"

The coils used in the strain survey were coils 2, 3, and 6. Two strain gages were installed over the upper surface EIDI coils in the circumferential (chordwise) and longitudinal (spanwise) directions. In addition, a single chordwise gage was utilized on the lower surface over coil 3. The test data are presented in Figs. 3-10 through 3-13.

These three coils were employed in five different IRT test runs. The selected strain measurements correspond to two different sets of electrical parameters for IRT test numbers (4) and (8). Each coil pair was pulsed twice

in each test with the sequence; (2,2), (3,3), and (6,6). These two test runs are summarized below.

IRT TEST	COIL (2)	COIL (3)	COIL (6)	Subjective Evaluation
(4)	400UF 900V 162 Joules	400UF 900V 162 Joules	400UF 800V 128 Joules	Fair, some residual
(8)	200UF 1250V 156 Joules	200UF 1250V 156 Joules	200UF 1120V 125 Joules	Clean!

The BCAC-767 slat is fabricated from 7075-T6 aluminium sheet 0.062 inches in thickness. The published mechanical properties for this material are; 78,000 psi ultimate strength, 68,000 psi yield strength, and 10,400,000 psi for the modulus of elasticity. From an examination of the strain plots one can conservatively state that the peak chordwise and spanwise strain have nearly identical occurrence times. Thus, the maximum peak stress is predicted on this basis, using a value of 0.30 for Poisson's ratio. In each case, the maximum stress will occur in the chordwise direction. These data are summarized below.

COIL LOCATION NUMBER (2):

IRT Test (4) Chordwise Peak: 2,710 micro-strain  
 162 Joules Spanwise Peak: 1,820 micro-strain  
 Upper Sfc. Maximum Stress: 37,200 psi  
 IRT Test (8) Chordwise Peak: 2,520 micro-strain  
 156 Joules Spanwise Peak: 1,590 micro-strain  
 Upper Sfc. Maximum Stress: 34,300 psi

COIL LOCATION NUMBER (3):

IRT Test (4) Chordwise Peak: 2,730 micro-strain  
 162 Joules Spanwise Peak: 1,840 micro-strain  
 Upper Sfc. Maximum Stress: 37,500 psi  
 Lower Sfc. Chordwise Peak: 3,030 Micro-strain  
 IRT Test (8) Chordwise Peak: 2,510 micro-strain  
 156 Joules Spanwise Peak: 1,600 micro-strain  
 Upper Sfc. Maximum Stress: 34,200 psi  
 Lower Sfc. Chordwise Peak: 2,810 micro-strain

COIL LOCATION NUMBER (6):

IRT Test (4) Chordwise Peak: 2,050 micro-strain  
 128 Joules Spanwise Peak: 1,010 micro-strain

Upper Sfc.	Maximum Stress:	26,900 psi
IRT Test (8)	Chordwise Peak:	2,100 micro-strain
125 Joules	Spanwise Peak:	974 micro-strain
Upper Sfc.	Maximum Stress:	27,300 psi

Coils 2 and 3 produce maximum stress values of 37,000 psi at the desired de-icing levels on the upper surface; this is extrapolated to 40,000 psi for the lower surface. While these values remain well below the yield strength for the material, the question of long term fatigue remains unanswered at this time. The skin mounted coil pair located at position 6, is clearly superior to the spar mounted configurations, with a maximum stress of 27,000 psi. The fatigue longevity of this configuration needs to be addressed.

#### IV. 2.5 Inch Radius Semi-Cylinder Studies.

##### A. Experimental Results.

During April 1984, a semi-cylindrical leading edge type structure was designed and tested by Mr. Robert Friedberg as partial fulfillment of his graduate study program at Wichita State University. The semi-cylinder was selected as a representative candidate for deicing studies, an experimental data base, and subsequent analytical modeling. The semi-cylinder is 66 inches in length, an inside radius of 2.5 inches, and skin thickness of 0.040 inches. The material used in the fabrication was 2024-T3. The semi-cylinder is attached to a reasonably rigid spar fabricated from a fiberglass covered 40 pound density 3/4 inch thick foam core, it has no internal ribs or bulkheads except the closure ribs at each end. The semi-cylinder is attached to the spar and closure ribs with No. 10 sheet metal screws spaced two inches center to center. The semi-cylinder was equipped with two coil configurations, a single coil and a pair of series connected double coils for two different IRT tests. The first IRT test was performed on May 19, 1984 and employed a single coil located at the nose and mid-length of the semi-cylinder as shown in Fig. 3-16. The coil had a nominal radius of 1.25 inches with 50 turns of rectangular copper conductor and shaped to conform to the internal radius with provision for a 0.010 inch air gap.

Acceleration data was established for the single coil configuration and is displayed in Figs. 3-14 and 3-15 for the energy level of 36 Joules as noted. The accelerometer used in the investigation was an Endevco Model 22, which has a total weight with the attached cable of 0.4 grams and a physical size of 0.14 inches diameter, 0.095 inches in height and a response level of approximately 12,000 g's. Mass loading of the light weight aluminium leading structures is an important consideration and this particular accelerometer has the largest g level per unit mass known to project personnel. Fig. 3-14 represents the spanwise variations of acceleration measured in three inch increments from mid-span. The data for  $S=+3"$  and  $S=-3"$  should of course be identical. The discrepancies shown are well within the variation of the shell boundary conditions and un-symmetric positioning of the coil. The spanwise response delays, indicated by the dashed line, is interesting and probably represents the longitudinal propagation of a circumferential bending wave. The velocity is on the order of 65,000 inches per second. The chordwise variations of acceleration, shown in Fig. 3-15, should again be equal for positions either side of the nose, e.g.  $C=+2"$  and  $C=-2"$ . It is further noted that the 200 microfarad capacitance results produces peak accelerations whose magnitude of 10 kilo-g's is approximately twice those corresponding to the 400 microfarad results. This is attributed to the increased rise time for the EIDI pulse for smaller values of capacitance, and dramatizes the structural

response sensitivity to changes in the EIDI electrical parameters.

Strain gages were installed on both the inner and outer surfaces of the semi-cylinder at mid-span. The position and numerical designation of each gage is noted in Fig. 3-16. Strain data was established for the single coil configuration for an energy level of 128 Joules; 400 microfarads and 800 volts. Compensated gages were installed and the DC-bridge process was employed for the measurements. The data is presented in Figs. 3-17 through 3-20 for each of the four gage positions as analog records and includes the principal occurrence times for strain peaks. Some data is further presented as bending and membrane strains. Peak occurrence times for the chordwise and spanwise peaks do not coincide, hence it is difficult to establish the maximum stress values. The experimental strains indicate maximum values of about 1100 micro-strain, which corresponds to maximum stresses on the order of 14,000 psi for the 128 Joule test condition. The energy level used in the IRT test of May 19, 1984 was 162 joules; 400 microfarads and 900 volts. The corresponding stress level for this test condition is approximately 17,700 psi.

An additional test was conducted on gage position (1) to establish the spanwise membrane strain for three different capacitance values and equal energy levels. The data is displayed in Fig. 3-21 and clearly indicates the decreasing rise time of the strain response as the capacitance is decreased. The current delivered to the coil is also displayed with the membrane strain. Case (3) of this test, evaluated for a capacitance of 100 microfarads, serves as a measure of the maximum strain-rate response experienced for a EIDI pulse. The peak of 1300 micro-strain occurring at 141 microseconds represents an approximate strain-rate of 10 per second, which could reach 40 to 50 per second for increased values of voltage. Most authorities, Ref. 3-5, consider values below 100 per second as a intermediate strain-rate regime where quasistatic stress-strain properties are still applicable. Strain-rates in excess of 1000 per second are normally associated with elastic-plastic shock wave propagation and hence the EIDI pulse may be classified as a very mild shock environment.

The semi-cylinder was configured with a pair of EIDI coils and a second IRT test was conducted on August 17, 1984. The coils were connected in series, placed at mid-span, and oriented at equal angles of 45 degrees measured from the nose. The radius of each coil was 0.875 inches and shaped to conform to the cylindrical surface with an air gap. The established de-icing level was approximately 170 to 200 joules. The 400 microfarad and 1000 volt test condition was subjectively evaluated as optimum. The double coil configuration failed to perform as well as the single coil and this is attributed to the angular position of the coils from the nose. An angle of less than 45 degrees or the ability to independently pulse each coil would

probably have been more efficient. A limited amount of strain data was acquired for the double coil configuration and this is presented in Fig. 3-22. During the August 17 IRT test, some data was acquired for the double coil configuration under icing conditions. The results confirmed earlier observations related to acceleration in that the peak values are reduced by approximately 20 to 30 per cent for the first pulse when ice is present on the airfoil. Circumferential bending strains for the double coil test exhibited reductions of approximately 15 to 25 per cent for the first coil pulse whereas the membrane strains remained basically unchanged.

## B. Analytical Results.

The semi-cylindrical leading edge structure was chosen for analytical study because of its geometric simplicity and the vast literature which exists for open cylindrical shells. Leissa, Ref. 3-6, reports that there are no less than 18,496 distinct problems for this shell corresponding to the numerous combinations of boundary conditions that may be selected for the four edges. An overwhelming majority of investigations have been directed to but one of these sets of boundary values and that is when all edges of the shell are supported by shear diaphragms. The semi-cylinder is further classified as a deep open shell requiring a consideration of the transverse shearing force resultants and the inclusion of tangential inertia effects for dynamic studies.

The boundary conditions for an open cylindrical shell supported by shear diaphragms are exactly satisfied by choosing trigonometric displacement functions of the form:

$$\begin{aligned} u &= A \cos(\lambda s) \sin(N\Theta) && \text{longitudinal displacement,} \\ v &= B \sin(\lambda s) \cos(N\Theta) && \text{transverse displacement,} \\ w &= C \sin(\lambda s) \sin(N\Theta) && \text{normal displacement;} \end{aligned}$$

where,  $\lambda s = M\pi x/L$   $R$ =shell radius  $L$ =shell length.

The parameters  $\lambda = M\pi/L$  and  $N$  are spatial wave frequencies with half wave lengths defined as follows:

$$\begin{aligned} (L/M) & \text{ longitudinal direction,} \\ (R\pi/N) & \text{ circumferential direction.} \end{aligned}$$

A computer code was written based on these ideal boundary conditions that employed both the Donnell-Mushtari and Love-Timoshenko equations of motion. The code was used in an attempt to duplicate some of the dynamic response effects observed in the experimental results. The values of 'M' and 'N' in the spatial wave frequency expressions are integers and combinations of each will produce a corresponding discrete resonant frequency and vibratory mode shape. The first analytic study was related to finding the maximum values of these integers for a selected bandwidth or cutoff frequency. The results of this study are summarized in the table below for a semicylindrical shell with the following geometric shape and material properties.

$L=66$  inches  $R=2.52$  inches  $H=0.040$  inches (thickness).

$E=10,500,000$  psi  $\nu=0.30$  Poisson's ratio

0.10 pounds per cubic inch weight density.

Bandwidth Hertz	M(max)	N(max)	Love-Timoshenko Mode Count
3,000	20	7	95
4,000	27	8	148
6,000	40	9	265
8,000	54	11	434
10,000	67	12	623

The calculated dynamic response of the spanwise and chordwise acceleration levels with a single coil placed at mid-span was performed using the electrical parameters; 400 microfarads and 424 volts. The cutoff frequency was selected as 10,000 Hertz and the results are displayed in Fig. 3-23. The structural damping parameter used in this investigation is noted as a 1 percent damping factor at 1,000 Hertz; thus a frequency of 4,000 Hertz would have a corresponding damping factor of 4 percent. The calculated response has several matching characteristics with the experimental response shown in Fig. 3-16, in spite of the fact that the boundary conditions do not match for the two results. In addition, the temporal behavior of the 400 microfarad pulse was synthesized from the 600 microfarad experimental result reported by Schrag, Ref. 3-1. It is further observed that 155 of the potential 623 modes were active or participated in the dynamic response, the remaining 468 modes were inactive due to the spatial symmetry of the pressure pulse. Moving the coil a slight distance in both the spanwise and chordwise directions from the symmetric nose and mid-length position will force a majority of the modes to participate, however the peak response values will change only slightly as shown in the upper portion of Fig. 3-24, even though 607 modes were active. The peak accelerations and corresponding occurrence times from Fig. 3-24 are noted below:

First Positive Peak: 3,619 g's at 112 microsec.

First Negative Peak: -2,960 g's at 288 microsec.

Fig. 3-25 is a display of the contribution of each of these 607 active modes to the two acceleration peaks noted above. The results are shown in an ascending frequency order and the two peak response accelerations have attained about 95 percent of their final value for a corresponding cutoff frequency of approximately 4,000 Hertz. This result is rather important for finite element shell studies, for it suggests that the approximate discrete model need only match the modal frequencies for the reduced bandwidth to produce a 92 percent confidence limit in peak response prediction. The lower portion of Fig. 3-24 represents the acceleration response corresponding to a

4,000 Hertz cutoff frequency.

Two additional plots, Figs. 3-26 and 3-27 are included to present the analytical predicted mid-span circumferential strain response for the outer and inner surface and may be compared directly to the experimental results displayed in Figs. 3-17 through 3-20. The correlations agree in that longitudinal strains are dominated by membrane effects, whereas bending behavior is dominant in the circumferential strain response. Again, the results only indicate similarity to the experimental results and the peak response occurrence times cannot be accurately matched until the boundary conditions and forces pulse characteristics are properly represented.

An additional analytical study related to the semi-cylindrical leading edge simulation is being conducted by two M.S. graduate students in Aeronautical Engineering. Mr. Peter Gien is documenting the closed form solution characteristics and Mr. Bryan Wilson is concerned with a matching finite element representation using the MSC/NASTRAN code. Their semi-cylinder is identical to the aforementioned study with the single exception of a selected 30 inch length. Their parallel investigations will result in direct comparisons of the acceleration and strain dynamic response using modal expansion solutions.

The finite element model employs the popular 'QUAD4' element and the study contains a correlation of the element size to the half wave lengths described above. Letting 'a' and 'b' be the longitudinal and chordwise dimensions of the 'QUAD4' element, the following requirements must be satisfied.

$$a \leq L/M \quad \text{and} \quad b \leq R/T/N.$$

Thus, the required size of the 'QUAD4' elements is determined from the values of 'M' and 'N', which in turn are dependent on the bandwidth or cutoff frequency. These results are summarized below for a 30 inch long semi-cylinder.

Bandwidth	Love-Timoshenko			a=L/M	b=R/N
Hertz	M(max)	N(max)	Mode Count	(inches)	(inches)
2,000	6	5	21	5.00	1.58
3,000	9	7	42	3.33	1.13
4,000	12	8	65	2.50	0.99
5,000	15	9	92	2.00	0.88
6,000	18	9	119	1.67	0.88
7,000	21	10	154	1.43	0.79
8,000	24	11	193	1.25	0.72

Based on these data, Mr. Wilson selected square "QUAD4" elements with a dimension of 0.75 inches. An eigensolution of this model exhibited a very strong mode correlation with the closed form results which may be summarized as follows:

Bandwidth Hertz	Mode Count	Frequency Maximum Error	Frequency Average Error
2,000	22	2.9 % @ 1948 Hz.	1.43 %
3,000	42	5.9 % @ 2744 Hz.	2.14 %
4,000	65	11.6 % @ 3874 Hz.	3.44 %
5,000	92	21.3 % @ 4556 Hz.	4.80 %

In general, the finite element model together with its discrete boundary conditions appears to present a slightly stiffer shell as 56 of the 65 frequencies are larger than the corresponding closed form solution values. It is also interesting to note that the Love-Timeshenko equations of motion yield the best correlation of frequencies with the finite element model and they are clearly superior to the Donnell Mushtari shell equations. The anticipated completion date for their final results and conclusions is May 1985.

Mr. Dan Christmore, who is a Ph.D. candidate in Aeronautical Engineering has presented a dissertation proposal that would extend the work of Mr. Gien and Mr. Wilson to the full 66 inch length semi-cylinder with boundary conditions selected to match the experimental model. This will hopefully permit a more accurate correlation of experimental and analytical results. His proposal also includes a finite element model analysis of a representative airfoil leading edge structure with a comparison to experimental results and some parametric studies related to coil selection and placement for a desired performance criteria.

## V. Recent Developments Related To EIDI Force Measurements.

The impulse strength of a EIDI pulse may be obtained from a basic ballistic pendulum test. Schrag, Ref. 3-1, and others Ref. 3-3, have published such results corresponding to various coil parameters, air gaps, and metallic target properties. In addition, Schrag has conducted a single experiment utilizing a special field measuring plate to establish both the normal spatial pressure and temporal distributions. The spatial integral of the of the pressure distribution data yields the temporal force whose time integral agreed closely with the ballistic pendulum result. The results of this experiment are summarized in Fig. 3-28.

Several different experimental procedures have been attempted to obtain a direct measurement of the temporal behavior of a EIDI force pulse. Most of these have given unsatisfactory results which are attributed to combinations of magnetic effects, mass loading, and eccentricities in the measurement transducer. A recent experimental investigation has been initiated that shows considerable promise. The procedure involves the longitudinal pulse propagation characteristics of a small diameter polycarbonate non-magnetic rod suspended as a pendulum. The basic experiment is summarized in Fig. 3-29. The solution to the one dimensional wave equation, when applied to a elastic rod, yields the following well known relationship.

$$f(0,t) = (\rho A c / 2) V(L, t + L/c)$$

where:  $f(0,t)$  = force pulse at  $x=0$ ,  
 $t$  = time,  
 $\rho$  = mass density of the rod,  
 $A$  = cross sectional area of the rod,  
 $L$  = length of the rod,  
 $c$  = velocity of propagation;  $c = E/\rho$ ,

$V(L, t + L/c)$  = particle velocity at  $x=L$ ,

$L/c$  = time delay for the rod, ( $\tau$ ).

This simple model is subject to the following limiting conditions:

- (1) The force pulse must correspond to a uniform stress over the cross section.
- (2) Radial inertia effects are not included in the mathematical model and thus dispersion is neglected.

(3) The rod material is elastic and energy dissipation is negligible; i.e., no damping.

The force pulse is approximately 1200 to 1400 microseconds in duration, thus the rod should have a delay time of 600 micro-seconds or larger. The 48 inch length of polycarbonate rod used in the experiments has a delay time of approximately 850 microseconds.

The experiment basically involves the measurement of acceleration at the free end of the rod, followed by an integration to yield the particle velocity, and then multiplying by the impedance ( $pAc/2$ ). A typical acceleration and corresponding particle velocity time response are presented in Fig. 3-30 for a 3 inch diameter rod, 49.2 inches in length. The velocity trace shows evidence of dispersion; e.g., a broadening of the pulse width for successive reflections and some attenuation due to material damping. It is difficult to establish the exact starting time for the force pulse due to the dispersive effects. Fig. 3-31 is a comparison of the force pulse developed by Schrag, Ref. 3-1, and the measured force pulse for two different arrival times;  $\tau=800$  and 850 microseconds as noted.

Fig. 3-32 presents the predicted force pulse for a 2 inch diameter polycarbonate rod 48 inches in length. The upper portion of the figure represents the measured response for a fixed value of capacitance, 600 microfarads, and three different values of voltage; 400, 500, and 600 volts. Theoretically the peak amplitudes should be proportional to the square of the voltage ratios. The measured results are remarkably accurate. The lower portion of the figure depicts the measured force pulse for three different values of capacitance while maintaining a constant energy value. The decrease in both the rise time and the first zero crossing time are entirely consistent with expectations.

Kolsky, Ref. 3-7, has presented a Fourier synthesis procedure that employs experimental dispersion and attenuation versus frequency relations to predict the correct form of a dispersed and attenuated pulse. The inverse of this technique is currently being investigated to serve as a classical form of pulse identification problem. Preliminary dispersion data has been established for the 2 inch diameter polycarbonate rod by passing the accelerometer signal through a narrow bandpass filter and noting the pulse arrival time,  $\tau$ . The phase velocity ( $L/\tau$ ) is thus established for the rod corresponding to the center frequency of the filter. The phase velocity at 250 Hertz is approximately 33,000 inches per second and increases to a stationary value of approximately 55,000 inches per second at 8,000 Hertz. This agrees closely with a static test where the modulus of elasticity was determined as 341,000 psi and a corresponding propagation velocity of 54,400 inches per second. It is anticipated that this experimental investigation will be completed by August 1985.

## VI. References

- (3-1) R. L. Schrag and G. W. Zumwalt, "Electro-Impulse De-icing: Concept and Electrodynamic Studies", AIAA 22nd Aerospace Sciences Meeting, Reno, NV, Jan. 9-12, 1984, Paper No. 84-0021.
- (3-2) W. D. Bernhart and G. W. Zumwalt, "Electro-Impulse De-icing: Structural Dynamic Studies, Icing Tunnel Tests and Applications", AIAA 22nd Aerospace Sciences Meeting, Reno, NV, Jan. 9-12, 1984, Paper No. 84-0022.
- (3-3) R. M. Bowley, et. al. "Production of Short Mechanical Impulses by Means of Eddy Currents", IEEE Proc., V. 130, Pt. B, No. 6, p.415-423, Nov. 1983.
- (3-4) Measurements Group, Inc., Raleigh, NC, "Strain Gages Operate in 50,000 Gauss Magnetic Fields for Fusion Research", Epsilonics, Vol. II, Issue 3, Dec. 1982.
- (3-5) J. A. Zukas, et. al., "Impact Dynamics", John Wiley & Son, New York, 1982.
- (3-6) A. W. Leissa, "Vibration of Shells", NASA SP-288, 1973.
- (3-7) H. Kolsky, "The Propagation of Stress Pulses in Viscoelastic Solids", Phil. Mag., 8, 1956, pp. 693-710.

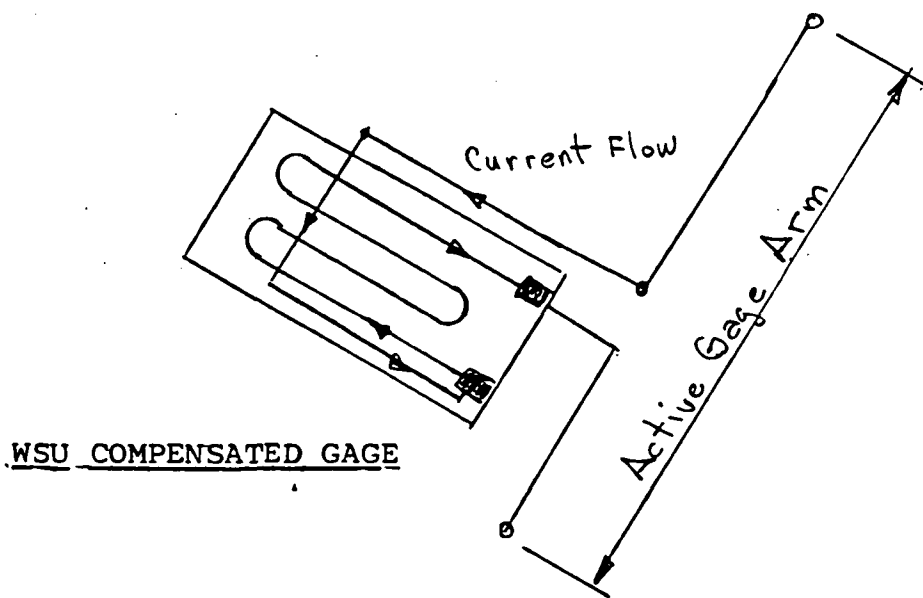
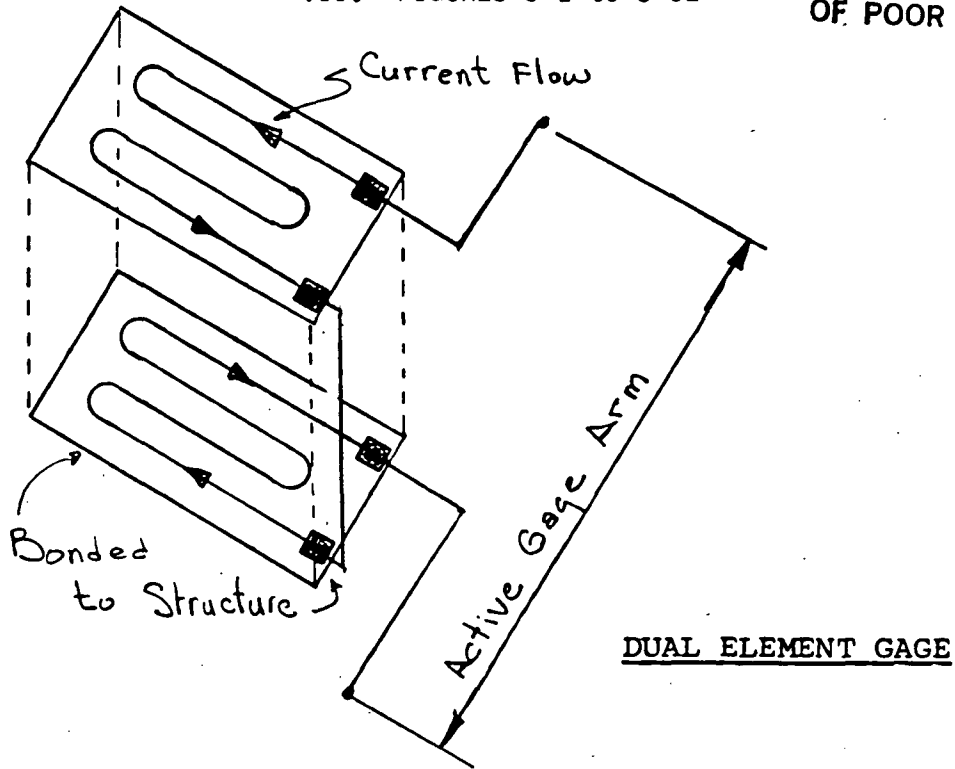
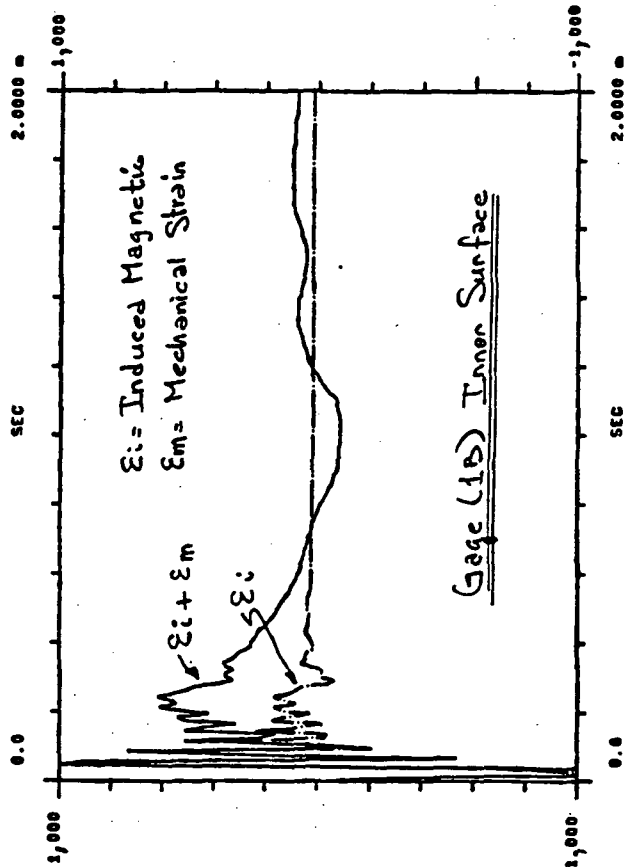
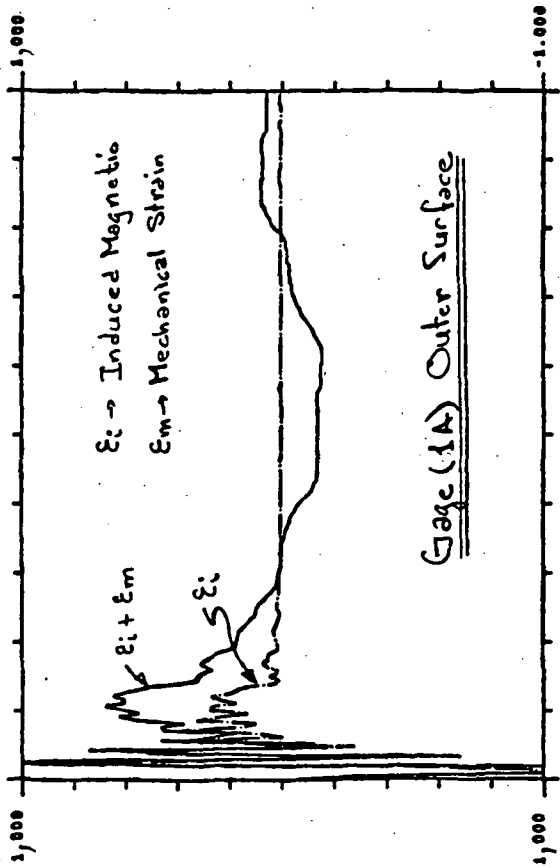
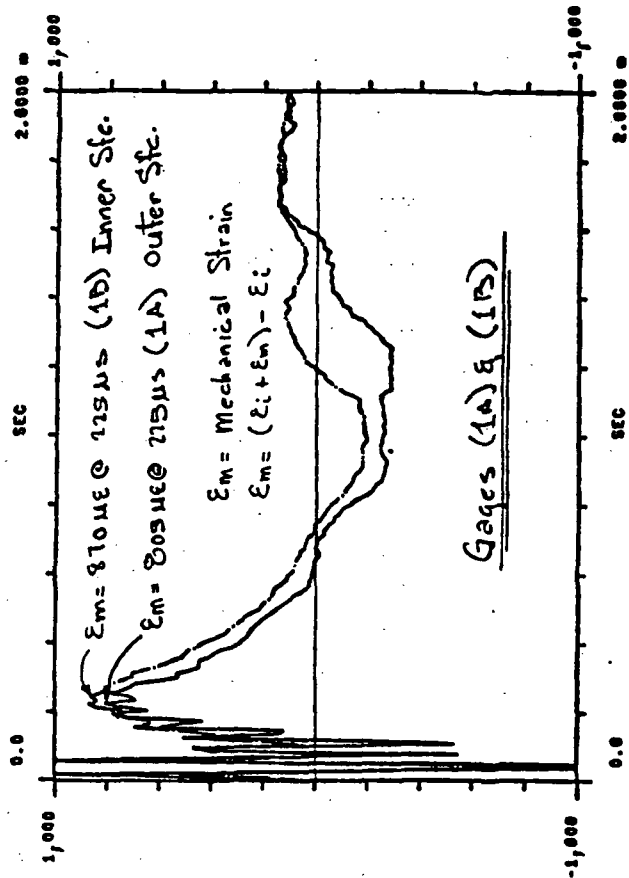


FIGURE 3-1. DUAL ELEMENT GAGE AND WSU COMPENSATED GAGE,



2.5" RADIUS SEMI-CYLINDER (SINGLE COIL). JULY 18, 1984.  
 LONGITUDINAL (SPANWISE) STRAIN: (C-400 V-800 126 JOULES).

ORIGINAL PAGE IS  
 OF POOR QUALITY

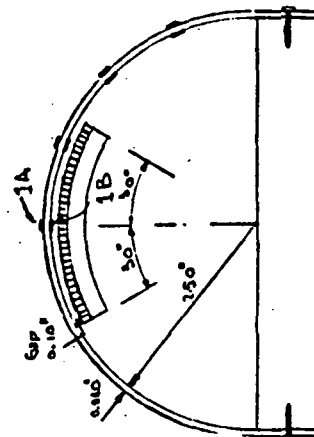


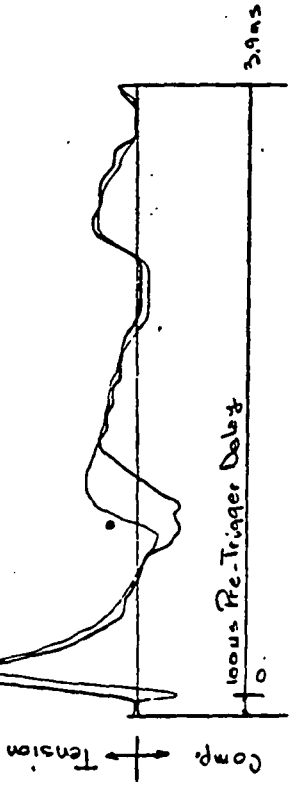
FIGURE 3-2. DC-BRIDGE STRAIN MEASUREMENT (10 MICRO-SECOND SAMPLE TIME).

Gages 1A & 1B

$\epsilon_m \rightarrow$  Mechanical Strain

$\epsilon_m (\epsilon_i + \epsilon_m) - \epsilon_i$

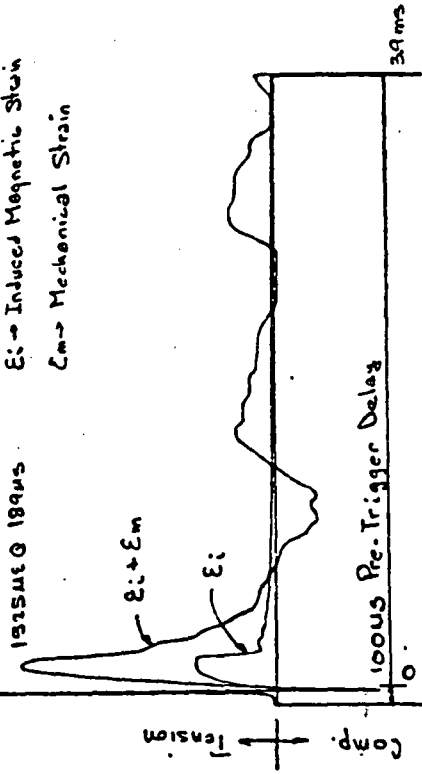
$\epsilon_m = 1038 \mu\epsilon @ 192 \mu s$  (1A) Outer Surface  
 $\epsilon_m = 898 \mu\epsilon @ 219 \mu s$  (1B) Inner Surface



Gage 1A. Outer Surface

$\epsilon_i \rightarrow$  Induced Magnetic Strain

$\epsilon_m \rightarrow$  Mechanical Strain

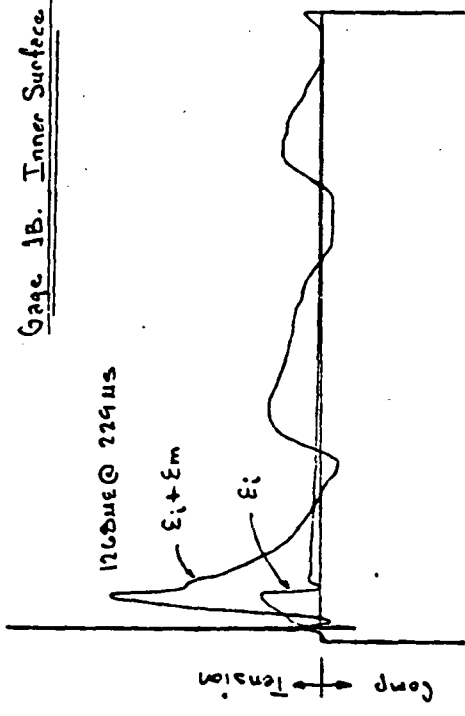


Gage 1B. Inner Surface

1760uT @ 219us

$\epsilon_i + \epsilon_m$

$\epsilon_i$



2.5" RADIUS SEMI-CYLINDER (SINGLE COIL). JULY 18, 1984.  
 LONGITUDINAL (SPANWISE) STRAIN: (C-400 V-800 V-800 128 JOULES).

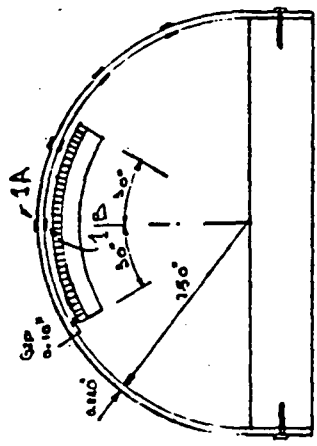


FIGURE 3-3. DC-BRIDGE STRAIN MEASUREMENT (1 MICRO-SECOND SAMPLE TIME).

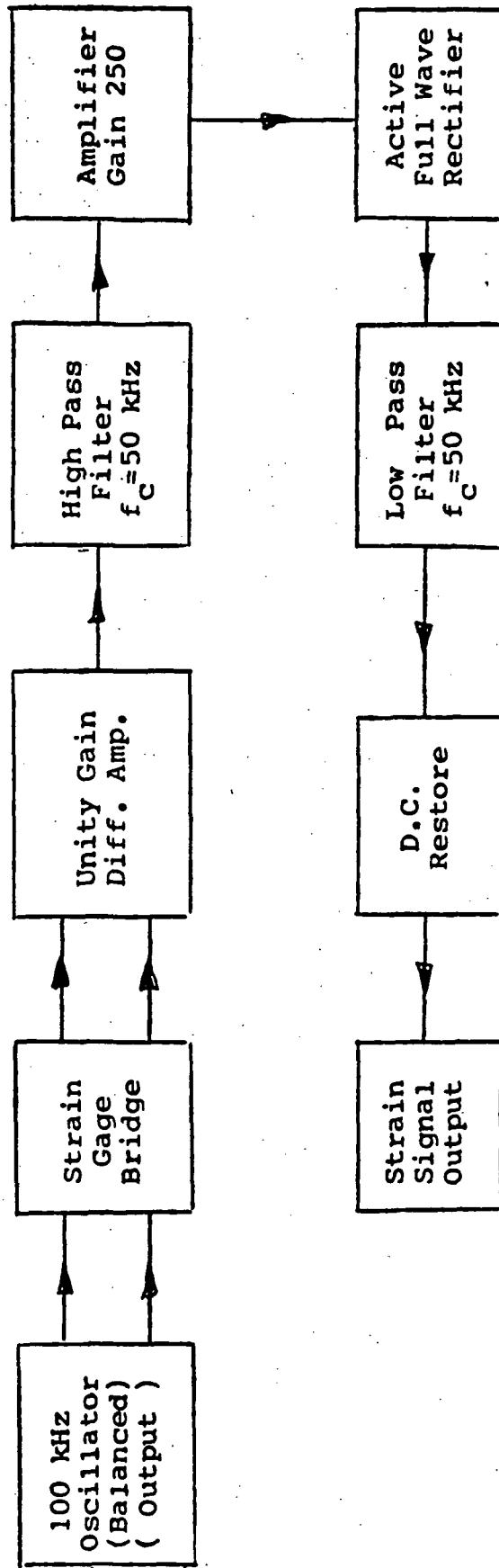


FIGURE 3-4. AC-BRIDGE STRAIN MEASUREMENT SYSTEM.

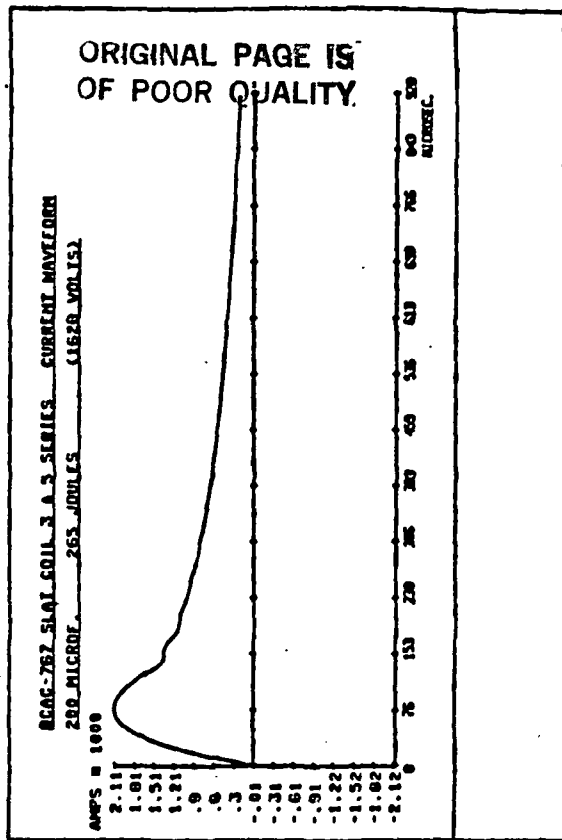
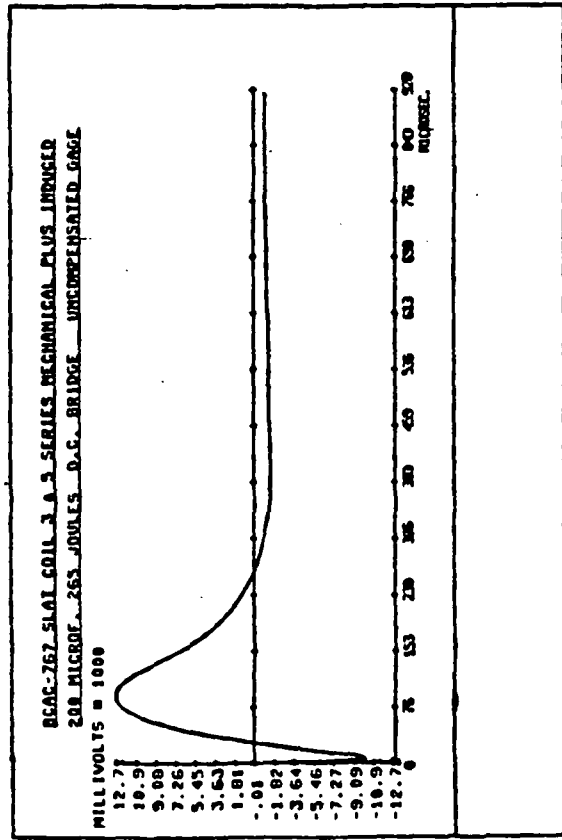
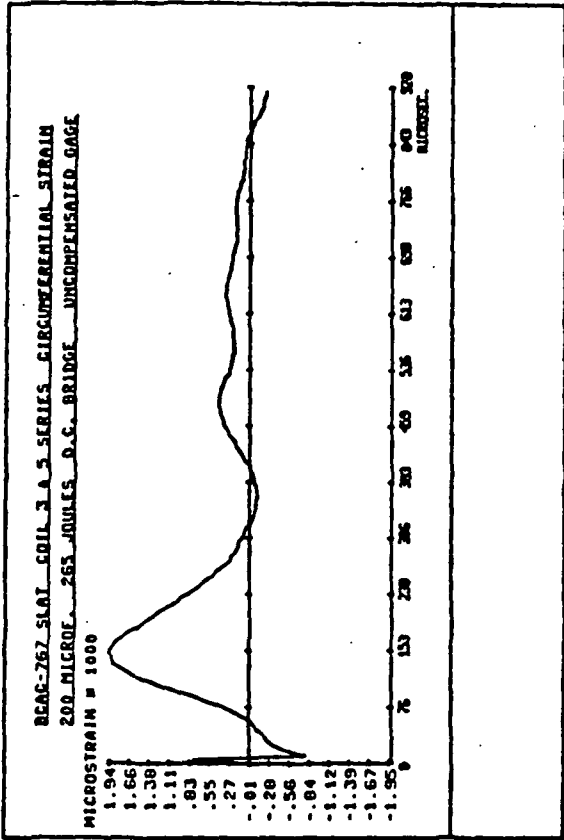
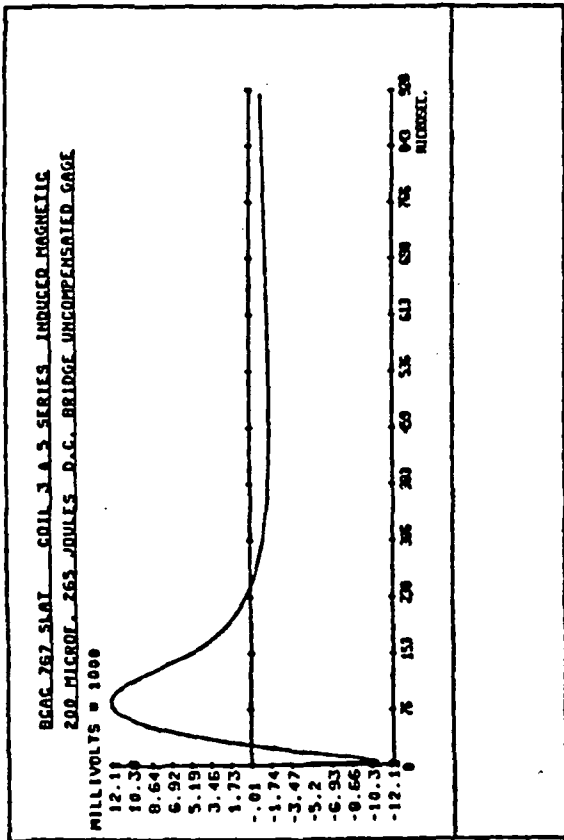


FIGURE 3-5. DC-BRIDGE STRAIN MEASUREMENT (NONCOMPENSATED GAGE).

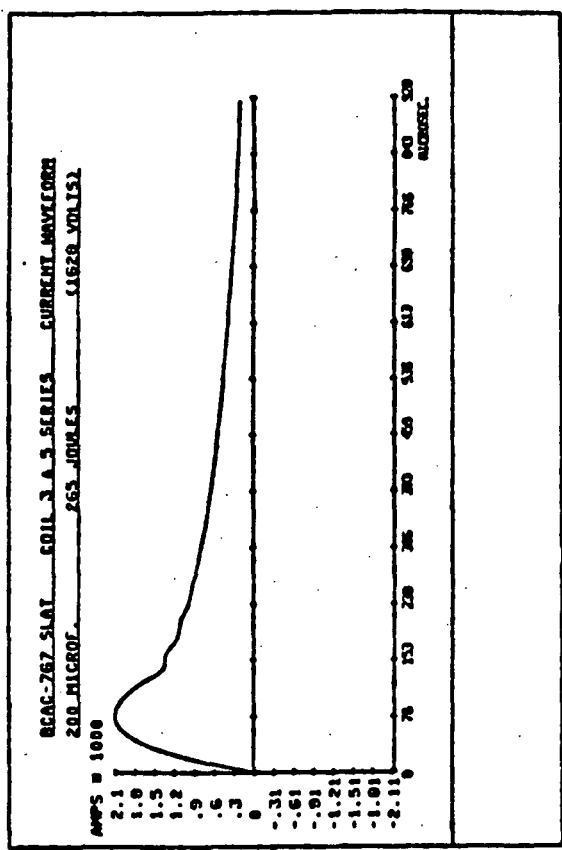
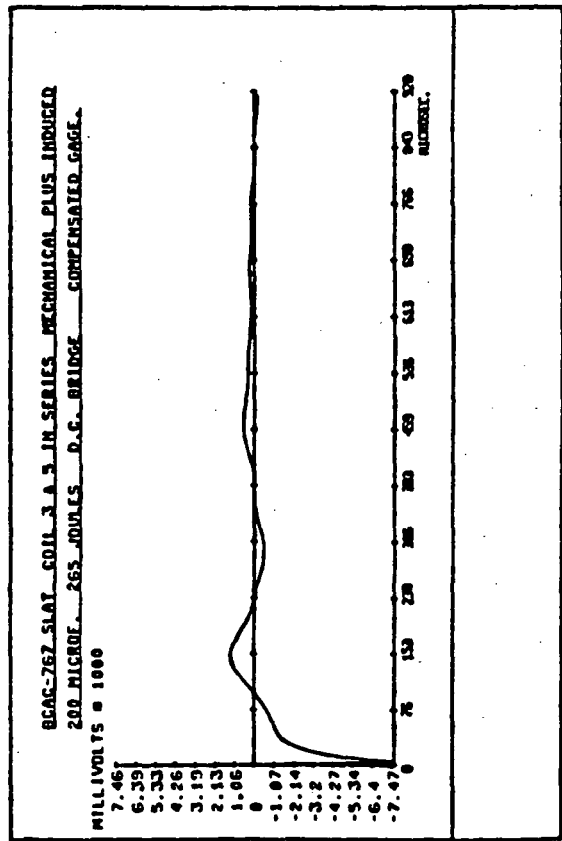
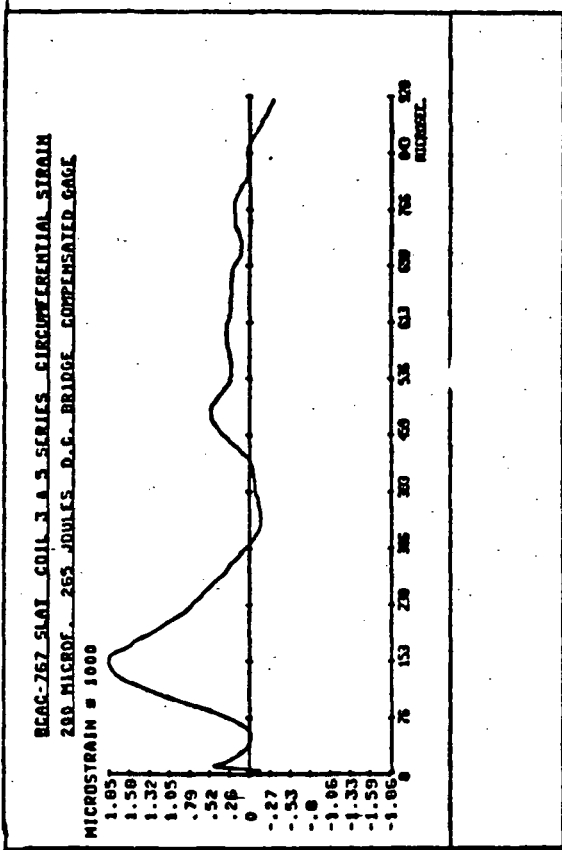
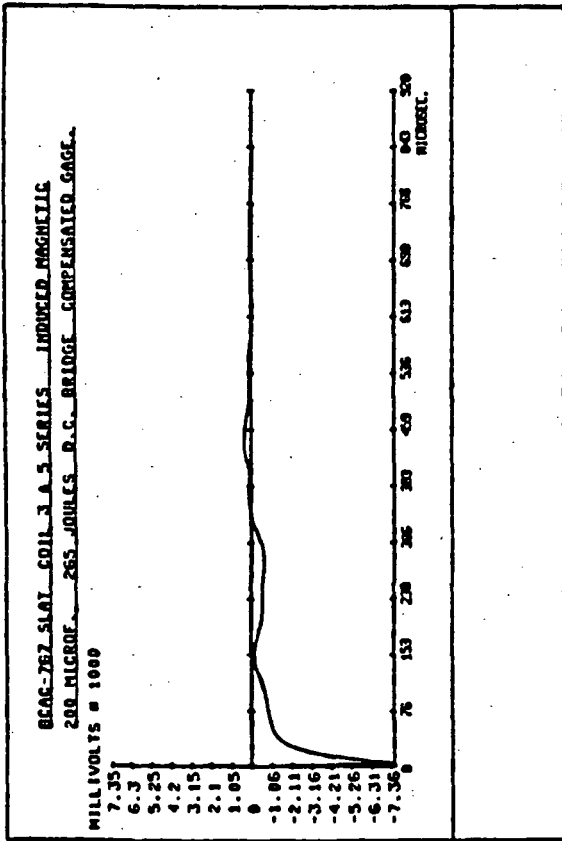


FIGURE 3-6. DC-BRIDGE STRAIN MEASUREMENT (COMPENSATED GAGE).

ORIGINAL PAGE IS  
OF POOR QUALITY

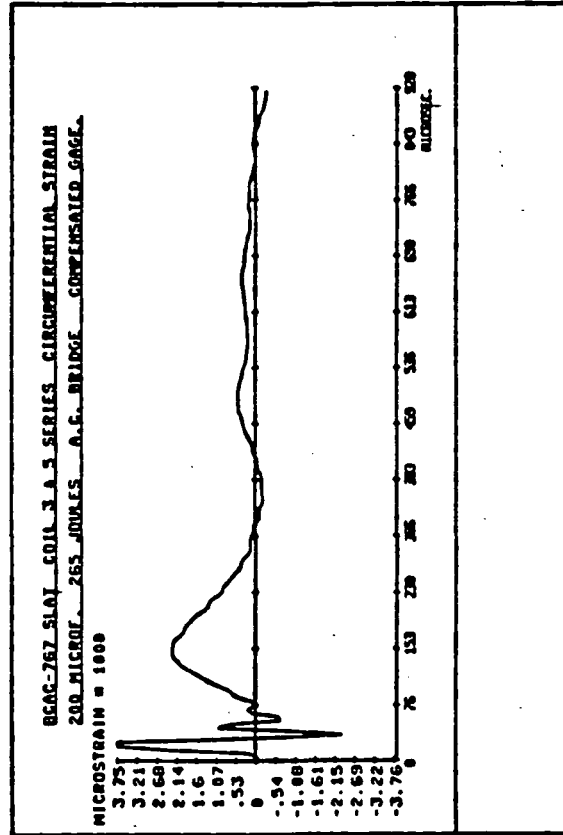
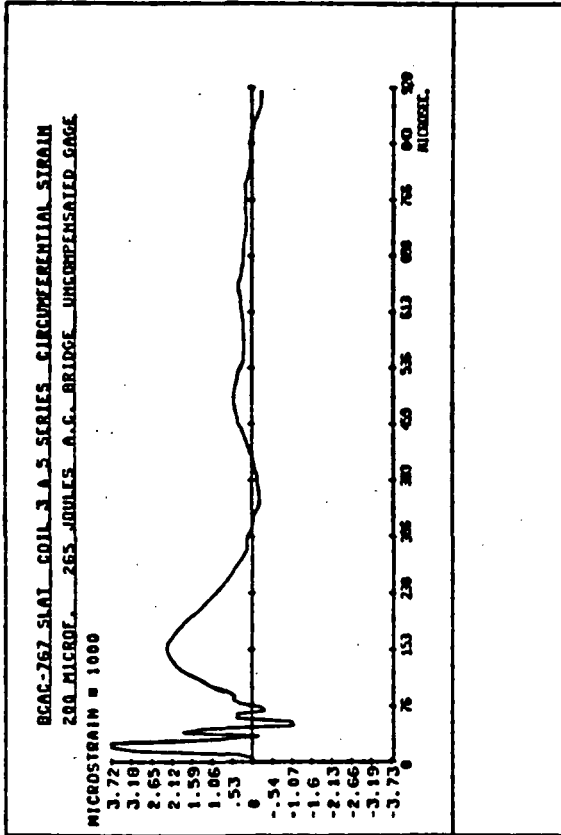


FIGURE 3-7. AC-BRIDGE STRAINS (NONCOMPENSATED AND COMPENSATED GAGE).

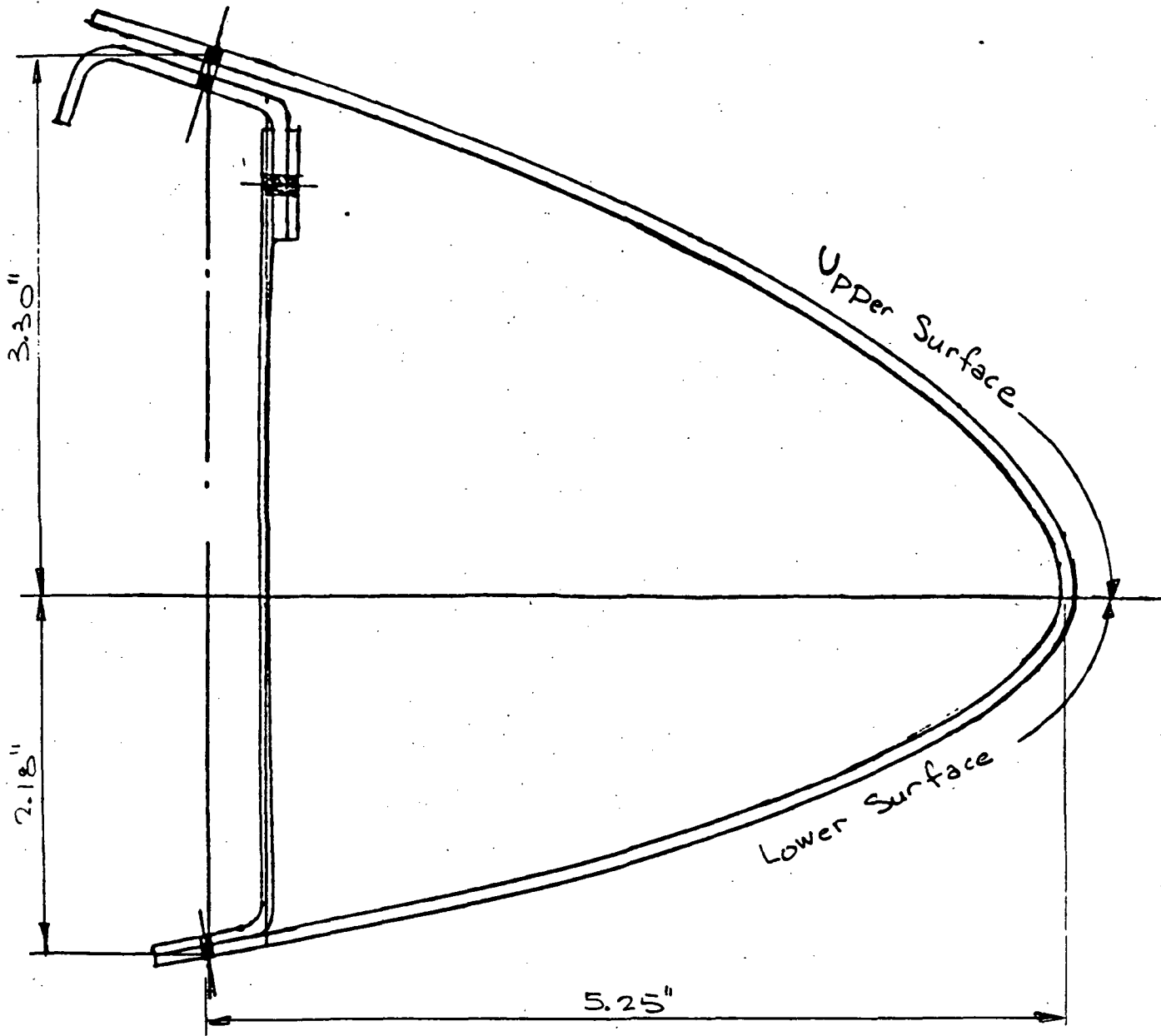


FIGURE 3-8. BOEING (BCAC) 767 LEADING EDGE SLAT CAVITY.

ORIGINAL PAGE IS  
OF POOR QUALITY

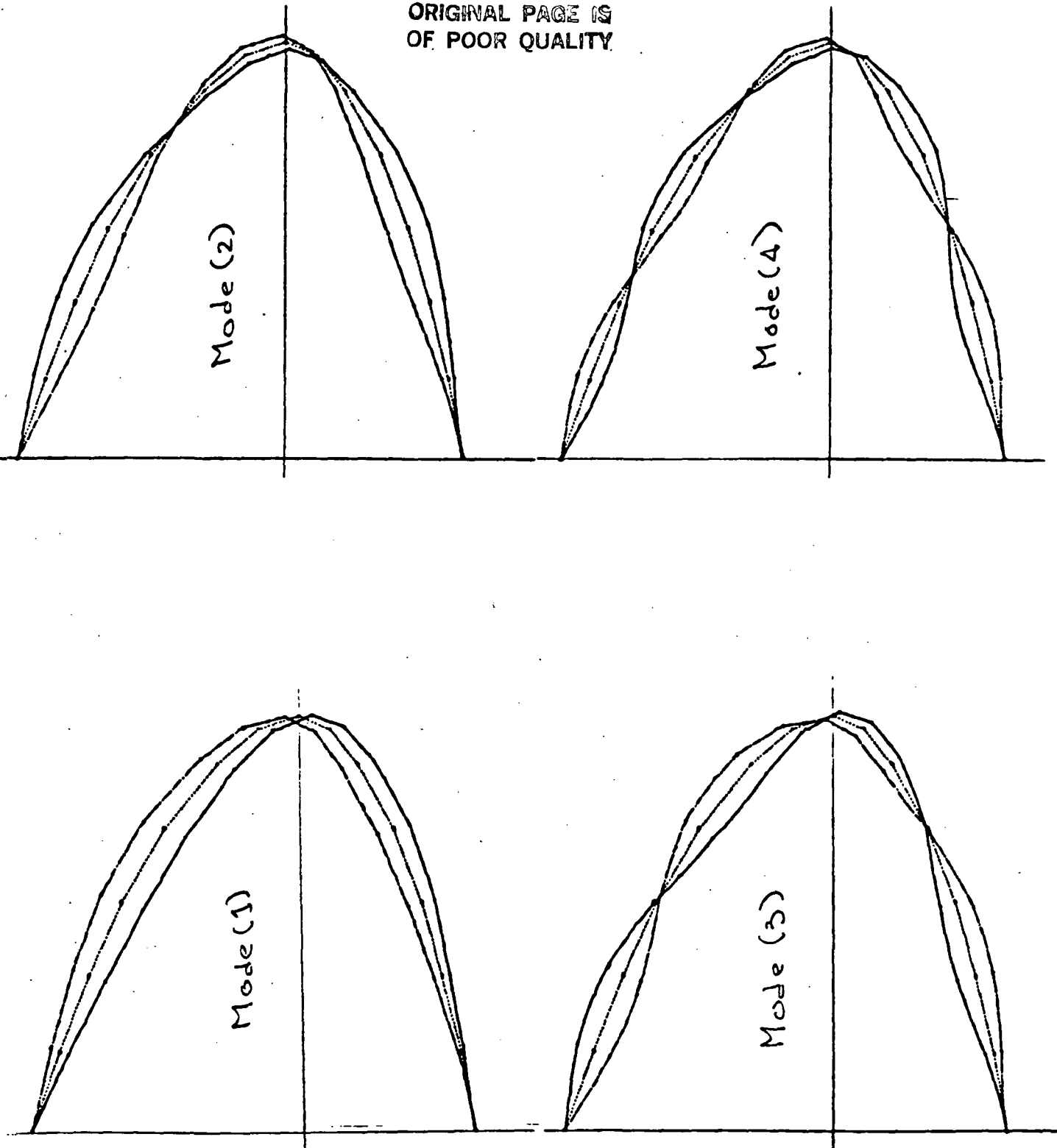


FIGURE 3-9. BCAC-767 L.E. SLAT. COPLANAR MODE SHAPES.

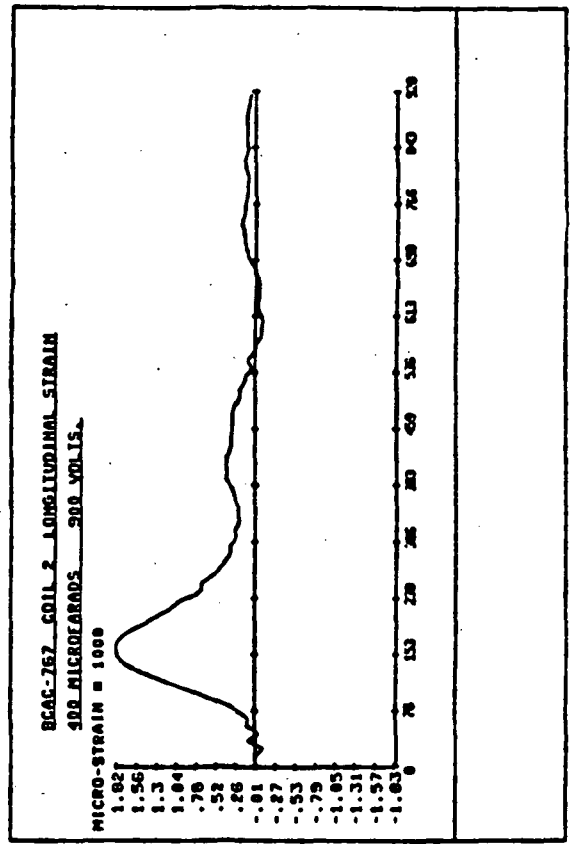
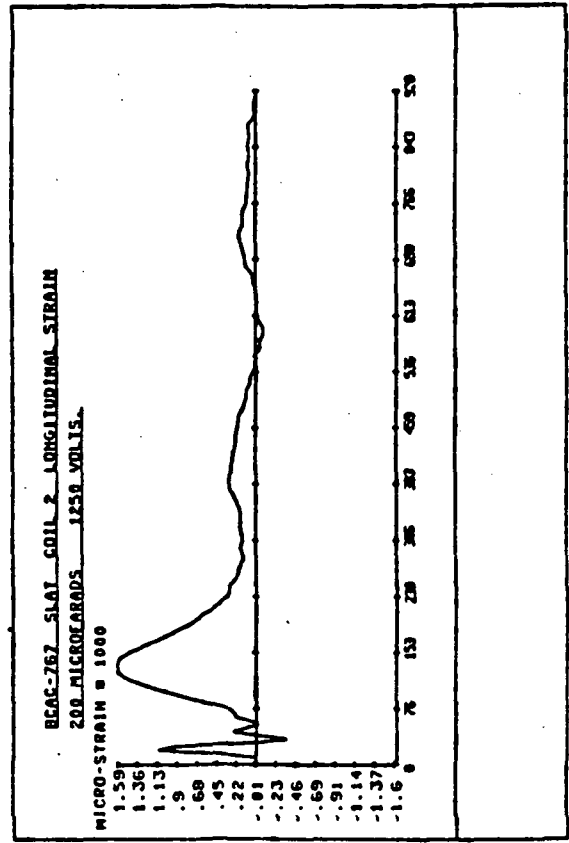
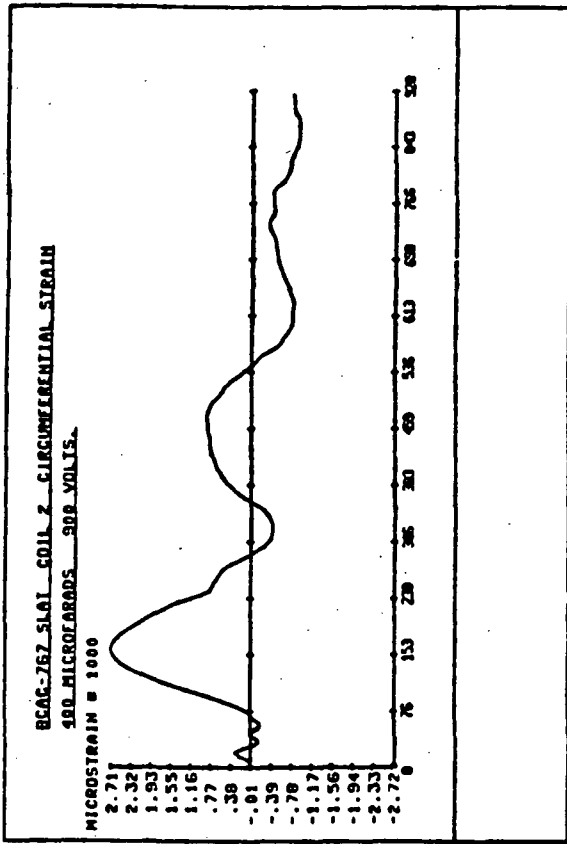
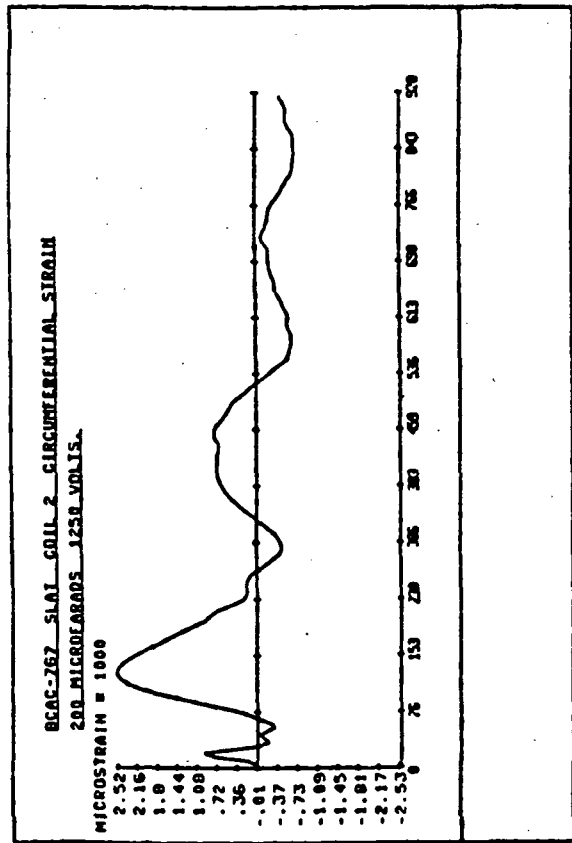


FIGURE 3-10. BCAC -767 L.E. SLAT. STRAINS AT COIL 2 (UPPER SURFACE).

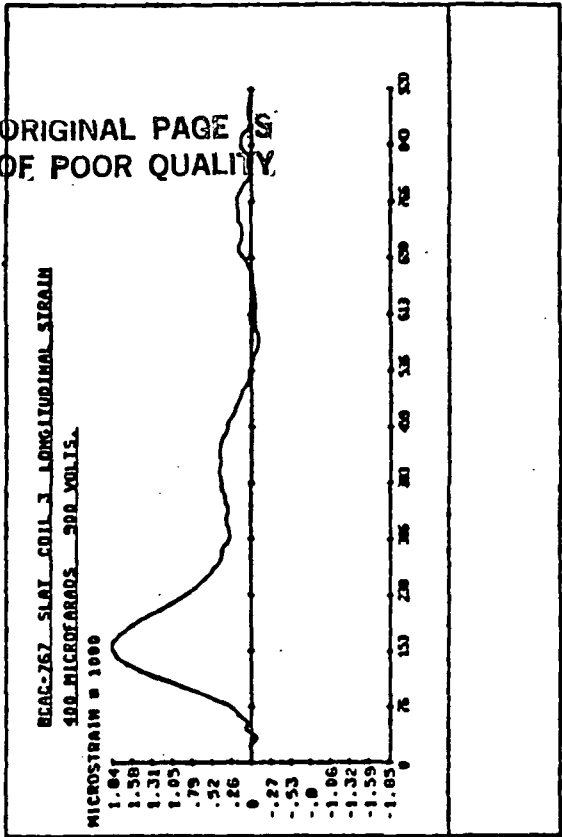
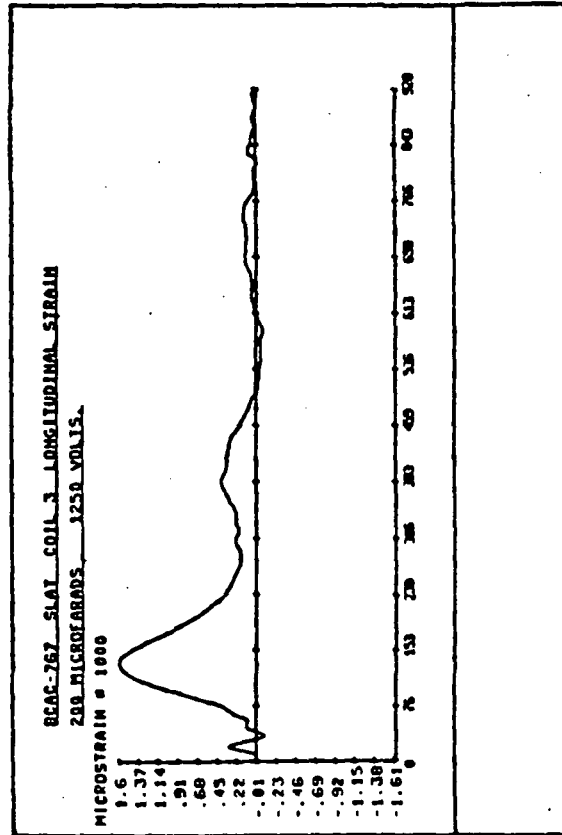
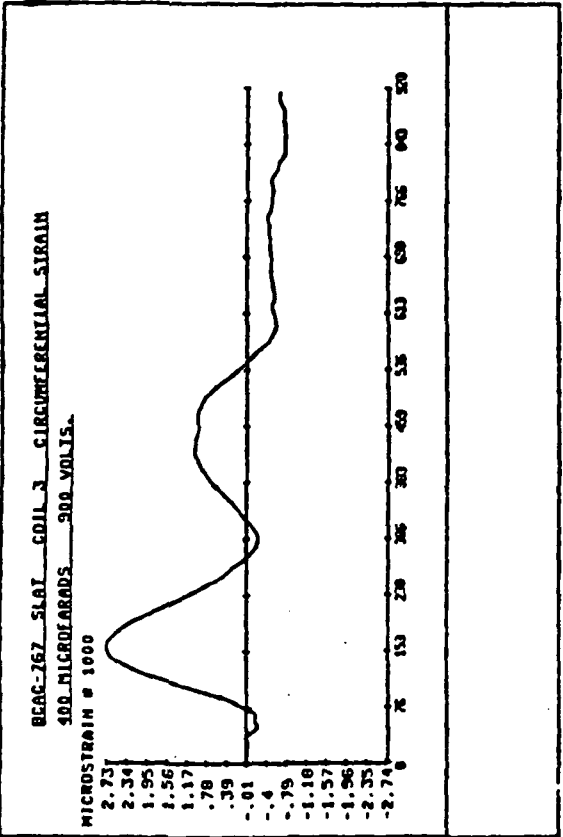
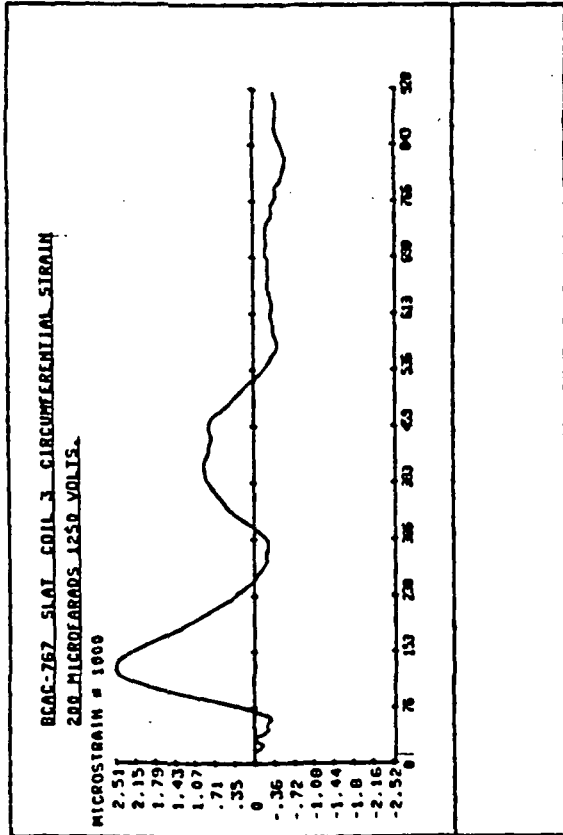


FIGURE 3-11. BCAC -767 L.E. SLAT. STRAINS AT COIL 3 (UPPER SURFACE).

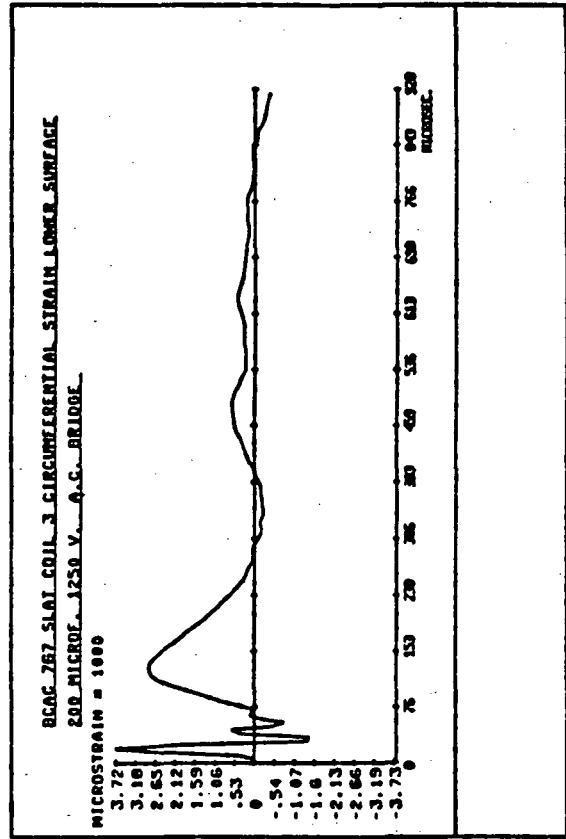
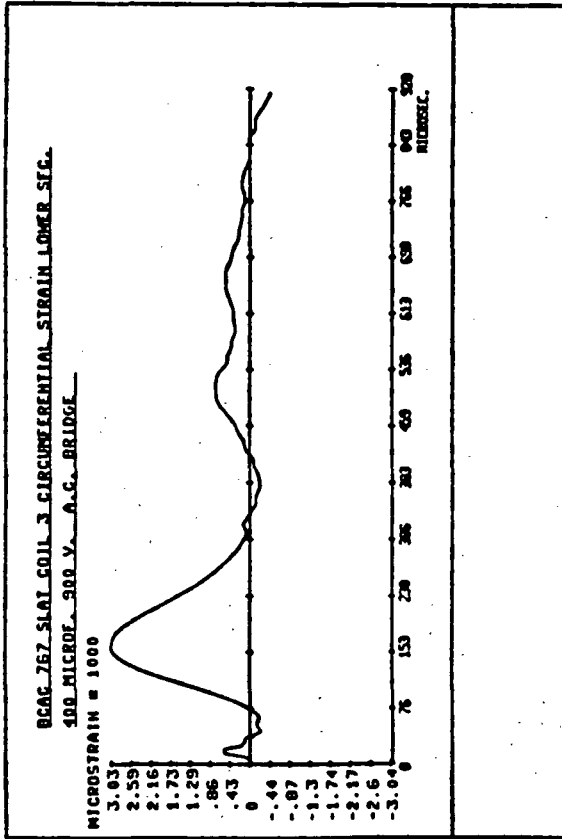
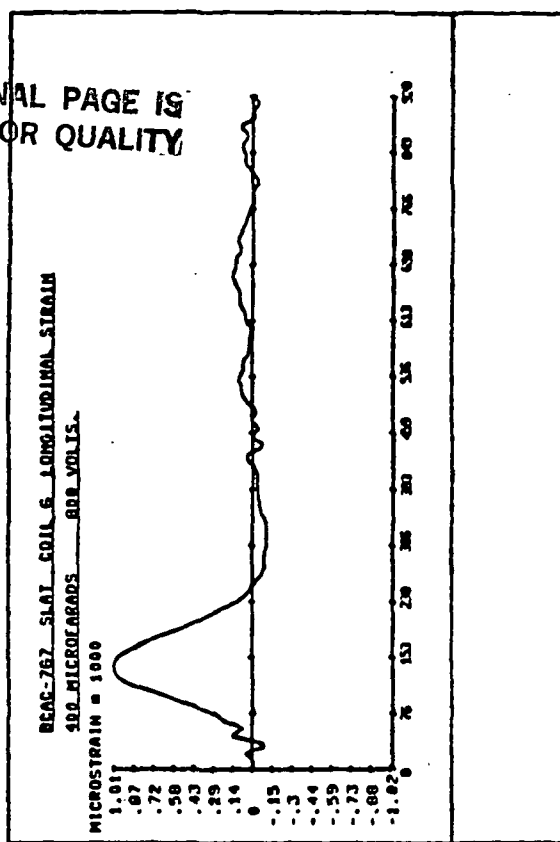
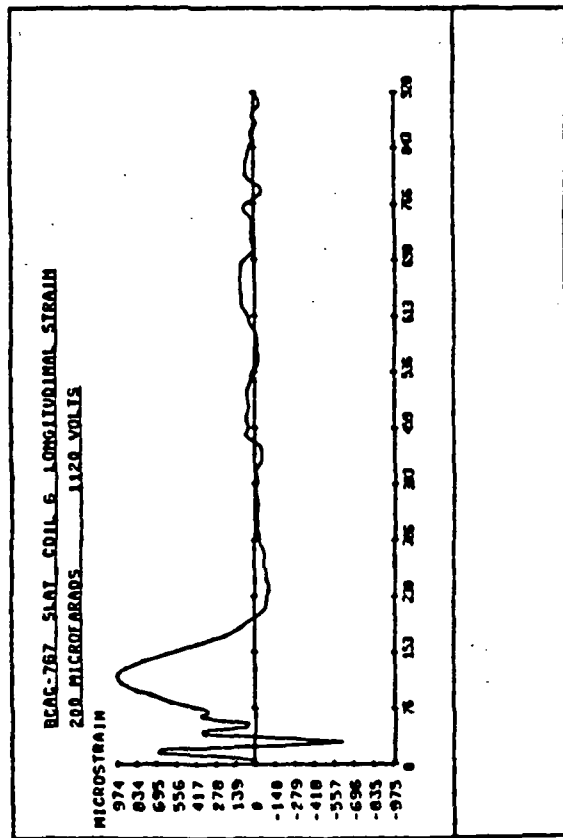
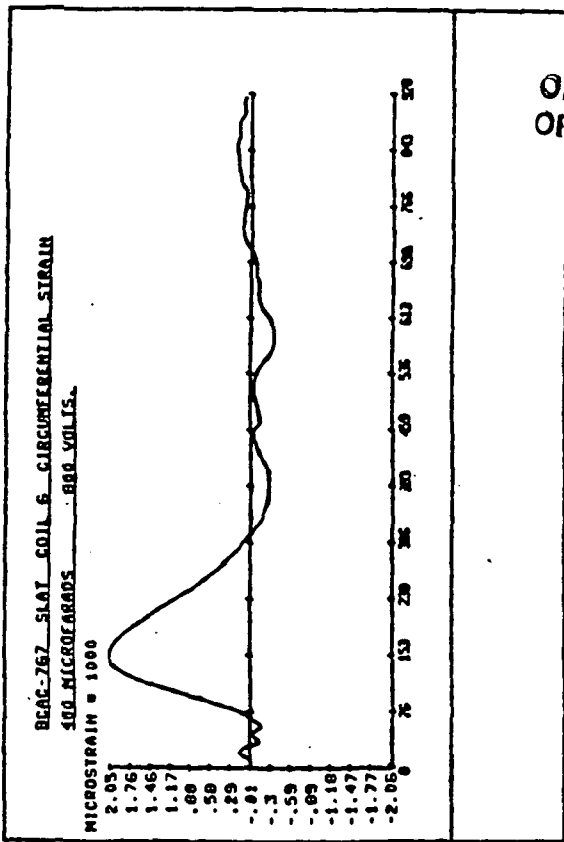
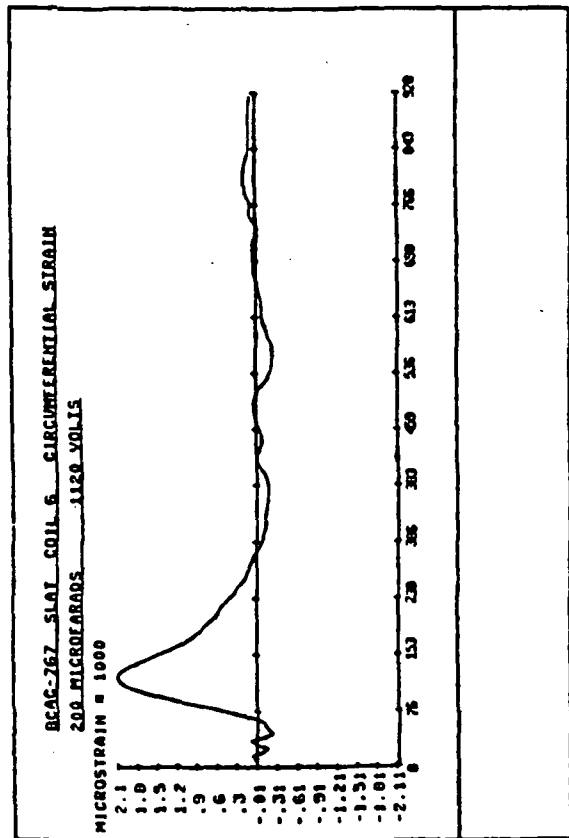
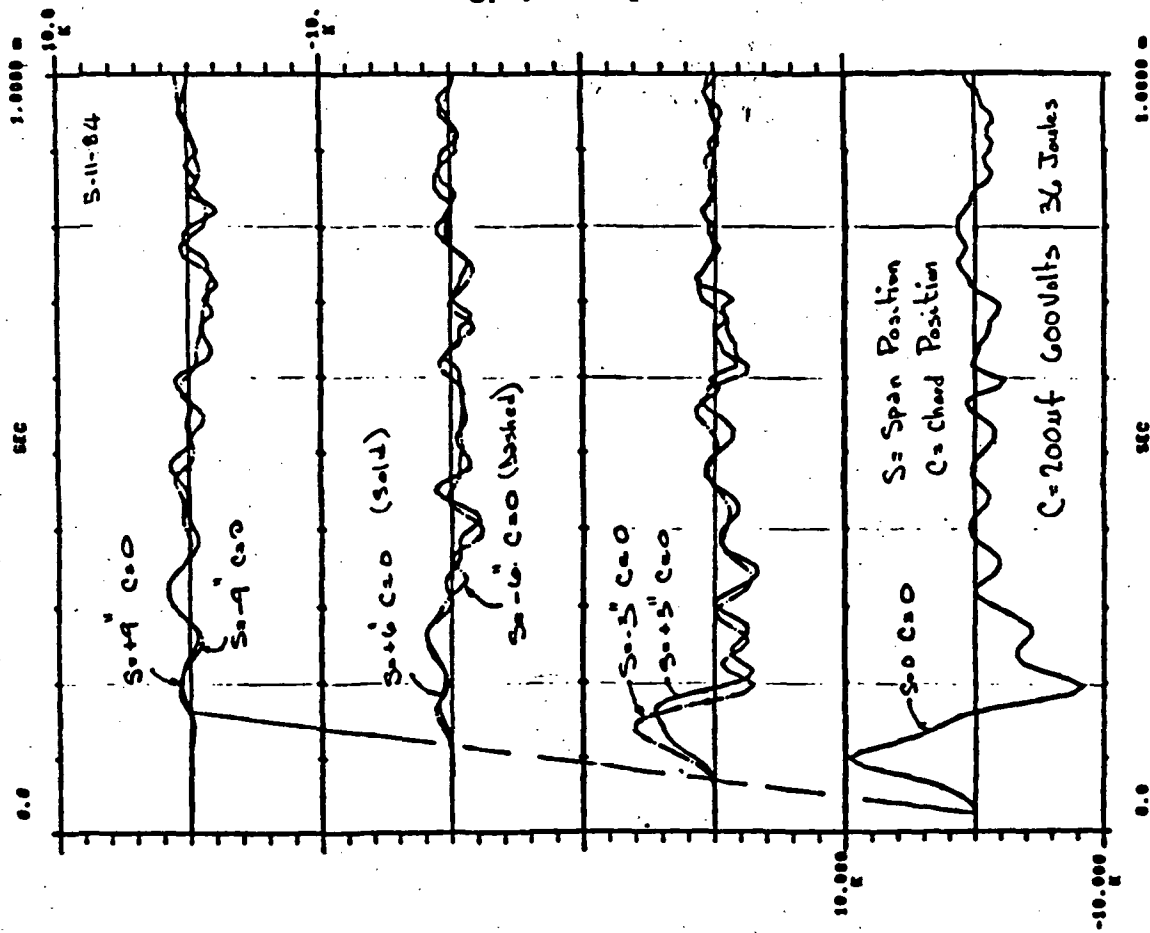


FIGURE 3-12. BCAC-767 L.E. SLAT. STRAINS AT COIL 3 (LOWER SURFACE).



ORIGINAL PAGE IS  
OF POOR QUALITY

FIGURE 3-13. BCAC-767 L.E. SLAT. STRAINS AT COIL 6 (UPPER SURFACE).



ORIGINAL PAGE IS  
OF POOR QUALITY

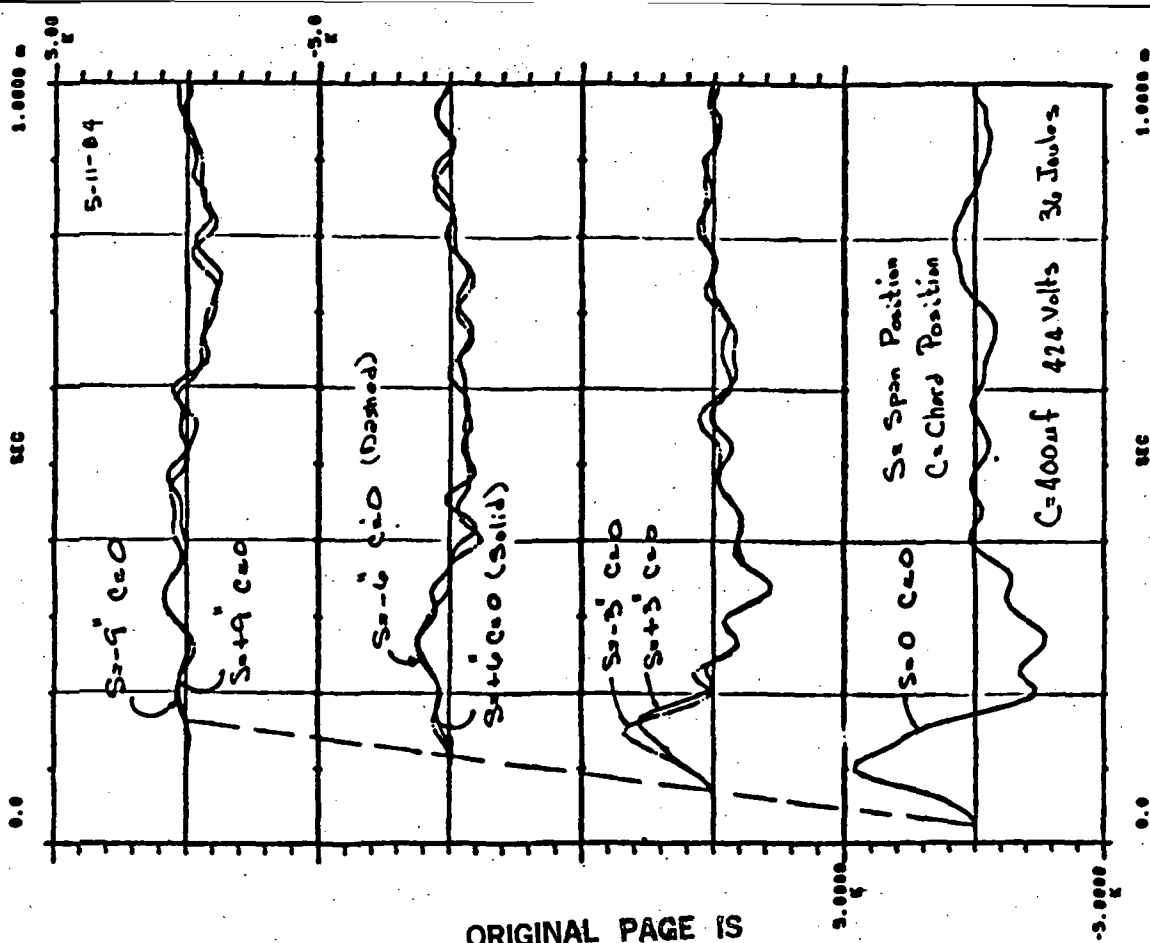
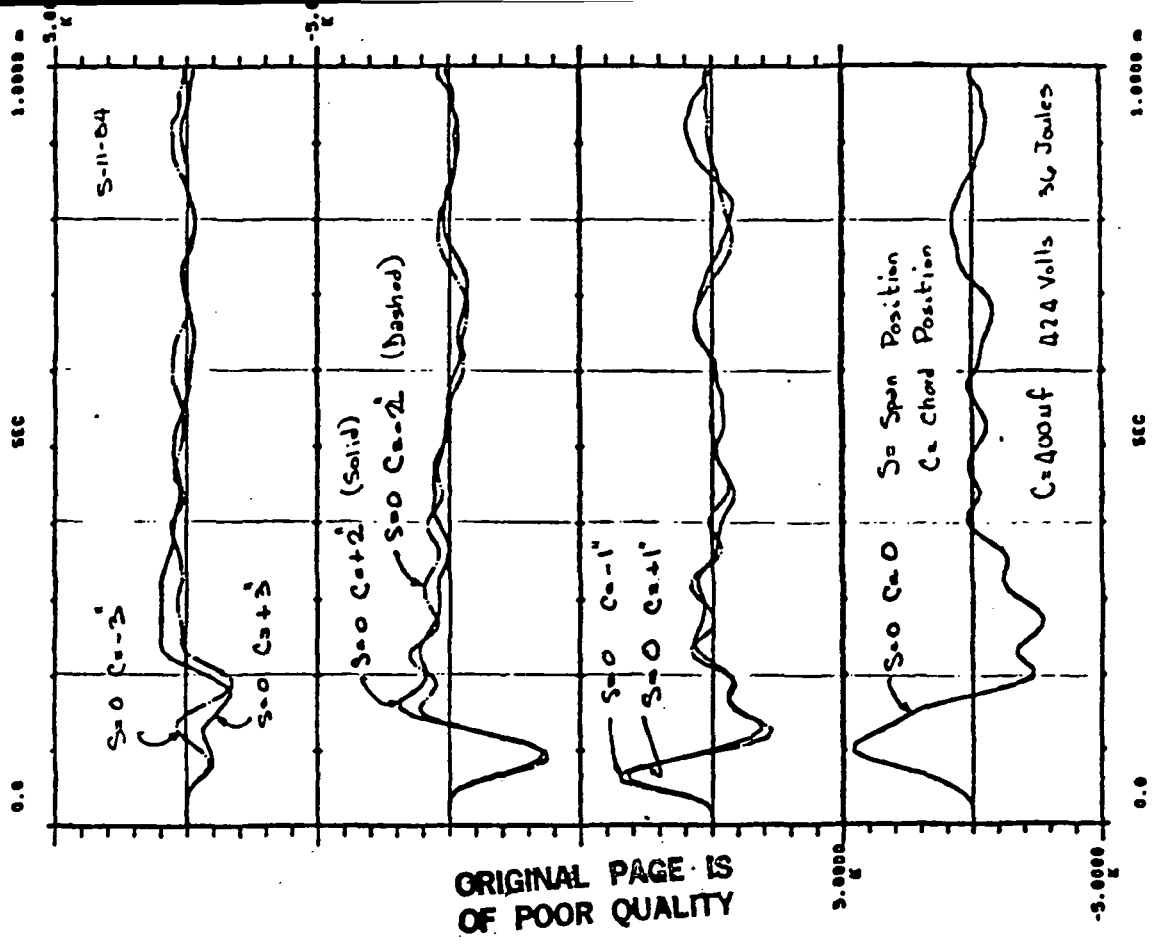


FIGURE 3-14. LONGITUDINAL (SPANWISE) ACCELERATION RESPONSE (g's).



ORIGINAL PAGE IS  
OF POOR QUALITY

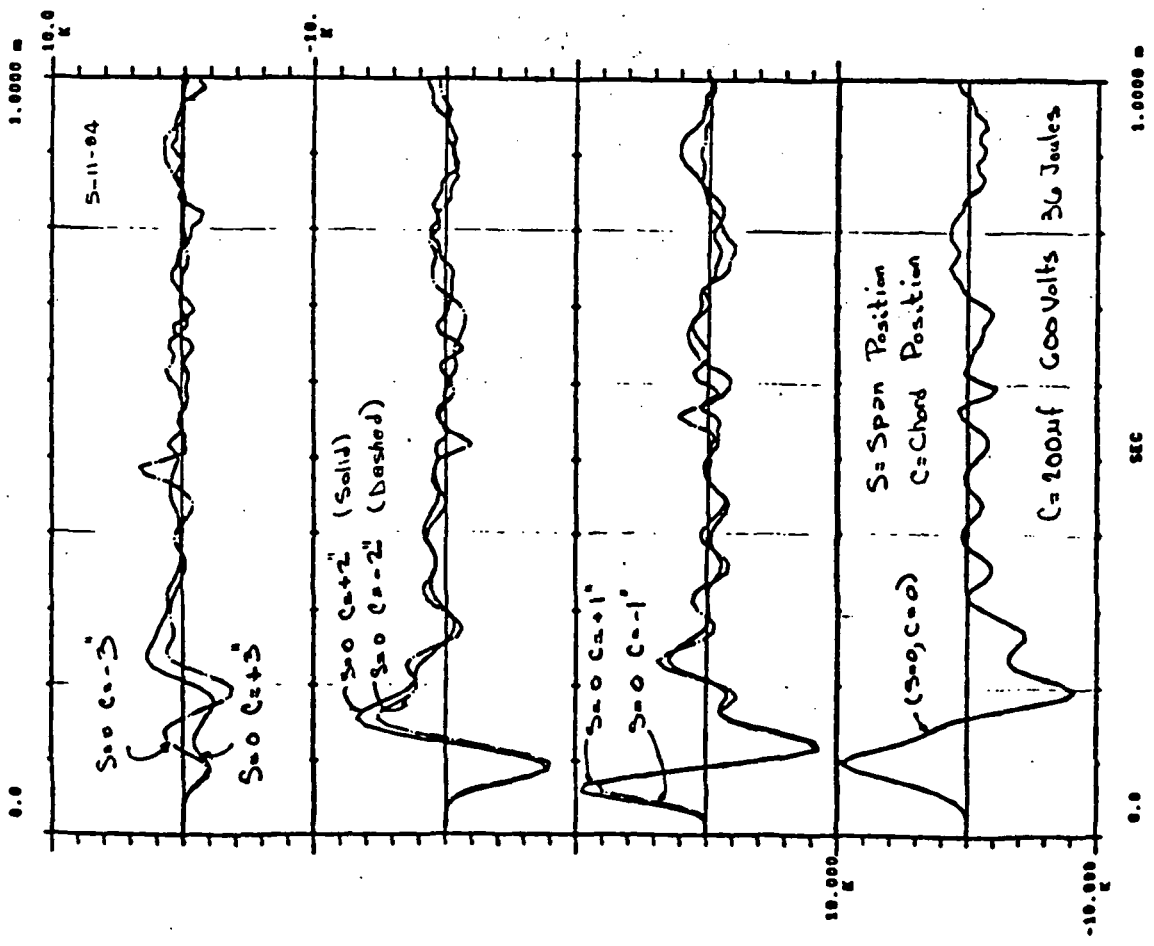
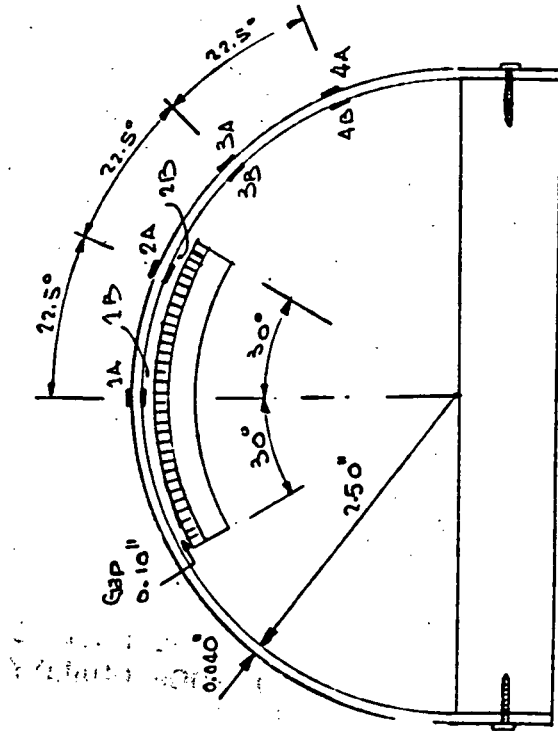
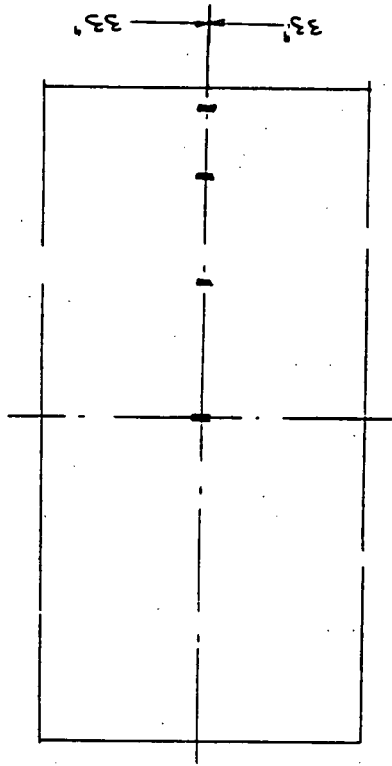
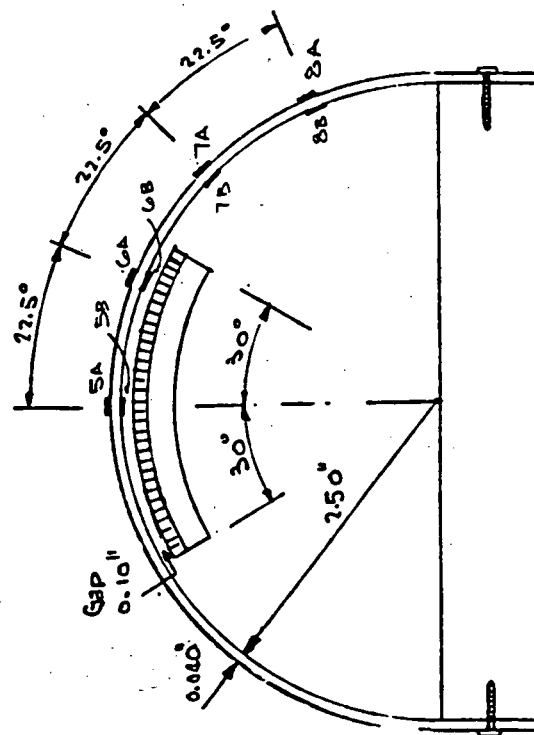
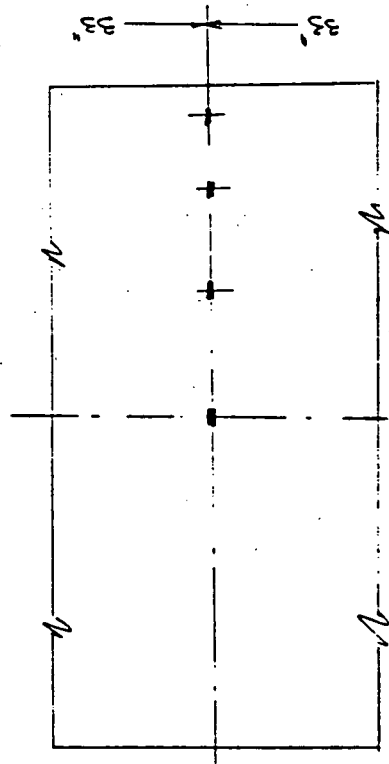


FIGURE 3-15. CIRCUMFERENTIAL (CHORDWISE) ACCELERATION RESPONSE (g's).



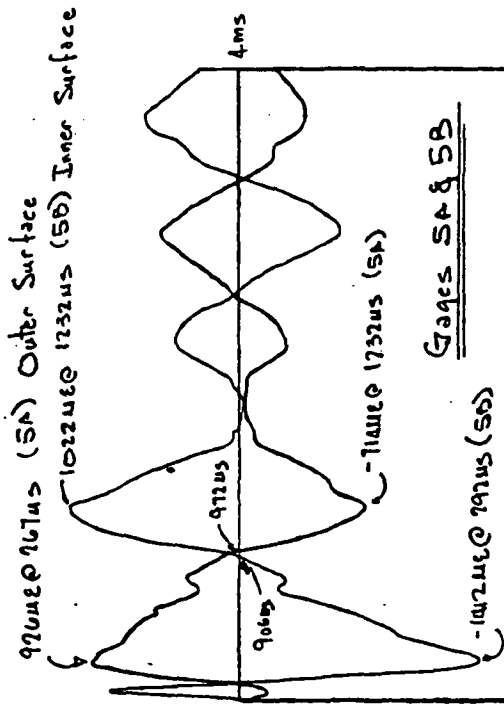
2.5" RADIUS SEMI-CYLINDER (SINGLE COIL).  
LONGITUDINAL (SPANWISE) STRAIN GAGE NUMBERS AND LOCATIONS.



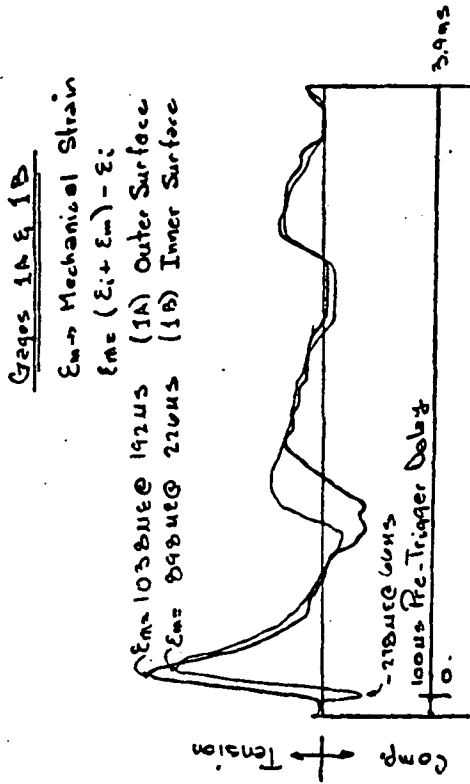
2.5" RADIUS SEMI-CYLINDER (SINGLE COIL).  
CIRCUMFERENTIAL (CHORDWISE) STRAIN GAGE NUMBERS AND LOCATIONS.

FIGURE 3-16. STRAIN GAGE NUMBERS AND LOCATIONS.

2.5° RADIUS SEMI-CYLINDER (SINGLE COIL). August 2, 1984.  
 CIRCUMFERENTIAL (CHORDWISE) STRAIN: (C-400 V=800 128 JOULES).



2.5° RADIUS SEMI-CYLINDER (SINGLE COIL). July 18, 1984.  
 LONGITUDINAL (SPANWISE) STRAIN: (C-400 V=800 128 JOULES).



ORIGINAL PAGE IS  
 OF POOR QUALITY

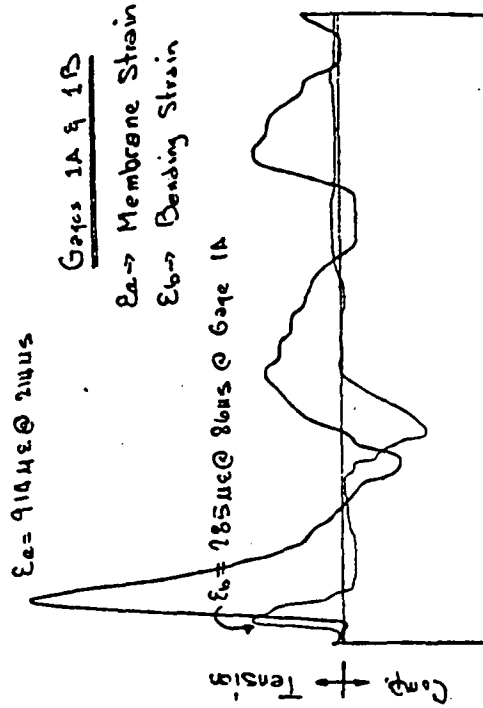
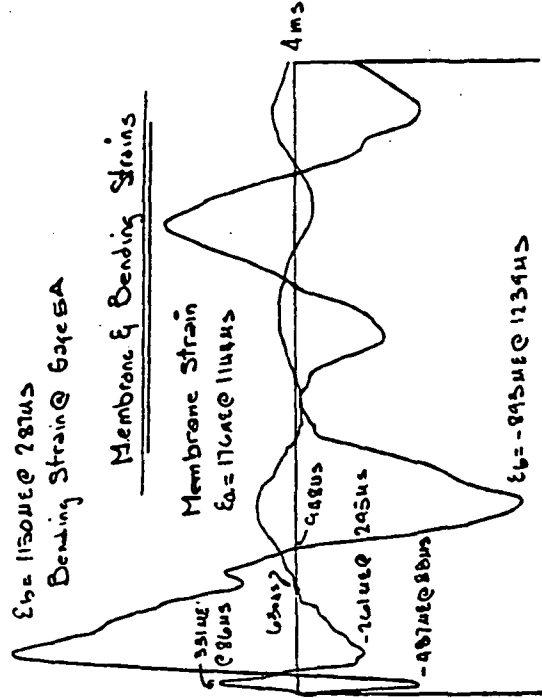


FIGURE 3-17. SEMI-CYLINDER STRAINS (GAGES 1 AND 5).

2.5" RADIUS SEMI-CYLINDER (SINGLE COIL).  
CIRCUMFERENTIAL (CHORDWISE) STRAIN: (C=400 V=800 128 JOULES).

August 2, 1984.

2.5" RADIUS SEMI-CYLINDER (SINGLE COIL). July 18, 1984.  
LONGITUDINAL (SPANWISE) STRAIN: (C=400 V=800 128 JOULES).

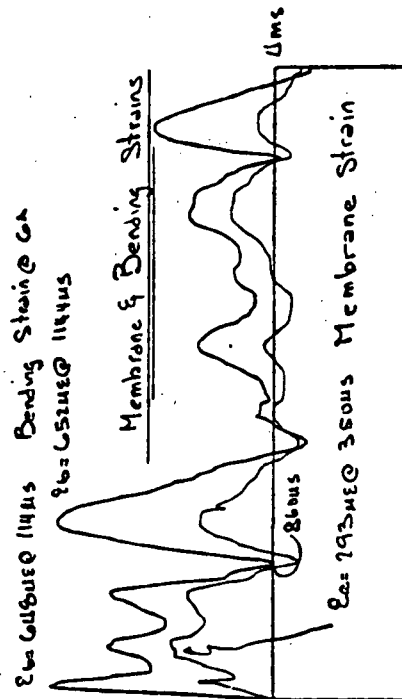
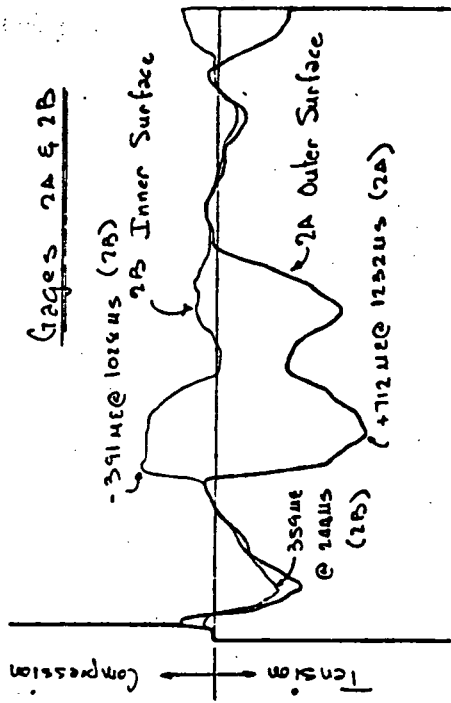
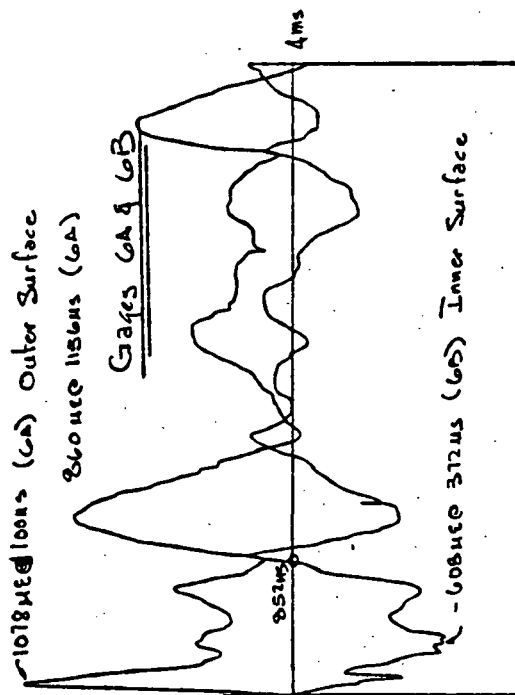
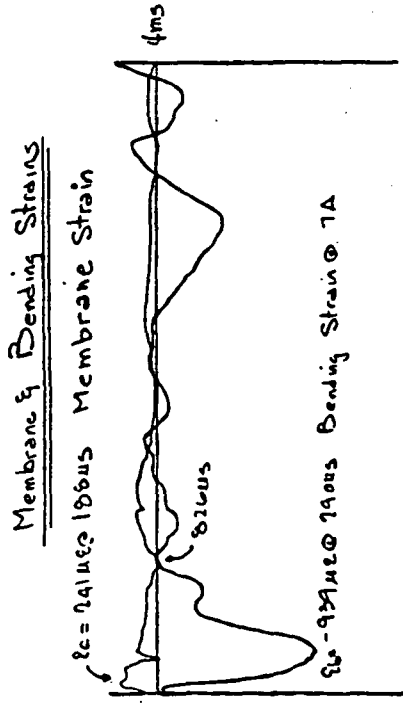
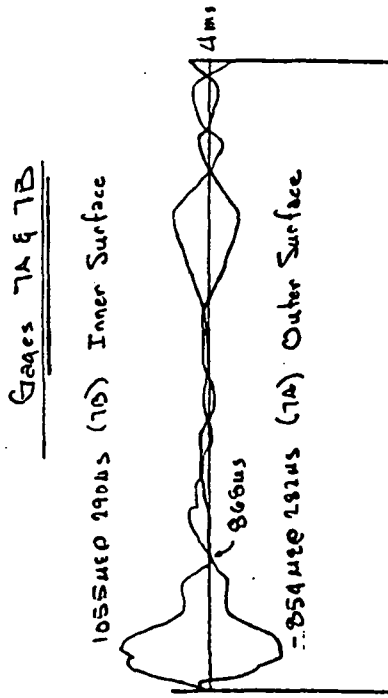


FIGURE 3-18. SEMI-CYLINDER STRAINS (GAGES 2 AND 6).

2.5" RADIUS SEMI-CYLINDER (SINGLE COIL). August 2, 1984.  
 CIRCUMFERENTIAL (CHORDWISE) STRAIN: (C=400 V=800 128 JOULES).



2.5" RADIUS SEMI-CYLINDER (SINGLE COIL). July 18, 1984.  
 LONGITUDINAL (SPANWISE) STRAIN: (C=400 V=800 128 JOULES).

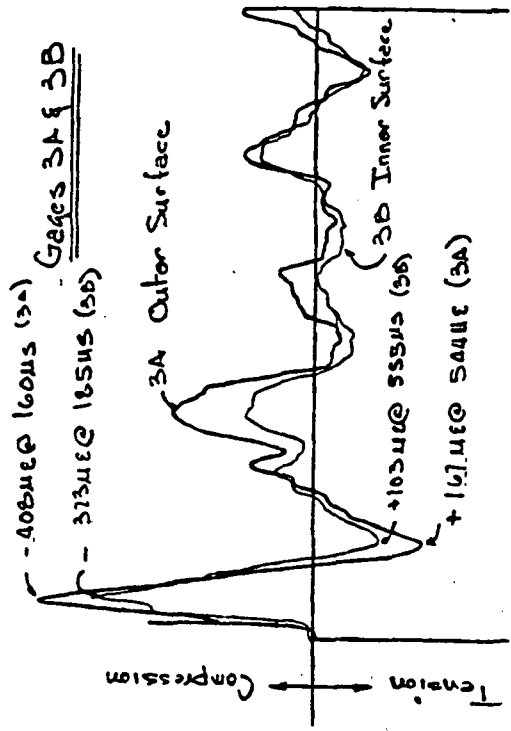
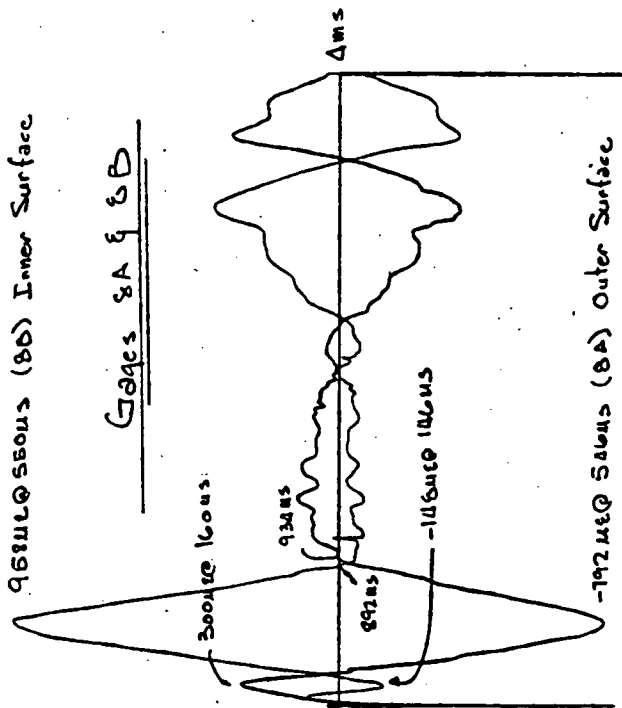


FIGURE 3-19. SEMI-CYLINDER STRAINS (GAGES 3 AND 7).

2.5" RADIUS SEMI-CYLINDER (SINGLE COIL). August 2, 1984.  
 CIRCUMFERENTIAL (CHORDWISE) STRAIN: (C=400 V=800 128 JOULES).

96311056015 (80) Inner Surface

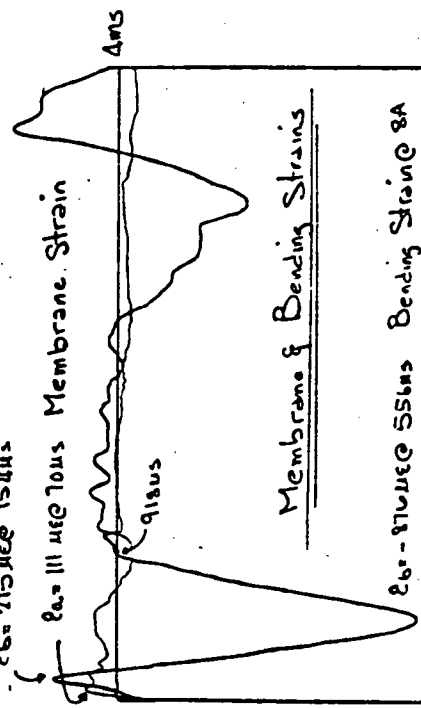
Gages 8A & 8B



-192140 @ 560ms (8A) Outer Surface

-860 215ms @ 154ms

Membrane & Bending Strains



860 215ms @ 55ms Bending Strain @ 8A

2.5" RADIUS SEMI-CYLINDER (SINGLE COIL). July 18, 1984.  
 LONGITUDINAL (SPANWISE) STRAIN: (C=400 V=800 128 JOULES).

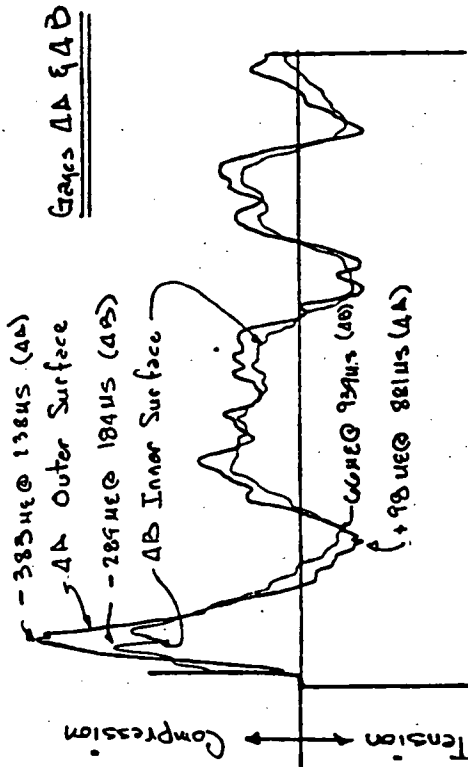
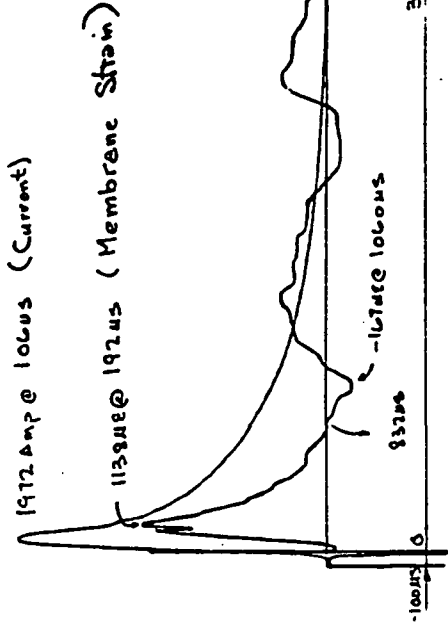
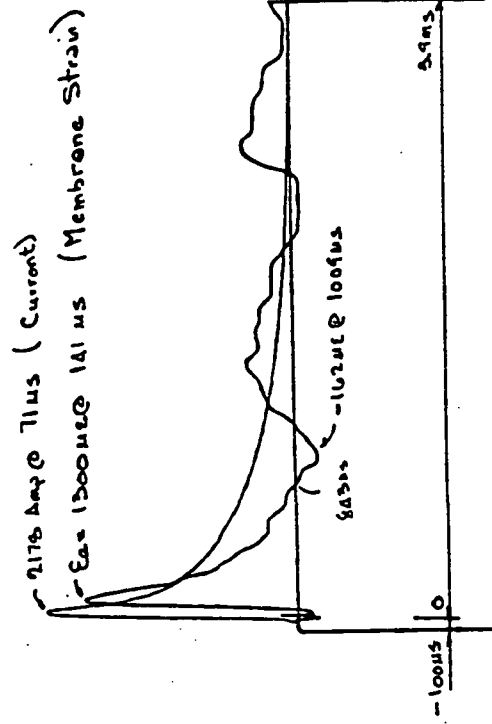


FIGURE 3-20. SEMI-CYLINDER STRAINS (GAGES 4 AND 8).

Case (7)  $C = 200 \mu\text{f}$   $V_0 = 1131 \text{ Volts}$  (1-23-84)



Case (8)  $C = 100 \mu\text{f}$   $V = 1600 \text{ Volts}$  (7-13-84)



7.5" Radius Semi-Cylinder July 23, 1984  
 Axial (Membrane) Strain at Gage Location 1.  
 A constant energy ( $\frac{1}{2} CV^2 = 128 \text{ J}$ ) for 3 values of capacitance.

Case (1)  $C = 400 \mu\text{f}$   $V = 800 \text{ Volts}$

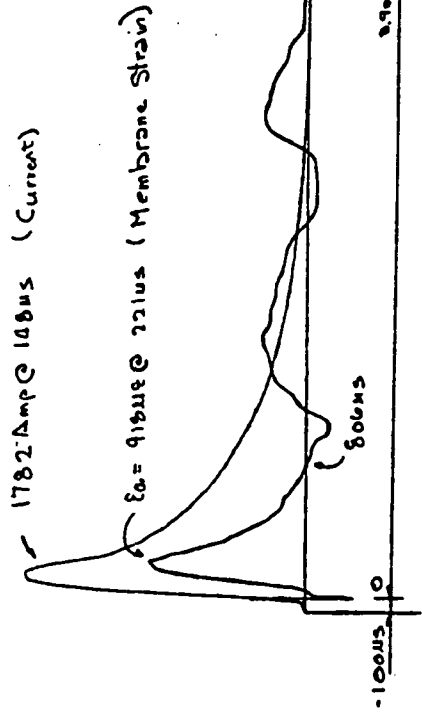


FIGURE 3-21. MEMBRANE STRAIN AT GAGE 1 FOR THREE VALUES OF CAPACITANCE.

2.5" RADIUS SEMI-CYLINDER (DOUBLE COIL). August 3, 1984.

CIRCUMFERENTIAL (CHORDWISE) STRAIN: (C=400 V=800 128 JOULES).

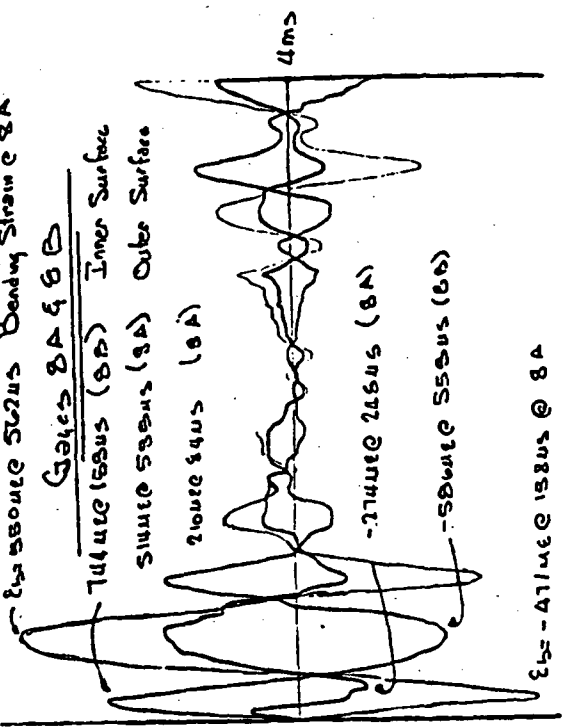
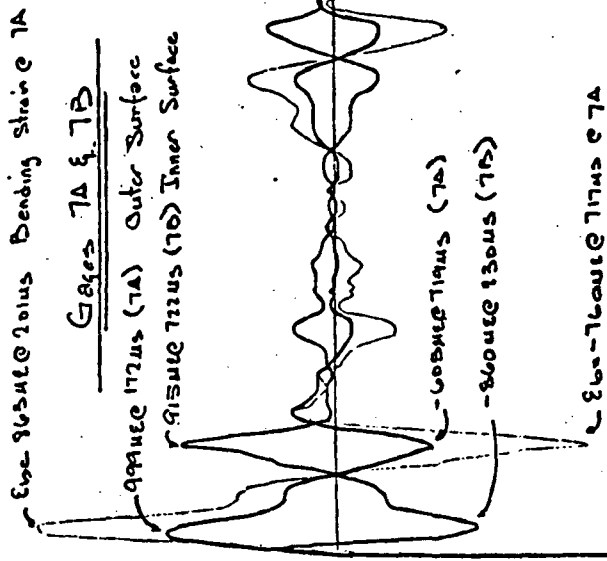
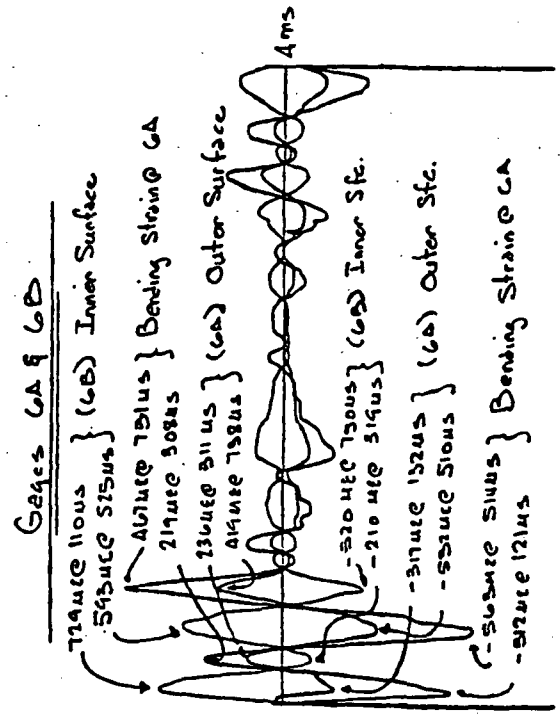
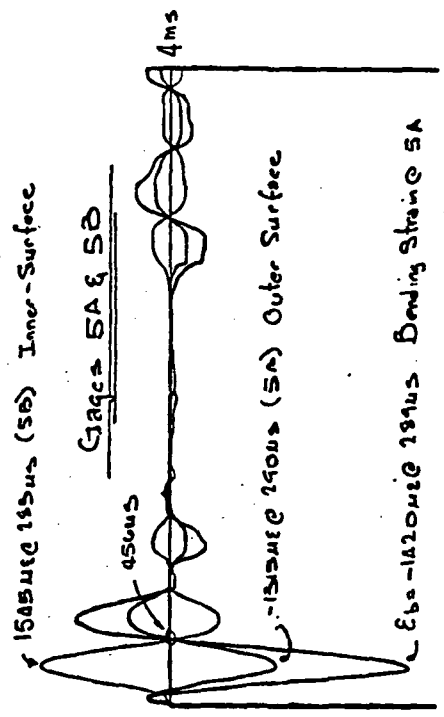


FIGURE 3-22. DOUBLE COIL CIRCUMFERENTIAL (CHORDWISE) STRAINS.

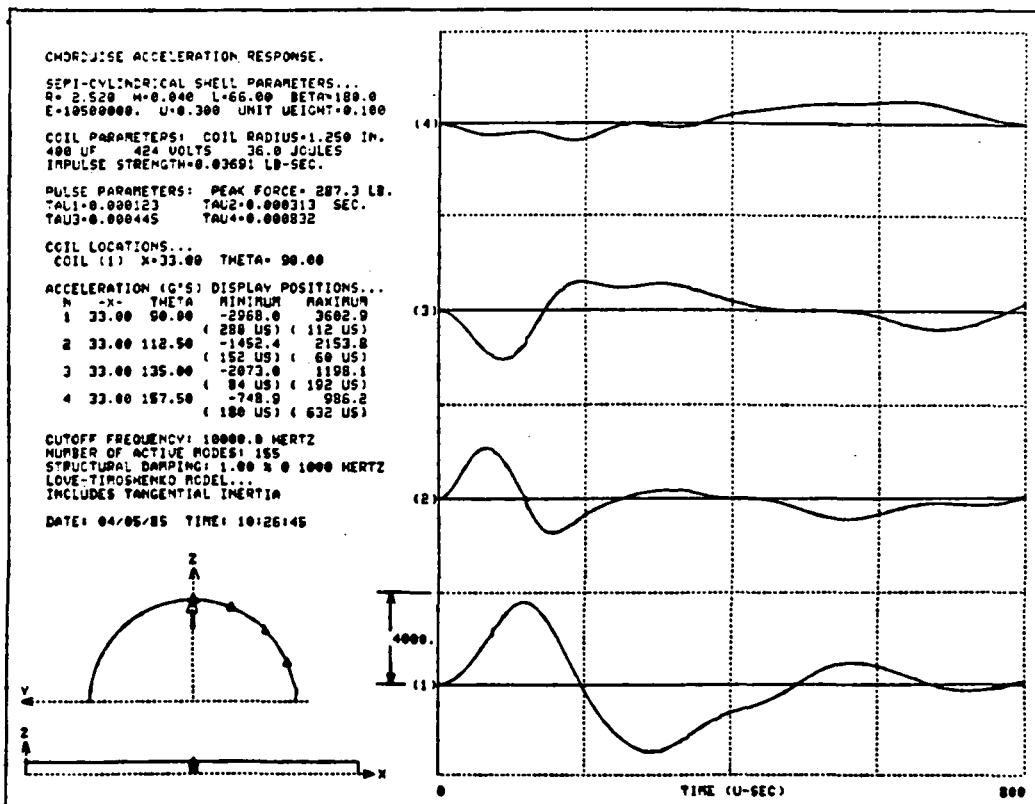
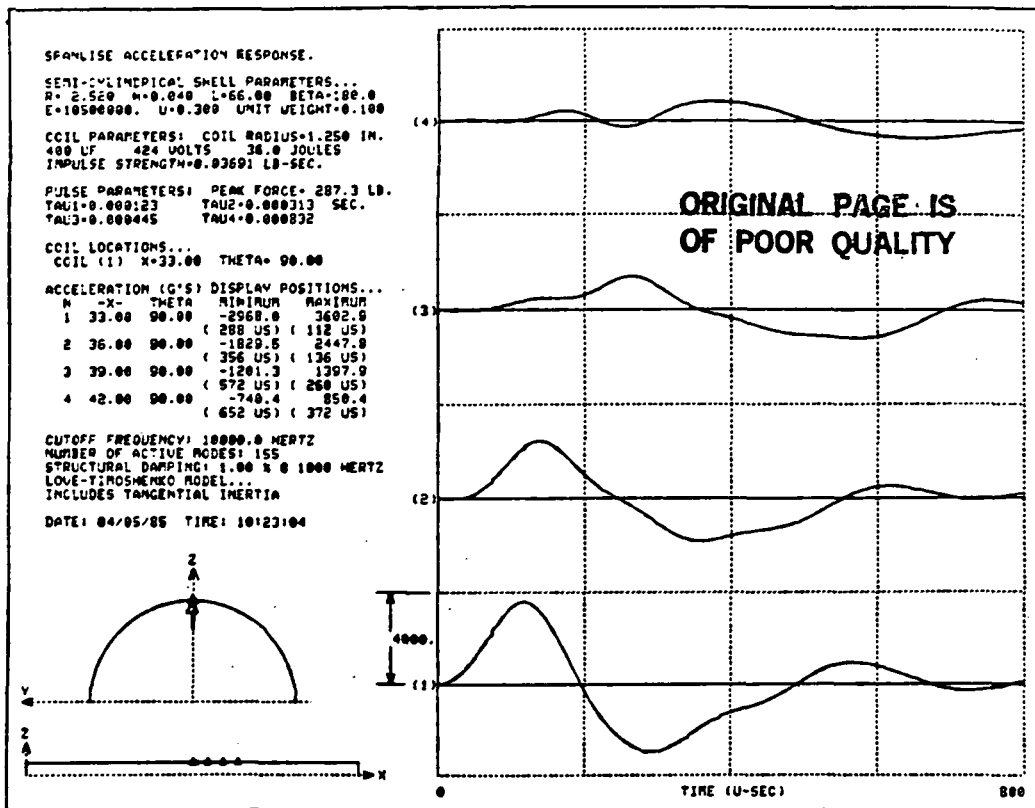


Figure 3-23 Spanwise and Chordwise Acceleration Response.

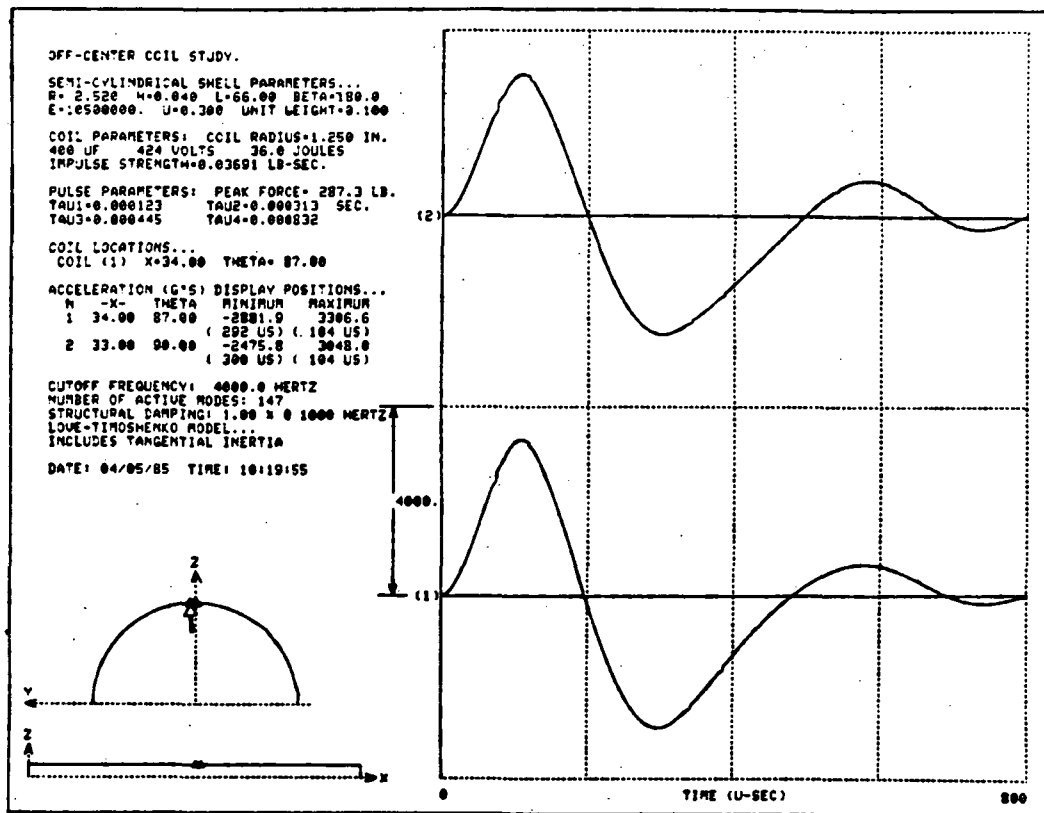
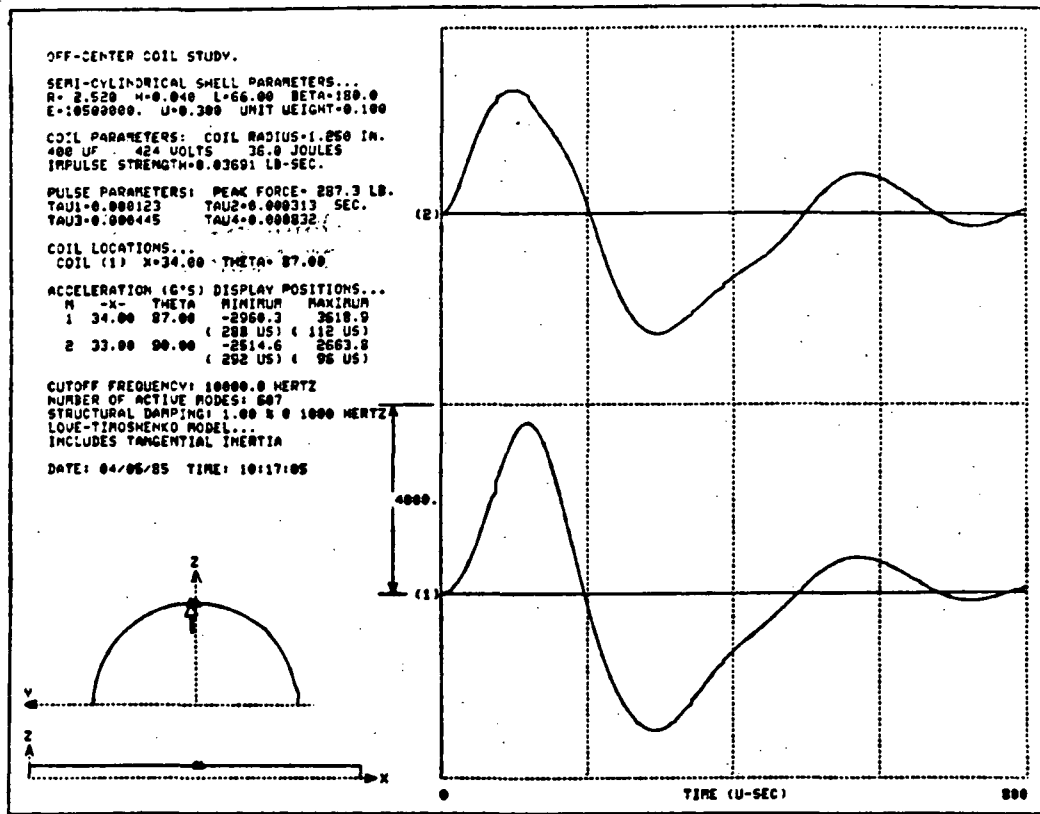
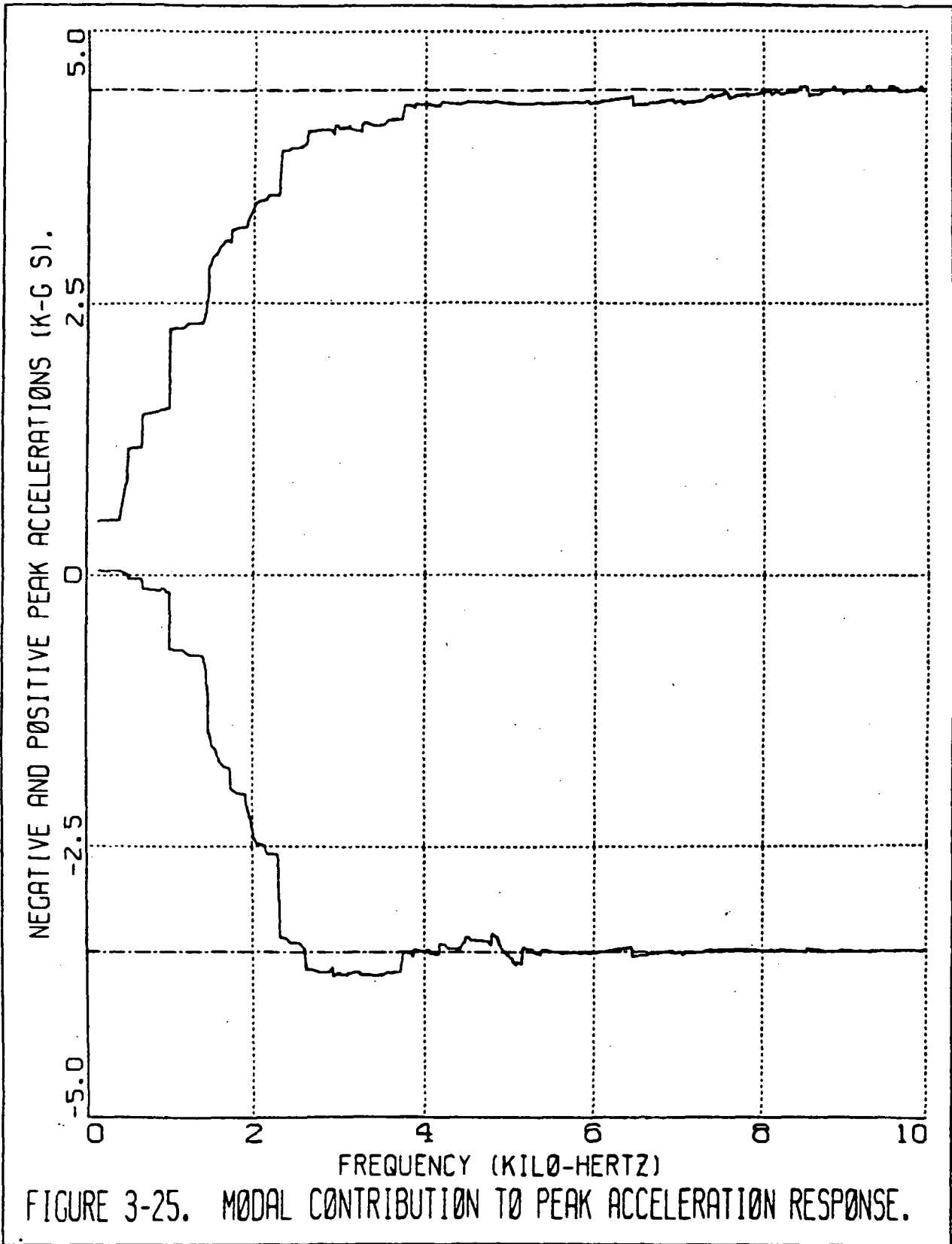


Figure 3-24 Peak Accelerations at Coil Location.

ORIGINAL PAGE IS  
 OF POOR QUALITY



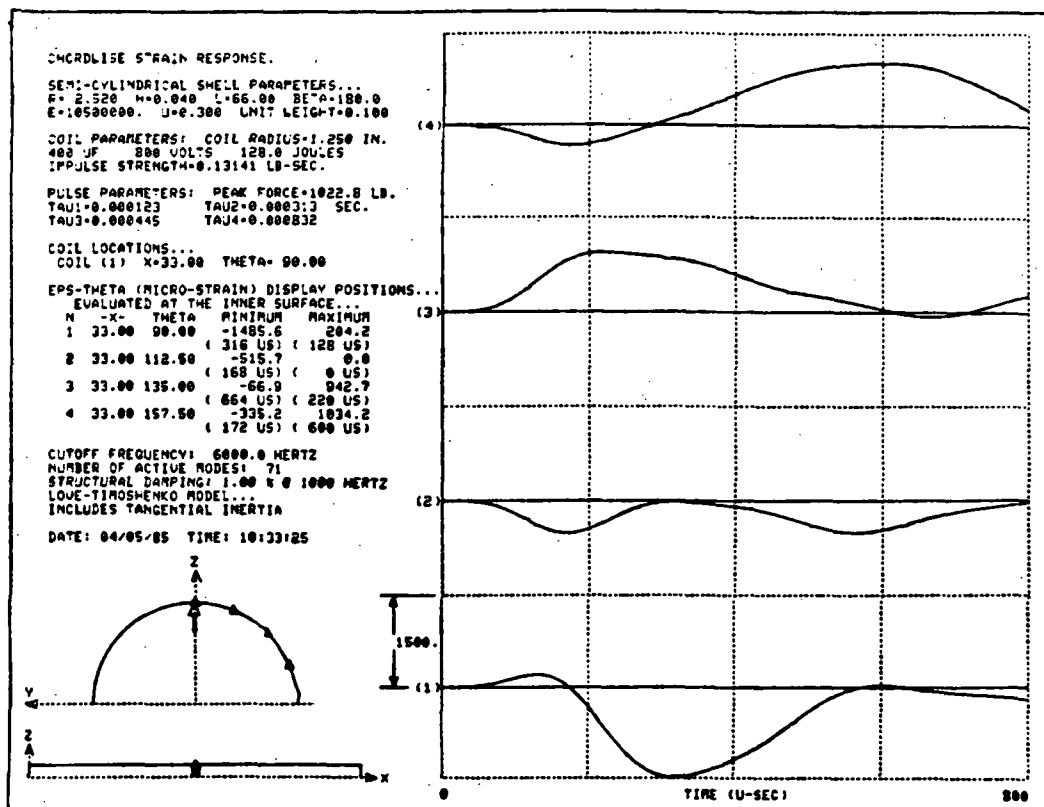
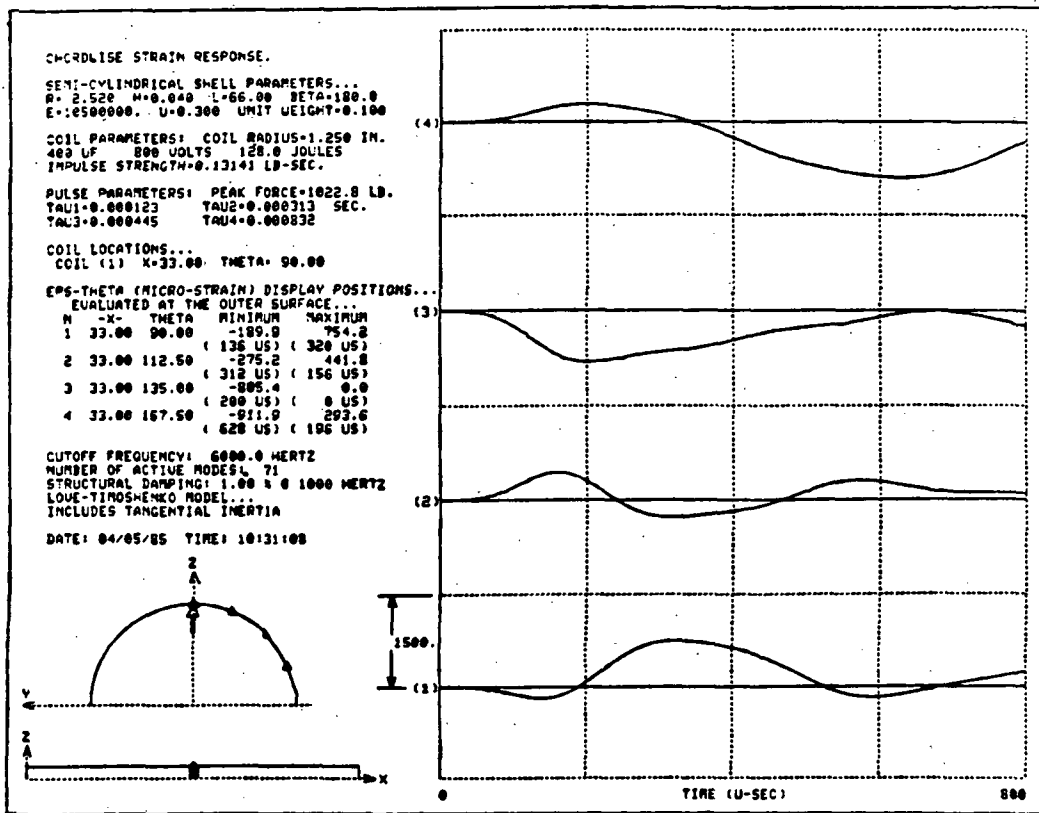


Figure 3-26 Circumferential Strain Response at Mid-Span.

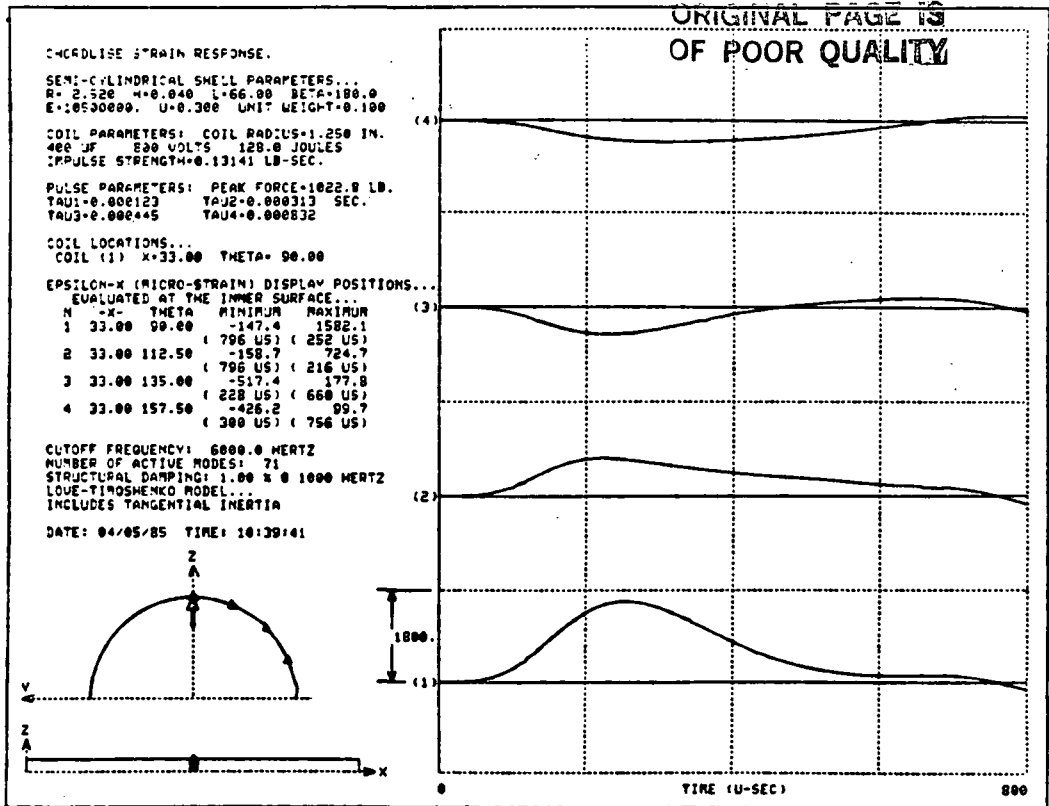
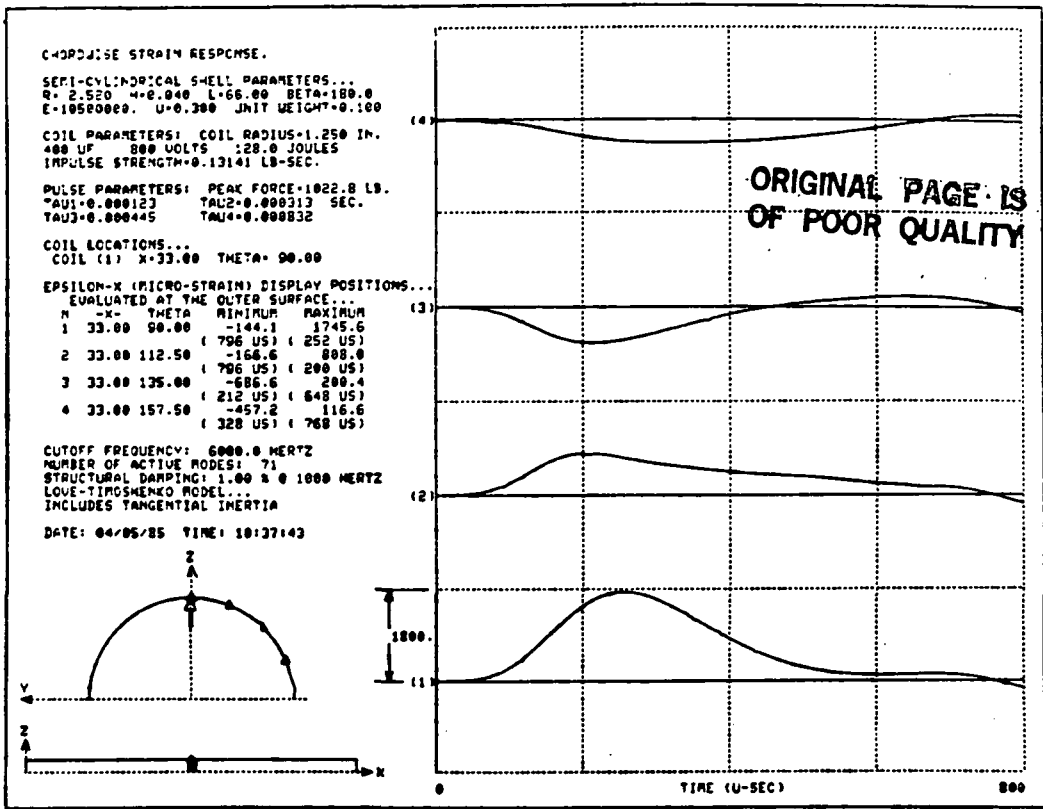


Figure 3-27 Longitudinal Strain Response at Mid-Span.

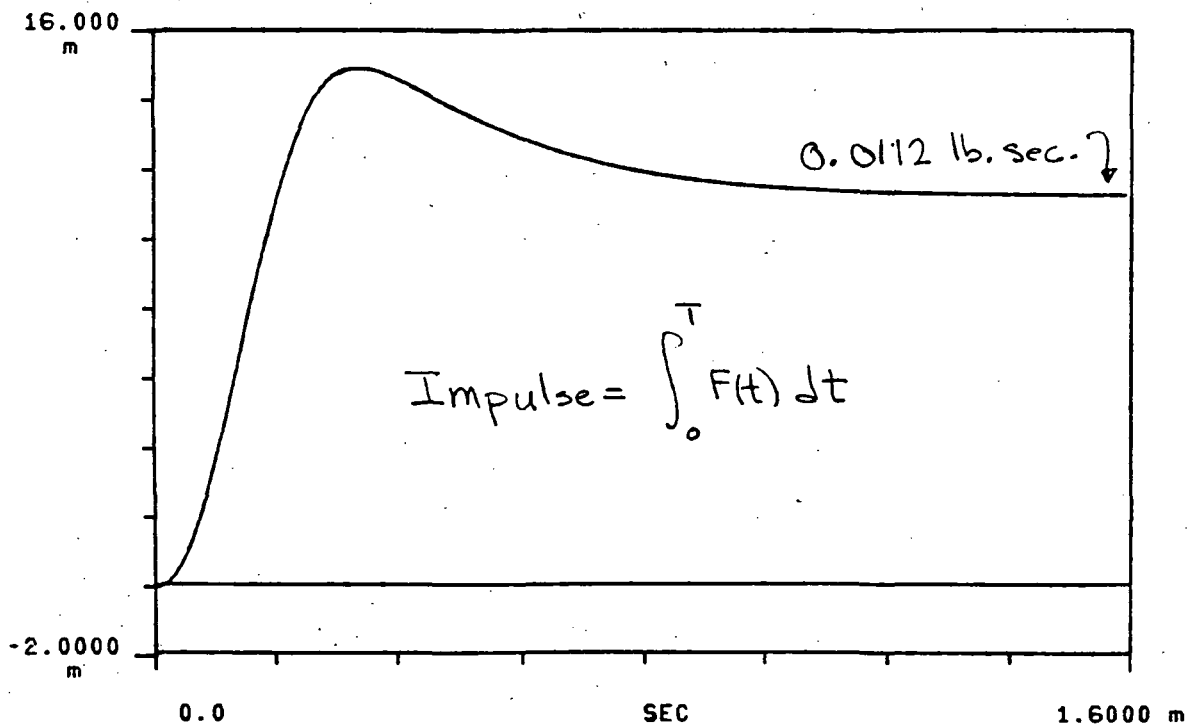
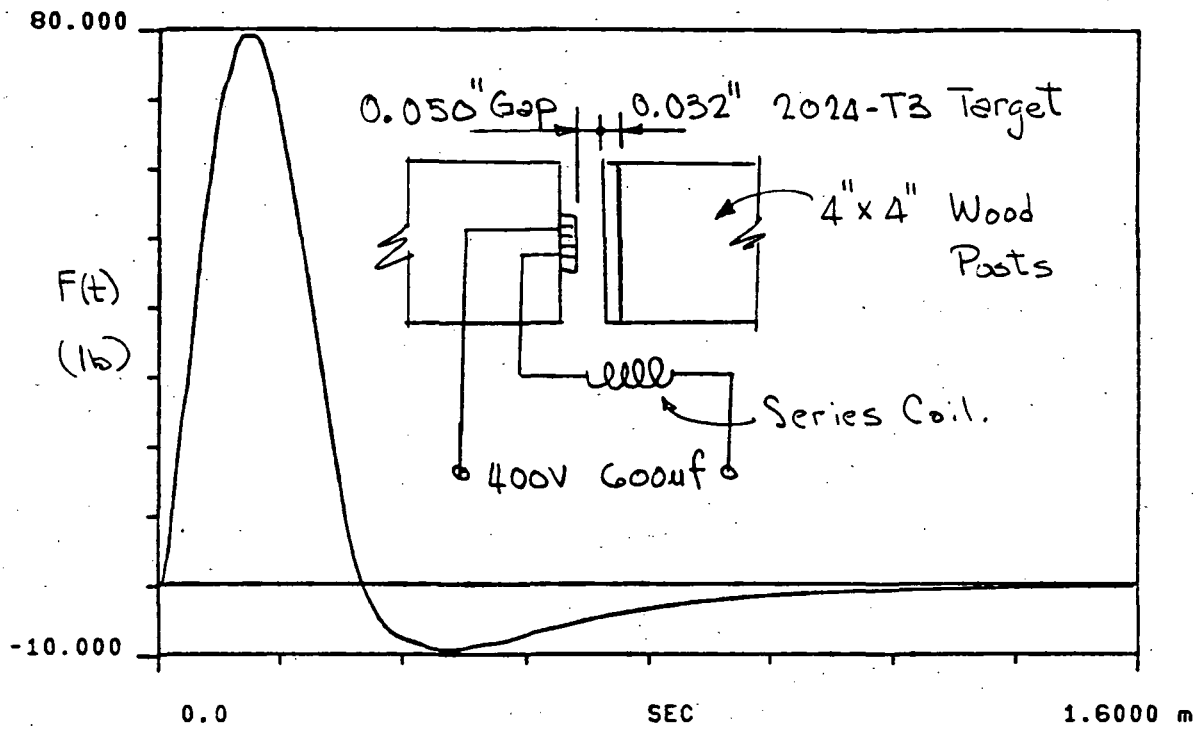


Figure 3-28 Schrag (Ref. 3-1) Force and Impulse Strength.

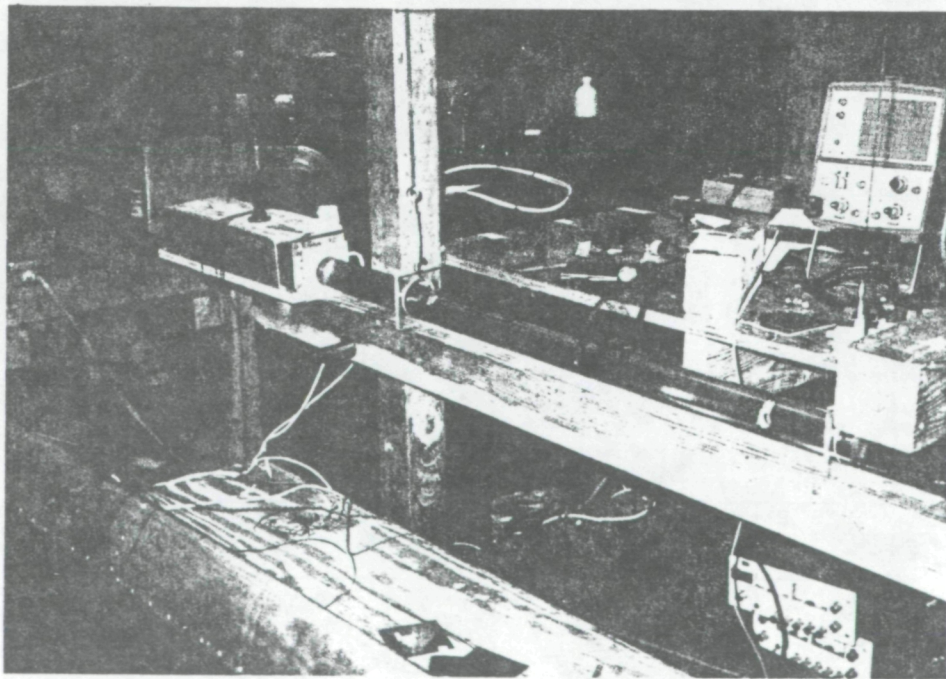
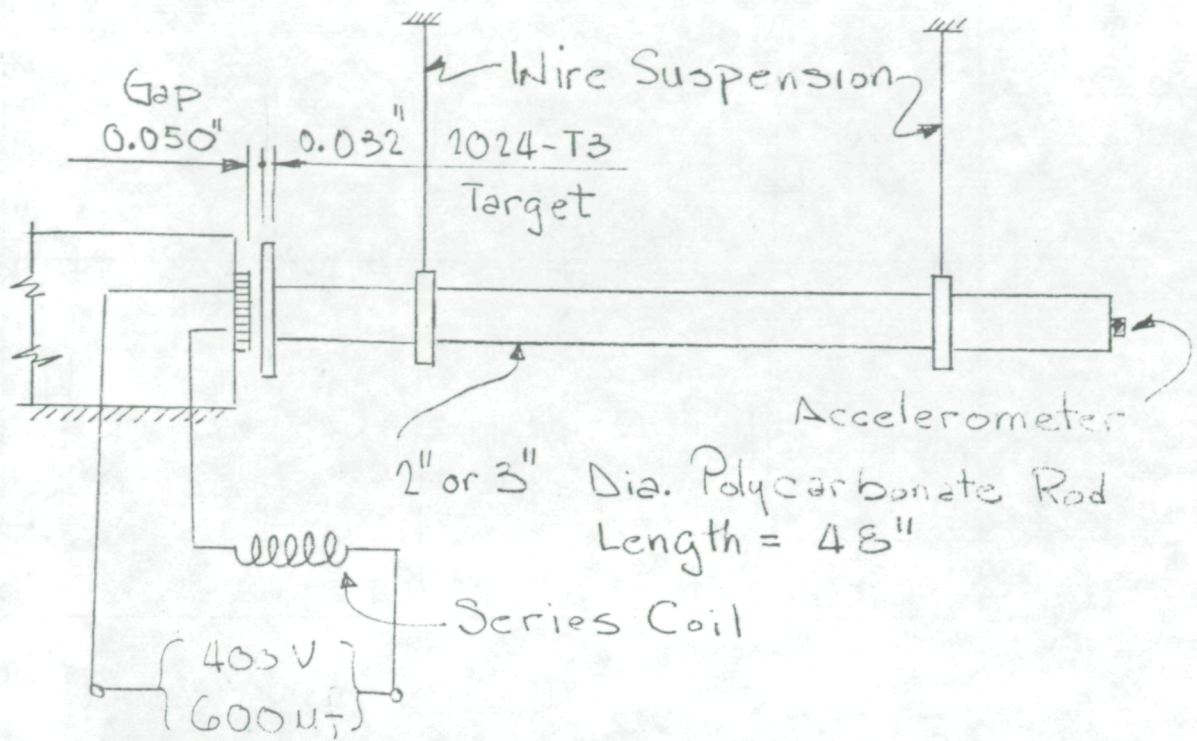


Figure 3-29 EIDI Force Measurement Experiment.

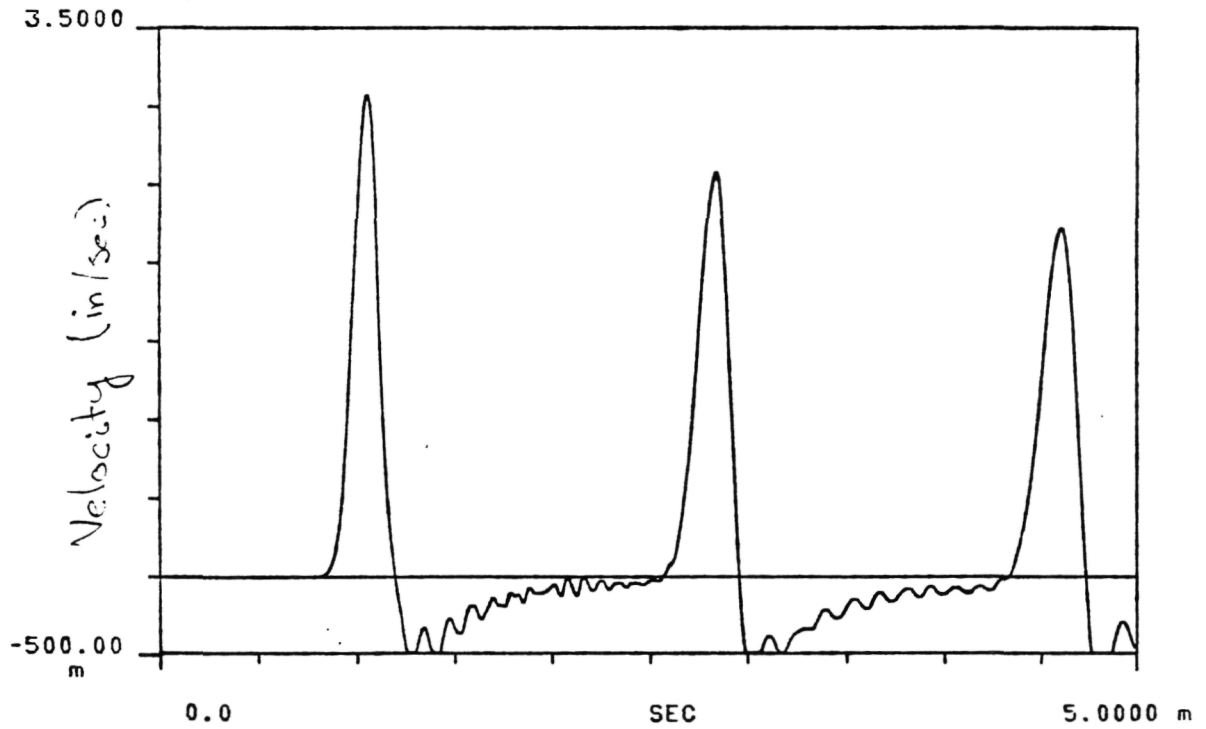
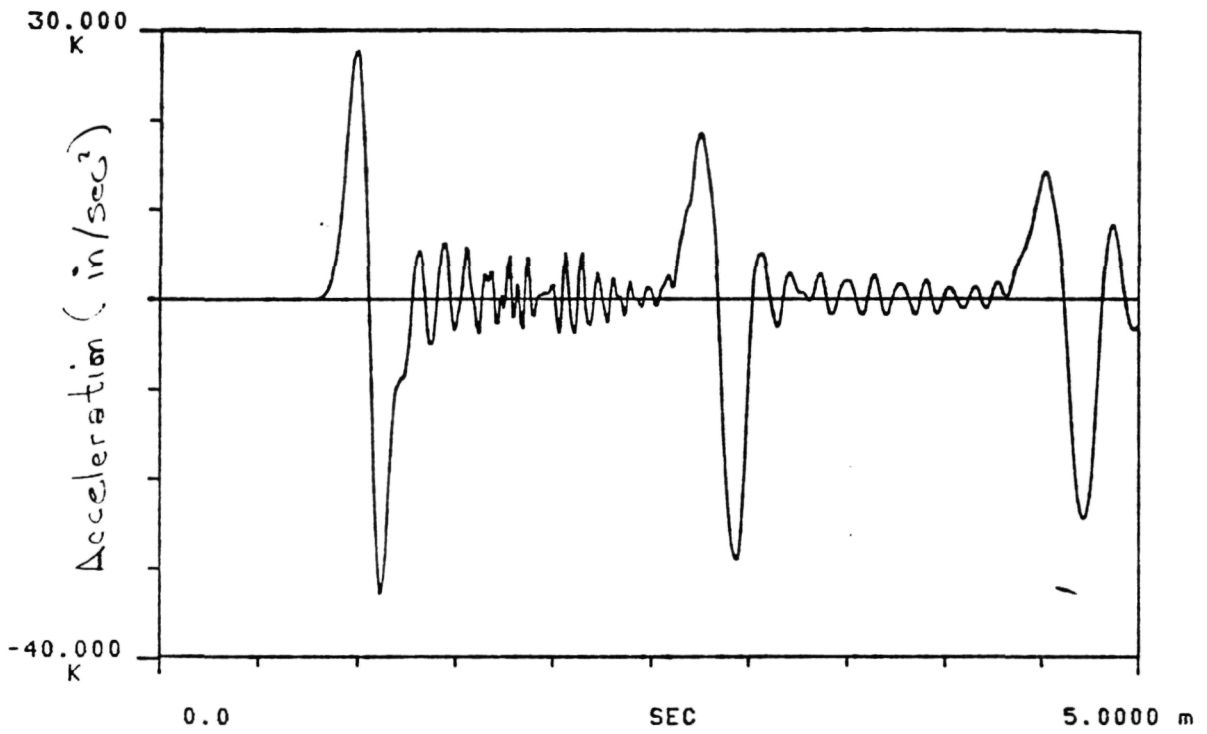


Figure 3-30 Acceleration and Velocity (3" Rod).

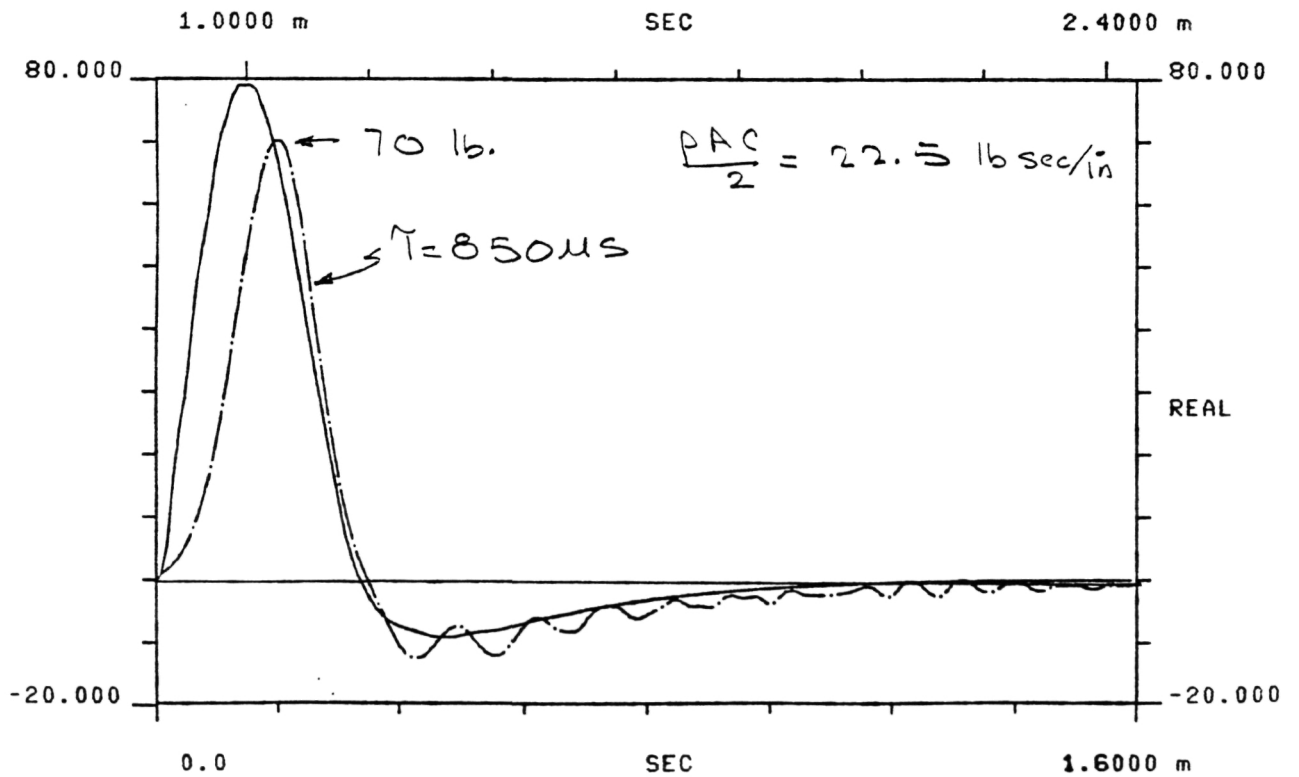
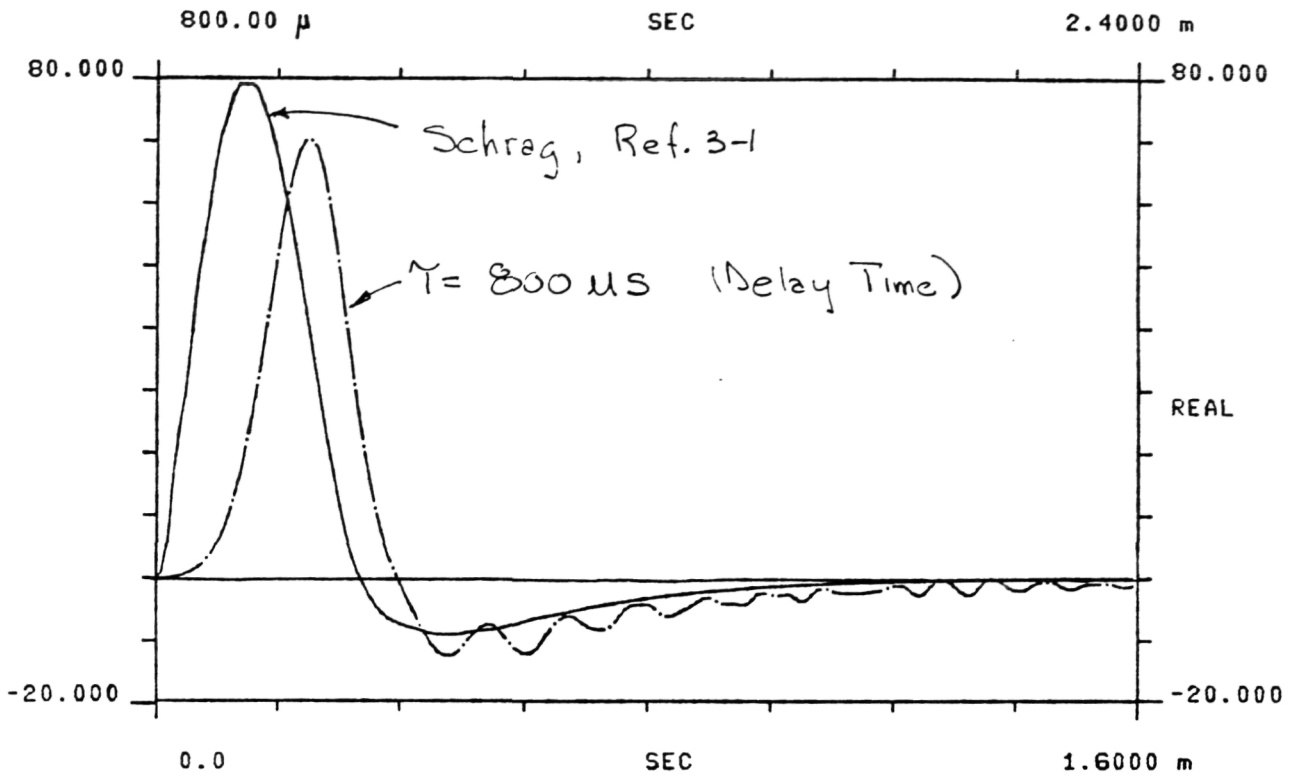


Figure 3-31 Measured Force vs. Schrag (3" Rod).



## CHAPTER 4. FABRICATION TECHNIQUES

Wichita State University supports EIDI research by fabricating coil and coil mounts, by fabricating models for laboratory, icing tunnel, and flight tests, and by installing instrumentation on these models.

Of these, WSU's first and most important function is the production and mounting of high quality electro-magnetic coils in various test models.

### Coil Wire Rolling

Coil wire starts with the purchase of annealed magnet strip wire insulated with a polyimide/polyester alloy. Virgin insulated wire, as received, measures approximately .033 x .180 inches. This is the smallest standard cross-section wire available from our sources.\* Rectangular wire is used because it provides the largest copper cross-section for a given coil cross-section.

However, the .033 inch thickness is too large for coil making. A wire rolling operation reduces the wire to a thickness of .021 to .026 inches for coil winding. Rolling is done in one pass to minimize work hardening of the wire and damage to the wire insulation. The virgin wire is squeezed between a milling machine arbor and a ball bearing outer race as shown in photo 4-1. Note that current practice has eliminated both the steel feed pipe and the take-up reel. Both the pipe and the take-up reel tended to scrape off the wire insulation. In addition, the take-up reel work hardens the copper wire.

Photo 4.2 shows wire thickness being checked during wire rolling. Typical finished dimensions are .024 x .195 inches (average). The word average is used because the wire comes from the mill with non-uniform dimensions, a condition which is worsened by our secondary rolling operation.

### Coil Making

Photo 4-3 shows the first step in coil winding, which is attaching an electrical connector to the wire. In this case, that connector is a gold plated brass pin. In addition to serving as a connector, the pin also serves to anchor the wire in the coil winding tool.

---

A custom-wire supplier has been found who may greatly simplify the process described here.

ORIGINAL PAGE IS  
OF POOR QUALITY

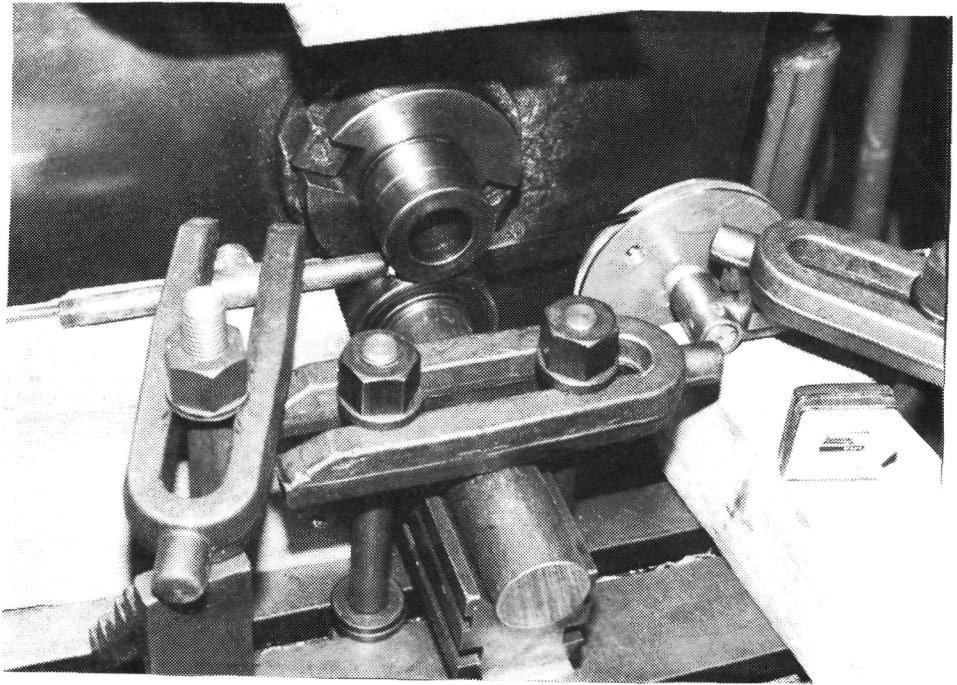


Photo 4-1

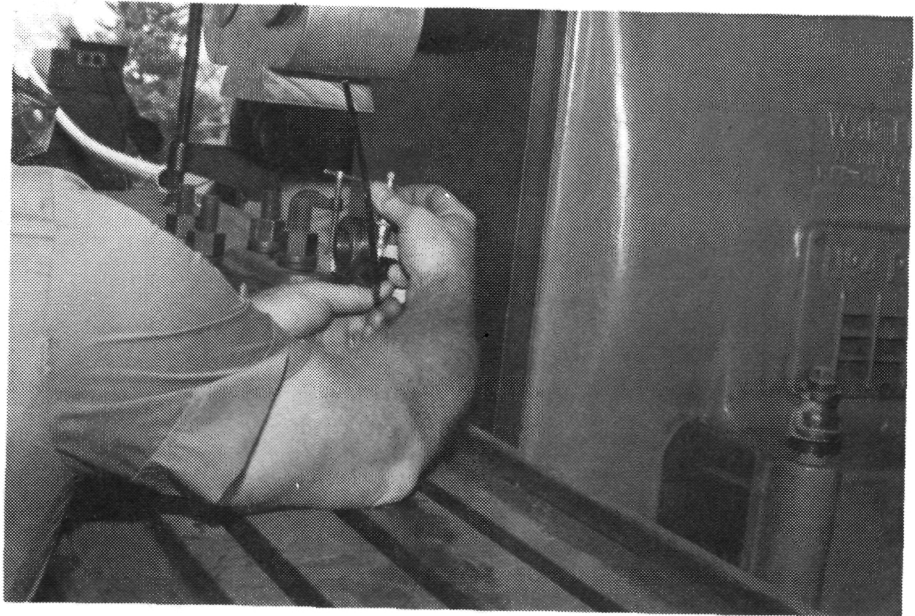
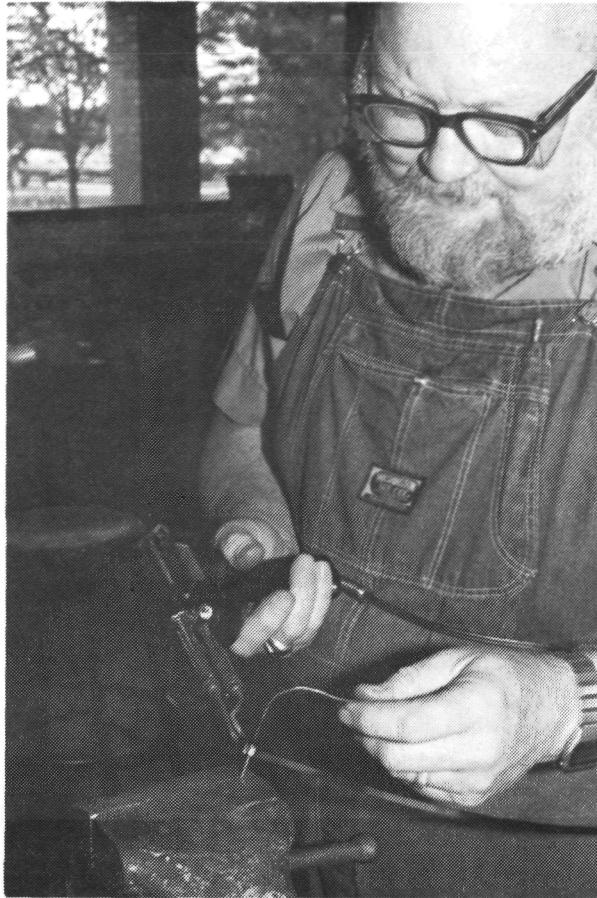


Photo 4-2



ORIGINAL PAGE IS  
OF POOR QUALITY.

Photo 4-3

Photo 4-4 shows the actual winding operation. Winding is done by hand.

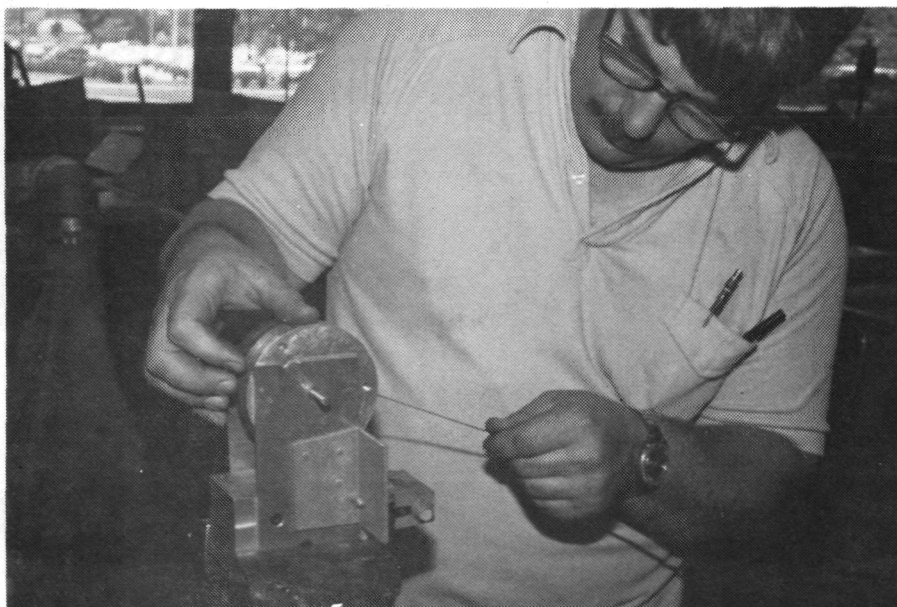


Photo 4-4

Many automated schemes of winding were tried, but hand winding has proven to produce better quality coils in about the same amount of time. Coils are either wound flat or curved depending on the coil installation.

Photo 4-5 shows the second electrical connector being soldered into place. Here again, the pin serves a secondary function which is holding the coil together during manufacture. In this case, the coil was wound flat.

The next step is adding a layer of 9.8 oz fiberglass, as shown in photos 4-6 and 4-7. The fiberglass serves three functions: 1) it provides insulation; 2) it gives the coil mechanical strength and integrity; and 3) it provides impact and scuff protection for the coil.

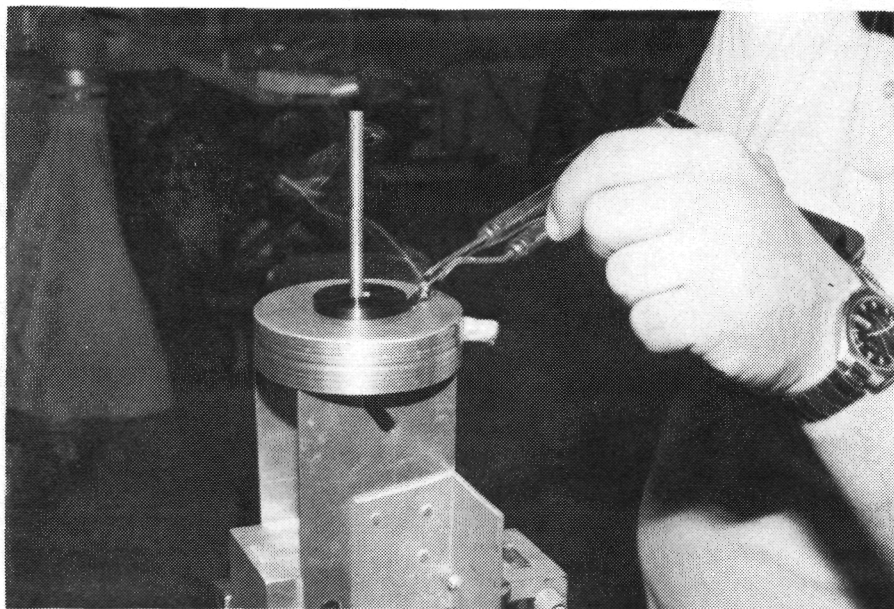


Photo 4-5



Photo 4-6



Photo 4-7

Photo 4-8 shows a heat lamp being used to speed epoxy/fiberglass cure time. Care must be taken at this time, because too much heat will degrade the insulating properties of the epoxy by making it porous from too much "out-gassing."



Photo 4-8

As mentioned earlier, coils must often be curved to match the contours of a leading edge. Photo 4-9 shows form blocks, which are one of three ways currently used to produce curvature. These particular form blocks are made of 40 lb/ft<sup>3</sup> polyurethane foam. Photo 4-9 shows the form blocks and the newly finished coil. Photo 4-10 shows the form blocks pressing a coil into shape.

ORIGINAL PAGE IS  
OF POOR QUALITY

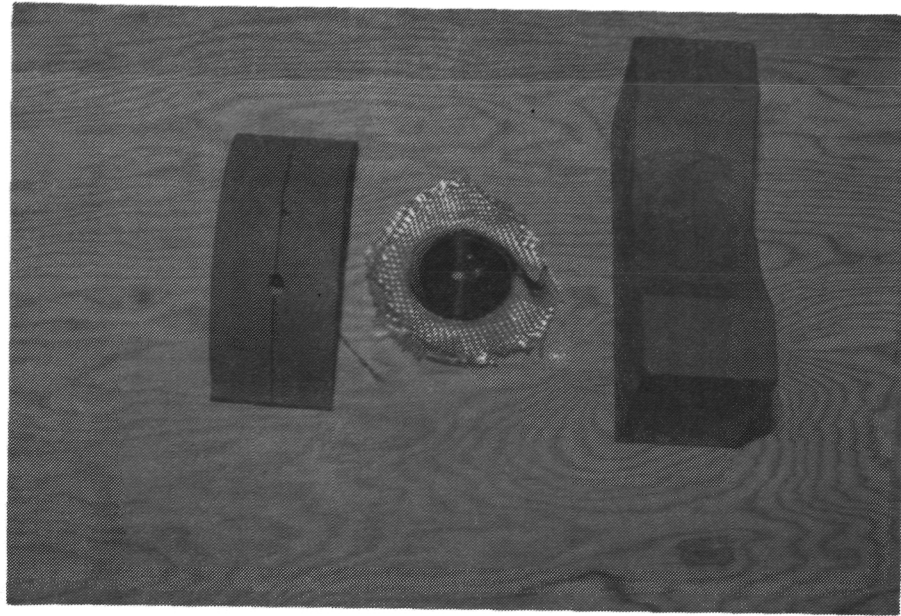


Photo 4-9

ORIGINAL PAGE IS  
OF POOR QUALITY

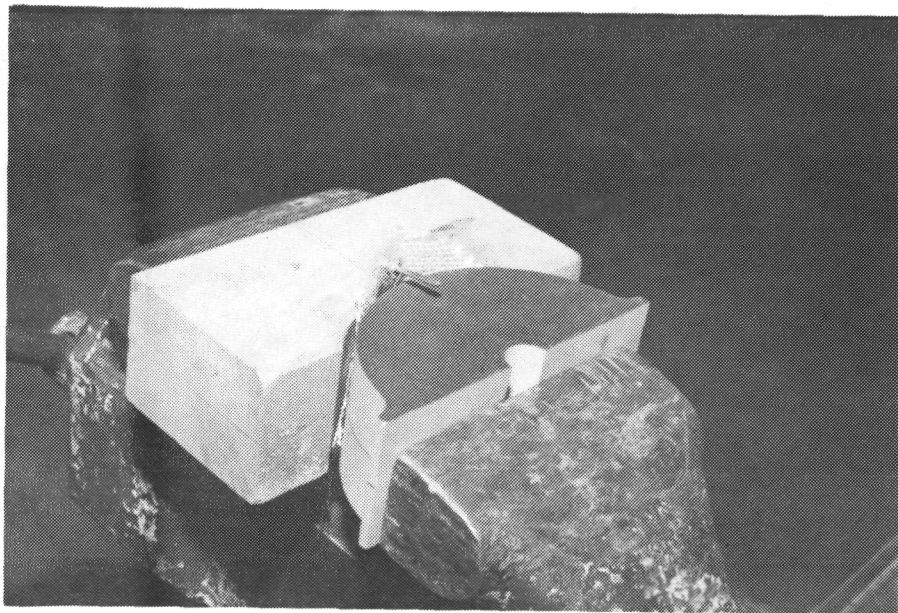


Photo 4-10

The second method is to wind the coil in a curved shape, a job which is more easily said than done.

The third method is to actually machine the coil to shape. Photo 4-11 shows this operation on a rotary die mill. This operation is only performed for high precision laboratory coils because it is a time consuming and difficult job. The very soft copper in the coils is nearly impossible to machine. Many different methods have been tried but nothing seems to work very well. After machining, the coils must be etched in concentrated nitric acid to remove electrical shorts induced by this machining.

After acid etching, manufacture is completed by repeating the steps shown in Photos 4-6 through 4-8.

### Coil Mounts

Fabricating coil mounts is the next step. Photos 4-12 through 4-15 illustrate the basic method used for making almost all coil mounts. While details may vary from coil mount to coil mount, the basic design philosophy is constant.

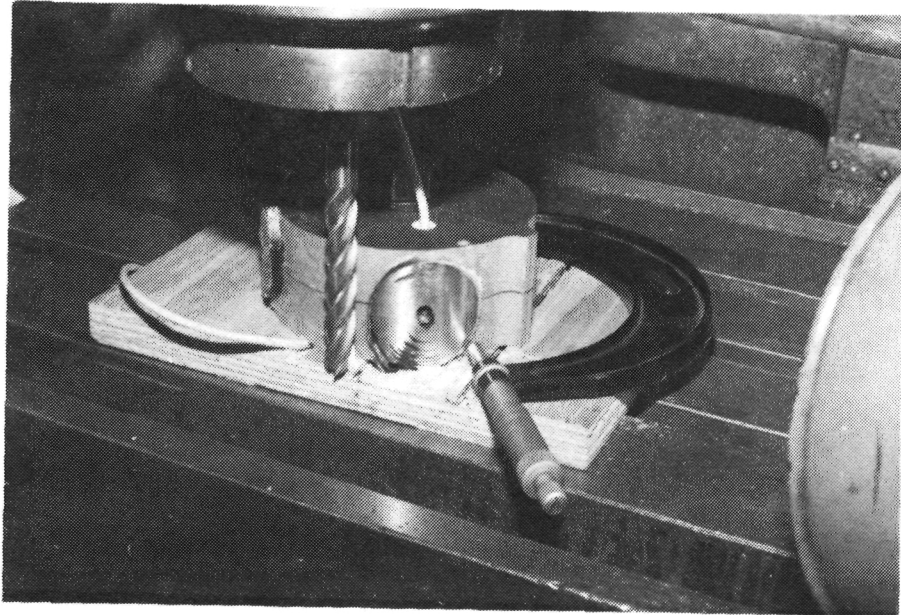


Photo 4-11

ORIGINAL PAGE IS  
OF POOR QUALITY

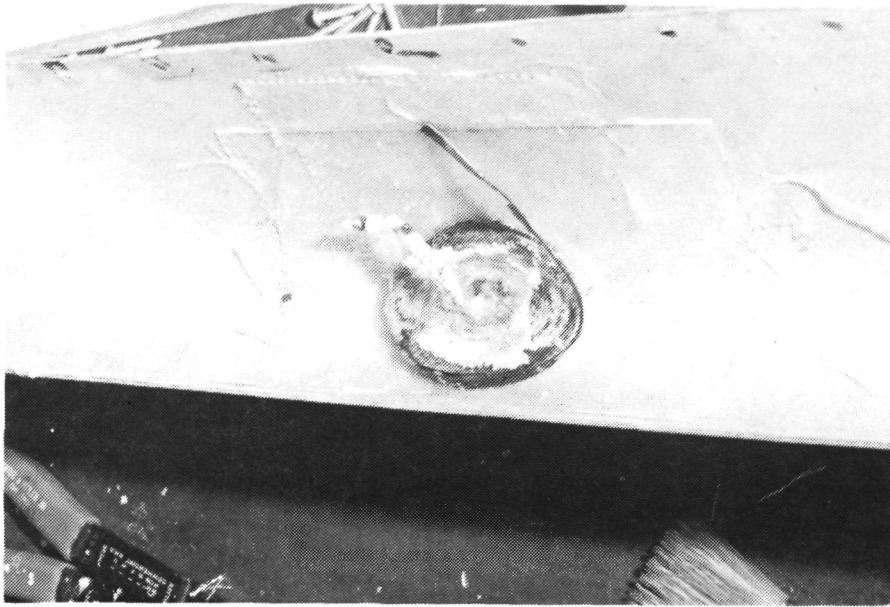


Photo 4-12

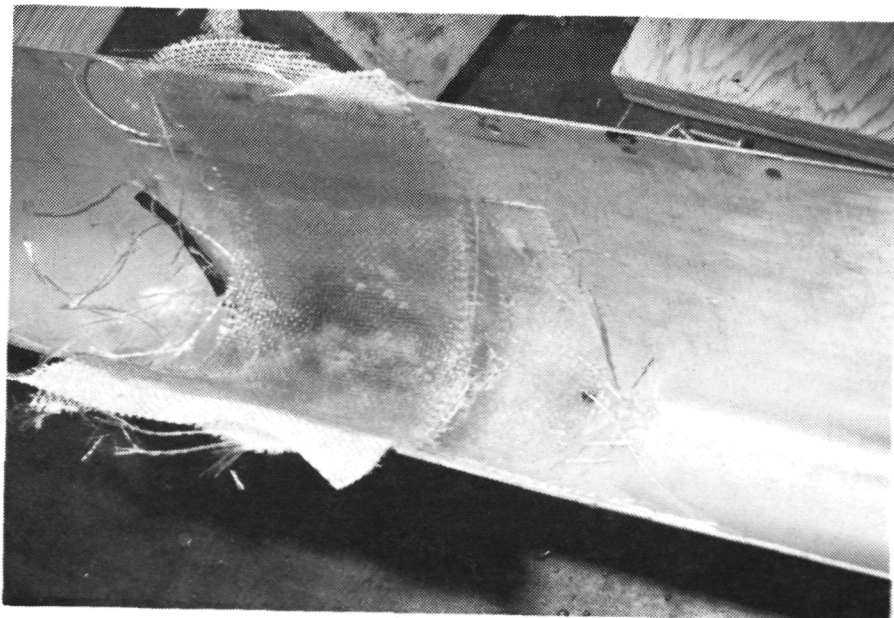


Photo 4-13

ORIGINAL PAGE IS  
OF POOR QUALITY



Photo 4-14

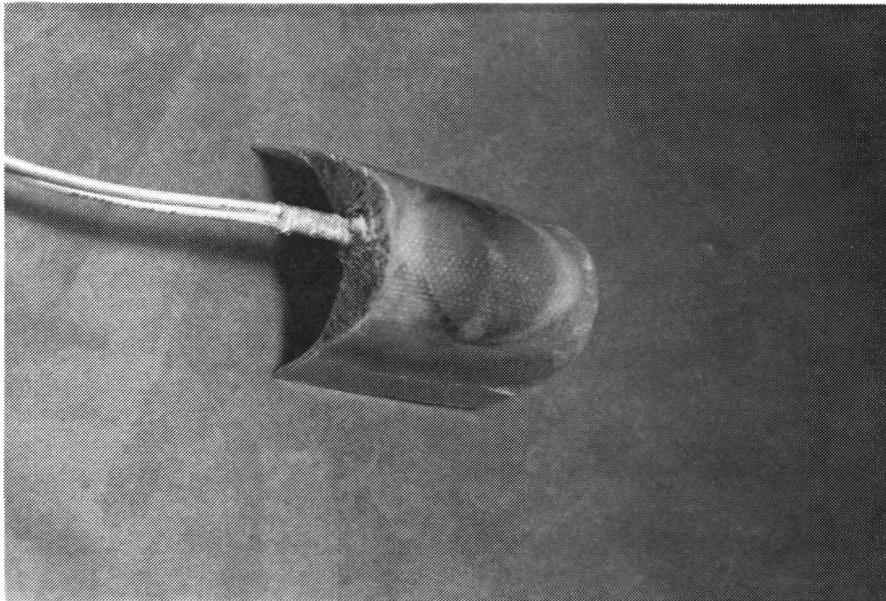


Photo 4-15

Coil mounts are made with epoxy/fiberglass and polyurethane rigid foam . Composites are used because they do not conduct electricity and because composite structures can be made both rigid and light. The first question is, "Why use fiberglass and not Kevlar or graphite?" Graphite is not used because it conducts electricity and Kevlar is not used because it's resistance to abrasion is much inferior to fiberglass.

Fiberglass seems to have the best mix of desired properties. These desired properties are high abrasion and impact resistance, structural stiffness, and good electrical insulating properties.

The second question is, "Why use polyurethane rigid foam as a composite sandwich material?" Polyurethane foam is used because it is compatible with epoxy/fiberglass construction and because polyurethane foam can be formulated to have good bearing strength and good impact resistance.

At this point, comments on the quality of available materials are appropriate. Regardless of manufacturer's guaranteed specifications, components must be chosen carefully. Not all epoxies work equally well, nor are all urethane foams equal. Specifications seem to mean very little. For epoxy, we use Gougeon "Brothers" West System. It's specifications are unimpressive when compared to competitive products, but it's performance is outstanding. Our two part pour-in-place urethane foam comes from General Plastics Inc. who also supplies our pre-cast rigid urethane blocks.

Now we will return to actual construction techniques. Photo 4-12 shows the first stages of mount construction. This photo shows the interior surface of a LearJet Model 55-Century III leading edge. The interior surface is treated with an epoxy release agent and then a two ply fiberglass spacer is laid up using the leading edge as a mold. This spacer is about .03 inches thick and appears as the long rectangular part in Photo 4-12. Spacers can be made of sheet wax or just about anything else. The spacer's sole purpose is to provide a .05 inch stand off distance between the interior surface of the leading edge and the opposing coil face and an .03 inch air gap between the coil mount and the interior surface of the leading edge. The spacer is discarded upon final installation.

The spacer is then trimmed to the desired size and treated with an epoxy release agent. A single ply of 9.8 oz fiberglass is laid up on the spacer and the leading edge. This ply is the outer layer of the coil mount and is the square part shown in Photo 4-12. The coil or coil pair is then

bonded to this outer layer. This layer provides abrasion protection, impact protection and electrical insulation for the coil, and is most important. Two more plies of fiberglass are added behind the outer layer completely capturing and encapsulating the coil. Total ply count now stands at 3 layers.

For lighter gauge leading edges of .03 inch or less only 2 layers of 9.8 oz fiberglass are required. The LearJet leading edge requires three plies because it is .063 inch thick and is extremely stiff. We now have a three ply arch with the exact shape of the leading edge less the thickness of the standoff spacer.

A three ply back plate arch is now added for extra strength. Photo 4-13 shows the spacer and the 3-ply back plate arch. The encapsulated coil appears as a dark shadow behind the semi-transparent back plate. Note that for lighter gauge aluminum leading edges 2 plies have the necessary strength. The six ply double arch is allowed to cure until it is almost hard. At this time the double arch is separated from the mold which is the leading edge and spacer. Next, the double arch is sawed to the desired size. Photo 4-14 shows the mount after removal and trimming to size.

Wire leads are then soldered to the coil, and the space between the two arches is filled with 2 part foam-in-place rigid urethane foam, Photo 4-15. In this case, 12 lb/ft<sup>3</sup> foam was used, however foam as light as 2 lb/ft<sup>3</sup> will work for light gauge leading edges.

### Electrical Leads

Care must be taken on the leads to the coil will fatigue with repeated coil firings. Photo 4-15 shows the best method found to date of connecting up coils; note the fiberglass strain relief which protects the two lead wires.

Placing screw terminals on coil mounts can lead to broken mounts or broken power cable terminals. The illustrated design arrangement eliminates exposed terminals and wires and provides double and triple insulation for all electrical components.

### Weight Estimates

Single coils have an outside diameter of about 2.5 inches and 40 turns. The wire measure about .025 x .195 inches, and completed coils weigh about 5 ounces.

Typical coil pairs are composed of two 30 turns coils having an outside diameter of 1.8 inches, and weighing 5.5 to 6.0 ounces.

Reducing coil thickness will reduce weight. A coil pair made from .025 x .100 inch wire should weigh 2 to 10 ounces depending on size and strength requirements. The mount in Photo 4-15 weighs about 3 ounces after subtracting the weight of the coil and lead wires.

An absolute minimum design weight using aluminum coils would appear to be in the 3 to 4 ounce range. A more practical design weight would be 5.0 to 7 ounces, a figure which has already been achieved.

### Coil Attachment

Coil mounts are attached to models in two ways. The first way is screw attachment to the front wing spar or to a false spar positioned ahead of the front wing spar.

The second method is direct bonding to the leading edge interior surface. The mount pictured in Photo 4-15 is a direct bonding type mount. The bonding surfaces are the flat, slightly extended strips adjacent to the table in the photograph. Bonding to the interior surface of the leading edge skin is a difficult task because the bond lines are subject to both peel and impact. To this point, only two adhesives have proven capable of performing this job, Loctite 324 and Gougeon Epoxy with natural fiber reinforcement. Of the two, Loctite 324 is easier to use. Aluminum 1100 series electro-magnetic doublers are also bonded to thin skins using Loctite 324 or Gougeon Epoxy.

### Icing Tunnel Models

Model preparation is another major task performed at WSU. WSU uses sheet metal and composite fabrication techniques which are common to all aircraft experimental shops. Unlike some wind tunnel test models, most EIDI models are actual parts or pieces taken from real aircraft. Photo 4-16 shows a LearJet Model 55 wing being prepared for Icing Tunnel tests. The wing has been sawed off to proper length and threaded steel angles have been added to accept a wind tunnel mounting plate. The LearJet wing has quite thick skin (.125 in) and so the angle brackets are attached to the skin. More commonly, angle are attached to wing spars. Photo 4-17 shows the model mounting plate. The plate bolts to the steel angles in the reinforced LearJet wing and in turn the plate/wing assembly bolts to the wind tunnel turntable. The plate measures 1/2 inch thick and is made of 6061 T-6 aluminum.

ORIGINAL PAGE IS  
OF POOR QUALITY

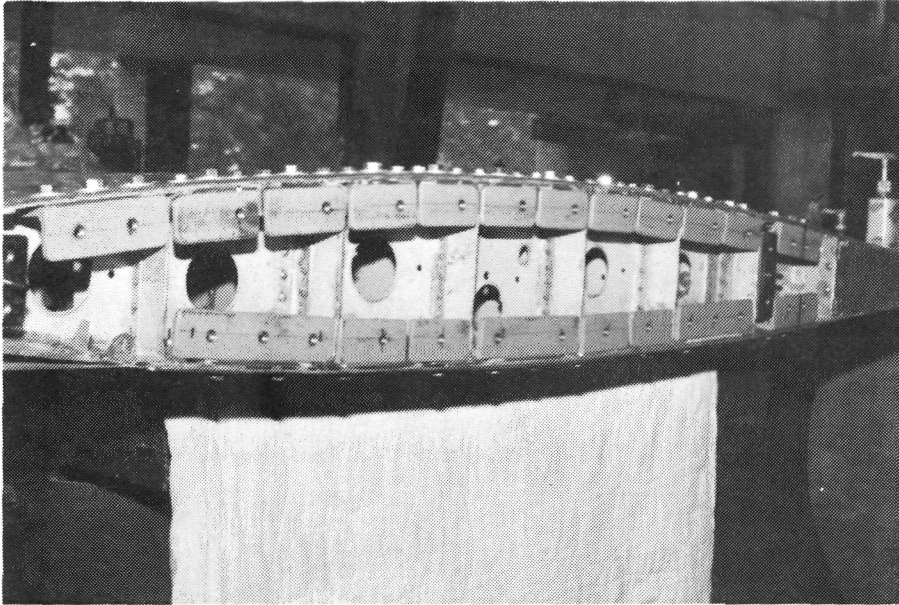


Photo 4-16

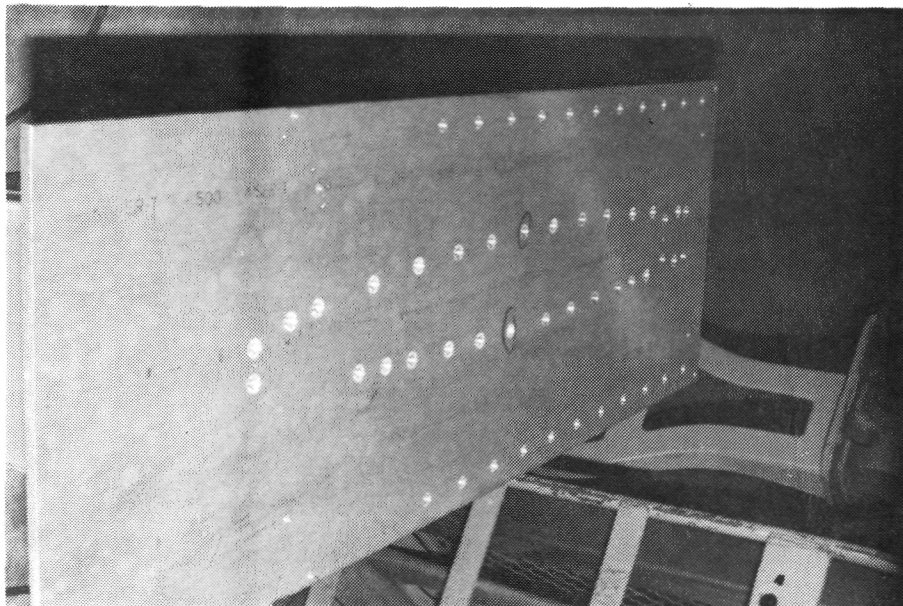


Photo 4-17

## Test Model Instrumentation

The third major WSU shop function is instrumenting test models. This primarily involves the installing of strain gages, but with a sinister twist. EIDI pulsers do terrible things to strain gages. Firstly, EIDI coils physically knock strain gages off the surface of the leading edges. Secondly, The coils electrically energize the gages, turning every strain gage into a miniature high voltage transformer.

Photos 4-18 through 4-20 show partial solutions to both problems.

The first problem, physical de-bonding, is eased by installing a thin sacrificial layer of fiberglass above the strain gage.

The second problem, electrical interference, is limited by special wiring techniques developed by Dr. Robert Schrag.

Strain gage installation starts with metal preparation. Metal preparation steps are:

1. De-grease the metal
2. Sand the metal with 60 to 100 grit sand paper
3. De-grease the metal
4. Mark the desired strain gage location with 6H drafting pencil
5. De-grease the metal
6. Acid etch the metal
7. Neutralize the metal with ammonium hydroxide solution
8. De-grease the metal twice
9. Bond strain gages to metal surfaces using M-Bond 200 or Perma-Bond 200 and adhesives. Step 9 is shown in the center of Photo 4-18.
10. Solder a small gauge insulated wire to one of the solder tabs (shown in bottom of Photo 4-18).
11. Solder a second small gauge insulated wire to the second solder tab and double back the wire across the middle of the strain gage, Photo 4-19. This doubling back causes the gage to self-cancel much of the induced error signal.
12. The two leads are now twisted together to again reduce induced signals; see Photo 4-19.
13. Finally a 4 mil layer of fiberglass cut on a 45° line is bonded over the gage to greatly slow gage debonding, Photo 4-20. The fiberglass is oriented to cause little or no strengthening to the metal while at the same time retaining the gage.



Photo 4-18

ORIGINAL PAGE IS  
OF POOR QUALITY

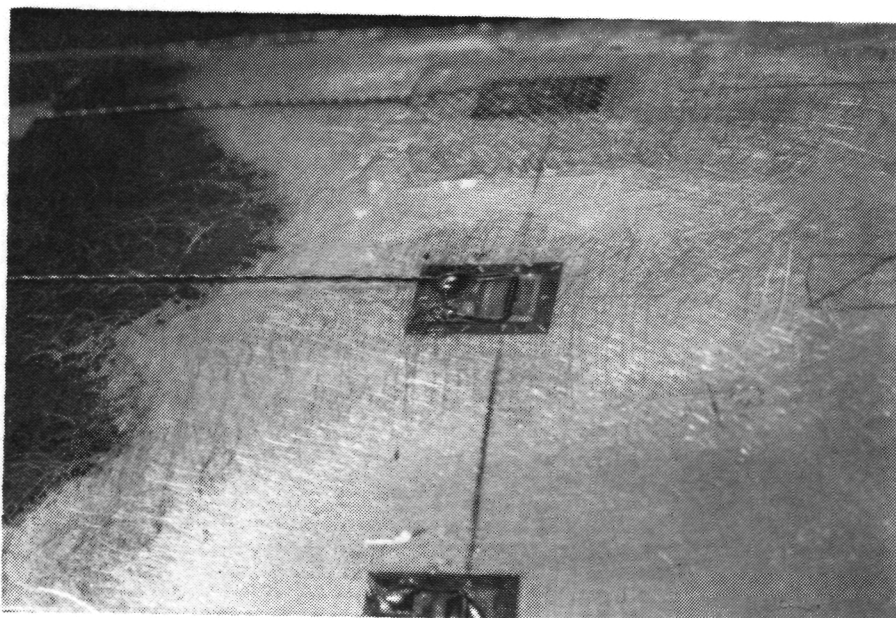


Photo 4-19

ORIGINAL PAGE IS  
OF POOR QUALITY

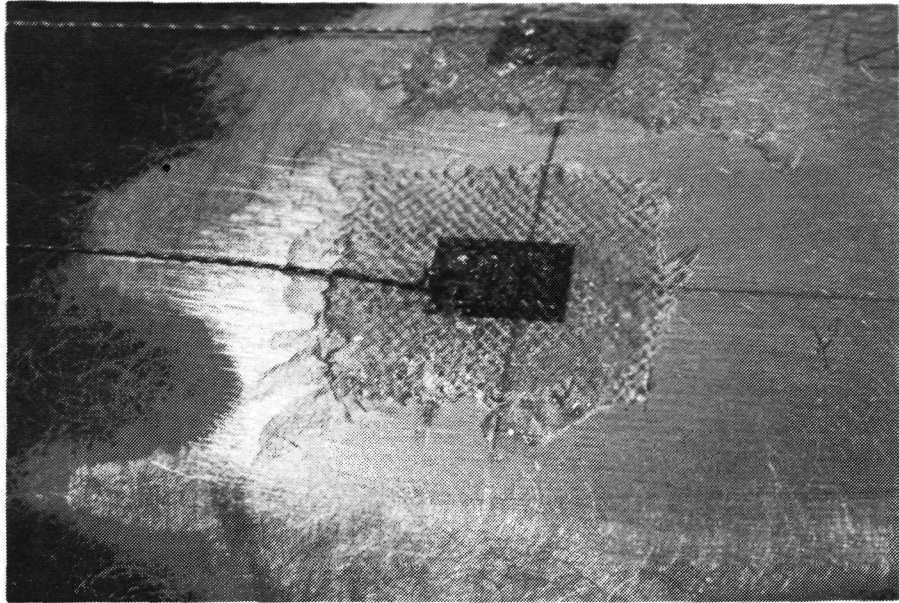


Photo 4-20

Strain gages being used have a resistance of 350 ohms, are temperature compensated and have a foil grid which measures  $1/8 \times 1/8$  inch.

## Chapter 5. ICING TUNNEL TESTS

An essential part of developing the EIDI system was testing in the NASA Icing Research Tunnel (IRT) at the Lewis Research Center in Cleveland, Ohio. This is a unique facility. The test section of 2 by 3 meters permits full-scale testing of many aircraft components such as wing sections, engine inlets and tail sections. Air speeds over 250 MPH and temperatures below 20°F can be obtained. The spray system provides a range of subcooled water droplets with median volume diameters from 10 to 20 microns and a fair range of liquid water content values.

The first test in Oct.-Nov. 1982 was a feasibility demonstration. This resulted in the decision to proceed with a full development project for the EIDI system. The eight test periods in the IRT are briefly summarized below.

### I. Oct. 25 - Nov. 5, 1982 Tests

#### A. Two Models Tested.

1. Beech Bonanza wing; aluminum leading edge, skin thickness 0.032 inches; tapered; very small distance from spar to high-light, giving a stiff leading edge.
2. Cessna 206 wing; aluminum leading edge, skin thickness 0.025 inches; no taper or twist; over 10 inches from spar to high-light gave a soft, flexible leading edge. Ribs were spaced from 9 to 15 inches apart.

#### B. Test Descriptions:

##### 1. Beech Bonanza Wing

\* Coils in 3 positions, 14 inches apart, racetrack shaped coils, two side coils in series at each position.

\* 31 runs

\* Tunnel conditions:

110 MPH	25°F	1.2g/m <sup>3</sup>	15 microns
110	25	2.4	20
160	25	0.83	14
160	25	1.7	20
230	25	10.6	12
230	25	1.2	20
110	5	1.2	15
160	5	0.83	14
160	5	1.7	20
230	5	0.6	12
110	20	2.4	20

## 2. Cessna 206 Wing

\* Coils in 3 positions between ribs, supported from beam-between-ribs. Coils were round; side pairs of coils were series wired. After 21st run, the center coil was replaced by a "racetrack" shaped coil at the nose.

\* 36 runs

\* Tunnel conditions:

110 MPH	25°F	1.2g/m <sup>3</sup>	15 microns
110	25	2.4	20
160	25	0.83	14
160	25	1.7	20
160	5	0.83	14
160	5	1.7	20
110	5	1.2	15
110	5	2.4	20
110	-15	1.2	15
160	-15	0.83	14
160	-15	1.7	20
110	29	1.2	15
110	29	2.4	20
160	29	0.83	14
160	29	1.7	20
160	15	1.7	20

In addition to the above variables, angle of attack and capacitance were also varied.

## C. Major Results and Conclusions

1. The EIDI system can de-ice two General Aviation wings, one stiff and one flexible in leading edge properties, over a wide range of atmospheric and icing conditions.
2. The energy required for a de-icing cycle was about 800 joules per foot of span.
3. High speed movies gave insight into the de-icing phenomenon.

## D. Participants

These tests were performed under W.S.U. direction with participation at the IRT by persons from Beech and Cessna Aircraft Companies and Simmonds-Precision. Beech and Cessna provided wing sections for the test models, while Simmonds designed and fabricated the power-and-sequencing box. This Simmonds-Precision power box has been used in all IRT tests to date with some modifications. It can supply up to 1800 volts at capacitances from 100 to 750 micro-farads.

## II. April 18-22, 1983 Tests

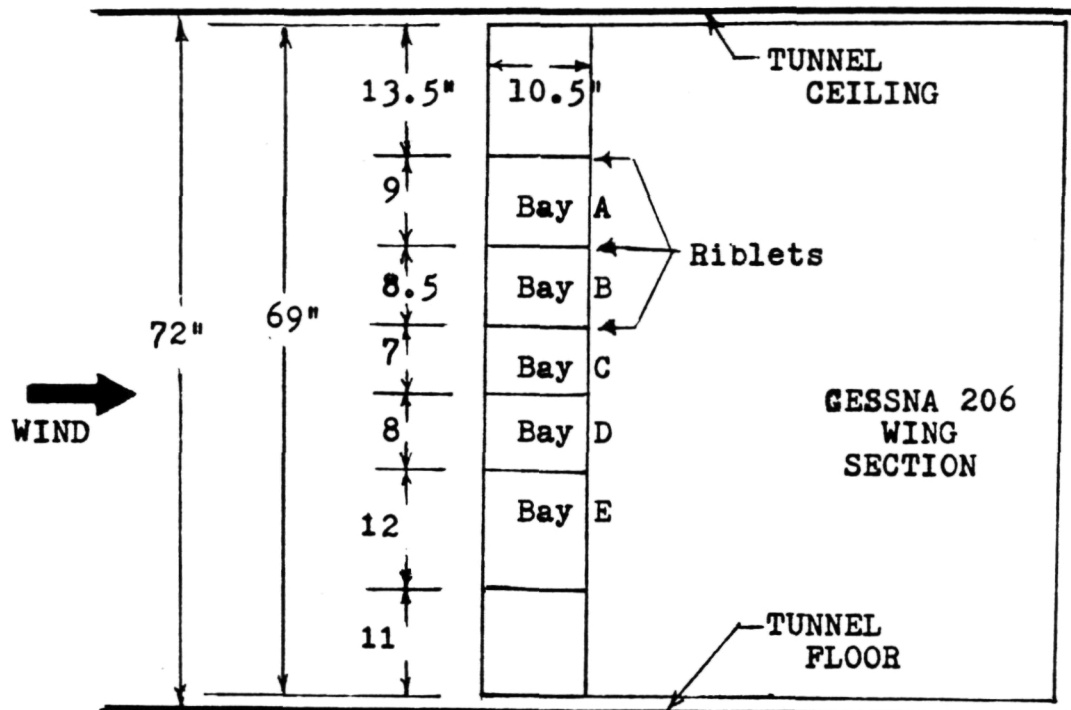
### A. Two Models Tested:

1. Cessna 206 wing with 0.025 aluminum leading edge skin.
2. Cessna 206 wing with 0.040 aluminum leading edge skin.  
Both were on an unswept, untapered, untwisted wing.

### B. Test Descriptions (See diagrams on the next two pages).

1. Cessna 206 wings; 0.025 inch aluminum skin.
  - \* Coils in 5 bays between ribs; 5 different coil-mount combinations.
  - \* 31 runs
  - \* Tunnel conditions were kept constant: 160 MPH, 15°F, 1.7 g/m<sup>3</sup>, 20 microns, 2° angle of attack, 600 uFd.
  - \* Primarily a comparison between different coil or mount designs.
  - \* Variations on a few runs were:
    - (a) reduce capacitance to 400 uFd.
    - (b) "full-cycle" voltage by removing the diode clamp.
    - (c) insertion of false spars to stiffen skins in 3 bays.
    - (d) reduced voltage to find number of impulses vs voltage to de-ice.
2. Cessna 206 wing; 0.040 inch aluminum skin.
  - \* Coils in 5 bays between ribs; 5 different coil-mount designs.
  - \* 28 runs
  - \* One bay had skin replaced by a graphite composite leading edge with a copper doubler.
  - \* Primarily a comparison between different coil/mount designs, two of which were different from those used for the previous, thin-skin, leading edge.
  - \* Variations on a few runs were:
    - (a) reduce capacitance to 200 uFd.
    - (b) "full-cycle" voltage cycle.
    - (c) insertion of false spars.
    - (d) application of de-icing fluid, ICEX, on the composite leading edge.
    - (e) gap between coil and skin filled with plastic material to see structural damping due to "no gap" condition.
    - (f) one run at air temperature 29°F.

ELECTRO-IMPULSE DE-ICER PLACEMENT IN WING FOR ICING  
TUNNEL TESTS, APRIL 18-22, 1983



Thin-Skin Leading Edge (0.025 in.)

- Bay A. Two Side Coils, With Doublers (Spar)\* (Zero Gap)\*
- Bay B. Two Side Coils (Spar) (Zero Gap)
- Bay C. One Nose Coil, With Doubler
- Bay D. One Nose Coil (Zero Gap)
- Bay E. Push-Pull Design (Spar) (Zero Gap)

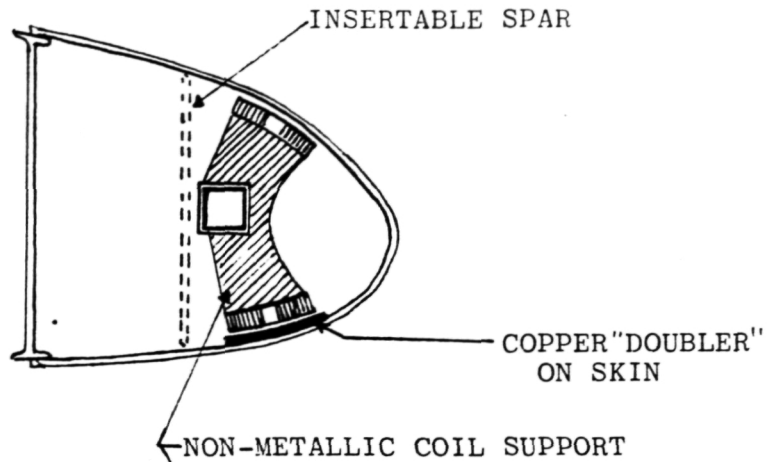
Thick-Skin Leading Edge (0.040 in.)

- Bay A. Two Side Coils, With Doublers (Spar)
- Bay B. Two Side Coils (Spar)
- Bay C. Two Side Coils Off-set Spanwise
- Bay D. One Nose Coil
- Bay E. Composite Leading Edge Inserted One Nose Coil of Inverse Design

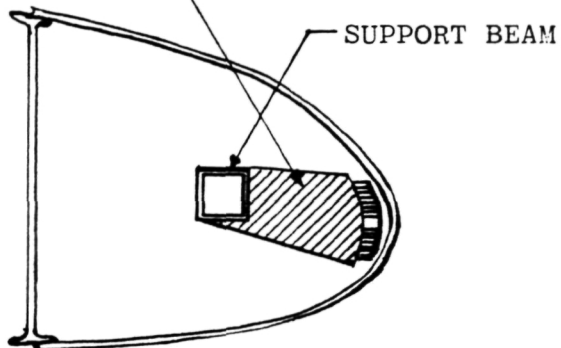
\*Indicates changes which can be made without removing the wing from the tunnel. A false spar will be inserted or a semi-soft plastic will be placed between the coil and skin to simulate the effect on skin movement of placing the coil directly against the skin.

COIL DESIGNS TESTED APRIL 18-22, 1983

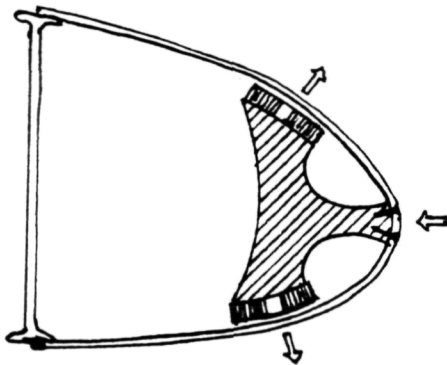
SIDE COILS



NOSE COIL

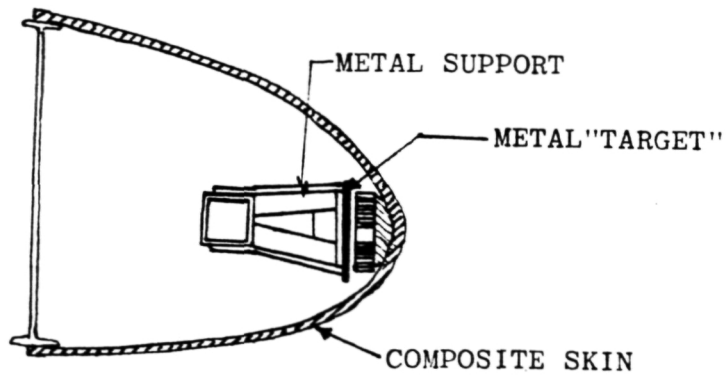


PUSH-PULL  
TYPE



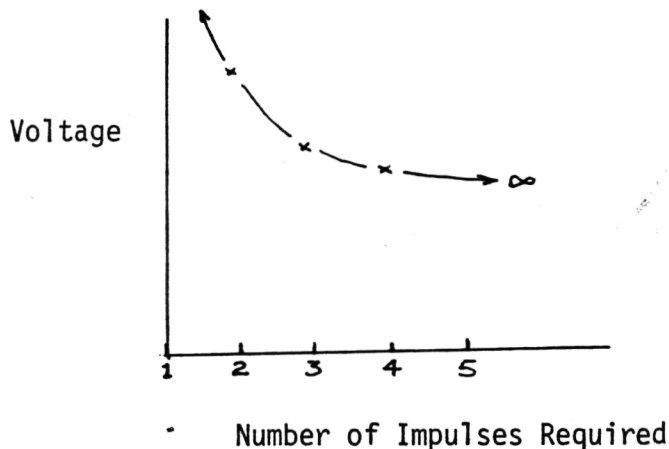
INVERSE TYPE

(COIL MOUNTED  
ON THE SKIN)



### C. Major Results and Conclusions

1. Using 0.050 inch aluminum doubler with the 0.025 inch skin decreases the required energy by 50% both for nose and side coils. For the 0.040 inch thick skin with side coils, the doubler advantage was (surprisingly) over 50%.
2. With doublers, de-icing energy was under 600 Joules per foot of span.
3. One bay had two side coils off-set spanwise from each other, at about the 1/3 span positions, in an attempt to twist the leading edge. This was inferior to aligned coils.
4. Anti-icing attempts were disappointing. Almost the same energy is required to expel 1/8 inch and 2 inches of ice thicknesses.
5. The optimum number of impulses at each coil is two or three. The general pattern is shown below.



### D. Participants

In addition to W.S.U. personnel, Alan Mueller of Cessna Aircraft Company, conducted the test. Cessna provided the leading edges; the wing model from the 1982 test was used again.

### III. August 15-18, 1983 Tests

#### A. One Model Tested:

A 50 inch span "glove" or "cuff" placed on a six-foot section of DHC-6 Twin Otter wing. The glove was identical in shape and material to the base wing, but extended three inches forward of the leading edge. Skin thickness was 0.025 inches with leading edge radius of 2.5 inches.

#### B. Test Descriptions:

\* four nose coils, one each in four 12.5 inch bays; separated by ribs. Coils were skin-mounted by rivets about 3 inches behind the stagnation line.

\* 35 icing runs.

\* Tunnel conditions:

100 MPH	28°F	1.4g/m <sup>3</sup>	= 10°
100	28	2.2	10
124	28	1.1	7
124	28	2.0	7
170	28	0.85	5
170	28	1.65	5
170	15	0.85	5
170	15	1.65	5
124	15	2.0	5
100	15	2.2	10
124	15	2.0	7
100	15	2.2	14
170	15	1.65	5
170	15	0.85	5
124	15	1.1	7
124	15	0.85	4 to 9 (varying)
124	15	1.1	7
124	30	2.0	7

\* Capacitance was fixed at 400 uFd. Doublers of 0.050 inch thick No. 1145 aluminum were riveted opposite the coils.

\* Coils were impulsed both singly, simultaneously by wiring adjacent-bay coils in series, and by series wiring of every other bay. Series connecting was done for 2, 3 and all 4 bays.

### C. Results and Major Conclusions.

1. When impulsed separately, energy required for de-icing was about 600 Joules per foot of span (3 impulses of 200 Joules each). This was reduced for series-connected coils as follows:

Coil Connections	Voltage Required	Energy (Joules/Ft.)
Single Bay	1000	600
Two Bays in Series	1100	363
Two Alternate Bays	1200	280 (center bay not completely clean)
Three Bays in Series	1200	280
Four Bays in Series	1400	292

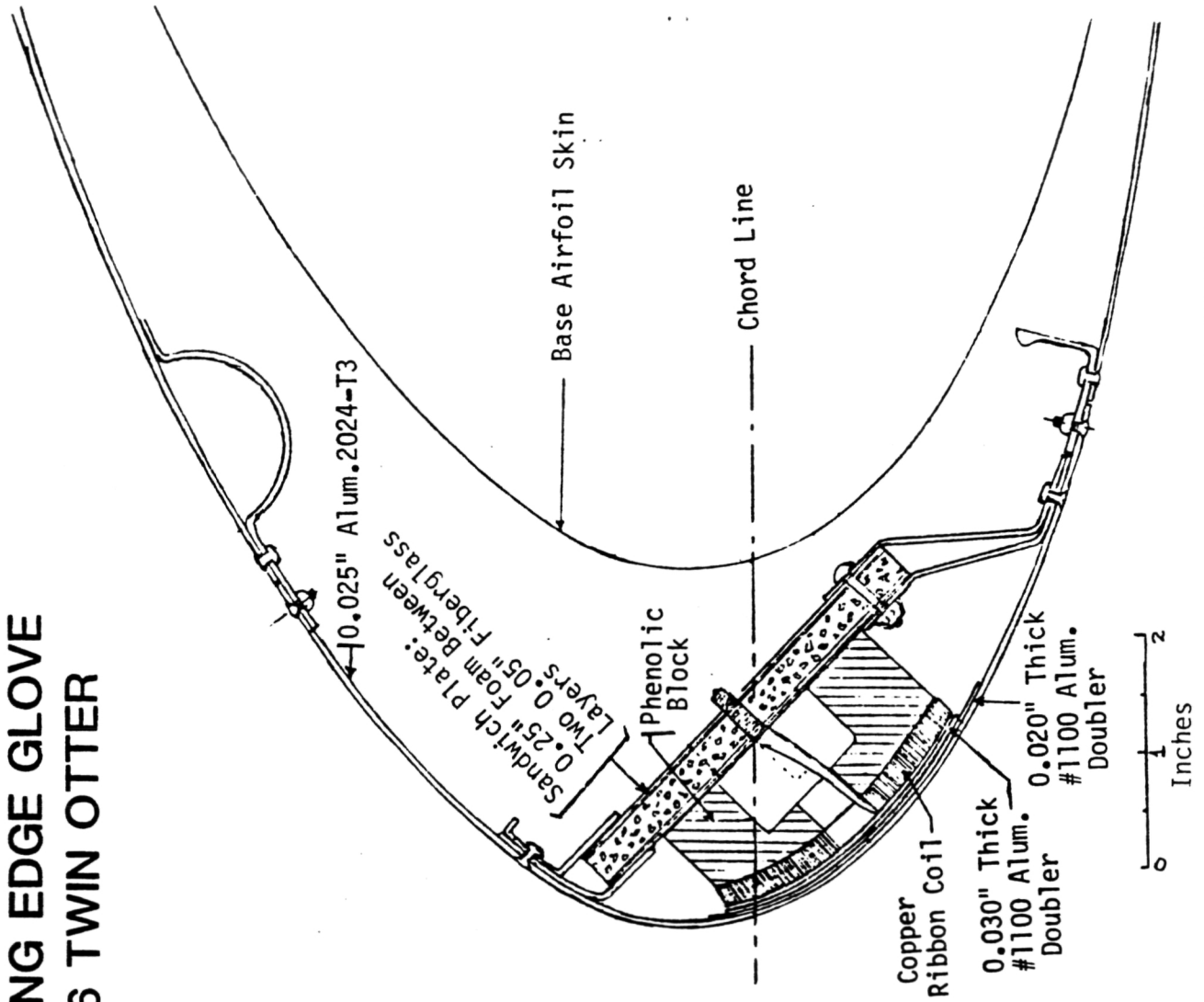
2. Some runs were made with continuous icing for up to 21 minutes with impulses 3 or 6 minutes apart. De-icing improved after the first impulse sequence in all cases.
3. When angle of attack was varied during the run, ice width was greater in the chord-wise direction, but ice expulsion was not affected.

### D. Participants

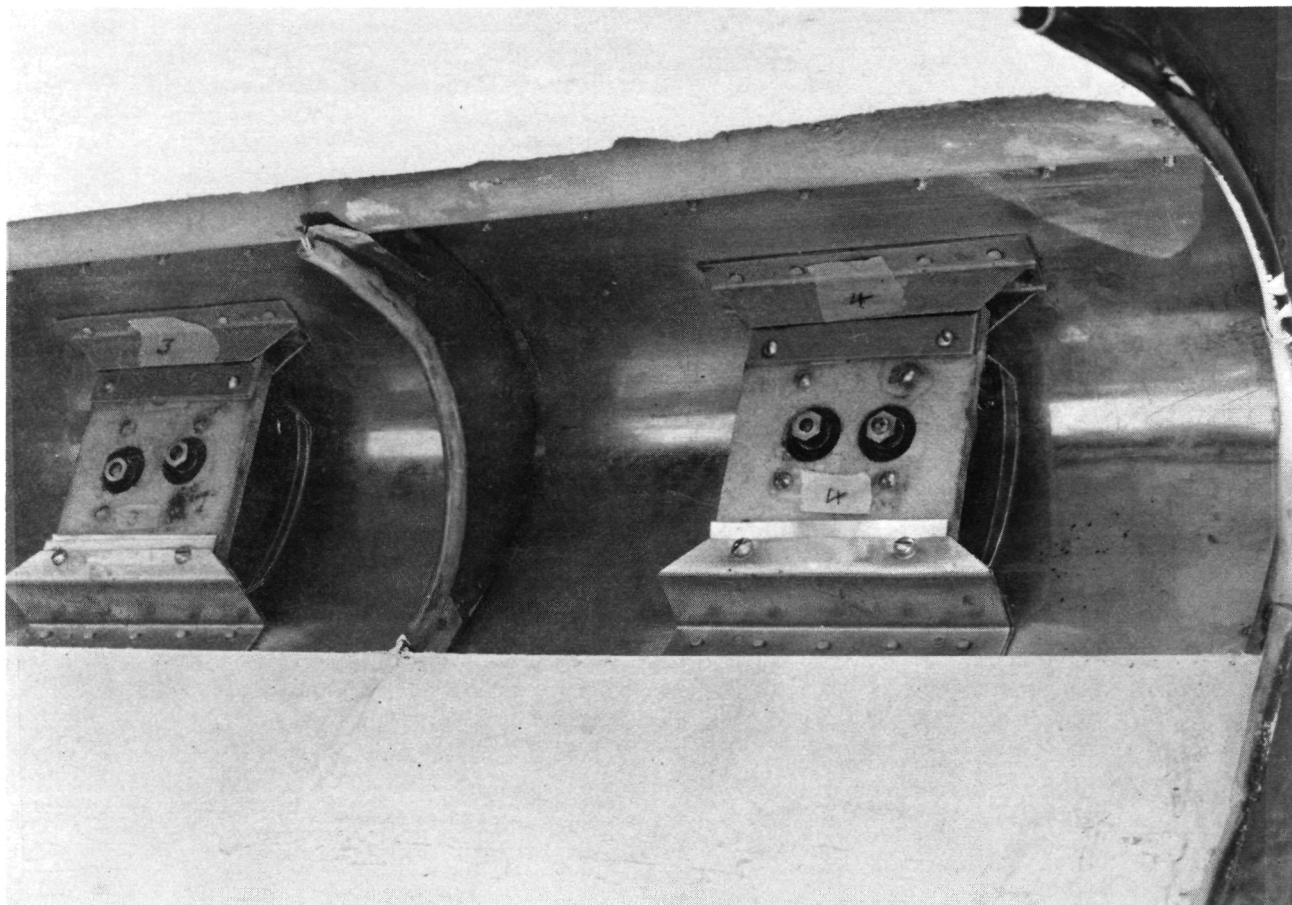
W.S.U. was joined by Robert Goehner of Simmonds-Precision for these tests.

# LEADING EDGE GLOVE DHC-6 TWIN OTTER

ORIGINAL PAGE IS  
OF POOR QUALITY



ORIGINAL PAGE IS  
OF POOR QUALITY



Coil Mounts Attached to the Skin  
of the Wing Glove for the DHC-6  
Twin Otter

#### IV. November 7-9, 1983 Tests

##### A. Two Models Tested:

1. The 50 inch Twin Otter glove (same as previous test).
2. A 34 inch span section from a LearFan wing made of Kevlar-epoxy composite. Coils were placed at the quarter and three-quarter positions, giving 17 inch spacing between coils. The leading edge had no ribs. A new type of coil mount was tested for use with composite wings. The coil was separated from the leading edge by a fiberglass-wrapped foam piece mounted on a thin aluminum plate. The plate was opposite the coil and provided the force to the foam wedge which transferred the impulse to the leading edge nose. Half of the composite surface was painted.

##### B. Test Descriptions

###### 1. Twin Otter glove.

\* Coils in the 4 bays were series-connected in two pairs of alternating bays (1-and-3; 2-and-4) for the first glove test series. Capacitance was kept at 400 micro Farads.

\* Only one coil was impulse for a second series while the electrical pulse time was varied by changing capacitance and adding external "dummy" coils in series. The purpose was to determine the optimum capacitance value.

\* 8 runs for first series; 11 runs for second series.

\* Tunnel Conditions:

100 MPH	28°F	1.4g/m <sup>3</sup>
124	28	1.1
170	28	0.85

###### 2. LearFan Composite Wing.

\* The two coils were impulsed separately and simultaneously.

\* 10 runs

\* Test Conditions:

160 MPH	25°F	0.83g/m <sup>3</sup>
---------	------	----------------------

\* Capacitance of 200, 400 and 600 microFarads.

##### C. Major Results and Conclusions.

1. For the Twin Otter (DHC-6) glove, the use of odd-and-even coil pairs reduced the needed impulses from 3 to 2 for good de-icing. The energy was thus reduced to about 200 Joules/ft.

2. For the second series of glove tests, the effect of capacitance was clear. The minimum energy for de-icing was obtained for 400 microFarads for this wing.
3. The Kevlar composite LearFan leading edge de-iced, but not well. Side coil impulses are probably needed. About 500 joules/ft. was required to de-ice.
4. Painted and unpainted Kevlar surfaces de-iced alike.

D. Participants

Mr. James Chase of LearFan took part in the test along with W.S.U. personnel.

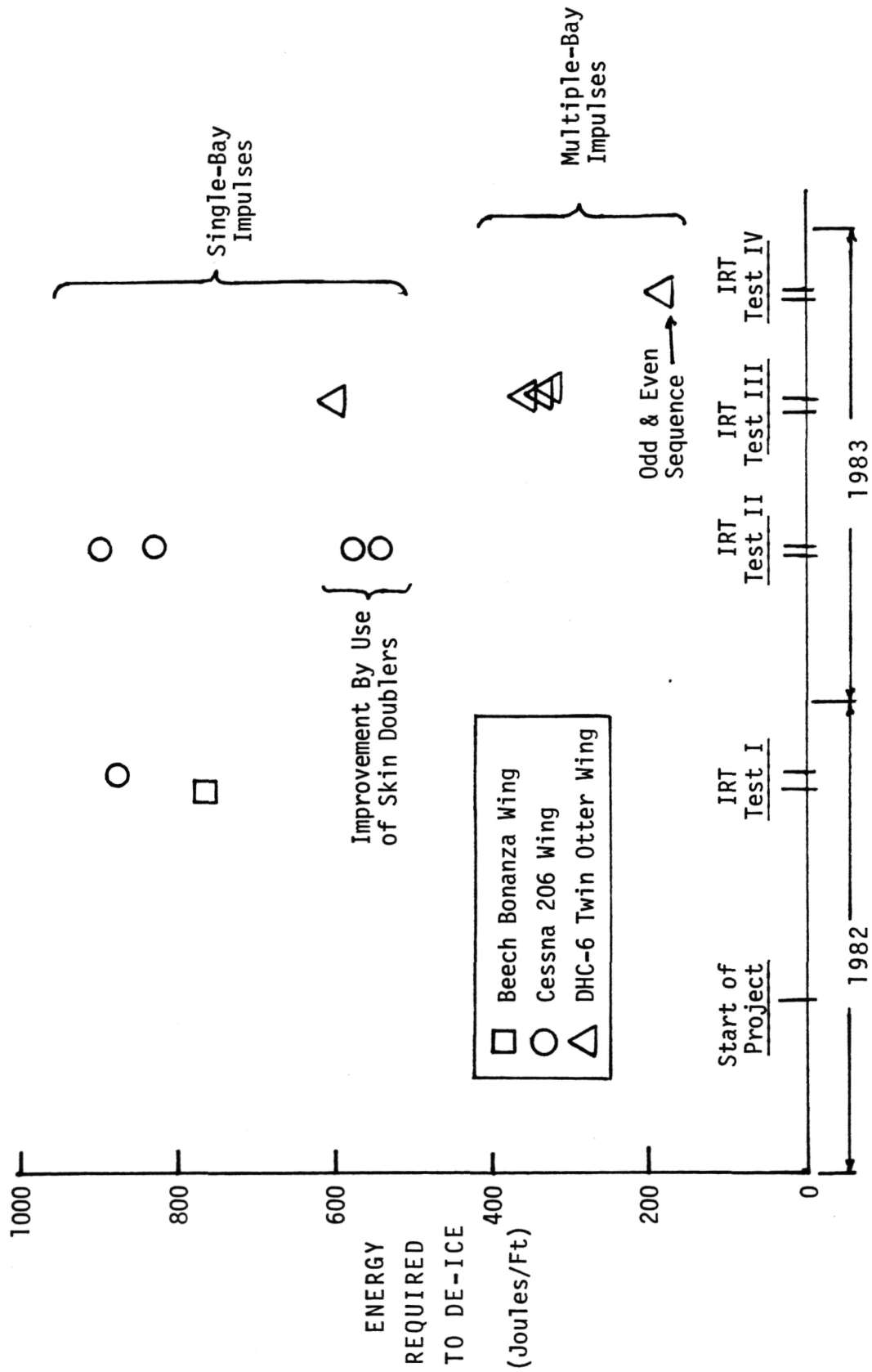
NOTE: At this point the energy required to de-ice a general aviation wing had been reduced dramatically, as shown in the table and plot on the following two pages.

SUMMARY OF RESULTS OF  
 ICING RESEARCH TUNNEL TESTS  
 OF  
 ELECTRO-IMPULSE DE-ICING

<u>DATE</u>	<u>WING</u>	<u>METHOD</u>	n =	<u>NO.IMPULSES PER POSITION</u>	<u>E = ENERGY (Joules/Ft)</u>	<u>ENERGY TO DE-ICE = nE</u>
Oct.1982	Beech Bonanza	Two Side Coils; Single Bay Hits.		2	383	766
Nov.1982	Cessna 206	Two Side Coils; Single Bay Hits.		2	440	880
Apr.1983	Cessna 206	Two Side Coils; Single Bay Hits.		2	450	900
	"	One Nose Coil; Single Bay Hits.		2	414	828
	"	Two Side Coils With Skin Doublers; Single Bay Hits.		2	289	578
	"	One Nose Coil With Skin Doubler; Single Bay Hits.		2	272	544
Aug.1983	DHC-6 Twin Otter	One Nose Coil With Skin Doubler; Single Bay Hits.		3	200	600
		Two-Bay Hits.		3	121	363
		Two-Bay With Bay Skipped Between		3	98	294
		Three-Bay Hits		3	96	288
		Four-Bay Hits		3	98	294
Nov.1983	DHC-6 Twin Otter	One Nose Coil With Skin Doubler; Two-Bay Hits, With "Odds-then-Evens" Sequence. (Bays 1 & 3 hit twice simultaneously, Then Bays 2 & 4 hit twice simultaneously.		2	90	180

Note: For this method,  
 four impulses  
 clean four bays.

These are plotted on the following page, with the "Total Energy Per Position Required To De-Ice" plotted against time when the tests were performed.



V. May 14-23, 1984 Tests

A. Four Models Tested:

1. Learjet wing with the standard (but modified) leading edge; skin thickness 0.063 inches; sweepback 17°.
2. Learjet wing with a composite material replacement leading edge which was 50% thicker and 100% stiffer, but had the same shape as the metal one.
3. A semi-cylinder of 5.0 inch diameter mounted with no sweepback; thickness 0.040 inches.
4. A Cessna 206 horizontal tail section; skin thickness 0.025 inches. This was tested to support the planned full-aircraft prototype program. Of the four models in this test, only this one had ribs in the leading edge.

B. Test Descriptions:

1. Learjet; metal leading edge.
  - \* Coils in 6 positions; 4 coil-mount combinations.
  - \* 15 runs with doublers added and 9 runs without doublers.
  - \* Tunnel conditions:

144 MPH	28°F	1.0g/m <sup>3</sup>
144	15	1.0
225	15	1.4
225	-10	0.6
  
2. Learjet; composite leading edge.
  - \* Coils in 6 positions; 5 types of coil/mountings.
  - \* 12 runs
  - \* Tunnel Conditions:

144 MPH	15°F	1.0g/m <sup>3</sup>
144	15	1.4
144	-10	0.6
  
3. Semi-cylinder
  - \* One nose coil at mid-span, spar mounted.
  - \* 13 runs
  - \* Tunnel conditions:

100 MPH	24°F	1.4g/m <sup>3</sup>
100	24	2.2
100	10	2.2
160	15	1.7

4. Cessna horizontal stabilizer

\* Coils in 4 positions; one without doublers.

\* 11 runs with the production-type rubber abrasion shield;  
tunnel conditions for this were:

100 MPH	28°F	1.4g/m <sup>3</sup>
124	28	1.1
160	28	0.83
160	15	0.83

\* 14 runs with the rubber abrasion shield removed;  
tunnel conditions for this were:

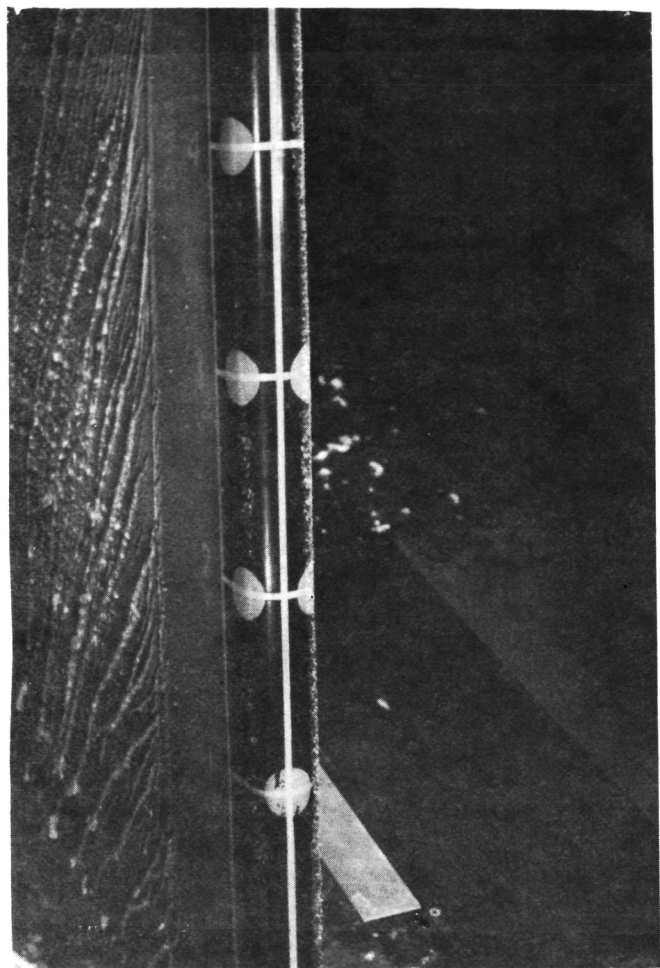
100 MPH	28°F	1.4g/m <sup>3</sup>
100	15	1.4
100	15	2.2
124	28	1.1
124	15	1.1
124	15	2.0
160	28	0.83
160	15	0.83

C. Major Results and Conclusions.

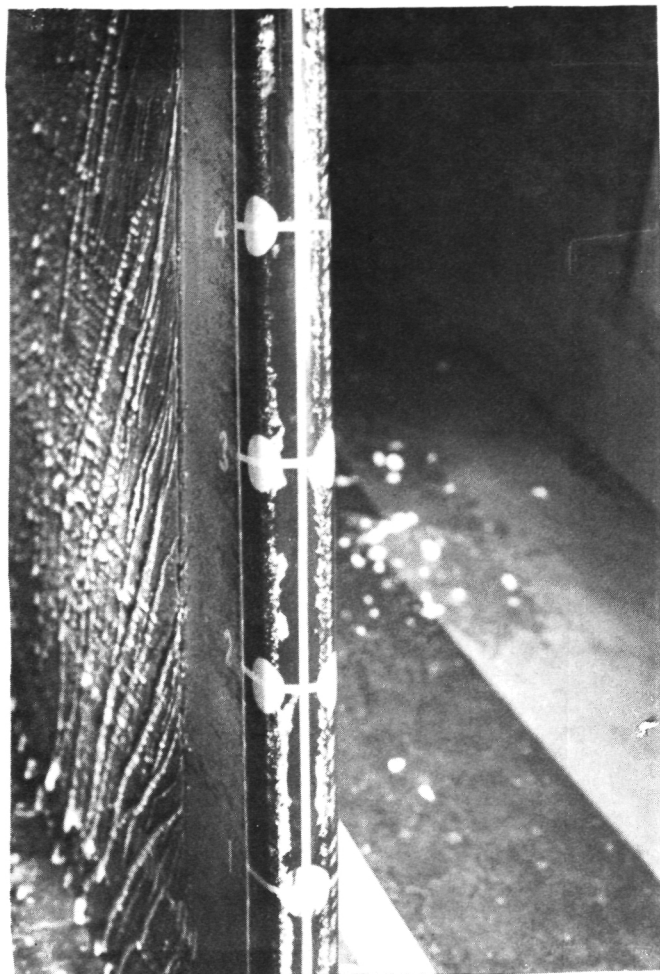
1. Learjet leading edge needs re-designed coil/mount system due to its peculiar, unsymmetrical shape.
2. Doublers are still helpful for 0.050" thick skins.
3. The composite material posed no special problem. It was only slightly more difficult to de-ice than its metal counterpart.
4. Painting the composite skin made no difference in de-icing.
5. The one coil in the semi-cylinder expelled ice from over five feet of length. Good high-speed movies were obtained for this.
6. The Cessna tail section was easily de-iced.

D. Participants

1. Gates-Learjet supplied the wing model and participated in the IRT test.
2. Cessna supplied an empennage for making the tail model and participated in the test.
3. Simmonds-Precision sent a participant for the IRT test.



20 micron droplet size  
1.4 g/m<sup>3</sup> LWC  
5 minutes spray  
700 volts/coil station



12 micron droplet size  
0.6 g/m<sup>3</sup> LWC  
10 minutes spray  
800 volts/coil station

Test Conditions For Both:

225 Miles/Hour Airspeed

15<sup>o</sup>F Air Temperature

4<sup>o</sup> Angle of Attack

400 MicroFarads

LEARJET ALUMINUM LEADING EDGE AFTER  
DE-ICING: ILLUSTRATION OF GREATER  
DIFFICULTY DE-BONDING SMALL-DROPLET  
ICE

VI. August 13-17, 1984

A. Three Models Tested:

1. A slat from the wing of a Boeing 767; sweepback  $34^{\circ}$ ; skin thickness, 0.062 inches. This portion of the slat was from a wing station about 65% of span from the fuselage.
2. The Learjet wing with its standard metal leading edge was returned for a second IRT test.
3. The 5 inch diameter semi-cylinder was returned with a side-coil pair at mid-span.

B. Test Descriptions:

1. Boeing 767

\* Coils in 6 positions; 3 coil/mount types.

\* 21 runs.

\* Tunnel conditions

170 MPH	28 <sup>o</sup> F	0.85g/m <sup>3</sup>
170	28	1.65
240	27	0.85
240	15	0.6
240	15	1.1
240	-10	0.54
240	-10	1.1

2. Learjet

\* Coils in 4 positions; 4 coil/mount types.

\* 22 runs

\* Tunnel conditions:

144 MPH	28 <sup>o</sup> F	1.0g/m <sup>3</sup>
144	15	1.0
225	15	1.0
225	15	1.4

3. Semi-cylinder

\* Two side-coils were spar-mounted in one mid-span position.

\* 14 runs

\* Recordings were made for signals from strain gages and, sub-miniature accelerometers mounted near the coils.

\* Tunnel conditions:

100 MPH	24 <sup>o</sup> F	2.2g/m <sup>3</sup>
100	15	1.4

### C. Major Results and Conclusions.

1. The Learjet wing still defied de-icing without unacceptable residual ice particles.
2. The Boeing 767 slat de-iced quite well using spar-mounted side-pair coils.
3. Best de-icing was achieved using very short electrical pulse times for the 767 slat; this gave higher skin stresses than desired. An optimized coil design and re-test is needed.
4. For the semi-cylinder, a nose coil is clearly superior to a pair of side coils. Good high-speed movies were obtained for the cylinder.
5. The skin-mounted coil-pair gave the best performance and lower stresses.

### D. Participants

W.S.U. was joined by three men from McDonnell-Douglas, one each from Boeing and Gates Learjet and two observers from the Lockheed-Georgia Co. Boeing supplied the B-767 slat.

A. Two Models Tested:

1. The Learjet wing was returned for a third set of tests. Three new coil/mount types were installed.
2. A Falcon Fanjet engine inlet (supplied by Rohr Industries) was equipped with EIDI coils.

B. Test Descriptions:

1. Learjet

\* 6 types of coil-and-mount configurations were tried in 6 positions.

\* 10 runs

\* Tunnel conditions:

144 MPH	28°F	1.0g/m <sup>3</sup>
144	15	1.0
225	15	0.6
225	15	1.4

2. Falcon Fanjet Engine Inlet

\* coils were placed in 8 equally-spaced positions; 6 coil/mount types.

\* 29 runs

\* Tunnel conditions:

110 MPH	27°F	1.2g/m <sup>3</sup>	= 0°
110	27	1.2	10
110	15	1.2	0
110	15	1.2	10
110	15	2.4	0
170	15	0.85	0 (with 66% blockage)
170	15	1.65	0
170	26	0.85	0
225	15	0.6	0
225	27	0.6	0

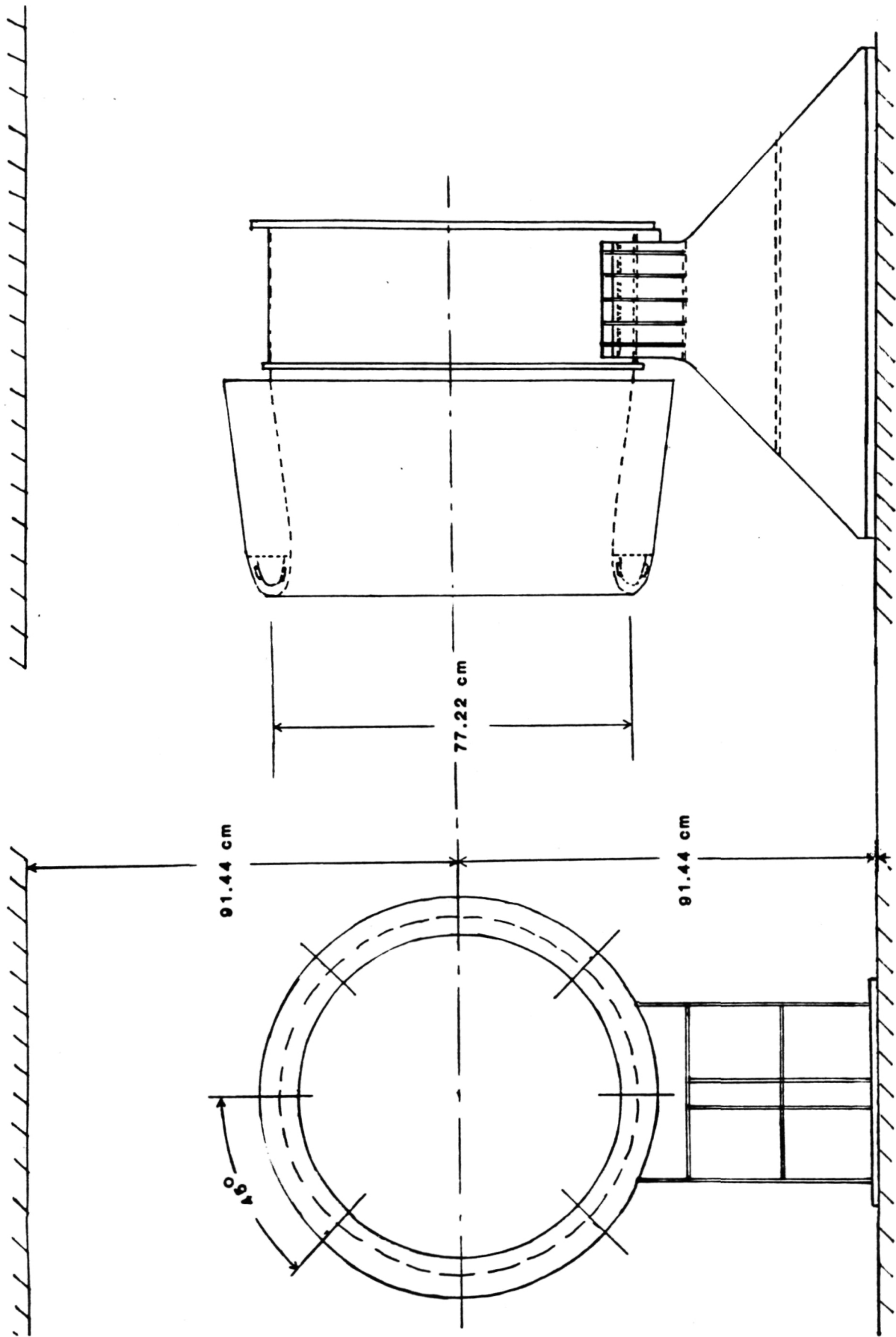
C. Major Results and Conclusions

1. A new transverse skin-mounted coil proved to be the most effective de-icer for both the Learjet wing and the engine inlet. It has the added advantage of very light weight. The only question concerning its usefulness is in its resistance to de-bonding during long-time use.
2. The Learjet wing was finally de-iced well by either of two coils, both using a single coil well off-set from the nose.

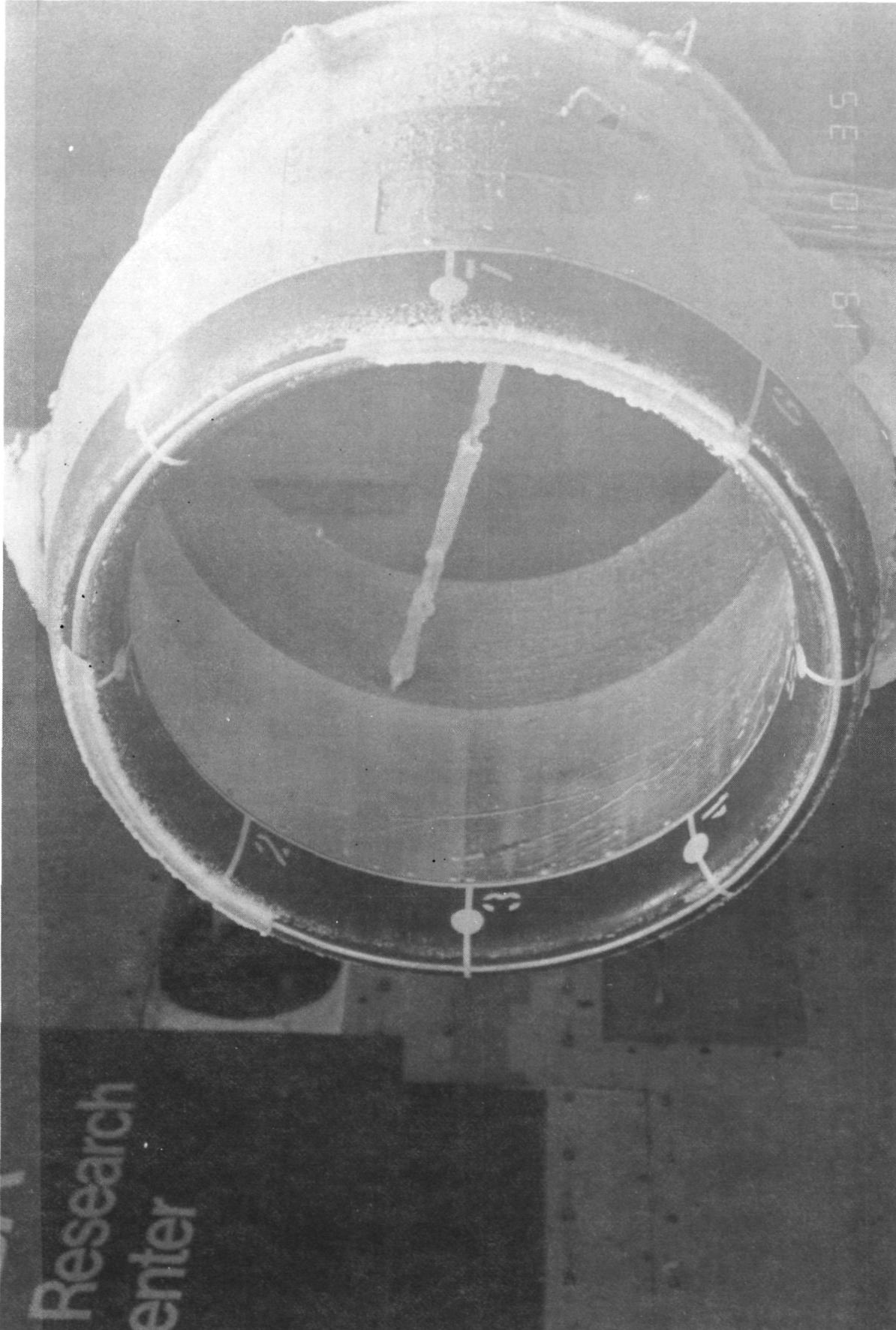
3. The engine inlet's curvature-induced stiffness was no problem for electro-impulse de-icing.
4. For the 36 inch diameter engine nacelle inlet, six coil positions are easily adequate.
5. Ice fragments were caught in a net and photographed for the engine inlet tests. These seem to be small enough to be safely ingested by a turbofan engine.

#### D. Participants

W.S.U. personnel were assisted by one industry participant from Simmonds-Precision, Cessna, Boeing, and Gates Learjet. Three participants were present from Rohr Industries.



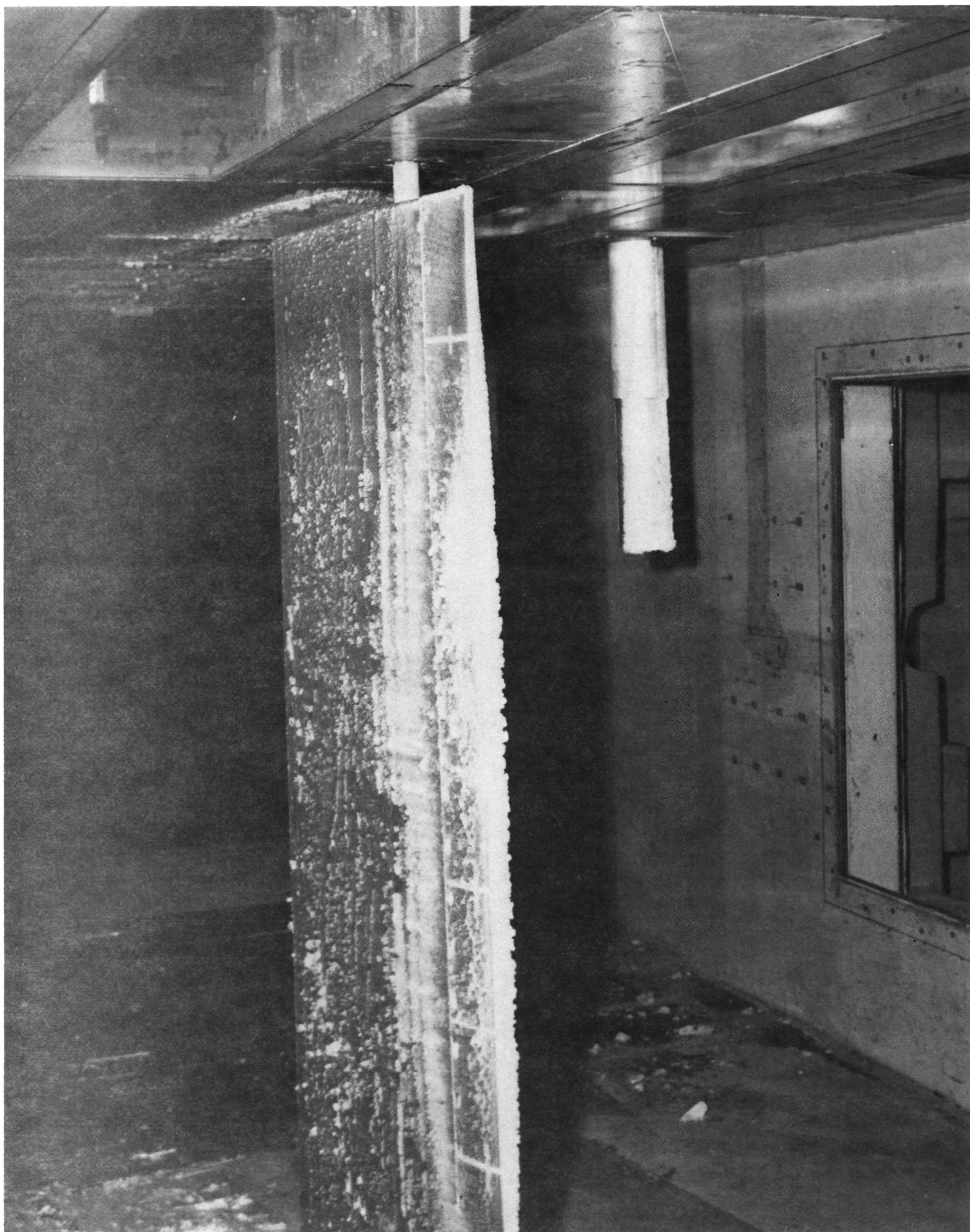
FALCQII FANJET 20 ENGINE INLET TEST MODEL



FALCON FANJET ENGINE INLET DURING DE-ICING CYCLE

COBRA HELICOPTER BLADE ICED

ORIGINAL PAGE IS  
OF POOR QUALITY





## VIII. Nov. 26 - Dec. 4 1984 Tests

### A. Six Models Tested

1. Cessna 206 horizontal stabilizer modified for retrofitting EIDI coils. A cuff extending the leading edge 3 inches was attached by rivets at the front spar.
2. Cessna 206 wing strut modified for retrofitting EIDI coils. A sheet metal (aluminum) airfoil shape was wrapped around the original elliptical-shaped strut .
3. Cessna 206 wing strut modified for new production to be more compatible with EIDI installation. Aluminum sheet airfoil was supported by an interior, load bearing, I-beam.
4. Cessna 206 wing section, outboard , skin thickness of 0.025 inches.
5. Cessna 206 wing section, inboard, modified for optimum EIDI rib spacing (18 inches) with 0.040 inch skin thickness.
6. Helicopter blade, mid-span section from AH-1 Cobra; this is an all-composite blade with 31 inch chord and slight twist.

### B. Test Descriptions

1. C-206 Horizontal Stabilizer; 0.032 inch aluminum skin.  
\* Two coil positions between 22 and 19 inch rib spacings; One position had side-pair coils mounted on an arch supported from the skin 3 inches behind the nose. The second had a composite beam version of the transverse skin-mount (band-aid) single coil on the pressure side of the leading edge. Doublers were used with all coils.

\* 48 runs

\* Tunnel conditions:

110 MPH	27°F	2.4g/m <sup>3</sup>	= 4°
110	27	1.2	4
160	27	1.7	0
160	27	0.83	0
110	10	2.4	-4
110	10	1.2	-4
160	10	0.83	0
160	10	1.70	0
160	-10	0.83	0

All of these were run with both metallized and electrolytic capacitors except the last two, which were done only with electrolytic.

\* To represent two or three coils in series, each coil was connected to one to two identical coils, outside the tunnel, which had "dummy" aluminum skins.

2. and 3. C-206 Wing Struts (Both types).

\* Two coil positions 24 inches apart; one position had side-pair coils supported on a skin-mounted arch; the second was a single "band-aid" mounted coil, one on one side only immediately behind the nose.

\* 42 runs

\* Tunnel conditions

110 MPH	27°F	2.4g/m <sup>3</sup>
110	27	1.2
160	27	1.7
160	27	0.83
110	10	2.4
110	10	1.2
160	10	1.7
160	10	0.83
160	-10	0.83

\* Electrolytic capacitors were used (500 microFarads).

4. C-206 Wing, 0.025" skin thickness.

\* A current-production leading edge was used which had 3 bays of differing span. In a 13 inch bay, a nose coil was mounted on an aluminum beam mounted to the ribs; In a 15 inch bay, a nose coil was mounted on a stiff, 6 inch long, composite bar attached (spanwise) to the skin at its ends; In a 17 inch bay, a band-aid type coil mount was placed on both upper and lower surfaces behind the nose; (these were wired separately). Doublers were used with all coils.

\* 19 runs

\* Tunnel Conditions

110 MPH	27°F	2.4g/m <sup>3</sup>
110	27	1.2
160	27	1.7
160	27	0.83

\* Electrolytic capacitors; 375 microFarads.

5. C-206 Wing; 0.040" skin thickness.

\* Three 18 inch bays each had identical nose coils, but were mounted differently. One was skin-mounted on a composite arch, one was a band-aid type, and one was supported by a composite rib mounted to the ribs. Doublers were used with all coils.

\* 32 runs

\* Electrolytic capacitors; 375 and 500 microFarads. Two

runs were made with metalized capacitors for comparison.

\* Tunnel conditions were the same as listed above for the horizontal stabilizer.

6. Helicopter blade

\* The outer 32 inches had an aluminum leading edge of 0.032 inch thick aluminum; the composite underneath was cut back to the first spar and two band-aid type coil mounts were placed 16 inches apart on the lower (pressure) surface. The inner 38 inches of the blade had an aluminum leading edge stretched against the solid composite leading edge, but bonded to it only aft of the nose region. Small "racetrack" shaped coils were recessed into the composite material and aluminum doublers bonded to the skin opposite them. Coil dimensions were 0.75 x 1.3 inches, and 0.125 inches thick. These were recessed into positions 8 inches part at three lower surface positions and 12 inches apart at two upper surface positions.

\* 15 runs

\* Tunnel conditions

230 MPH	27°F	1.2g/m <sup>3</sup>	= 10°
230	27	0.6	10
230	27	0.6	0
230	10	1.2	5
230	10	0.6	5
230	-10	1.2	5
230	-10	0.6	5

\* Metallized Capacitors, 400 microFarads.

C. Major Results and Conclusions

1. For the horizontal stabilizer, rib spacings of 22 inches are acceptable. Coils can be connected for three side-pairs in series and impulsed three times to de-ice with the 375 microFarads electrolytic capacitors. This gives a total energy of 246 Joules per foot of span. The band-aid type, similarly connected, would require 215 J/ft.
2. The wing struts de-iced well with three impulses using about 200 J/ft. The band-aid mounts were somewhat superior to side-pair types.
3. For the wing leading edges, the beam-between-ribs and simple band-aid coil mounts de-iced well. The attempts to devise a rigid band-aid mount were not successful. Energy required was about 400 J/ft. with three impulses.

4. For the helicopter blade, the outer section was used as a comparison with similar sized wing tested previously. This de-iced easily, but is not typical of a helicopter leading edge structure. The inner blade section was believed to be a viable helicopter EIDI design. Best de-icing was achieved using the three lower surface mini-coils in series with 1300 volts and three impulses. This gave 400 Joules per foot of span as energy requirement. Ice shedding was good for all cases. A continuous icing run was made with de-icing every 2 minutes for 10 minutes; Results were very good. Attempts to use only two coils 16 inches apart were unsuccessful. Upper surface coils used alone or in series with lower coils were inferior to lower coils impulsed alone.

#### D. Participants

W.S.U. test conductors were joined by industrial participant representatives from Cessna, Simmonds-Precision, and Kaman Aerospace Co.

#### IX. References

- 5-1. G.W. Zumwalt and A.A. Mueller, "Flight and Wind Tunnel Tests of an Electro-Impulse De-Icing System," AIAA/NASA General Aviation Technology Conference, Hampton, VA, July 10-12, 1984. AIAA Paper No. 84-2234.
- 5-2. G.W. Zumwalt, "Icing Tunnel Tests of Electro-Impulse De-Icing of an Engine Inlet and High-Speed Wings," AIAA 23rd Aerospace Sciences Meeting, Reno, Nevada, January 14-17, 1985. AIAA Paper No. 85-0466.

## Chapter 6. FLIGHT TESTS

At the date of writing, two flight test series have been completed and a third is beginning. The two completed flights were reported in Ref. 6-1.

### I. NASA Icing Research Aircraft

During January, 1984, the EIDI system was tested in twenty-one flights from NASA Lewis Research Center over the Lake Erie area in the well-instrumented NASA/Lewis Icing Research Aircraft, a DeHavilland DHC-6 Twin Otter. Robert Friedberg of W.S.U. operated the EIDI Equipment on the flight. NASA pilots were Rich Ranaudo and Robert McKnight. The purposes were:

1. To make direct comparisons between the EIDI performance in the icing tunnel and in natural icing conditions.
2. To explore possible electro-magnetic interference (EMI) problems.
3. To obtain flight operation experience safely in natural icing with an aircraft and crew having extensive prior experience flying in icing conditions.

Twenty-one flight were made from NASA/Lewis in Cleveland, Ohio, over the Lake Erie area in January, 1984.

#### A. Equipment Used

A power supply-and-sequencing box was designed and built by Simmonds-Precision. While considerably lighter than that used in the IRT tests, this was still a research tool rather than a production model. It provided capacitance of 400 uFd and voltage from 800 to 1200, with automatic sequencing of either 2 or 3 impulses per station as fast as the capacitors recharged, an interval of 3 to 4 seconds.

Since the aircraft was already fitted with deicing boots, a cuff section was constructed for the tests which would not interfere with boot operation. The cuff (or "glove") was a 50 inch long section constructed from a cannibalized DHC-6 wing, and its leading edge extended 3 inches forward of the wing's leading edge. Thin fences were placed at each end to minimize end effects on the flow. Like the main wing, the cuff section was unswept with ribs at 12.5 inch spanwise spacing, and had a leading edge made of 2024 T-3 aluminum, 0.025 inches thick, with radius of approximately 2.5 inches. The cuff was placed at about two-thirds semi-span position from the fuselage on the right wing as shown in Figure 6-1. The cuff assembly was fabricated and coils installed by WSU, and tested first in the Icing Research Tunnel, as described in 5. IV.

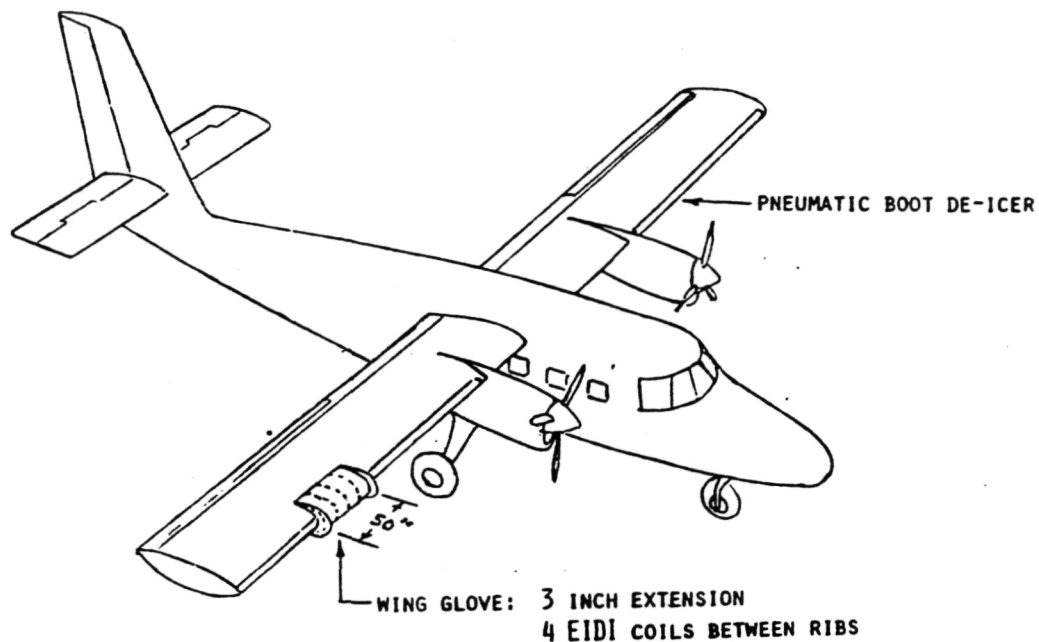


Fig. 6-1 DHC-6 Twin Otter Aircraft  
for E.I.D.I.

A single, contoured coil was placed at the center of each bay, mounted on a composite plate which was riveted to the skin about 4 inches aft of the leading edge. The coils had 40 turns of copper ribbon wire, 0.024 x 0.190 inches, giving a 2.5 inch coil diameter. An aluminum doubler, 0.050 thick, was bonded to the inside of the skin opposite the coil, with a gap of 0.050 inches between doubler and coil. The coils were connected in alternating pairs and were impulsed two times each (bays 1-and-3 twice, then 2-and-4 twice) with 1000 volts at 400 uFd. This gave an energy of 96 joules per impulse per foot of span per impulse.

Cameras are installed in right side of the forward fuselage, including a stereoscopic system to permit determination of ice shapes.

#### B. Test Procedures

Due to the effect of Lake Erie on the atmosphere above it, a wide variety of icing conditions are available during the winter months. The pilots sought a range of temperatures and ice types. Rime ice was encountered on 3 flights, clear glaze ice on 8 flights, and mixed on the remaining 10.

Indicated airspeeds were 85 to 140 knots at altitudes 3000 to 6000 feet. Ice thickness ranged from 0.1 to nearly 1.0 inches. Air temperatures were  $-8$  to  $-3^{\circ}\text{C}$  ( $17.5$  to  $27^{\circ}\text{F}$ ). Generally, ice was collected at almost constant speed, but on four tests the speed was varied (three decreasing and one increasing), with resulting angle of attack change, to obtain a wider ice collection on the wing.

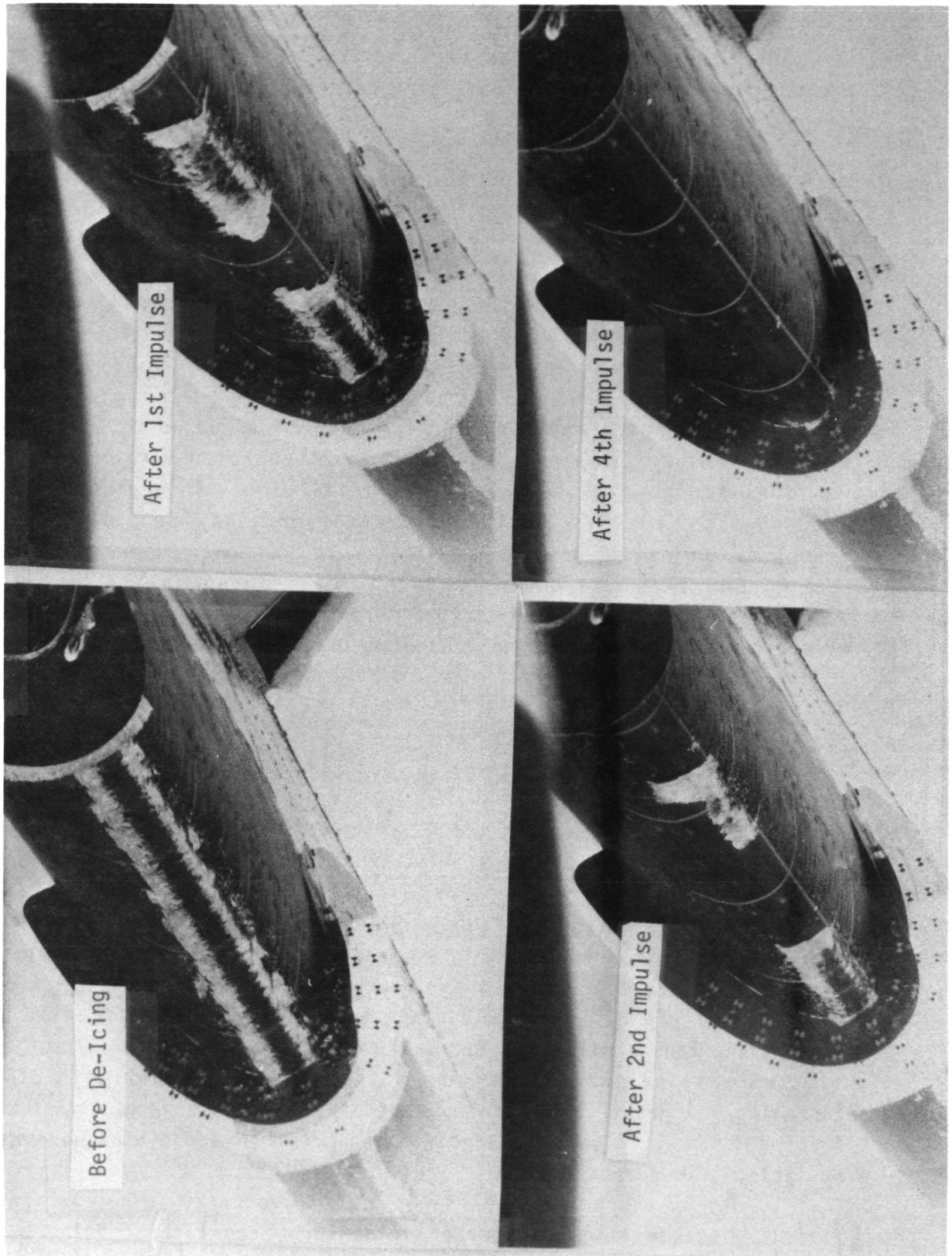


Fig. 6-2 Removal of Natural Ice Shown in Four Impulses.

After the desired ice was accreted, the altitude was increased to reach a cloud-free atmosphere for obtaining good photographs.

### C. Results

Figure 6-2 shows a sequence during de-icing, with pictures taken at about 4 second intervals. For this test, conditions were: TAS 139 knots, altitude 3075 ft, outside air temperature  $-5^{\circ}\text{C}$ , LWC  $0.38 \text{ g/m}^3$ , ice thickness about 0.7 inches.

Ice removal was very good, being (by pilots' testimony) always better than the adjacent boots. Two de-icing attempts were judged to be fair-to-poor. If a very thin layer of ice (about 0.1 inch) was pulsed, then only half of the ice was shed. A second sequence of impulses removed half of the residual. Changing speed during ice accretion had no noticeable effect. When ice was accumulated beyond about 2% chord on top or bottom, some residual ice tended to be left after de-icing. This suggests that for leading edges of this 2.5 inch radius or greater, two coils (upper and lower) may be needed rather than the single nose coil.

No EMI problems could be found, even though all flight and data acquisition instruments were turned on and monitored. The sound made by the electrical discharge could not be heard inside the cabin in flight.

### D. Conclusions

The system worked well and de-iced the aircraft well and reliably. The natural icing was easier to remove than that encountered in the icing tunnel.

## II. Cessna TV 206 Flights (1984)

In February-March 1984, Cessna Aircraft company made fifteen flight over the Wichita, Kansas area in a Cessna 206 partially protected by an EIDI system. Alan A. Mueller of Cessna's Pawnee Division was Project Engineer and operated the EIDI system during these flights. The 206 pilot was Doug Bassett and tanker pilot was Tom Wallis. Prior to this time, the C-206 wing had two test series in the NASA Icing Research Tunnel with EIDI coils installed. A grant from the State of Kansas Advance Technology Commission enabled W.S.U. to give more specific support than would otherwise have been possible. The purposes were:

1. To expand experience with the EIDI system/206 wing combination to include flight in tanker icing spray and natural icing conditions in addition to the previous wind tunnel experience.
2. To bring experience in-house for both the operational and design aspects of the system.

3. To increase the visibility and credibility of the program within the company.

Fifteen flights were made over the Wichita, Kansas, area during February-March, 1984.

#### A. Equipment Used

The test vehicle was the engineering prototype Turbo-206, a single engine, propeller-driven, high wing, six-place aircraft. Wichita State University personnel fabricated and installed seven, 2.25 inch diameter electro-impulse coils in a production leading edge assembly supplied by Cessna. The EIDI coils were supported by composite beams suspended between ribs. Doublers and gaps were similar to those in the Twin Otter. The modified leading edge was then installed on the TU-206 in the Cessna experimental shop. The portion of the right wing that was to be de-iced was painted black to make the ice more visible and the rib locations were highlighted with a yellow stripe to mark the bays; Fig. 6-3. Coil locations were marked, and the bays identified, with three inch numbers. Seven bays were equipped, having rib spacings varying from 7 to 18 inches, for a total span of 8 feet. Metal tabs with 1/2 inch wide stripes were mounted on the wing leading edge as an aid in gauging the ice thickness. In addition to the wing installation, a pair of coils were installed in the wing strut. Two, 1.5 inch diameter coils, wired in series, were embedded in foam inside the strut. (Note that the number 8 on the strut is not over the coils but is about 8 inches above the coils).

The coils were connected in alternating pairs (1-3, 2-4, 5-7, and 6-8) and were pulsed two or three times each. The EIDI control box and power supply were the same as those used in the DHC-6 tests, above.

The tanker used was a Cessna 404 equipped with two 100 plus gallon water tanks, a pump system, and spray bars mounted on top of the vertical tail. About forty minutes of spray time was available on each flight, with a spray plume about 4 feet wide. The 206 is shown in formation with the tanker during ice accretion in Figure 6-4.

Documentation was provided by camera(s) mounted in the blister on top of the 206 cowl and cameras in the tanker and/or a separate photo chase plane.

#### B. Test Procedures

After locating an altitude where the desired temperatures were available, the tanker pilot would turn on the spray pump. Once started the pump could not be stopped without freezing the spray system. Unable to see the test vehicle, the tanker pilot was required to hold altitude, heading and airspeed so that the pilot of the 206 test vehicle could maneuver behind him and position the spray over the portion of the airframe to be iced.

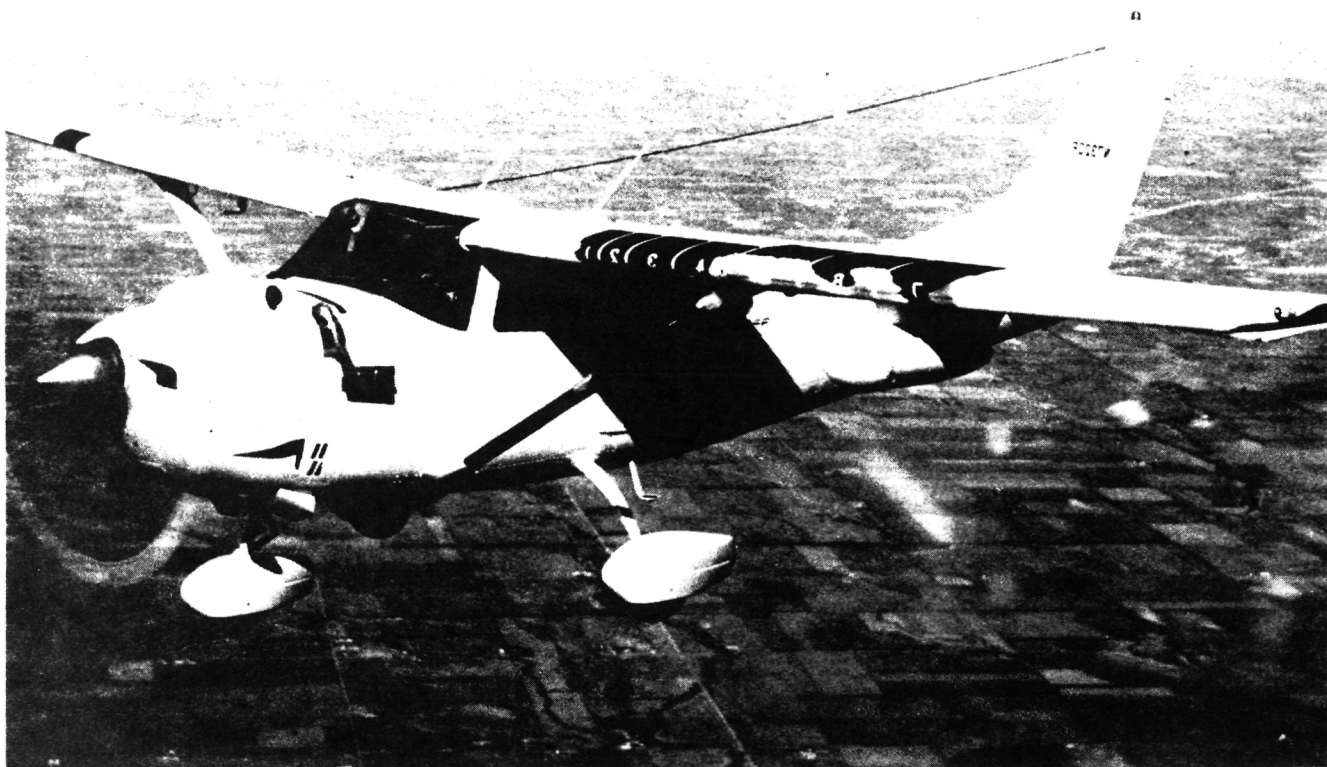


Fig. 6-3 Cessna TU 206 Test Aircraft

ORIGINAL PAGE IS  
OF POOR QUALITY



Fig. 6-4 Cessna 206 with Icing Tanker

As the ice accumulated the airspeed decreased due to drag, and the pitch attitude increased. A typical flight would start at 115 to 120 KIAS and would decrease to about 95 KIAS by the time 1/2 inch of ice had built up. This required close coordination between the two aircraft on airspeed control.

For most of the test program, a photographer rode in the tanker which required the 206 to move out of the water spray and reform on the left wing of the tanker. Starting with flight 12, a separate photo chase plane was used which allowed the 206 to remain in the water spray during the de-ice cycle. This was found to have a significant effect on the operation of the system as discussed below.

The primary form of data acquisition was photographic. On the early flight a video camera was mounted in the cowl camera housing, and a 35mm still camera was carried in the tanker. The video camera allowed the flight test engineer to monitor the image while it was being recorded. Since no processing was required, it provided instant review of the flight on the ground after the test. On later flights, the video camera was replaced with a 500 frames per second movie camera and a 35mm still frame camera with a motor drive. The video camera was used from the tanker as a back-up in case the other cameras should fail to operate. On the last flights the video camera in the tanker was replaced by a 16mm movie camera running at normal speed and a 35mm still camera in a photo chase plane. Each media added its own unique contribution to the understanding of the de-icing mechanism on the electro-impulse system.

### C. Tanker Ice

Twelve flights were made with tanker icing. The photo sequence shown in Figure 6-5 was taken on flight 5. This sequence illustrates the clearing pattern adopted for the bulk of the tests. Three pulses were sent to alternating pairs of bays wired in series. Bay 6 was wired in series with the coil pair in the strut. The two stage clearing action of fracture and expel are clearly shown. In this test, two pulses were adequate to clear the bays. However, on other tests three pulses were required. In all cases, each impulse had energy of less than 140 joules per bay.

Test conditions were varied on subsequent flights to cover a range of temperatures and ice thicknesses. The system was successful in clearing ice ranging in thickness from 1/10th of an inch to in excess of one inch. The temperature was varied from 5° to 30°F. The most difficult ice to clear was the extremely thin, warm ice. In this case, some residue was left on the rib locations with approximately 90% of the area between the ribs clean.

On the flights using a separate photo chase plane the system was activated while the airplane remained in the water spray. This caused a significant degradation in system effectiveness. Up to three cycles of the

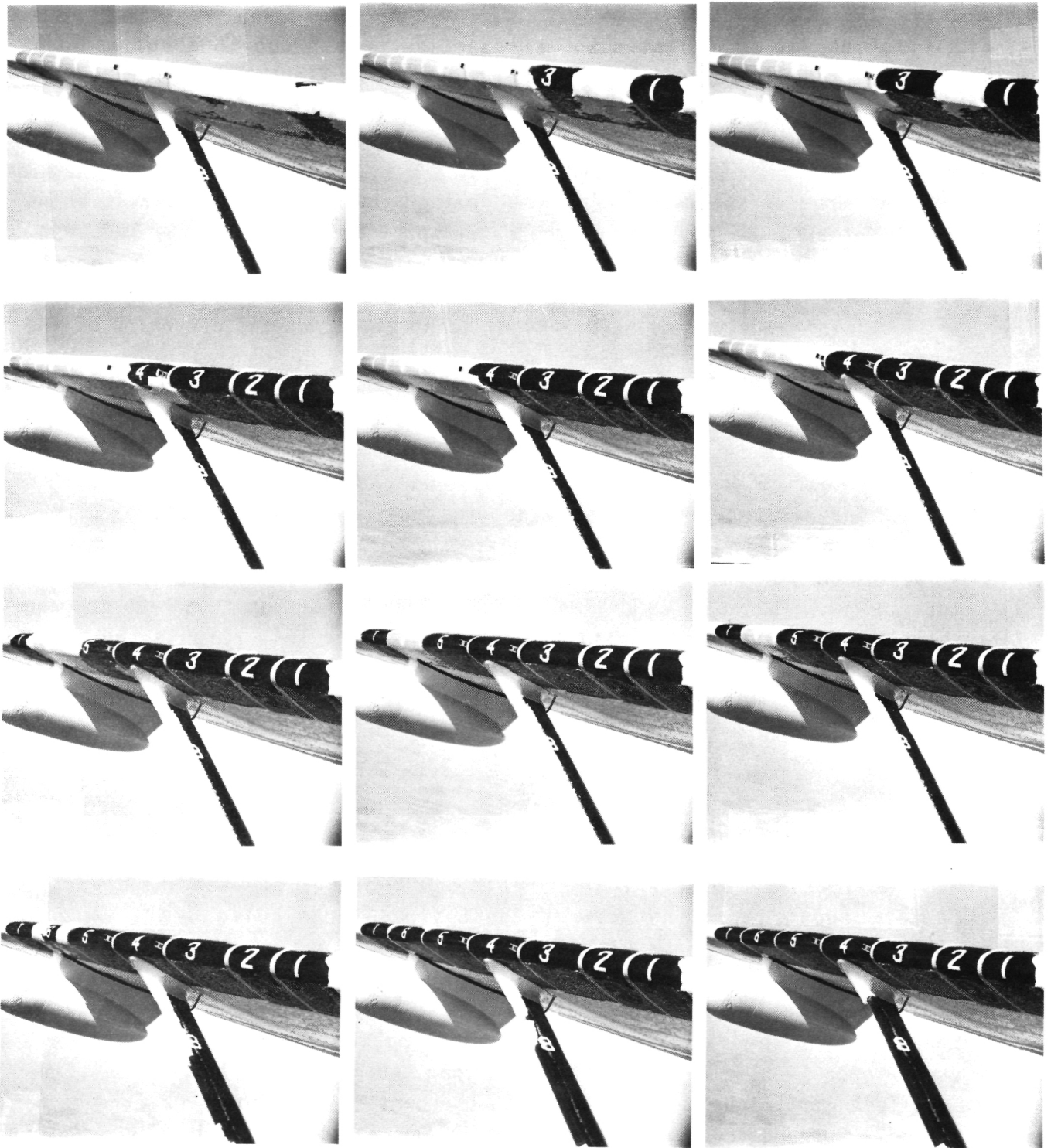


Fig. 6-5 De-icing Sequence of Cessna 206 Wing  
with Tanker Spray Ice

ORIGINAL PAGE IS  
OF POOR QUALITY.

system were required to clear ice that had cleared easily in one cycle on previous tests. There were three significant variables different on these tests. The presence of liquid water on the surface of the ice caused the fractures in the ice to fill with water. This water apparently damped the action of subsequent pulses and allowed the ice to refreeze between cycles. It was also estimated that the 206 was flown closer to the tanker than on previous flights and that the water in the tanker was warmer than on earlier flights. This tended to create a greater amount of runback with clear ice extending 12 to 14 inches along the lower surface of the wing. Examination of the high speed movies revealed that ice was being fractured and pushed free of the wing, only to be pushed back into its original location by the air pressure and held by the ice ridge behind it.

#### D. Natural Ice

Natural ice flights were limited due to safety consideration. Other than the de-icing provided by the EIDI system and propeller de-ice, there were no other de-ice provisions on the airplane. We were therefore limited to icing conditions with warm air below and clear skies above. The two natural icing encounters were in thin stratus layers with a low liquid water content (not measured). One quarter inch of ice took approximately 20 to 25 minutes to accumulate and was a soft agglomerate of ice particles. This resulted in a considerable residue after the first clearing cycle. This residue provided seed points from which the next accretion grew and seemed to promote a more rapid and solid ice growth resulting in more complete clearing of the second ice build-up. Figure 6-6 shows the clearing cycle in light natural icing.

#### E. EMI/RFI

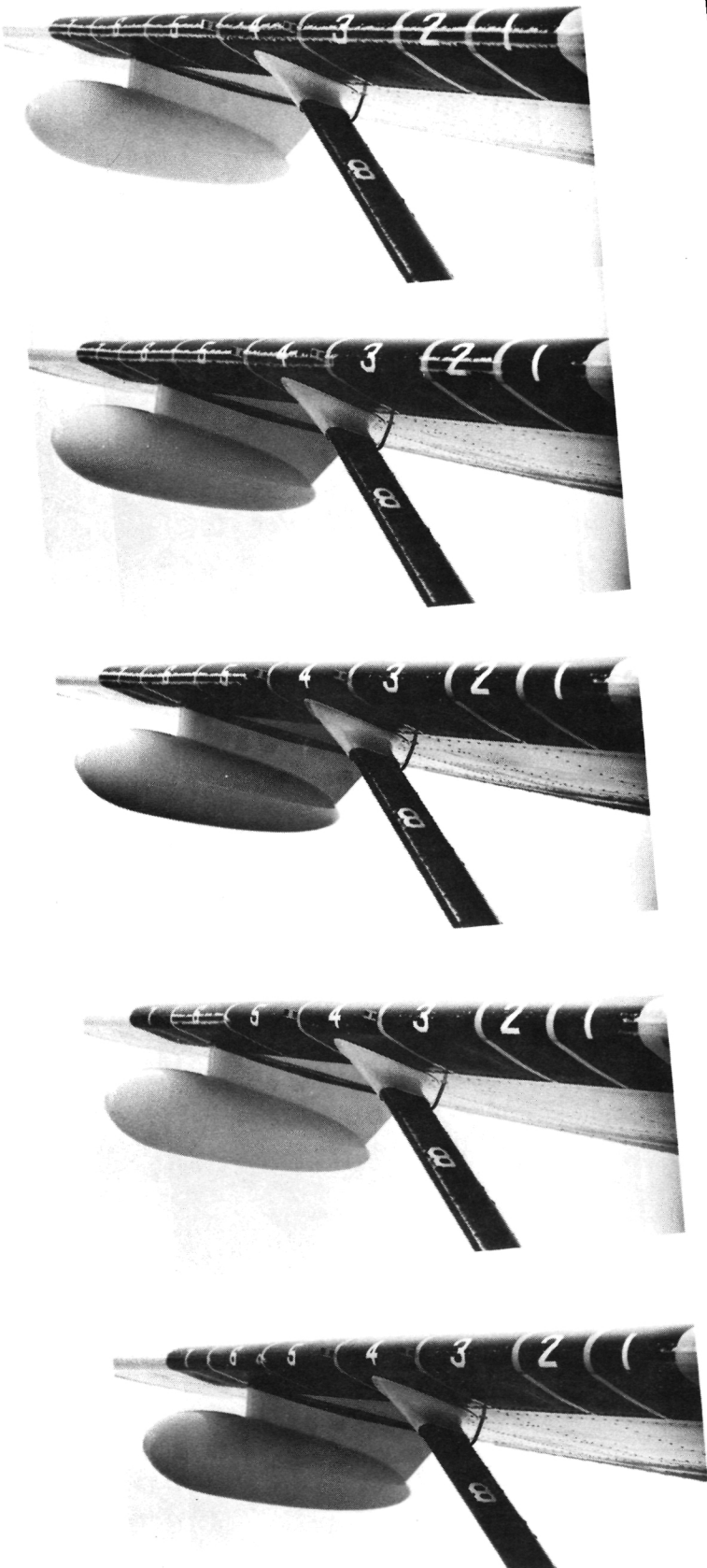
There was no evidence of any electro-magnetic or radio frequency interference problems on any of the flights. The equipment installed on all flights included two digital display NAV/COMs, ADF, RNAV, Autopilot, and Weather radar. In addition there was a LORAN-C installed for part of the flights with no detrimental effect on its operation.

#### F. Noise

The noise level when operated on the ground is quite startling but in the air is noticeable but not disconcerting. It may even be comforting to know that the system is working without requiring constant monitoring. A production aircraft would be quieter with a full interior installed in the cabin and some soundproofing in the wing root.

ORIGINAL PAGE IS  
OF POOR QUALITY

Fig. 6-6 Natural Ice De-icing  
Sequence



## G. Conclusions

It is important that the coil mounts be stiff. The original mounts were too soft and absorbed some of the de-icing energy.

System components must be properly matched. Coils wound a little small had the compounding effect of reducing efficiency and limiting the voltage of the system due to approaching the current capacity of the SCR's.

Ice thickness ranging from 1/10th inch to over one inch can be shed successfully. As in the tunnel, warm soft ice is the most difficult to clear.

The presence of liquid water on the surface of the ice can effect the system operation. There are probably two mechanisms at work here: (1) The water coming out of the tanker was quite warm and did not cool to near freezing before impinging on the aircraft. This kept the ice temperature near the freezing point. (2) Liquid water on the surface quickly fills the cracks after the first pulse, damping subsequent pulses, and then refreezes. The quantity and temperature of this water probably does not represent natural ice. It does, however, point out the need to look at the effect of flight in natural ice near the freezing point.

In general, tanker ice is more difficult to shed than natural ice. Since the system was able to shed the tanker ice on all tests, natural ice should provide no significant surprises. Reference 6-2 gives further details of this test.

As a result of this test, Cessna Aircraft Company decided to install a complete prototype EIDI system in the C-206 for a thorough evaluation in natural icing. Anticipating both new production installations and retrofit, several design changes were made from the wing and strut installation tested above. In addition, empennage installations were designed. Changes were made in wing rib spacings and skin thickness to be more congenial to the EIDI components, and to the strut and tail to facilitate EIDI installation under both field and factory conditions. All these changes were tested in the IRT on Nov.-Dec. 1984 and are currently being incorporated in the C-206 for flight tests to address certification issues.

## III. References

6-1 Zumwalt, G.W. and A.A. Mueller, "Flight and Wind Tunnel Tests of an Electro-Impulse De-Icing System", AIAA/NASA General Aviation Technology Conference, July 10-12, 1984, Hampton, VA. AIAA Paper No. 84-2234.

6-2 Mueller, A.A., D.R. Ellis and D.C. Bassett, "Flight Evaluation of an Electro-Impulse De-Icing System on a Light General Aviation Airplane." AIAA/AHS Aircraft Designs, Systems and Operations Meeting, San Diego, CA., October 1984. AIAA Paper No. 84-2495.

## CHAPTER 7. PLANS AND PROSPECTS

At this juncture, the EIDI group at Wichita State University can design a system for general aviation aircraft with considerable confidence. This ability rests on the empirical data and experience reported here. For larger, transport category aircraft, more testing of similar type needs to be done to define system parameters and design optimums, but no intrinsic difficulties are seen. Helicopters pose special problems, which are discussed briefly in a Section of the Appendix; more testing is planned in the Icing Research Tunnel. More engine inlet de-icing testing is scheduled.

From the outset it was proposed to go beyond this empirical base for the design of Electro-Impulse De-Icing applications. The ultimate aim is to be able to mathematically model (1) the structural dynamics; (2) the electro-dynamics and (3) the ice removal effects so that a system can be designed without tunnel testing. From the start, an approximate, two-dimensional analysis of the natural vibratory modes of the leading edge was computed as the first step in the design. Then circuit computations gave an estimate of current pulse times to match the structural mode frequencies. The computer modeling being performed as two Ph.D. dissertations should lead to a design method which minimizes the reliance on insight and intuition based on the type of experience now residing only in the W.S.U. group.

After three years of rather heavy funding, the NASA support is expected to diminish. The technology has been developed and demonstrated to the point where U.S. industries or other government agencies can continue much of the development and provide the support for further research.

PRECEDING PAGE BLANK NOT FILMED

CHAPTER 8

APPENDIX

W.S.U. Participants on E.I.D.I. Project  
(to March 1985)

- Glen W. Zumwalt, Ph.D., Distinguished Professor  
of Aeronautical Engineering, Project Director, May 1982 to March 1985.
- Robert L. Schrag, Ph.D., Professor of Electrical Engineering,  
Leader of Electro-Dynamic Research, May 1982 to March 1985.
- Walter D. Bernhart, Ph.D., Professor of Aeronautical Engineering,  
Leader of Structural Dynamic Research, May 1982 to March 1985.
- Thangavel Paramasivam, Ph.D., Ass't. Professor of Aeronautical Engineering,  
Research on Composite Materials Dynamics, May 1982 to March 1983.
- Robert Friedberg, M.S.A.E., Research Associate in Aeronautical Engineering,  
Leader of Manufacturing Methods, May 1982 to March 1985.
- Robert E. Henderson, M.S.E.E., Instructor of Electrical Engineering, January  
1984 to March 1985.
- Curtis Luginbill, Chief Technician, Dec. 1982 to Dec. 1983.
- Fred Cook, Chief Technician, Jan. 1984 to Apr. 1984.
- Vernon L. Hagnauer, Chief Technician, May 1984 to March 1985.
- B. Keith Wilson, B.S.A.E., Research Assistant, Jan. 1984 to March 1985.
- Peter Gien, B.S.A.E., Research Assistant, May 1984 to March 1985.
- Elias Bounajm, M.S.A.E., Research Assistant, Sept. 84 to March 1985.
- Dan Chrismore, M.S.A.E., Doctoral Fellow, Aug. 1984 to March 1985.
- Michael Schmitt, Student Assistant, Feb. 1984 to March 1985.
- John Schwartz, Student Assistant, Feb. 1984 to March 1985.
- Mondhes Yahiaoui, Student Assistant, Feb. 1985 to March 1985.

## INDUSTRIAL PARTICIPANTS

Beech Aircraft Company, 9707 E. Central, Wichita KS 67201  
Harold Riesen 316/681-7944

Boeing Commercial Aircraft Co., P.O. Box 3707, Seattle, WA 98124  
Douglas Cozby, M.S. 47-03 206/237-6003

Cessna Aircraft Company, P.O. Box 7704, Wichita KS 67277  
Alan Mueller 316/946-6956

Electro-Delta, Inc., P.O. Box 8, White Oak TX 75693  
George Massey 214/759-3942

Gates Learjet Corp., P.O. Box 7707, Wichita KS 67277  
Allyn Heinrich 316/946-2881

Lear Fan Corp.(U.S.), Box 60000, Reno NV 89506  
Ian Gilquist 702/972-2647

Douglas Aircraft Div. of McDonnell-Douglas Co., 3855 Lakewood Blvd,  
Long Beach CA 90846  
David Blyther 213/593-8126

Rohr Industries, Inc., P.O. Box 878, Chula Vista CA 92010  
Herman A. Rosenthal, M.Z. 19T, 619/691-3420  
Don Nelepovitz, M.Z. 19T, 619/691-3004

Simmonds-Precision Co., Engine Systems Div., P.O. Box 310, Norwich NY 13815  
Jack Chearmonte 607/335-5113

Sikorsky Aircraft Co., North Main St., Stratford CT 06601  
Robert Flemming 203/386-5789

## Prospects and Problems for Applying EIDI to Helicopter Blades

The need for de-icing is greater for helicopters than for any other aircraft. Only recently has a helicopter been certified by F.A.A. for flight into known icing conditions; one "limited conditions" certification has been given Sikorsky by the British BCAR. The small blades collect ice proportionately better than fixed wings and can tolerate only small accumulations since power requirements rise quickly with icing. Pneumatic boots are only beginning to be available for rotors and electro-thermal power requirements impose a severe penalty. Thus, electro-impulse must be examined for meeting this need.

Several design decisions can be made immediately. The power-and sequencing box would be placed in the core section of the rotating mechanism. Power for this would be supplied through commutator rings at low voltage and nearly continuous flow to recharge the capacitors. The small space available in the blades will probably force the SCRs to be in the center column also. Thus, the coils will be connected by a rather large number of wires to the central power box, and will be pulsed in opposing blades simultaneously to maintain symmetry.

There are several problems, and these will require some re-designing of rotor blades if EIDI is to be used. Many rotor blades have a main spar which is a hollow, flattened-oval, tube. Spars have been metallic but are now beginning to be made of composite materials. It seems likely that electro-impulse can be used only with the composite spars. Forward of the spar is a plastic (e.g., phenolic) material forming the leading edge. This is often protected by a metal abrasion strip, a thin sheet having good abrasion resistance (usually titanium) wrapped around and bonded to the leading edge for about 15% of the chord. Alternately, a rubber-like abrasion shield may be needed.

Electro-impulse coils could be recessed into the plastic leading edge material with a gap between the coil and the metal shield. A doubler would probably be needed, bonded to the inner surface of the abrasion shield immediately over the coil to provide adequate electrical conductivity.

The abrasion shield must be free to move normal to its surface to expel ice, so bonding of the shield would have to be restricted to its upper and lower sides well downstream of the nose. Some gaps will be necessary between the shield and its supporting composite under-structure, since the metal must be able to move at least 0.2mm in the nose region. Realizing that this metal shield frequently impacts objects at high speeds (birds, hail, sand, bugs,), maintaining adequate free movement will be a challenge. . . but it may be possible.

Coils may be made in the familiar flat spiral shape with two opposing coils in the upper and lower nose at the same span station, or an elongated oval winding might be used, with only one coil at a given span location. There seems to be adequate space for a coil to be recessed into the plastic nose material.

A major problem is the lack of space forward of the spar for running the needed number of insulated wires to the coils. This problem is compounded by the space required for coils and by the practice of imbedding lead weights in the nose at frequent span locations.

Where can space be found for the power cables to the EIDI coils? The most obvious available space is inside the hollow spar, but this suggestion is rejected by some rotor designers since it implies drilling holes in the spar at each coil station to attach the power wires. Holes are undesirable due to stress concentrations which compromise structural integrity. In addition, it is a common practice to apply a constant small air pressure (or vacuum) inside the hollow spar to detect cracks. Some sort of feed-through electrical connector may be needed which will be acceptable to the structural designers of the rotor blade.

Of course, the distributed weights of the EIDI components must be included in the aeroelastic analysis and design of the blade. This calls for the EIDI system to be a part of a redesigned blade; EIDI is not an add-on system for helicopter blades.

1. Report No. NASA CR-174919		2. Government Accession No.		3. Recipient's Catalog No.	
4. Title and Subtitle Analyses and Tests for Design of an Electro-Impulse De-Icing System				5. Report Date May 1985	
				6. Performing Organization Code	
7. Author(s) G.W. Zumwalt, R.L. Schrag, W.D. Bernhart, and R.A. Friedberg				8. Performing Organization Report No. AR 85-1	
				10. Work Unit No.	
9. Performing Organization Name and Address Wichita State University College of Engineering Wichita, Kansas				11. Contract or Grant No. NAG 3-284	
				13. Type of Report and Period Covered Contractor Report	
12. Sponsoring Agency Name and Address National Aeronautics and Space Administration Washington, D.C. 20546				14. Sponsoring Agency Code 505-45-54	
15. Supplementary Notes  Interim report. Project Manager, John J. Reinmann, Propulsion Systems Division, NASA Lewis Research Center, Cleveland, Ohio 44135.					
16. Abstract De-icing of aircraft by using the electro-magnetic impulse phenomenon is an idea which has been proposed and demonstrated in several European countries. However, it has not been available as a developed system due to lack of research on the basic physical mechanisms and necessary design parameters. The de-icing is accomplished by rapidly discharging high voltage capacitors into a wire coil rigidly supported just inside the aircraft skin. Induced eddy currents in the skin create a repulsive force resulting in a hammer-like force which cracks, de-bonds and expels ice on the skin surface. The promised advantages were very low energy, high reliability of de-icing and low maintenance. In 1982, under NASA Lewis Research Center sponsorship, Wichita State University organized a consortium of aerospace companies to work with the University to develop the method, which was termed Electro-Impulse De-Icing (EIDI). This interim report summarizes nearly three years of effort and includes analytical studies and the results of testing done in the laboratory, in the NASA Icing Research Tunnel and in flight. It is shown that the design must be done with clear understanding of both the electro-dynamic and structural dynamic phenomena, and the interaction between them. If properly designed, EIDI has been demonstrated to be an effective and practical ice protection system for small aircraft, turbojet engine inlets, elements of transport aircraft, and shows promise for use on helicopter rotor blades. Included in the report are practical techniques of fabrication of impulse coils and their mountings. The use of EIDI with nonmetallic surface materials is also described.					
17. Key Words (Suggested by Author(s))  Electro-impulse de-icing Aircraft Ice Protection			18. Distribution Statement  Foreign distribution excluded. Available from NASA Industrial Applications Centers.		
19. Security Classif. (of this report) Unclassified		20. Security Classif. (of this page) Unclassified		21. No. of pages 196	22. Price*

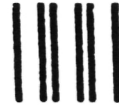
National Aeronautics and  
Space Administration

**Lewis Research Center**  
Cleveland, Ohio 44135

Official Business  
Penalty for Private Use \$300

**SECOND CLASS MAIL**

ADDRESS CORRECTION REQUESTED



Postage and Fees Paid  
National Aeronautics and  
Space Administration  
NASA-451

**NASA**

---